Doctoral Thesis (2006)

Studies on Molecular Structures, Electronic Spectra, and Reactivities of Uranyl(V) and -(VI) Complexes

Koichiro Mizuoka

Department of Nuclear Engineering
Graduate School of Science and Engineering
Tokyo Institute of Technology

Supervisor
Associate Professor Yasuhisa Ikeda

Contents

List of Figures

List of Tables

Chapter 1

Introduction

One of the largest issues of human beings in the 21st century is the energy source. Still now, nuclear power is one of the most powerful energy sources in spite of the disasters of the atomic bombs. However, after the use of the nuclear power, a large amount of “dirty wastes” is left. Here, “dirty” means chemically and radioactively toxic. To develop optimal techniques for treating such dirty wastes from the nuclear fuel cycle, accumulation of basic data of actinoid chemistry is essential. Especially, in reprocessing process of spent nuclear fuel and geological disposal of high level radioactive wastes, the knowledges on actinoid chemistry must be necessary, because their main processes are exactly chemical. Thus, basic properties and behaviors of the actinoid elements must be important and should be understood. In this chapter, the details of background, motivation, and objectives of this doctoral thesis are presented.

1.1 Actinyl Ions

The word “actinoid” refers elements with atomic number from 89 (actinium) to 103 (lawrencium), which are lying at the lowest row of the periodic table. At the ground state of the neutral atom of each actinoid element, valence electrons occupy 5f, 6d, and 7s orbitals as follows. For a comparison, the electronic configurations of lanthanoid elements with the

57 La $5d6s^2$	58 Ce $4f^15d6s^2$	59 Pr $4f^36s^2$	60 Nd $4f^46s^2$	61 Pm $4f^56s^2$	62 Sm $4f^66s^2$	63 Eu $4f^76s^2$	64 Gd $4f^75d6s^2$	65 Tb $4f^96s^2$	66 Dy $4f^{10}6s^2$	67 Ho $4f^{11}6s^2$	68 Er $4f^{12}6s^2$	69 Tm $4f^{13}6s^2$	70 Yb $4f^{14}6s^2$	71 Lu $4f^{14}5d6s^2$
89 Ac $6d7s^2$	90 Th $6d^27s^2$	91 Pa $5f^26d7s^2$	92 U $5f^36d7s^2$	93 Np $5f^46d7s^2$	94 Pu $5f^67s^2$	95 Am $5f^77s^2$	96 Cm $5f^76d7s^2$	97 Bk $5f^97s^2$	98 Cf $5f^{10}7s^2$	99 Es $5f^{11}7s^2$	100 Fm $5f^{12}7s^2$	101 Md $5f^{13}7s^2$	102 No $5f^{14}7s^2$	103 Lr $5f^{14}6d7s^2$

corresponding number of the valence electrons are also shown here. From this table, most lanthanoid elements have nf^{m-2} $(n+2)s^2$ electronic configuration at ground state ($n = 4$, $m = Z - 54$, where Z is the atomic number) with some exceptions; La ($5d6s^2$), Ce ($4f^15d6s^2$), Gd ($4f^75d6s^2$), Lu ($4f^{14}5d6s^2$). In the actinoids, most elements has similar electronic configuration to that of the lanthanoid elements in the same column. On the other hand, one can find that the valence electrons of Pa, U, and Np also occupy the 6d orbital in spite of the same number of them with Pr, Nd, and Pm, respectively. Such an aspect is also observed in the difference between the electronic configurations of Ce ($4f^15d6s^2$) and Th ($6d^27s^2$). These facts imply that the energy difference between the 5f and 6d orbitals is smaller than that between 4f and 5d ones. Thus, the 5f orbitals are not shielded by outer shells as largely as the 4f orbitals. Actually, it is known that the 5f orbitals can participate to the bonding with other elements.

As a result of the weakly shielded 5f orbital, the lighter actinoid elements from Pa to Am can exist at pentavalent or higher oxidation states. The electronic configurations of these species are summarized in Table 1.1. In aqueous solution, the actinoid elements in such high oxidation states (V, VI, and VII) is hydrolyzed, and consequently, forms an actinyl ion (AnO_2^{n+}; $n = 1, 2, 3$) as follows.[1)]

$$An^{(n+4)} + 2H_2O \longrightarrow AnO_2^{n+} + 4H^+ \tag{1.1}$$

As can be seen from Eq. 1.1, the actinoid elements in the high oxidation states act as strong acids in water. The actinyl ions of Pa, U, Np, Pu, and Am are named with suffix “-yl” instead of “-ium”, *i.e.*, protoactinyl, uranyl, neptunyl, plutonyl, and americyl, respectively. Essentially, the actinyl ions have linear O=An=O structure. Thus, the bare actinyl ions belong to

Table 1.1. Electronic configuration of actinoid elements at various oxidation states

An	III	IV	V	VI	VII
$_{91}$Pa	[Rn]$5f^2$	[Rn]$5f^1$	**[Rn]**	–	–
$_{92}$U	[Rn]$5f^3$	[Rn]$5f^2$	[Rn]$5f^1$	**[Rn]**	–
$_{93}$Np	[Rn]$5f^4$	[Rn]$5f^3$	**[Rn]$5f^2$**	[Rn]$5f^1$	[Rn]
$_{94}$Pu	[Rn]$5f^5$	**[Rn]$5f^4$**	[Rn]$5f^3$	[Rn]$5f^2$	[Rn]$5f^1$
$_{95}$Am	**[Rn]$5f^6$**	[Rn]$5f^5$	[Rn]$5f^4$	[Rn]$5f^3$	–

* [Rn]: closed electronic configuration of radon.

[Rn] = $1s^22s^22p^63s^23p^63d^{10}4s^24p^64d^{10}4f^{14}5s^25p^65d^{10}6s^26p^6$.

** **Bold**: most stable oxidation state.

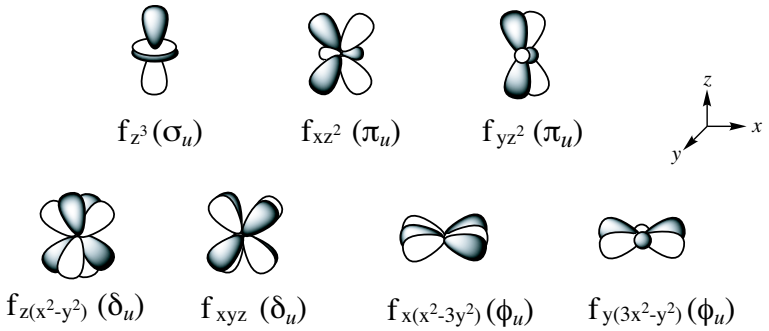

Figure 1.1. Schematic shapes of real function of f orbitals.

$D_{\infty h}$ point group. The linearity of actinyl ions is considered to be due to a contribution of the 5f orbitals. The schematic shapes of real functions of f orbitals are shown in Figure 1.1. The axial oxygen atoms in the actinyl ions have a total of six possible linear combinations of their 2p orbitals (σ_u, σ_g, $2 \times \pi_u$, and $2 \times \pi_g$). All of the atomic orbital combinations allowed by symmetry with either 5f or 6d orbitals in the actinoids are shown in Figure 1.2.[2)] It should be noted that the ungerade (u) symmetry combinations (σ_u, $2 \times \pi_u$) in Figure 1.2 are not possible in use of any d orbitals. For example, the axial oxygen atoms in the uranyl compounds adopt a *trans*- (linear) configuration, while the structures of VO_2^+ (vanadyl ion) and MoO_2^{2+} (molybdenyl ion) have *cis*- (bent) geometry.[3)]

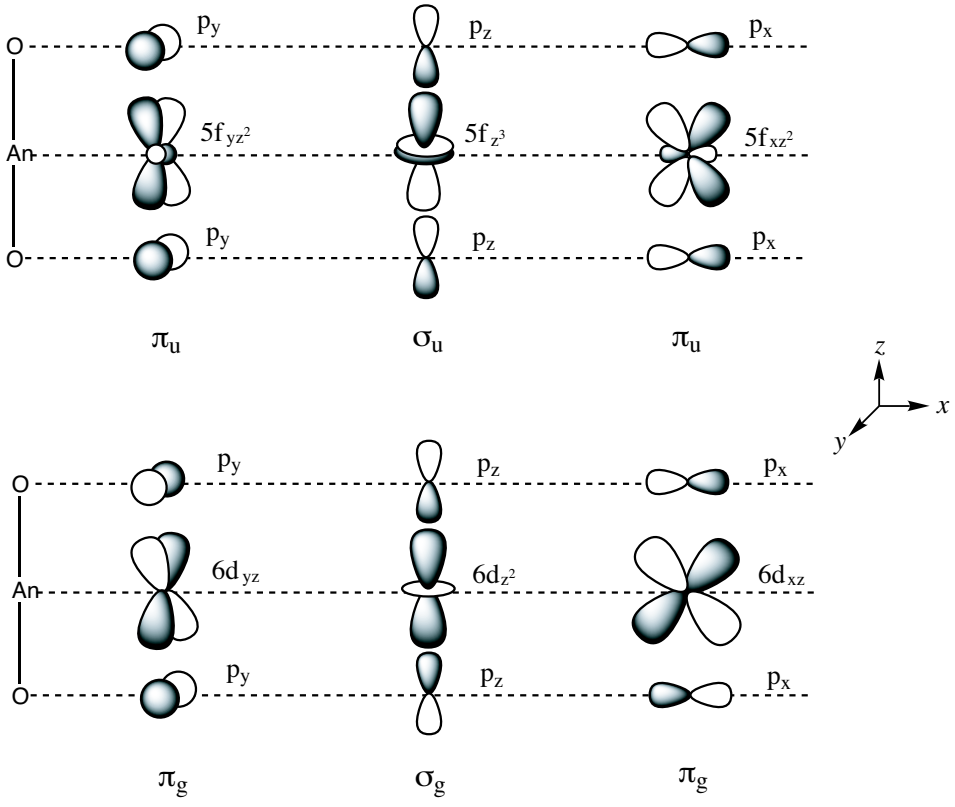

Figure 1.2. Scheme of symmetry allowed combinations of atomic orbitals in actinyl ions.

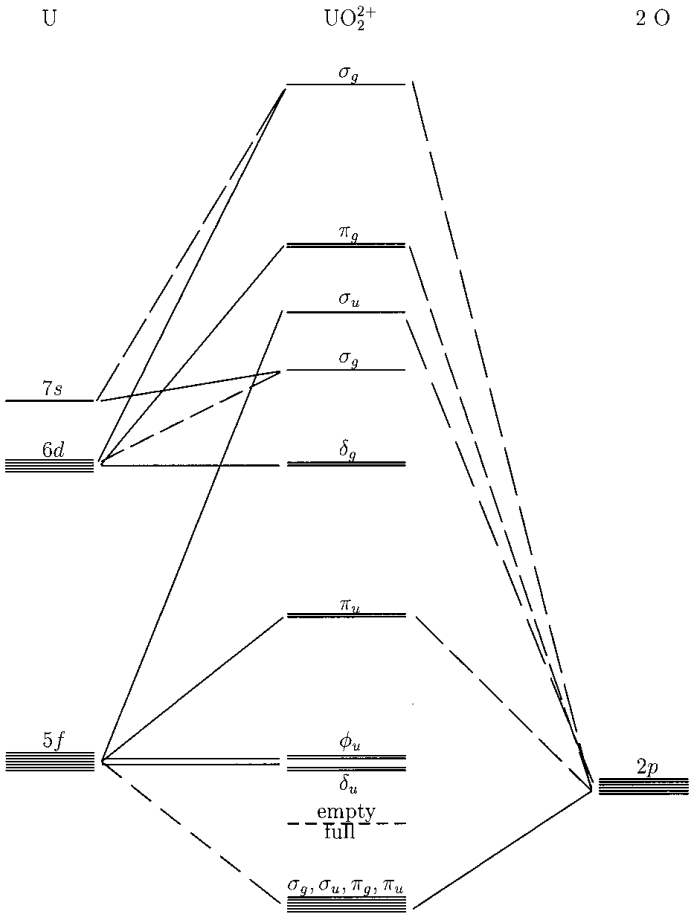

Figure 1.3. MO diagram of bare $U^{VI}O_2^{2+}$ by Matsika *et al.*[4)]

Because of the participation into the bonding between the axial oxygen and center uranium, it can be predicted that the 5fσ_u, 5fπ_u, 6dσ_g, and 6dπ_g orbitals have anti-bonding characters. Figure 1.3 shows the molecular orbital diagram calculated by Matsika *et al.*[4)] As predicted, the 5fσ_u, 5fπ_u, 6dσ_g, and 6dπ_g orbitals become the anti-bonding MO, while the 5fδ_u, 5fϕ_u, and 6dδ_g orbitals which are not participated in the formation of the actinyl ion remain as non-bonding orbitals.

X-ray diffraction studies of a number of crystalline uranium(VI) salts have experimentally demonstrated the existence of uranyl(VI) ion in solid state. They were summarized by King.[5)] In $UO_2Cl_2(OPPh_3)_2$, $[UO_2(O_2C_2H_4CO_2)\cdot H_2O]$, and $UO_2(NO_3)_2(OPPh_3)_2$, it was found that a linear O–U–O group existed. Furthermore, it was clarified that each uranium atom in $BaUO_4$, α-$SrUO_4$, β-$SrUO_4$, $MgUO_4$, $PbUO_4$, $CuUO_4$, Li_2UO_4, α-Na_2UO_4, β-Na_2UO_4, $CaUO_4$, UO_3, U_3O_8, and so on is surrounded by oxygen atoms; four or six of such oxygen atoms (O(II)) lie in a plane with the uranium atom all at a distance longer than the remaining two oxygens (O(I)), which lie above and below the uranium atom on a straight line perpendicular to the plane of the O(II) oxygen atoms. In $CaUO_4$, the U–O(II) distance is 2.30 Å, while the U–O(I) distance is 1.96 Å. It seems likely that the U–O(II) bonds are principally of ionic character, and crystals of $CaUO_4$ are composed of Ca^{2+}, $U^{VI}O_2^{2+}$, and

O^{2-} ions. Further, UO_3 can readily dissolve in an acidic aqueous solution according to the following reaction.

$$UO_3(s) + 2HA(aq) \longrightarrow UO_2^{2+} + 2A^- + H_2O \tag{1.2}$$

where HA and A^- are the arbitrary acid and its conjugate base (*e.g.*, A = Cl, NO_3 and so on), respectively. This phenomenon indicates the existence of the uranyl(VI) moiety in UO_3. Crandall has studied the formula of uranyl ion in solution by using ^{18}O-enriched water as a tracer in the exchange reaction of oxygen atoms coordinated to uranium.[6] As a result, it has been showed that the uranyl ion exists as $U^{VI}O_2^{2+}$ even in diluted hydrochloric acid solution. Nowadays, it is well accepted that the actinyl ions has the linear $[O{=}An{=}O]^{n+}$ structure in both solid and solution states.

1.2 Uranyl(VI), the Most Popular Actinyl Ion

The most well-known actinyl ion is the uranyl(VI), $U^{VI}O_2^{2+}$, which has the radon-like closed shell electronic configuration, $[Rn]5f^0$. The hexavalent state is the most stable oxidation state of uranium. Thus, a large number of studies on uranyl(VI) have been reported.

The uranyl(VI) ion also has characteristic linear structure as described above. The U=O distance (R_{UO}) in the uranyl(VI) ion has been measured for a large number of compounds. The values is ranging from 1.5 Å (uranyl–8-hydroxyquinolinate) to 2.08 Å (α-UO_3), and the average is 1.77 Å. Since bare uranyl(VI) ion belongs to $D_{\infty h}$ point group, the O=U=O symmetric stretching (ν_1) is Raman-active, while the asymmetric stretching (ν_3) is IR-active. The ν_1 and ν_3 peaks of the uranyl(VI) ion generally appear in the ranges of 800–880 cm^{-1} and 900–960 cm^{-1}, respectively.[7] The force constants of the U=O bond (F_{UO}) range from 2.60 mdyne·$Å^{-1}$ (α-UO_3) to 10.8 mdyne·$Å^{-1}$ ($UO_2Br_4^{2-}$). The average values are in the range of 6.0–7.3 mdyne·$Å^{-1}$. There seems to be a relationship between R_{UO} and F_{UO}. Actually, Jones[8] has rationalized R_{UO} with F_{UO} by using Badger's law[9] as follows.

$$R_{UO} = \beta F_{UO}^{-\frac{1}{3}} + d_{UO} \tag{1.3}$$

In Eq. 1.3, β is about 1.08 for all pairs of elements if one element has atomic number greater than 18, and d_{UO} is intrinsic value for each uranyl(VI) compound. McGlynn *et al.*[10] have corrected Eq. 1.3 to explain their results systematically obtained as follows.

$$R_{UO} = 1.993 F_{UO}^{-\frac{1}{3}} + 0.666 \tag{1.4}$$

Furthermore, Veal *et al.*[11] has expressed R_{UO} with the ν_3 frequency in cm^{-1} (Eq. 1.5).

$$R_{UO} = 81.2 \nu_3^{-\frac{2}{3}} + 0.895 \tag{1.5}$$

These empirical relationships between R_{UO} and F_{UO} or ν_3 are standing on the systematic investigations for vibrational spectra of widely various uranyl(VI) compounds.

The uranyl(VI) ion can play a role as an acid in aqueous solution even after the formation of $U^{VI}O_2^{2+}$ in Eq. 1.1 as follows.

$$m U^{VI}O_2^{2+} + n H_2O \rightleftarrows (U^{VI}O_2)_m(OH)_n^{2m-n} + n H^+ \tag{1.6}$$

In fact, uranyl(VI) salts are distinctly acid in the aqueous solution and it has also been known that large amounts of UO_3 can be dissolved in aqueous solutions of uranyl(VI) salts. The

Table 1.2. Equilibrium constants ($K^{\circ}_{\mathrm{hydro}}$) for the hydrolysis of uranyl(VI) ion at 298.15 K, 0.1 MPa, and zero ionic strength[12, 13)]

Reaction	$\log K^{\circ}_{\mathrm{hydro}}$ [a]
$U^{VI}O_2^{2+} + H_2O \rightleftarrows U^{VI}O_2(OH)^{+} + H^{+}$	-5.250 ± 0.240
$U^{VI}O_2^{2+} + 2H_2O \rightleftarrows U^{VI}O_2(OH)_2 + 2H^{+}$	-12.150 ± 0.070
$U^{VI}O_2^{2+} + 3H_2O \rightleftarrows U^{VI}O_2(OH)_3^{-} + 3H^{+}$	-20.250 ± 0.420
$U^{VI}O_2^{2+} + 4H_2O \rightleftarrows U^{VI}O_2(OH)_4^{2-} + 4H^{+}$	-32.400 ± 0.680
$2U^{VI}O_2^{2+} + H_2O \rightleftarrows (U^{VI}O_2)_2(OH)^{3+} + H^{+}$	-2.700 ± 1.000
$2U^{VI}O_2^{2+} + 2H_2O \rightleftarrows (U^{VI}O_2)_2(OH)_2^{2+} + 2H^{+}$	-5.620 ± 0.040
$3U^{VI}O_2^{2+} + 4H_2O \rightleftarrows (U^{VI}O_2)_3(OH)_4^{2+} + 4H^{+}$	-11.900 ± 0.300
$3U^{VI}O_2^{2+} + 5H_2O \rightleftarrows (U^{VI}O_2)_3(OH)_5^{+} + 5H^{+}$	-15.500 ± 0.120
$3U^{VI}O_2^{2+} + 7H_2O \rightleftarrows (U^{VI}O_2)_3(OH)_7^{-} + 7H^{+}$	-32.200 ± 0.800
$4U^{VI}O_2^{2+} + 7H_2O \rightleftarrows (U^{VI}O_2)_4(OH)_7^{+} + 7H^{+}$	-21.900 ± 1.000

[a] Logarithmic equilibrium constant of the hydrolysis of uranyl(VI) ion at 298.15 K, 0.1 MPa, and zero ionic strength.

hydrolytic reactions of uranyl(VI) have been exhaustively studied. Grenthe *et al*. have summarized a series of the equilibrium constants of the hydrolysis of the uranyl(VI) ion as shown in Table 1.2.[12, 13)] In this table, the largest value of $\log K^{\circ}_{\mathrm{hydro}}$ is -2.700 ± 1.000 of the reaction: $2U^{VI}O_2^{2+} + H_2O \rightleftarrows (UO_2)_2(OH)^{3+} + H^{+}$. This data suggests that the hydrolysis of the uranyl(VI) ion will start from pH 3–4.

A very large number of inorganic and organic anions and electron donating neutral molecules coordinate to the uranyl(VI) ion by strong (probably covalent) bonds to form uranyl(VI) complexes. Normally, such ligands are positioned in the equatorial plane of the uranyl(VI) ion. The number of coordination sites in the equatorial plane of the uranyl(VI) ion varies from 3 to 6 as shown in Figure 1.4. In these geometries, the pentagonal and hexagonal bipyramidal ones are most popular. The simplest uranyl(VI) complex is its hydrated perchlorate salt; $U^{VI}O_2(ClO_4)_2{\cdot}nH_2O$. The crystal structures of $U^{VI}O_2(ClO_4)_2{\cdot}nH_2O$ ($n = 5, 7$) were analyzed by Alcock *et al.*[14)] and refined by Fischer.[15)] In their reports, the linear uranyl(VI) ion was surrounded by 5 water molecules, *i.e.*, the geometry of this uranyl(VI)aqua complex is pentagonal bipyramidal. Interestingly, Fischer has also found that the perchlorate anion (ClO_4^{-}), which is generally known to have little coordination ability to metal ions, can also interact with the uranyl(VI) ion. The resulting pentagonal bipyramidal complex is $U^{VI}O_2(ClO_4)_2(H_2O)_3$. The uranyl(VI) ion can also form its complex with various chelating ligands. The typical ligands for uranyl(VI) are, for example, β-diketonates,[16–22)] Schiff bases,[23–39)] phthalocyanines,[40, 41)] macrocycles,[42–49)] and so on.

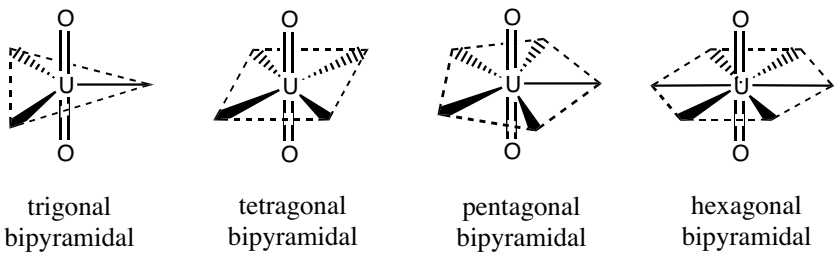

Figure 1.4. Schematic geometries of uranyl(VI) complexes.

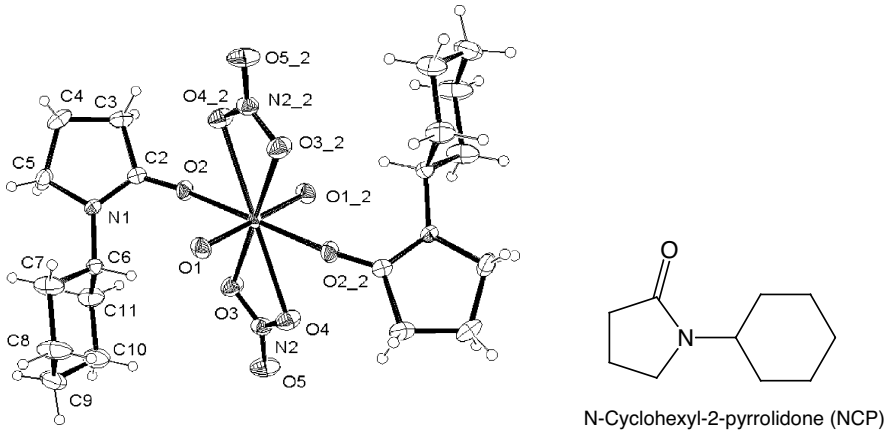

Figure 1.5. Structure of $U^{VI}O_2(NO_3)_2(NCP)_2$ (NCP = *N*-cyclohexyl-2-pyrrolidone) drawn as thermal ellipsoid plot at 40% probability level reported by Varga *et al.*[58)]

Traditionally, a series of the uranyl(VI) nitrates have been studied in detail, because this species is quite important in the nuclear engineering, especially in the purification of uranium to prepare the nuclear fuel and to reprocess the spent fuel from the power plant. The comprehensive review in such an engineering field was published previously.[50)] In this field, the uranium species is normally purified by using the solvent extraction in the hydrocarbon/HNO_3 aq. biphasic system from the crude materials, and the most popular extractant is tri-*n*-butylphosphate (TBP), which works as shown in Eq. 1.7.

$$U^{VI}O_2^{2+}(aq) + 2NO_3^-(aq) + 2TBP(aq) \rightleftarrows U^{VI}O_2(NO_3)_2(TBP)_2(org) \qquad (1.7)$$

More chemically detailed review was written by Casellato *et al.*[51)] The authors' focus was especially in the molecular structures and vibrations of the actinide nitrates. According to them and the references in this review, the nitrate anion (NO_3^-) generally coordinates to the uranyl(VI) ion as a bidentate ligand, resulting the hexagonal bipyramidal uranyl(VI) nitrate complexes as shown in Figure 1.4. When two NO_3^- coordinate to the uranyl(VI) ion, this uranyl(VI) nitrate complex has more two unidentate ligands *e.g.*, H_2O, ($U^{VI}O_2(NO_3)_2(H_2O)_2$) at *trans*-position in the hexagonal equatorial plane. From some structural characterizations for $U^{VI}O_2(NO_3)_2L_2$ (L = tri-*n*-butylphosphine oxide, di-*n*-butylphosphate, trimethylphosphate, triisobutylphosphate),[52–55)] the resulting $U^{VI}O_2(NO_3)_2(TBP)_2$ in Eq. 1.7 is also considered to have such a *trans*-geometry. Auwer *et al.* have studied the coordination sphere in various U, Np, and Pu nitrates in HNO_3 aqueous solution containing TBP with X-ray absorption spectroscopy, in which the oxidation states of these actinoid elements were VI for U, Np, and Pu and IV for Np and Pu.[56)] In their analyses for the X-ray absorption spectra, each actinyl(VI) ion coordinates two NO_3^- and two TBP molecules. Recently, Varga *et al.* have found the new unidentate ligand for the uranyl(VI) nitrate, *N*-cyclohexyl-2-pyrrolidone (NCP), which functions as a selective precipitant for the uranyl(VI) ion from its nitric acid aqueous solution.[57,58)] The molecular structure of $U^{VI}O_2(NO_3)_2(NCP)_2$ determined by the X-ray crystallography is shown in Figure 1.5. The selectivity of NCP and its derivatives to the uranyl(VI) ion rather than other metal ions and their capabilities as precipitants in the reprocessing process have been confirmed by Koshino *et al.*[59)]

One of the environmentally important uranyl(VI) complex is the carbonate, because of the sufficiently high concentration of CO_3^{2-} in natural environment and the large stability

of this complex. The equilibrium constants for the formation of the uranyl(VI) carbonate complexes at 298.15 K, 0.1 MPa, and zero ionic strength are shown below.[13)]

$$U^{VI}O_2^{2+} + CO_3^{2-} \overset{K_1}{\rightleftarrows} U^{VI}O_2(CO_3)(aq) \qquad (1.8)$$
$$\log K_1^\circ = 9.940 \pm 0.030$$

$$U^{VI}O_2^{2+} + 2CO_3^{2-} \overset{\beta_2}{\rightleftarrows} U^{VI}O_2(CO_3)_2^{2-} \qquad (1.9)$$
$$\log \beta_2^\circ = 16.610 \pm 0.090$$

$$U^{VI}O_2^{2+} + 3CO_3^{2-} \overset{\beta_3}{\rightleftarrows} U^{VI}O_2(CO_3)_3^{4-} \qquad (1.10)$$
$$\log \beta_3^\circ = 21.840 \pm 0.040$$

From these data, the third stepwise formation constant of $U^{VI}O_2(CO_3)_2^{2-} + CO_3^{2-} \rightleftarrows [U^{VI}O_2(CO_3)_3]^{4-}$ is calculated as $\log K_3^\circ = 5.230 \pm 0.037$. This $\log K_3^\circ$ value indicates that the major species of the uranyl(VI) carbonate under a condition with a presence of sufficient amount of CO_3^{2-} is $[U^{VI}O_2(CO_3)_3]^{4-}$. An ORTEP view of $K_4[U^{VI}O_2(CO_3)_3]$ reported by Brittain *et al.*[60)] is shown in Figure 1.6. The uranium atom in $[U^{VI}O_2(CO_3)_3]^{4-}$ is surrounded by the hexagonal bipyramidal coordination environment. In Figure 1.6, the R_{UO} value is 1.80 Å close to its average and U–O(1), U–O(2), and U–O(3) distances in its equatorial plane is 2.43 Å. To neutralize the highly negative charge of $[U^{VI}O_2(CO_3)_3]^{4-}$, the counter cations are located in interconnected vacancies between the coordinated CO_3^{2-}, and as a result, forming continuous chains. Such a phenomenon is also confirmed in the crystal structures of $Na_2Ca[U^{VI}O_2(CO_3)_3]\cdot xH_2O$ by Coda *et al.*[61)], $Cs_4[U^{VI}O_2(CO_3)_3]$ by Mereiter.[62)] Differing from most other heavy metal carbonates, sodium salt of $[U^{VI}O_2(CO_3)_3]^{4-}$ is water-soluble. Therefore, the sodium salt of $[U^{VI}O_2(CO_3)_3]^{4-}$ is important for the separation of the uranium from ores.

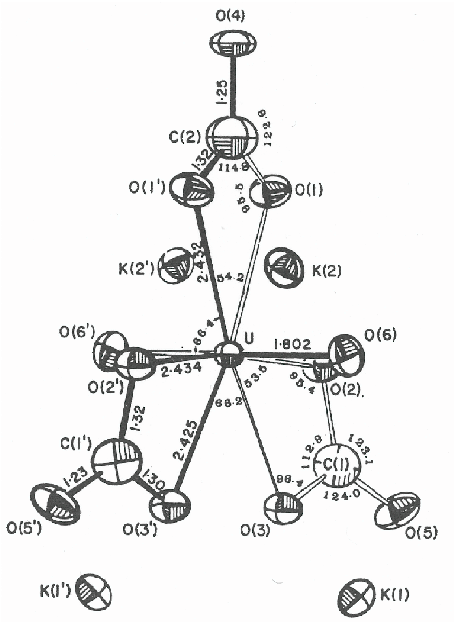

Figure 1.6. ORTEP view of $K_4U^{VI}O_2(CO_3)_3$ reported by Brittain *et al.*[60)]

Generally, the axial oxygen of the uranyl(VI) ion is quite inert in acidic aqueous media unless irradiated by UV light.[6,63] Gordon and Taube proposed that the exchange reaction between the oxygen atoms of the uranyl(VI) ion and water in 1 M (= mol·dm^{-3}) perchloric acid solution is catalyzed by the uranyl(V) ion ($U^{V}O_2^+$) generated by UV irradiation as follows.

$$UO_2^{2+} + e^- \xrightarrow{h\nu} UO_2^+ \tag{1.11}$$

$$UO_2^+ + H_2O^* \longrightarrow UO_2^{*+} + H_2O \tag{1.12}$$

$$UO_2^{*+} + UO_2^{2+} \longrightarrow UO_2^+ + UO_2^{*2+} \tag{1.13}$$

where O^* denotes the isotope labeled oxygen atom. The half-life for the axial oxygen in the uranyl(VI) ion in 1 M $HClO_4$ aq. was estimated as 40 000 h. On the other hand, Clark *et al.* has found that the axial oxygen in the uranyl(VI) ion can easily exchange with the water oxygen in 3.5 M tetramethylammonium hydroxide.[64] In such a medium, the major uranyl(VI) species is $U^{VI}O_2(OH)_n^{(2-n)}$ ($n = 4, 5$). They analyzed the ^{17}O NMR spectra of this sample solution at different temperatures by using NMR line-broadening method,[65] and obtained the activation enthalpy ($\Delta H^{\ddagger}$), entropy ($\Delta S^{\ddagger}$), and the apparent first-order rate constant (k_{ex}) of the oxygen exchange reaction in this basic medium as $\Delta H^{\ddagger} = 41 \pm 1$ kJ·mol^{-1}, $\Delta S^{\ddagger} = -75 \pm 17$ J·mol^{-1}·K^{-1}, and $k_{ex} = 18 \pm 6$ s^{-1} at 283 K. For the significant acceleration of the oxygen exchange between the uranyl(VI) ion and water in the basic aqueous media, Clark *et al.* have proposed two mechanisms; (1) direct mechanism in which the proton in the coordinated OH^- transfers to the axial oxygen, (2) water assisted mechanism in which one of the protons in the water molecule binding to the coordinated OH^- through a hydrogen bond transfers to the axial oxygen. In nonaqueous solvents, the axial oxygen is generally considered to be stable, because the ν_3 peak due to the uranyl(VI) moiety can be observed even in the IR spectrum of such a system.

On the other hand, the exchange reaction of the equatorial ligands of the uranyl(VI) complexes may occur more readily than that of the axial oxygen atoms. To investigate such an exchange reaction in the uranyl(VI) complexes, the NMR spectroscopy has been used frequently.[66–82] Fratiello *et al.* have estimated lifetimes of the water molecule coordinating to the uranyl(VI) ion in water–acetone and water–dimethyl sulfoxide–acetone mixtures as *ca.* 5×10^{-3} s.[66,67] Ikeda *et al.*[68] also studied the H_2O exchange reaction in the uranyl(VI) aqua complex in mixtures of water, acetone, and/or DMSO (dimethyl sulfoxide), and obtained the first-order rate constant ($k_{H_2O} = 9.80 \times 10^5$ s^{-1} at 298 K)[1] and activation parameters ($\Delta H^{\ddagger} = 41.4 \pm 2.1$ kJ·mol^{-1}, $\Delta S^{\ddagger} = 8 \pm 11$ J·mol^{-1}K^{-1}). In the reports by Fratiello *et al.*,[66,67] the hydration number in the uranyl(VI) aqua complex has been evaluated as 4 from the peak area in the ^1H NMR spectra. In these literatures, the authors mentioned "The addition of acetone procudes a reduction of the dielectric constant of the medium, eventually to that of acetone, about 20 at 25°C, at high concentrations of this component. Even though the ^1H NMR measurements are made at −85 to −100°C, the bulk dielectric constant should still be only about 35, a much lower value than that of pure water. Thus, if inner-shell complex formation is induced in solution, a decrease in the cation hydration number should be noted." Actually, the hydration number in the crystal structure of the perchlorate salt was determined as 5, *i.e.*, $U^{VI}O_2(H_2O)_5^{2+}$.[14,15] Bardin *et al.* have also estimated the hydration number surrounding the uranyl(VI) ion in the H_2O/acetone mixture as 5 from the ^1H NMR spectrum.[75] They considered that such a difference between the hydration numbers estimated from the NMR

[1] This rate constant was calculated for $U^{VI}O_2(H_2O)_4^{2+}$ by Ikeda *et al.*[68]

peak area should be caused by the accuracy of the measurements, *i.e.*, the higher magnetic field instruments (300 and 400 MHz) used by Bardin *et al.* would produce more accurate result than the previous ones[66–68] (maximum 200 MHz). The first-order rate constant at 298 K and activation parameters in the exchange reaction of water molecule in $U^{VI}O_2(H_2O)_5^{2+}$ evaluated by Bardin *et al.* fluctuated as $k_{H_2O} = 10^4 \sim 10^5$ s^{-1}, $\Delta H^{\ddagger} \approx 30$ kJ·mol^{-1}, and $\Delta S^{\ddagger} \approx 19$ or 800 J·mol^{-1}K^{-1}.[75] Farkas *et al.* further investigated the H_2O exchange reaction in $U^{VI}O_2(H_2O)_5^{2+}$ from ^{17}O NMR spectra measured by the 500 and 800 MHz instruments, and obtained the first-order rate constant ($k_{H_2O} = (1.30 \pm 0.05) \times 10^6$ s^{-1} at 298 K) and the activation parameters ($\Delta H^{\ddagger} = 26.1 \pm 1.4$ kJ·mol^{-1}, $\Delta S^{\ddagger} = -40 \pm 5$ J·mol^{-1}K^{-1}).[76] Additionally, they also performed the quantum chemical calculation for the uranyl(VI) aqua complexes and combined the experimental and theoretical results. Recently, Vallet *et al.* estimated the energies of the activation and the intermediate in the water exchange reaction of $U^{VI}O_2(H_2O)_5^{2+}$ by using the quantum chemical calculation.[83] Their results suggested that such a reaction in $U^{VI}O_2(H_2O)_5^{2+}$ proceeds through the associative mechanism in which the additional ligand (water) will bind to $U^{VI}O_2(H_2O)_5^{2+}$ in the intermediate.

Tóth *et al.* have studied the CO_3^{2-} exchange reaction in $[U^{VI}O_2(CO_3)_3]^{4-}$ by using ^{13}C NMR spectroscopy.[71] According to their result, the CO_3^{2-} exchange reaction in $[U^{VI}O_2(CO_3)_3]^{4-}$ occurs *via* the dissociative mechanism in which the coordination number of the ligand will decrease in the intermediate, that is, the intermediate should be $[U^{VI}O_2(CO_3)_2]^{2-}$ as follows.

$$[U^{VI}O_2(CO_3)_3]^{4-} \underset{k_{-1}}{\overset{k_1}{\rightleftharpoons}} [U^{VI}O_2(CO_3)_2]^{2-} + CO_3^{2-} \tag{1.14}$$

The estimated values of $\Delta H^{\ddagger}$, $\Delta S^{\ddagger}$, and k_1 of Eq. 1.14 were 82±11 kJ·mol^{-1}, 50±30 J·mol^{-1}·K^{-1}, and 13 ± 3 s^{-1}, respectively. The k_{-1} value was derived from the relationship, $k_{-1} = K_3 k_1$, resulting $k_{-1} \simeq 10^7$ M^{-1}·s^{-1} In the further investigation by Tóth *et al.*,[72] it was found that there is the second path involving H^+ other than Eq. 1.14. The proton-catalyzed CO_3^{2-} dissociation from $[U^{VI}O_2(CO_3)_3]^{4-}$ was proposed for an alternative path.

The exchange reactions of unidentate ligands (L) in the uranyl(VI) complexes, $U^{VI}O_2(L)_5^{2+}$ and $U^{VI}O_2(\beta$-diketonato$)_2$L (L = *N*,*N*-dimethylformamide, *N*,*N*-dimethylacetoamide, *N*,*N*-diethylformamide, trimethyl phosphate, triethyl phosphate, dimethyl sulfoxide, tetrahydrofuran; β-diketonato = acetylacetonato, 1,1,1-trifluoroacetylacetonato, 1,1,1,5,5,5-hexafluoroacetylacetonato) in nonaqueous solvents have also been investigated and discussed the details concerning the rate constants and mechanisms.[69, 70, 78–82]

For the properties of the actinyl ions and related species, many kinds of studies, not only experimental, but also theoretical and computational, have been reported.[3, 4, 10, 84–116] According to Denning *et al.*[3] and Matsika *et al.*[4], the ground state of the uranyl(VI) ion is,

$$(1\pi_u)^4(1\pi_g)^4(1\sigma_g^+)^2(1\sigma_u^+)^2;\ {}^1\Sigma_g^+ \tag{1.15}$$

In this configuration of the uranyl(VI) ion at the ground state, it is unusual that the energy levels of the occupied σ MOs are higher than those of the occupied π MOs. This phenomenon has been explained by anti-bonding overlap between the σ-oriented oxygen $2p_z$ orbitals and the toroidal lobes of the uranium $6d_{z^2}$ and $5f_{z^3}$ orbitals.[3]

Essentially, uranyl(VI) compounds have intense yellow color. This is considered to be due to the following electronic excitation in the uranyl(VI) ion.

$$(1\pi_u)^4(1\pi_g)^4(1\sigma_g^+)^2(1\sigma_u^+)^2;\ {}^1\Sigma_g^+ \longrightarrow (1\pi_u)^4(1\pi_g)^4(1\sigma_g^+)^2(1\sigma_u^+)^1(\phi_u, \delta_u)^1;\ {}^1\Phi_g \text{ or } {}^1\Delta_g \tag{1.16}$$

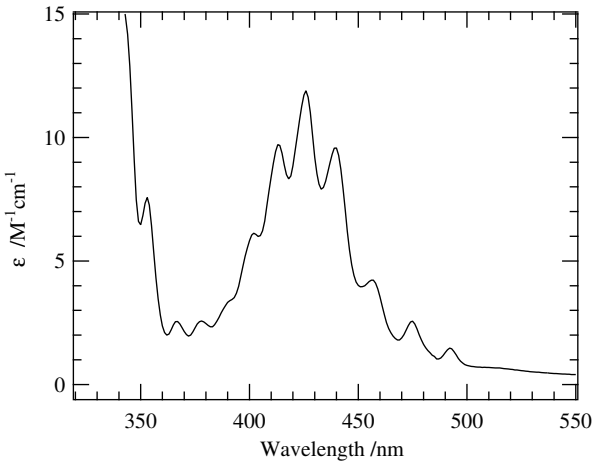

Figure 1.7. UV-visible absorption spectrum of uranyl(VI) perchlorate in 1-butyl-3-methylimidazolium nonafluorobutanesulfonate ionic liquid at room-temperature.[117)]

This transition is classified into the ligand-to-metal charge transfer (LMCT) from the 2p orbitals in the axial oxygen atom to the 5fδ_u and/or ϕ_u orbitals in the center uranium. The typical absorption spectrum of the uranyl(VI) ion is shown in Figure 1.7.[117)] As can be seen from this spectrum, the absorption bands due to such LMCT in the uranyl(VI) ion appear at 350∼500 nm with vibronic structures. The excited states (configuration) in this transition are predicted as $^1\Phi_g$ ($\sigma_u\phi_u$) or $^1\Delta_g$ ($\sigma_u\delta_u$). These LMCT transitions, $^1\Sigma_g^+ \rightarrow {}^1\Phi_g$ and $^1\Sigma_g^+ \rightarrow {}^1\Delta_g$ are spin-allowed, but forbidden because of the transitions between the energy states with same parity ($g \rightarrow g$, g: gerade). Therefore, the molar absorptivity (ϵ; $\mathrm{M^{-1}{\cdot}cm^{-1}}$) of the LMCT absorption bands is low (0.3∼20 $\mathrm{M^{-1}{\cdot}cm^{-1}}$) and their intensities should be borrowed from the vibrinic coupling. Görller-Walrand and Vanquickenborne discussed which coupling scheme is suitable to describe the spin-orbit effect in the uranyl(VI) ion. In their conclusion, a molecular Russell-Saunders ((Λ, S)) coupling scheme is most appropriate, and other schemes ((ω, ω) and intermediate) cannot rationalize the energy splittings and the spectral intensities. Görller-Walrand *et al.*[95,96)] and McGlynn *et al.*[84)] reported that a large number of the uranyl(VI) complexes with widely different ligands, coordination numbers, and symmetries exhibits remarkably similar LMCT absorption bands, and concluded that the perturbation order in the uranyl(VI) compounds is,

$$V_{\mathrm{ax}} \gg e^2/r_{ij} \geq H_{\mathrm{SO}} > V_{\mathrm{eq}} \tag{1.17}$$

where V_{ax}, e^2/r_{ij}, H_{SO}, and V_{eq} are the axial ligand field potential, the electrostatic potential, the spin-orbit hamiltonian, and the equatorial ligand field potential, respectively.

Today, comprehensive reviews for the physical and chemical properties of various uranyl(VI) compounds are available, for example, "*The Chemistry of the Actinide Elements*" by Katz *et al.*[1)] and "*Chemical Thermodynamics of Uranium*" by Grenthe *et al.*[12)] These reviews are summarizing not only for uranyl(VI), however even limiting in the uranyl(VI) species, their ranges are quite vast.

1.3 Actinyl Ions with $5f^1$ Configuration

Uranyl(VI), which is the most popular actinyl ion as described above, has no unpaired electron in its 5f orbital. Therefore, in the study on the uranyl(VI) species, it is not possible to observe the properties caused by the 5f electron directly. In the actinyl ions, uranyl(V) ($U^{V}O_2^+$), neptunyl(VI) ($Np^{VI}O_2^{2+}$), and plutonyl(VII) ($Pu^{VII}O_2^{3+}$) have [Rn]$5f^1$ configuration, which is the simplest electronic configuration in $5f^n$ system. Thus, these species are most essential for the systematic interpretation for the properties of whole actinyl species with $5f^n$ configuration. From Figures 1.1 and 1.2, the 5f orbitals being free from the interaction with the 2p orbitals in the axial oxygen atoms are $5f\phi_u$ and $5f\delta_u$. Hence, the unpaired electron in the *bare* actinyl ions with the $5f^1$ configuration should be located in one of these non-bonding 5f orbitals, *i.e.*, its predicted ground state is,

$$(1\pi_u)^4(1\pi_g)^4(1\sigma_g^+)^2(1\sigma_u^+)^2(\delta_u)^1;\,^2\Delta_u \tag{1.18}$$

$$(1\pi_u)^4(1\pi_g)^4(1\sigma_g^+)^2(1\sigma_u^+)^2(\phi_u)^1;\,^2\Phi_u \tag{1.19}$$

It may be expected that the $5f\delta_u$ orbital is positioned lower in energy than $5f\phi_u$, because the former (δ: $\lambda = 2$) has the lower angular momentum around the z axis than latter (ϕ: $\lambda = 3$). In fact, according to the quantum chemical calculation by Matsika *et al.*,[4] the $5f\delta_u$ orbital is located at slightly lower energy level than $5f\phi_u$ as shown in Figure 1.3. However, their positions may invert with the equatorial ligand field and/or the spin-orbit coupling. Actually, the electronic configuration of a neptunyl(VI) compounds, $NaNp^{VI}O_2(CH_3COO)_3$ and $RbNp^{VI}O_2(NO_3)_3$, was determined as $^2\Phi_{5/2u}$ (Eq. 1.19) by experimental values of their magnetic susceptibilities.[89]

1.3.1 Uranyl(V) ion; $U^{V}O_2^+$

The pentavalent state is the most unstable oxidation state of uranium in solution.[1] In order to observe the uranyl(V) species, electrochemical and photochemical reduction of uranyl(VI) to uranyl(V) were attempted by many researchers.[118–153] However, the uranyl(V) species are generally unstable in acidic aqueous system, because of the disproportionation (Eq. 1.20).[120–124]

$$2U^{V}O_2^+ + 4H^+ \rightleftarrows U^{4+} + U^{VI}O_2^{2+} + 2H_2O \tag{1.20}$$

The following mechanism has been suggested for Eq. 1.20.

$$U^{V}O_2^+ + H^+ \longrightarrow UOOH^{2+} \tag{1.21}$$

$$U^{V}O_2^+ + UOOH^{2+} \longrightarrow U^{VI}O_2^{2+} + UOOH^+ \tag{1.22}$$

$$UOOH^+ \longrightarrow \text{stable U(IV)} \tag{1.23}$$

The rate-determining step is considered to be Eq. 1.22. The logarithmic equilibrium constant of Eq. 1.20 has been evaluated as 6.23 ± 0.08[154] and 6.07 ± 0.06,[12] which are quite larger than that of the corresponding disproportionation of neptunyl(V), -6.40 in 1 M $HClO_4$ and -1.62 in 1 M H_2SO_4.[1] Furthermore, one must consider the pH region in which these uranium species are stable towards their hydrolyses. According to Kraus *et al.*,[118,119] the optimum pH range for stable presence of the uranyl(V) species in aqueous solution is from 2 to 4, which is narrower than that of plutonyl(V) (pH = 2~6). Due to the unusual instability of the uranyl(V) species, any data have not been accumulated systematically.

Sipos and co-workers have studied the electrochemical reaction mechanism of uranyl(VI), uranyl(V), U^{4+}, and U^{3+} ions in perchloric acid aqueous solutions by using polarography and cyclic voltammetry.[126] They proposed the reaction mechanisms including the disproportionation in acidic aqueous system (Eq. 1.20). Even in nonaqueous system, Gritzner and Selbin[129] reported that a brown colloidal precipitate expected as UO_2 was produced after the reduction of uranyl(VI) to uranyl(V) in dimethyl sulfoxide (DMSO). Ikeda and co-workers have studied the electrochemical properties of $[U^{VI}O_2(L)_5]^{2+}$ (L = DMSO, *N*,*N*-dimethylformamide (DMF)), $U^{VI}O_2(\beta\text{-diketonato})_2L$ (β-diketonato = acetylacetonato, 1,1,1-trifluoroacetylacetonato, 1,1,1,5,5,5-hexafluoroacetylacetonato, thenoyltrifluoroacetonato, benzoyltrifluoroacetonate, and dibenzoylmethanato), and $U^{VI}O_2$(salen)L (salen = *N*,*N'*-disalicylideneethylenediaminato) in L as solvent.[140–143] As a result, they have proposed that the uranyl(V) complexes including multidentate ligand(s) can exist more stably than those having only unidentate ones. However, there are no reports of the nonaqueous system of the stable uranyl(V) species.

The attempts to clarify the spectroscopic properties of uranyl(V) species in aqueous media[127] and organic solvents have been performed previously.[129–135] Such studies suggested that the uranyl(V) species have characteristic absorption bands at around 750, 950, and 1500 nm in visible and near infrared regions. However, the sample solutions in these reports were mixtures of uranium(IV), uranyl(V), and uranyl(VI) species, and the absorption bands of uranyl(V) were assigned only by comparing the absorption spectra of such sample solutions with those of uranium(IV) and uranyl(VI).

On the other hand, it has been known that some uranyl(V) species might be produced stably in molten alkali and alikaline-earth chloride mixtures.[144, 145] Adams *et al.* reported that the uranyl(V) species in LiCl–KCl, LiCl–$MgCl_2$, and NaCl–KCl–$MgCl_2$ eutectics show similar electronic spectra at around 690, 870, and 1510 nm.[144] Furthermore, Khokhryakov also observed that the uranyl(V) speceis in CsCl–NaCl and NaCl–KCl melts have absorption bands at around 615, 715, and 1560 nm and tried to assign them.[145] However, the structures of the uranyl(V) species in these molten salt systems have not been identified. Although the knowledges of the spectrum of the pure uranyl(V) species and its exact structure are necessary to interpret its electronic spectrum, the spectroscopic properties of the uranyl(V) species are still uncertain.

A uranyl(V) carbonato complex in basic carbonate aqueous solutions is known as only one system that the uranyl(V) complex can exist stably.[147–153] This system was found by Cohen.[147] According to his report, the uranyl(V) species is stable in the aqueous system at pH $\geq$ 11 and $Na_2CO_3 \geq 1$ M. Ferri *et al.* have determined the stoichiometry of CO_3^{2-} per uranyl(V) ion in this complex by using a potentiometric titration.[149] The result was 3, *i.e.*, its chemical formula is $[U^{V}O_2(CO_3)_3]^{5-}$. The logarithmic formation constant of Eq. 1.24 was evaluated as $\log\beta_3^\circ = 6.950 \pm 0.360$.[2]

$$U^{V}O_2^+ + 3CO_3^{2-} \overset{\beta_3}{\rightleftarrows} [U^{V}O_2(CO_3)_3]^{5-} \tag{1.24}$$

According to a study of extended X-ray absorption fine structure (EXAFS) by Docrat *et al.*,[153] the structure of $[U^{V}O_2(CO_3)_3]^{5-}$ can be considered to be similar to that of $[U^{VI}O_2(CO_3)_3]^{4-}$, *i.e.*, the coordinated CO_3^{2-} in $[U^{V}O_2(CO_3)_3]^{5-}$ are equivalent each other. Cohen

[2]This is the corrected value at 298.15 K, 0.1 MPa, and zero ionic strength from the most recent report, "*Update on the Chemical Thermodynamics of Uranium, Neptunium, Plutonium, Americium and Technetium*"[13]. The original value of $\log\beta_3$ reported in *Inorg. Chem.* **1983**, *22*, 3162–3165. is 13.3 ± 0.4 in 3 M $NaClO_4$ aq.[149]

has also reported that $[U^{V}O_2(CO_3)_3]^{5-}$ shows its characteristic absorption bands at around 765, 980, and 1120 nm in visible-NIR region, and that the solution of $[U^{V}O_2(CO_3)_3]^{5-}$ is almost colorless.[147] Mizuguchi and co-workers have measured the UV-visible absorption spectra of $[U^{V}O_2(CO_3)_3]^{5-}/[U^{VI}O_2(CO_3)_3]^{4-}$ redox couple (Eq. 1.25)[3] at various potentials with spectroelectrochemical technique.[152]

$$[U^{VI}O_2(CO_3)_3]^{4-} + e^- \rightleftarrows [U^{V}O_2(CO_3)_3]^{5-} \tag{1.25}$$

As a result, the decolorization with the reduction from $[U^{VI}O_2(CO_3)_3]^{4-}$ to $[U^{V}O_2(CO_3)_3]^{5-}$ was spectrophotometrically confirmed as the disappearance of the LMCT absorption bands of $[U^{VI}O_2(CO_3)_3]^{4-}$ at around 450 nm. Unfortunately, the electronic spectrum of $[U^{V}O_2(CO_3)_3]^{5-}$ in the wavelength region longer than 1350 nm has not been observed, because of the strong absorption of H_2O as the solvent. Since no stable uranyl(V) species with identified structures other than $[U^{V}O_2(CO_3)_3]^{5-}$ are known, the spectroscopic properties of the uranyl(V) complexes cannot be discussed systematically.

The structural properties of the uranyl(V) species are also uncertain. With the reduction from uranyl(VI) to uranyl(V), it has been predicted theoretically that the U=O bond distance (R_{UO}) lengthens about 0.05~0.08 Å, and that the ν_1 and ν_3 stretching in the uranyl moiety show red-shifts.[108,110] In fact, Docrat *et al.* have clarified that the R_{UO} value increases with the reduction of $[U^{VI}O_2(CO_3)_3]^{4-}$ (1.80 Å) to $[U^{V}O_2(CO_3)_3]^{5-}$ (1.90 Å) in their EXAFS study.[153] Furthermore, Madic *et al.* have observed the red-shift of the ν_1 peak in the Raman spectra with the reduction from $[U^{VI}O_2(CO_3)_3]^{4-}$ (ν_1 = 812 cm^{-1}) to $[U^{V}O_2(CO_3)_3]^{5-}$ (ν_1 = 759 cm^{-1}).[151] However, these structural data of the uranyl(V) species are limited only in $[U^{V}O_2(CO_3)_3]^{5-}$. Additionally, no data concerning the ν_3 peak, which will be observed in IR spectra, are available.[4] Jones and Penneman have studied the IR properties of the alternative actinyl(V/VI) species (neptunyl(V/VI) and americyl(V/VI)).[155] They reported that the reduction from $An^{VI}O_2^{2+}$ to $An^{V}O_2^{+}$ causes the red-shift of the ν_3 peak of O=An=O, *i.e.*, An=O bond strength is weakened. The shifts for An = Np and Am are 145 and 107 cm^{-1}, respectively. Thus, in the case of An = U, it is expected that the ν_3 peak in O=U=O is shifted to lower wavenumber by *ca.* 100~150 cm^{-1} with the reduction from uranyl(VI) to uranyl(V).

On the other hand, some compounds containing $U^{V}X_n^{5-n}$ species (X = F, Cl, OC_2H_5; $n = 5, 6$), which have no axial oxygen atoms, have been reported previously, and Selbin and Ortego reviewed them.[125] According to them, the $U^{V}X_n^{5-n}$ species have characteristic absorption bands in visible and NIR regions as shown in Figure 1.8. Generally, the crystal field surrounding the center uranium in the $U^{V}X_n^{5-n}$ species was treated as an octahedral one (O_h).[5] The electronic configuration, $5f^1$, allows only the $^2F_{5/2}$ and $^2F_{7/2}$ term level which is split by spin-orbit coupling into two levels. Moreover, the crystal field in $U^{V}X_n^{5-n}$ will further

[3] Various formal potential ($E^{\circ\prime}$) values of Eq. 1.25 were reported such as −0.714, −0.730, −0.7459, −0.749, −0.815, and −0.859 V *vs.* Ag/AgCl, which were summarized by Grenthe *et al.* in "*Chemical Thermodynamics of Uranium*"[12]. In this thesis, the $E^{\circ\prime}$ value of Eq. 1.25 under the present experimental condition has been re-evaluated by using spectroelectrochemical technique. Details are in Section 3.1.

[4] Even for $[U^{V}O_2(CO_3)_3]^{5-}$, it should be difficult to measure its IR spectrum, because the solvent H_2O is a strong absorber of IR rays.

[5] Since there are no axial oxygens, the perturbation order shown in Eq. 1.17 cannot be applied. Therefore, the crystal fields surrounding the center uranium in $U^{V}X_n^{5-n}$ were treated by using O_h point group. Furthermore, the spin angular momentum of U^{5+} is half-integer (1/2) because of the $5f^1$ configuration. This means that the introduction of "double group" is required in the discussion including both crystal field and spin-orbit coupling. Here, O_h^* (or O^*) double group corresponds to the O_h single group. Details are presented in Chapter 6.

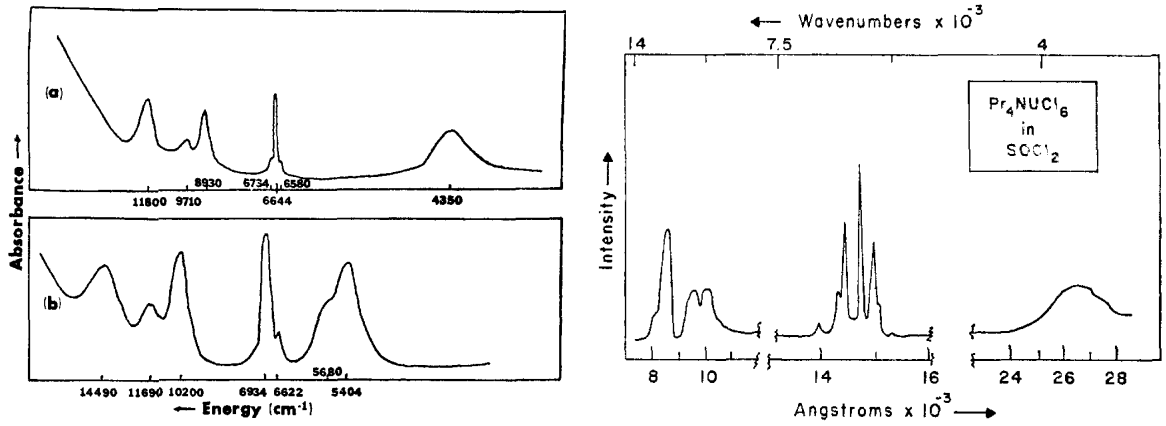

Figure 1.8. Visible and near-infrared electronic absorption spectra of $U^{V}X_n^{5-n}$ species. Left: (a) $U^{V}Cl_5 \cdot SOCl_2$ in CCl_4 and (b) $[U^{V}(OC_2H_5)_5]_2$ in CCl_4. Right: $(C_3H_7)_4NU^{V}Cl_6$ in $SOCl_2$.[125)]

split the foregoing degenerate levels as follows.

$$^2F_{5/2} \longrightarrow \Gamma_7 + \Gamma_8$$
$$^2F_{7/2} \longrightarrow \Gamma_6 + \Gamma_7' + \Gamma_8'$$

Hence, one should predict at least four transitions to be possible in the $U^{V}X_n^{5-n}$ species, namely $\Gamma_7 \rightarrow \Gamma_8$, $\Gamma_7 \rightarrow \Gamma_7'$, $\Gamma_7 \rightarrow \Gamma_8'$, and $\Gamma_7 \rightarrow \Gamma_6$, in which the odd electron resides in the lowest Γ_7 level in the ground state. In Figure 1.8, not just four bands, but rather at least four groups of the absorption bands were observed. The additional bands were suggested to be the result of different vibronic transition and/or removal of the degeneracy arising from the lowering of the symmetry.[6]

Selbin and Ortego also included the matter of the uranyl(V) species in their review.[125)] However, they described that the knowledge of uranyl(V) is extremely limited and a great deal more work needs to be done before uranyl(V) may even be considered as well characterized. This was stated in 1969, but still now no sufficient information of uranyl(V) has been available.

1.3.2 Other 5f¹ Systems: Neptunyl(VI) and Plutonyl(VII)

The neptunyl(VI) ($Np^{VI}O_2^{2+}$) is one of the alternative $5f^1$ actinyl ions. Structural properties of the neptunyl(VI) ion are almost identical with those of uranyl(VI). On the other hand, the stability of the neptunyl(VI) ion is completely different from that of uranyl(V) in spite of the isoelectronic configuration. The neptunyl(VI) ion is stable in both acid and basic media. Thus, pure sample of the neptunyl(VI) species can be prepared and studied. The absorption

[6]Some of the pertinent theoretical predictions were predicted by the authors of the references in the review by Selbin and Ortego;[125)] (1) The doublet levels (Γ_7, Γ_7', Γ_6) arising from Kramer's degeneracy are predicted to be stabilized by spin-orbit coupling and would be unaffected by Jahn-Teller distortions. (2) Jahn-Teller effects are important in the behavior of the quadruply degenerate Γ_8 leveles. These levels are predicted to split into two doublets when the octahedron distorts. The Γ_8 levels may also interact with the vibration modes. (3) Vibrational selection rules indicate that the totally symmetric vibrational mode, A_{1g}, can couple with the electronic transitions. (4) The odd vibrational modes of the molecule are predicted to couple most strongly with the electronic transitions.

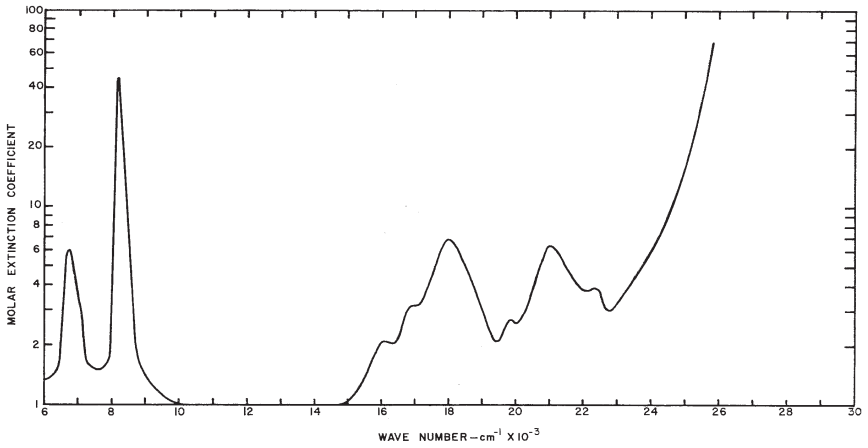

Figure 1.9. Absorption spectrum of the neptunyl(VI) ion in 1 M H(D)ClO_4 aq. summarized by McGlynn and Smith.[89)]

spectra of the neptunyl(VI) ion in $HClO_4$ aqueous solutions have been reported by Sjoblom *et al.*,[156)] Waggener,[157)] and Hagan *et al.*[158)] According to their papers, the neptunyl(VI) ion shows its characteristic absorption bands at around 1223 and 1480 nm in NIR region. Friedman and Toth have reported that the neptunyl(VI) ion in 0.1, 0.5, 1.0, and 4.0 M HNO_3 also has the characteristic bands at *ca.* 1200 nm, which does not show any significant dependences on the acid concentration.[159)] Figure 1.9 shows the typical absorption spectrum of the neptunyl(VI) ion in aqueous system summarized by McGlynn and Smith.[89)] According to their assignment, the neptunyl(VI) ion in 1 M H(D)ClO_4 aq. has the characteristic absorption bands due to f–f transition at ~2000 ($^2\Phi_{5/2u} \rightarrow {}^2\Delta_{3/2u}$), 6752 ($^2\Phi_{5/2u} \rightarrow {}^2\Phi_{7/2u}$), 8168 ($^2\Phi_{5/2u} \rightarrow {}^2\Delta_{5/2u}$), 18180 ($^2\Phi_{5/2u} \rightarrow {}^2\Pi_{1/2u}$), 21100 ($^2\Phi_{5/2u} \rightarrow {}^2\Pi_{3/2u}$), and ~24000 cm^{-1} ($^2\Phi_{5/2u} \rightarrow {}^2\Sigma_u^+$).[7] Leung and Wong studied the absorption spectrum of the neptunyl(VI) ion doped into a $CsU^{VI}O_2(NO_3)_3$ single crystal cooled at liquid nitrogen or liquid helium temperature. They observed very complicated absorption peaks including Zeeman effects by Kramer's doublets in $[Np^{VI}O_2(NO_3)_3]^-$, and assigned 6 peaks at 4802.9, 6212.1, 6220.8, 7185.2, 10613, 15480 cm^{-1} to the f–f transitions in the neptunyl(VI) ion with $5f^1$ configuration. Further investigations for the polarized absorption spectra of $[Np^{VI}O_2Cl_4]^{2-}$ and $[Np^{VI}O_2(NO_3)_3]^-$ doped into single crystals of the corresponding uranyl(VI) compounds were performed by Denning *et al.*[101, 102)] They also reported that the absorption peaks attributable to the f–f transitions in the neptunyl(VI) ion appear at ~1000, 6880.4, ~7990, 17241.4, and 20080.8 cm^{-1} for $[Np^{VI}O_2Cl_4]^{2-}$, and 6459.0, 9420.2, 17843.6, and 20816.3 cm^{-1} for $[Np^{VI}O_2(NO_3)_3]^-$. Therefore, if the electronic spectrum of pure uranyl(V) species is recorded, it can be compared with those of the neptunyl(VI) species.

The plutonyl(VII) species is also isoelectronic with the uranyl(V). However, this species is presented only in the strongly basic aqueous system ($[OH^-] > 7$ M), and considered to exist as $Pu^{VII}O_5^{3-}$ rather than $Pu^{VII}O_2^{3+}$. The anion of plutonyl(VII) is a very powerful oxidizing agent, for example, it oxidizes water to oxygen when $[OH^-] < 7$ M. Available data concerning the properties of the plutonyl(VII) species is limited only in the characteristic absorption peak at 635 nm with $\epsilon = 530\ M^{-1}\cdot cm^{-1}$.[1)]

[7]Wavenumber ($\tilde{\nu}$ /cm^{-1}) and wavelength (λ /nm) have a relationship, $\tilde{\nu} = 10^7/\lambda$.

1.4 Objectives in This Doctoral Thesis

As described above, the chemistry of uranyl(VI) is well understood, while that of uranyl(V) is almost unknown. However, the knowledges of basic properties of uranyl(V) must be essential to complete the actinoid chemistry, because uranyl(V) has the $5f^1$ electronic configuration which is simplest in the actinyl species with $5f^n$ configuration. Thus, the elucidation of the chemistry of uranyl(V) is the most important objective of this doctoral thesis.

The most probable candidate of the stable uranyl(V) complex is $[U^{V}O_2(CO_3)_3]^{5-}$, of which the stability has already been confirmed. Therefore, $[U^{V}O_2(CO_3)_3]^{5-}$ in the aqueous system was selected in this study. Based on the proposal by Ikeda *et al.*,[140–143] *N,N'*-disalicylidene-*o*-phenylenediaminate (saloph) and dibenzoylmethanate (dbm) were selected as multidentate ligands expected to stabilize the uranyl(V) species in nonaqueous systems. The saloph ligand is one of the most popular tetradentate Schiff bases reported by Pfeiffer *et al.*[23] It has been known that the uranyl(VI) complex coordinated with saloph generally contains a unidentate ligand (L). Indeed, Bandoli *et al.* reported a single crystal X-ray analysis for the uranyl(VI) complex with saloph and ethanol (EtOH); $U^{VI}O_2$(saloph)EtOH.[24] To study the effect of L on the stabilities of $[U^{V}O_2(saloph)L]^{-}$complexes, two kinds of the uranyl(VI) saloph complexes with DMF and DMSO as L, $U^{VI}O_2$(saloph)DMF and $U^{VI}O_2$(saloph)DMSO, were prepared here. Moreover, to examine the effects of multidentate ligand type on the properties of the uranyl(V) and -(VI) complexes, dbm which is bidentate was used as an alternative ligand. The resulting uranyl(VI) dbm complex was $U^{VI}O_2(dbm)_2$DMSO. In this study, the electrochemical techniques were used to prepare the uranyl(V) complex from the uranyl(VI) one in both aqueous and nonaqueous systems. Therefore, the electrochemical redox behavior of each uranyl(VI) complex has been studied. Furthermore, to discuss the properties of the uranyl(V) complexes, it must be necessary to know those of the corresponding uranyl(VI) complexes. Hence, the characterizations of the uranyl(VI) complexes were also performed.

In this thesis, I have tried to elucidate the properties concerning molecular structures, electronic spectra, and reactivities of uranyl(V) and -(VI) complexes in aqueous and nonaqueous systems with an especial interest in uranyl(V). This doctoral thesis is composed by 7 chapters as follows.

Chapter 1 Introduction.

Chapter 2 Syntheses and characterizations of uranyl(VI) complexes, $Na_4[U^{VI}O_2(CO_3)_3]$, $U^{VI}O_2$(saloph)DMF, $U^{VI}O_2$(saloph)DMSO, and $U^{VI}O_2(dbm)_2$DMSO, using single crystal X-ray analysis, IR (Raman) spectroscopy, and NMR spectroscopy.

Chapter 3 Spectroelectrochemistry of $[U^{VI}O_2(CO_3)_3]^{4-}$ in aqueous carbonate solution with an optical transparent thin-layer electrode cell and ligand exchange reaction of $[U^{V}O_2(CO_3)_3]^{5-}$ using ^{13}C NMR spectroscopy.

Chapter 4 Electrochemistries and spectroelectrochemistries of $U^{VI}O_2$(saloph)DMF, $U^{VI}O_2$(saloph)DMSO, and $U^{VI}O_2(dbm)_2$DMSO in nonaqueous systems.

Chapter 5 Structural changes of uranyl moiety with reduction from U(VI) to U(V) using IR spectroelectrochemical technique.

Chapter 6 Electronic spectra of uranyl(V) complexes.

Chapter 7 Conclusion.

Chapter 2

Syntheses and Characterizations of Uranyl(VI) Complexes[1]

[1]In this chapter, the oxidation state of uranium in all compounds is VI. Thus, to simplify the writing, the superscript roman number indicating the oxidation state on U was abbreviated.

2.1 $Na_4[UO_2(CO_3)_3]$

2.1.1 Experimental Details

Synthesis of $Na_4[UO_2(CO_3)_3]$. Aqueous solution (10 ml) of $UO_2(NO_3)_2{\cdot}nH_2O$ (3.5 g) was mixed with saturated aqueous solution of Na_2CO_3 (50 ml, Kanto Chemical Co. Ind.). After the stirring at 80°C for 10 min, the mixture was cooled to room temperature. The yellow powder of $Na_4[UO_2(CO_3)_3]$ was filtered off and washed with 40 vol.% EtOH aqueous solution.

Other Materials. Deuterium oxide (ACROS, 99.8 atom% D) and ^{13}C-enriched Na_2CO_3 (ISOTEC, 99 atom% ^{13}C) were used as received. All other chemical used in this section were of reagent grade.

Methods. Characterization of $Na_4[UO_2(CO_3)_3]$ was performed by using an IR spectrophotometer (SHIMADZU FTIR-8400S), a Raman spectrophotometer (JASCO RMP-200), a UV-visible absorption spectrophotometer (SHIMADZU UV-3150), and an NMR spectrometer (JEOL JNM-LA300WB FT NMR SYSTEM, ^1H: 300.4 MHz, ^{13}C: 75.45 MHz).

2.1.2 Results and Discussion

An IR spectrum of the yellow product in KBr was measured by a diffuse reflectance method. The resulting IR spectrum was depicted by a black solid line in Figure 2.1. Characteristic peaks of CO_3^{2-} were observed at 703, 736 cm^{-1} (ν_4), 1064 cm^{-1} (ν_1) and 1348, 1560 cm^{-1} (ν_3). These assignments were performed on the basis of the previous report by Nakamoto.[160] Overlapping of two peaks at 829 and 852 cm^{-1} was observed. The peak at 852 cm^{-1} might be attributable to the O=U=O asymmetric stretching (ν_3) in the uranyl(VI) moiety, which usually appears in a region from 900 to 950 cm^{-1}. Thus, the peak at 852 cm^{-1} might be too low to assign it to the ν_3 one of the uranyl(VI) moiety. On the other hand, these peaks also have possibility of the out-of-plane deformation (ν_2) of CO_3^{2-} in $[UO_2(CO_3)_3]^{4-}$, because the ν_2 peak of CO_3^{2-} in its salts is observed in a region from 850 to 879 cm^{-1}.[160]

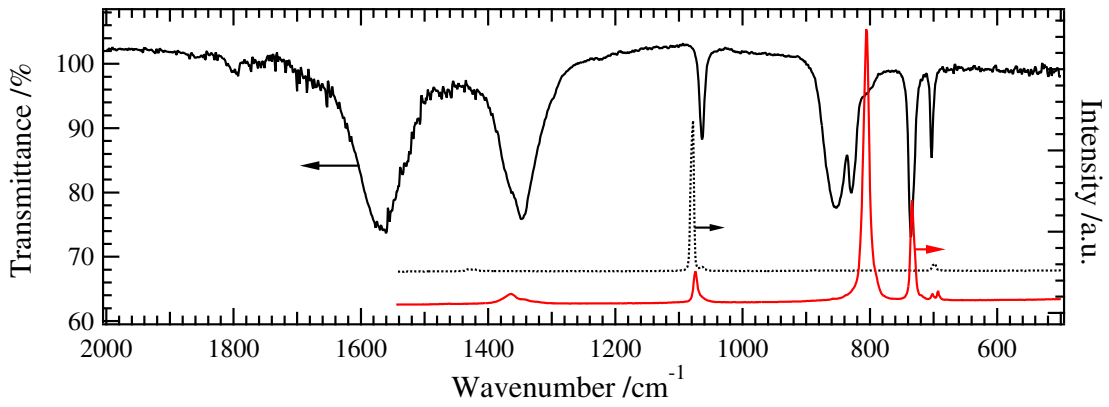

Figure 2.1. Vibrational spectra of $Na_4[UO_2(CO_3)_3]$. Black line: IR, red line: Raman. Black dotted line is the Raman spectrum of Na_2CO_3 for a comparison.

Therefore, the presence of the uranyl(VI) ion in the yellow product cannot be concluded only from the IR spectrum.

Since the uranyl(VI) species also shows the O=U=O symmetric stretching (ν_1) in a Raman spectrum, such a spectroscopy should be one of the good tool to confirm the presence of the uranyl(VI) ion in the product. The Raman spectrum of the yellow product was drawn by a red line in Figure 2.1 with that of Na_2CO_3 in a black dotted line. The characteristic peaks of CO_3^{2-} were also observed at 734, 702, and 693 cm^{-1} (ν_4), 1075 cm^{-1} (ν_1), and 1364 cm^{-1} (ν_3) for the product (red solid line) and 699 cm^{-1} (ν_4), 1079 cm^{-1} (ν_1), and 1421, 1430 cm^{-1} (ν_3) for Na_2CO_3 (black dotted line). The ν_2 peak in CO_3^{2-} was not be detected in both Raman spectra. The assignments of these Raman peaks agree with those of the corresponding IR peaks (black solid line) and the Raman peaks reported previously.[151] The peak at 806 cm^{-1} in the red line can be attributed to ν_1 of the uranyl(VI) moiety in $Na_4[UO_2(CO_3)_3]$. This Raman peak is comparable with that observed in an aqueous solution (0.18 M UO_2^{2+}, 2 M Na_2CO_3) at 812 cm^{-1} by Madic *et al.*[151].

As a result, it is most likely to assign the IR peak at 852 cm^{-1} to ν_3 of the uranyl(VI) moiety and the other one at 829 cm^{-1} to ν_2 of CO_3^{2-} in $Na_4[UO_2(CO_3)_3]$. The similar overlapping was also observed in the systems of $(gua)_4[UO_2(CO_3)_3]$, $(gua)_2[UO_2(CO_3)_2]$, and $(gua)_6[(UO_2)_3(CO_3)_6]\cdot 6.5H_2O$ (gua = $C(NH_2)_3^+$, guanidinium cation) by Allen *et al.*[161] They reported that the uranyl(VI) ν_3 peak was generally "masked" by the strong ν_2 CO_3^{2-} out-of-plane deformation.

The presence of the uranyl(VI) ion could also be confirmed by means of the UV-visible absorption spectroscopy. The UV-visible absorption spectrum of an aqueous solution prepared by dissolving the yellow powder of $Na_4[UO_2(CO_3)_3]$ (5.5×10^{-2} M) and Na_2CO_3 (1.0 M) is shown in Figure 2.2. As can be seen from this figure, the characteristic absorption bands due to the charge transfer from the axial oxygen to the center uranium (LMCT) in the uranyl(VI) ion was observed at around 450 nm with a resolved vibronic structure. The spectral features and the molar absorptivities (ϵ) are comparable that of $[UO_2(CO_3)_3]^{4-}$ reported

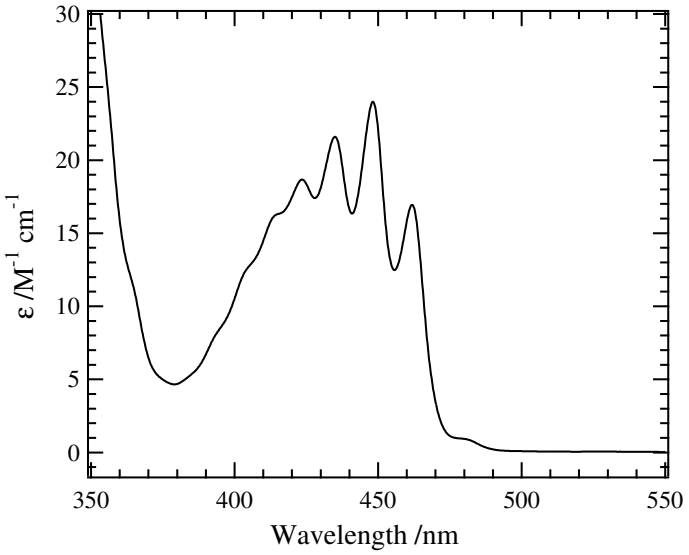

Figure 2.2. UV-visible absorption spectrum of the aqueous solution dissolving $Na_4[UO_2(CO_3)_3]$ (5.5×10^{-2} M) and Na_2CO_3 (1.0 M).

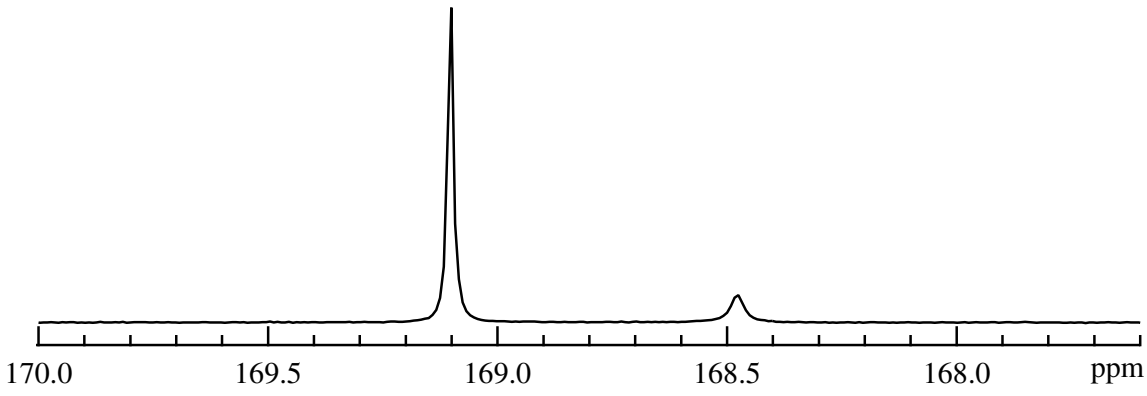

Figure 2.3. ^{13}C NMR spectrum of D_2O solution dissolving $Na_4[UO_2(CO_3)_3]$ (4.09×10^{-2} M) and $Na_2{}^{13}CO_3$ (5.74×10^{-1} M).

by Mizuguchi *et al.*[152)]

Furthermore, the ^{13}C NMR spectrum of a D_2O solution dissolving $Na_4[UO_2(CO_3)_3]$ (4.09×10^{-2} M) and $Na_2{}^{13}CO_3$ (5.74×10^{-1} M) was measured at room temperature. The resulting NMR spectrum is shown in Figure 2.3. The signals due to the free and coordinated CO_3^{2-} were detected at 169.10 and 168.48 ppm, respectively.[71, 72, 162)] The area ratio indicates that the coordination number of CO_3^{2-} around the uranyl(VI) ion is 2.89 ± 0.03. In conclusion, the uranyl(VI) species exists as $[UO_2(CO_3)_3]^{4-}$ even in the aqueous solution with the presence of the excess amount of free CO_3^{2-}, which is obvious from its quite large stability constant ($\log\beta_3 = 21.840 \pm 0.040$ at $I = 0$).[13)]

2.2 UO_2(saloph)DMF

2.2.1 Experimental Details

Synthesis of UO_2(saloph)DMF. Ethanol (EtOH) solution of *o*-phenylenediamine (5.4 g, Kanto) was mixed with hot ethanol solution containing salicylaldehyde (11.72 g, Aldrich, 98%). This mixture was stirred and refluxed at 78°C for 3 h. The resulting orange precipitate of *N,N'*-disalicylidene-*o*-phenylenediamine (H_2saloph, see Figure 2.4) was filtered off, and washed with EtOH. This product was recrystallized from ethyl acetate. The EtOH solution containing $UO_2(NO_3)_2{\cdot}nH_2O$ (2.0 g) was added to the hot EtOH solution containing H_2saloph (1.3 g) under vigorous stirring. The mixture was refluxed for 2 h at 78°C, and cooled at −18°C for 1 week. The orange precipitate of UO_2(saloph)EtOH was filtered off and washed with EtOH. The UO_2(saloph)EtOH (0.3 g) was dissolved in *N,N*-dimethylformamide (4 ml, DMF, Kanto). The solution was heated at 80°C with stirring for 3 h. The excess DMF was removed by evaporation at 100°C under vacuum. The deposited orange needle crystals of UO_2(saloph)DMF were filtered off and washed with mixture of dichloromethane and ether (1 : 4 vol.). Single crystals of UO_2(saloph)DMF suitable for X-ray crystallography were obtained from a solution of UO_2(saloph)DMF in a mixed solvent of dichloromethane and DMF.

Synthesis of $[UO_2(saloph)]_2$. Dichloromethane solution dissolving UO_2(saloph)DMF or UO_2(saloph)DMSO (see Section 2.3) was concentrated by slow evaporation of the solvent at ambient condition until crystals of $[UO_2(saloph)]_2$ deposited. The resulting crystals of $[UO_2(saloph)]_2$ were suitable for the single crystal X-ray analysis.

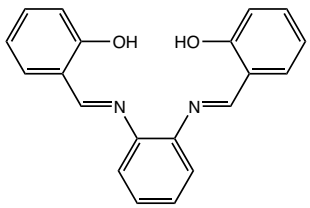

Figure 2.4. Schematic structure of *N,N'*-disalicylidene-*o*-phenylenediamine (H_2saloph).

Other Materials. Dichloromethane-d_2 (ACROS, 99.8 atom% D) and chloroform-*d* (ACROS, 99.8 atom% D) were used for NMR measurements without further purification. All other chemicals used were of reagent grade.

Methods. Characterizations of UO_2(saloph)DMF and $[UO_2(saloph)]_2$ were performed by using the IR spectrophotometer, NMR spectrometer, and single crystal X-ray diffractmeter (Rigaku RAXIS RAPID).

Details in Single Crystal X-ray Analyses. The single crystal X-ray analyses for UO_2-(saloph)DMF and $[UO_2(saloph)]_2$were performed with the following procedure. Single crystal of each uranyl(VI) complex was mounted on a glass fiber, and put into the low temperature nitrogen gas flow. Intensity data were collected by using imaging plate area detector in

Rigaku RAXIS RAPID with graphite monochromated Mo-Kα radiation (λ = 0.71075 Å). The structures of these uranyl(VI) complexes were solved by direct (*SIR 92*)[163] or heavy-atom Patterson methods[164] and expanded using Fourier techniques.[165] All non-hydrogen atoms were refined anisotropically. Hydrogen atoms were refined using the riding model (C–H bond, aromatic: 0.95 Å, methyl: 0.98 Å). The final cycle of full-matrix least-squares refinement on F^2 was based on observed reflections and parameters, and converged with unweighted and weighted agreement factors, R and wR. The weighing schemes for the refinements of UO_2(saloph)DMF·CH_2Cl_2, $[UO_2(saloph)]_2$, and $[UO_2(saloph)]_2$·0.5CH_2Cl_2 by SHELXL-97[166] were $w = 1/[\sigma^2F_o^2 + (0.0262P)^2 + 5.3741P]$, $w = 1/[\sigma^2F_o^2 + (0.0256P)^2 + 46.5808P]$, and $w = 1/[\sigma^2F_o^2 + (0.0396P)^2 + 60.3343P]$, respectively ($P = F_o^2 + 2F_c^2)/3$). Plots of $\sum w(|F_o| - |F_c|)^2$ versus $|F_o|$, reflection order in data collection, $\sin\theta/\lambda$, and various classes of indices showed no unusual trends for these uranyl(VI) complexes. The maximum (minimum) peaks on the final difference Fourier maps for UO_2(saloph)DMF·CH_2Cl_2, $[UO_2$-(saloph)$]_2$, and $[UO_2(saloph)]_2$·0.5CH_2Cl_2 corresponded to 0.964 (−0.740), 1.726 (−2.211), and 2.490 (−2.984) e^-·Å^{-3}, respectively. Neutral atom scattering factors were taken from Cromer and Waber.[167] Anomalous dispersion effects were included in F_c[168]; the values for $\Delta f'$ and $\Delta f''$ were those of Creagh and McAulley.[169] The values for the mass attenuation coefficients were those of Creagh and Hubbell.[170] All calculations were performed by the CrystalStructure crystallographic software package.[171] Crystal data and other data collection parameters of UO_2(saloph)DMF·CH_2Cl_2 and $[UO_2(saloph)]_2$ are summarized in Tables 2.1 and 2.2, respectively. The crystallographic information files of UO_2(saloph)DMF·CH_2Cl_2, $[UO_2(saloph)]_2$, and $[UO_2(saloph)]_2$·0.5CH_2Cl_2 are in Appendixes A, B, and C, respectively.

2.2.2 Results and Discussion

In the diffuse reflectance IR spectrum of UO_2(saloph)DMF in KBr (Figure 2.5), the typical peaks due to O=U=O asymmetric stretching (ν_3) of the uranyl(VI) moiety, C=N stretching in saloph, and C=O stretching in DMF were observed at 905, 1609, and 1651 cm^{-1}, respectively. Since the corresponding IR peaks of the free H_2saloph and DMF appear at 1615 and 1720 cm^{-1}, respectively, such red shifts of these peaks indicate the coordination of saloph and DMF to the uranyl(VI) ion. Furthermore, IR peaks due to -OH stretching of

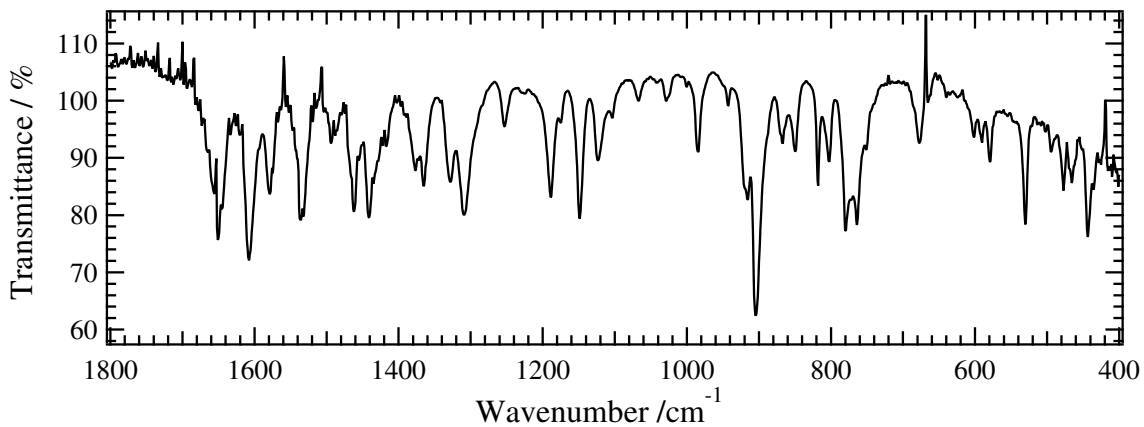

Figure 2.5. IR spectrum of UO_2(saloph)DMF in KBr.

H_2saloph at around 3500 cm^{-1} were not observed for the present uranyl(VI) complex. This means the deprotonation from H_2saloph. As a consequence, the formation of UO_2(saloph)-DMF was confirmed.

To analyze the molecular structure of UO_2(saloph)DMF, the single crystal X-ray analysis was carried out. The crystallographic data and ORTEP view of UO_2(saloph)DMF are shown in Table 2.1 and Figure 2.6, respectively. The resulting crystal of UO_2(saloph)DMF contained one molecule of dichloromethane used as the solvent in the recrystallization. It was found that UO_2(saloph)DMF has the pentagonal bipyramidal geometry with the axial O=U=O moiety, which is one of the most popular structures of the uranyl(VI) complexes. Because of the completely conjugated π electron system of saloph with three benzene rings bridged by two azomethine groups, usually this ligand has been known to have large planarity in its metal complexes.[172–174] However, the coordinated saloph in UO_2(saloph)DMF is largely distorted about 35° as seen from Figure 2.6. This is due to the bulky size of the center uranium. Such distortion was also reported for the analogous uranyl(VI) saloph complex with ethanol, UO_2(saloph)EtOH, by Bandoli *et al.*[24] The U=O bond distances in UO_2(saloph)DMF are 1.776(2) and 1.788(2) Å and the uranyl(VI) moiety is almost linear

Table 2.1. Crystallographic data of UO_2(saloph)DMF·CH_2Cl_2

Empirical formula	$C_{24}H_{23}Cl_2N_3O_5U$	Temparature (°C)	−150.0
Formula weight	742.38	D_{calc} (g·cm^{-3})	1.969
Crystal system	monoclinic	Crystal size (mm)	0.30 × 0.30 × 0.30
Space group	$P2_1/n$ (#14)	Crystal color and shape	orange, block
a (Å)	10.667(4)	F_{000}	1416
b (Å)	9.608(3)	$2\theta_{max}$ (°)	55.0
c (Å)	24.859(10)	Observed data	5734
β (°)	100.65(3)	R [a]	0.0258
V (Å^3)	2503.9(16)	wR [b]	0.0650
Z	4	S (Goodness of fit) [c]	1.119

[a] $R = \Sigma||F_o| - |F_c||/\Sigma|F_o|$, [b] $wR = [\Sigma(w(F_o^2 - F_c^2)^2)/\Sigma w(F_o^2)^2]^{1/2}$, [c] $S = [\Sigma w(F_o^2 - F_c^2)^2/(N_o - N_v)]^{1/2}$, $w = 1/[\sigma^2 F_o^2 + (0.0262P)^2 + 5.3741P)]$ where $P = (F_o^2 + 2F_c^2)/3)$

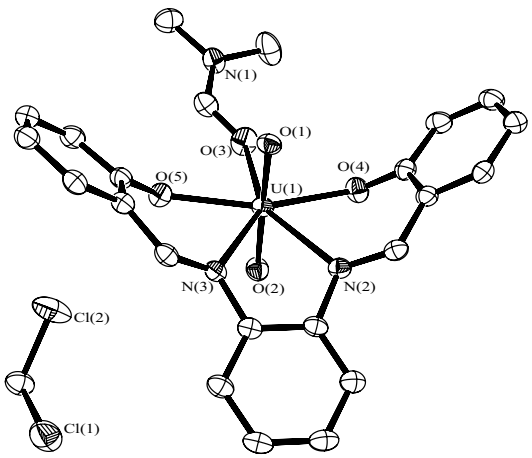

Figure 2.6. ORTEP view of asymmetric unit of UO_2(saloph)DMF·CH_2Cl_2. Probability: 50%. Bond distances (Å); U(1)–O(1): 1.776(2), U(1)–O(2): 1.788(2), U(1)–O(3): 2.410(3), U(1)–O(4): 2.260(3), U(1)–O(5): 2.275(3), U(1)–N(2): 2.549(3), U(1)–N(3): 2.539(3). Bond angle (°); ∠O(1)–U(1)–O(2) = 176.94(11).

(∠O(1)–U(1)–O(2) = 176.94(11)). These results are characteristics of uranyl(VI) complexes as described in Chapter 1. The U(1)–O(4) and U(1)–O(5) bond distances (2.26–2.28 Å) are shorter than U(1)–N(2) and U(1)–N(3) (2.54–2.55 Å). Such a difference implies that the coordination of the oxygen atoms in saloph are stronger than the nitrogen atoms. The bond distance between the oxygen atom in DMF and the center uranium is 2.410(3) Å, which is longer than U(1)–O(4) and U(1)–O(5). It seems that the coordination of DMF through its oxygen atom in UO_2(saloph)DMF is not so strong as those of saloph.

To investigate behavior of UO_2(saloph)DMF in solution, ^{1}H NMR spectroscopy was utilized. The ^{1}H NMR spectra of dichloromethane-d_2 solution dissolving the crystals of UO_2(saloph)DMF·CH_2Cl_2 are shown in Figure 2.7. The very complicated signals in a region from 6.7 to 8.0 ppm are due to the phenyl groups of saloph (12H). At −60°C, two doublet signals due to the methyl groups in the free and coordinated DMF[2] appeared at 2.83 and 3.36 ppm, respectively, which coalesced into one peak with an increase in temperature. The existence of the free DMF and such a coalescence of the signals indicate the partial dissociation of the coordinated DMF from UO_2(saloph)DMF and the exchange reaction between the free and coordinated DMF. The same phenomena were also observed in the case of the formyl groups of the free and coordinated DMF which showed the NMR signals at 7.92 and 9.14 ppm at −60°C, respectively. Furthermore, two singlet signals attributable to the azomethine group of saloph were observed at 9.39 and 9.66 ppm. Both azomethine signals

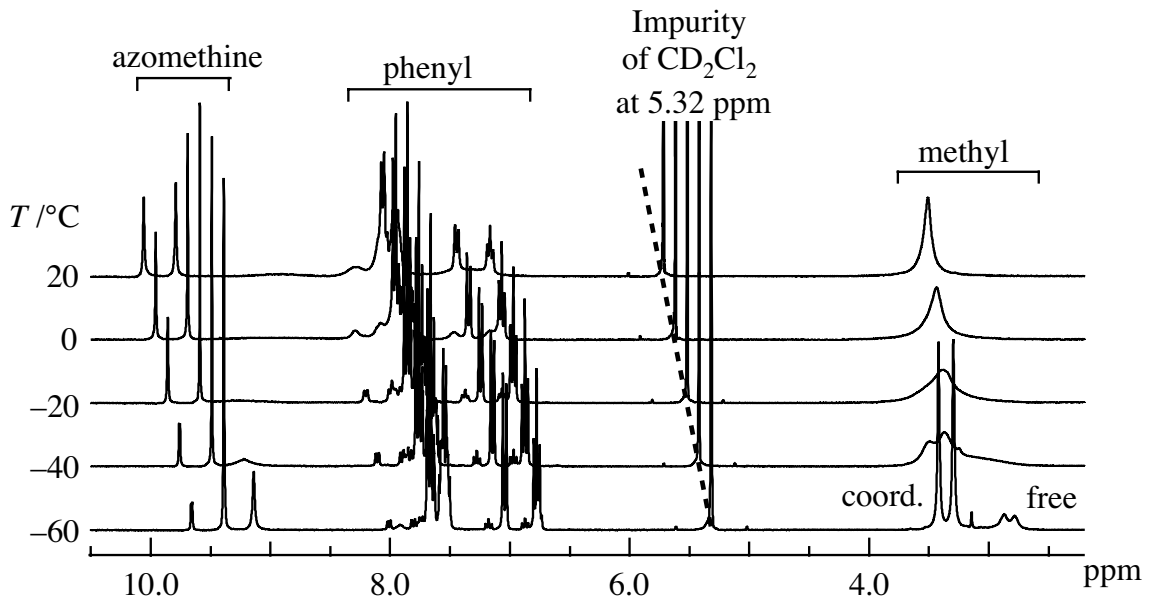

Figure 2.7. ^{1}H NMR spectra of dichloromethane-d_2 solution dissolving UO_2(saloph)DMF at various temperatures.

[2]The doublet signals are due to the following chemical exchange between the methyl groups nearer to and further from the carbonyl oxygen in DMF.

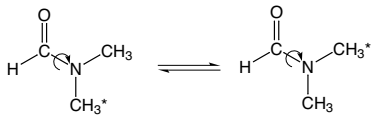

where asterisk is a typographical distinction only.

are in lower field than that of free H_2saloph (8.65 ppm). Thus, the uranyl(VI) complexes coordinated with saloph have two different forms in this system. At −60°C, the peak areas of the azomethine signals (2H) at 9.39 and 9.66 ppm correspond to those of the methyl signals (6H) of the coordinated (3.36 ppm) and free (2.83 ppm) DMF in 1 : 3 ratios, respectively. Therefore, these azomethine signals in Figure 2.7 can be assigned to those in UO_2(saloph)DMF (9.39 ppm) and the DMF dissociated uranyl(VI) species (9.66 ppm). With an increase in temperature from −60 to 20°C, the intensities of the azomethine signals at 9.39 and 9.66 ppm decreased and increased, respectively. Additionally, when a small amount of free DMF was added into the sample solution of Figure 2.7, the azomethine signal due to the DMF dissociated uranyl(VI) species was vanished, whereas that due to UO_2(saloph)DMF did not show any changes. Therefore, an equilibrium reaction between UO_2(saloph)DMF and the DMF dissociated uranyl(VI) species should occur in this system. It must be noted that the line-widths of the azomethine signals at 9.39 and 9.66 ppm have no significant temperature dependences in spite of the line-broadening of the signals due to the free and coordinated DMF for their exchange reaction. This means that the equilibrium between UO_2(saloph)-DMF and the DMF dissociated uranyl(VI) species is independent of the DMF exchange reaction in UO_2(saloph)DMF. The similar phenomena were also observed in chloroform-*d* solution dissolving UO_2(saloph)DMF.

From the dichloromethane solution dissolving UO_2(saloph)DMF, some red crystals deposited. The single crystal X-ray analysis was also performed for this crystal. As a result, this crystal was found to be a dinuclear uranyl(VI) complex consisting of two UO_2(saloph) fragments, $[UO_2(\text{saloph})]_2$. The crystallographic data and ORTEP views of the asymmetric units of $[UO_2(\text{saloph})]_2$ are shown in Table 2.2 and Figure 2.8, respectively. The geometry around each uranyl(VI) ion is also pentagonal bipyramidal. The bond distances between the center uranium and the bridging oxygen atom in each UO_2(saloph) fragment, U(1)–O(4), U(2)–O(8), U(3)–O(11), and U(4)–O(15), are 2.39–2.40 Å, which is longer than those including the non-bridging oxygen atom; 2.20–2.23 Å (U(1)–O(3), U(2)–O(7), U(3)–O(12), and U(4)–O(16)). Such difference of U–O bonds should be caused by bridging between UO_2(saloph) fragments. The lengths of the bridges, U(1)–O(8), U(2)–O(4), U(3)–O(15), and U(4)–O(11), are 2.46–2.49 Å, which are longer than the bond distance between the uranium and the oxygen atom in DMF of UO_2(saloph)DMF (2.410(3) Å). The saloph ligands are distorted in a similar manner to that in UO_2(saloph)DMF (Figure 2.6). The distortion of saloph results the

Table 2.2. Crystallographic data of $[UO_2(\text{saloph})]_2$

Empirical formula	$C_{40}H_{28}N_4O_8U_2$	Z	4
Formula weight	1168.72	Temparature (°C)	−180.0
Crystal system	triclinic	D_{calc} (g·cm^{-3})	1.945
Space group	$P\bar{1}$ (#2)	Crystal size (mm)	$0.20 \times 0.10 \times 0.10$
a (Å)	15.689(7)	Crystal color and shape	red, block
b (Å)	16.044(5)	F_{000}	2176
c (Å)	17.642(7)	$2\theta_{\text{max}}$ (°)	55.0
α (°)	67.00(3)	Observed data	17643
β (°)	78.25(3)	R^a	0.0578
γ (°)	81.72(3)	wR^b	0.1082
V (Å^3)	3992(3)	S (Goodness of fit) ^{c}	1.022

^{a} $R = \Sigma||F_o| - |F_c||/\Sigma|F_o|$, ^{b} $wR = [\Sigma(w(F_o^2 - F_c^2)^2)/\Sigma w(F_o^2)^2]^{1/2}$, ^{c} $S = [\Sigma w(F_o^2 - F_c^2)^2/(N_o - N_v)]^{1/2}$, $w = 1/[\sigma^2 F_o^2 + (0.0256P)^2 + 46.5808P)]$ where $P = (F_o^2 + 2F_c^2)/3)$

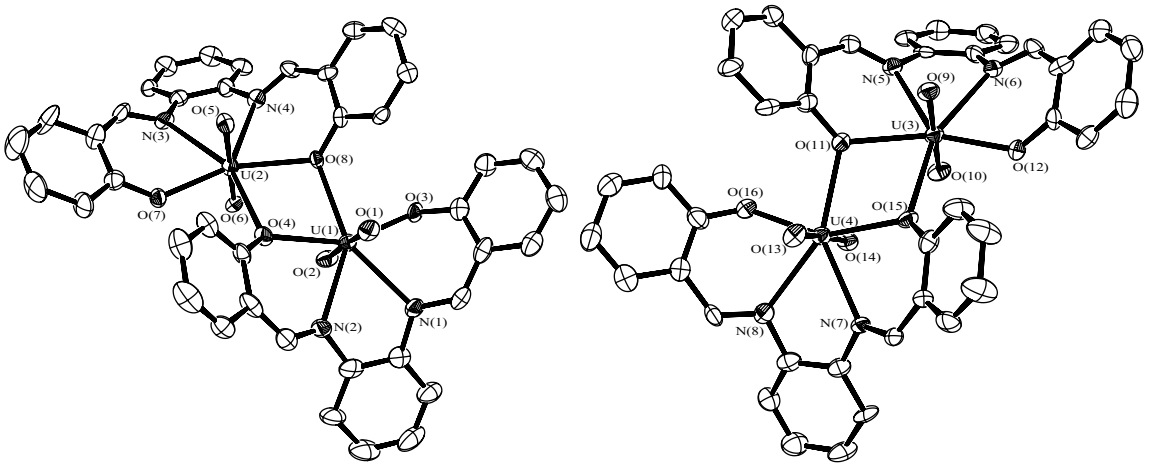

Figure 2.8. ORTEP views of racemic units of $[UO_2(saloph)]_2$. Probability: 50%. Bond distances (Å); U(1)–O(1): 1.769(7), U(1)–O(2): 1.774(7), U(1)–O(3): 2.233(7), U(1)–O(4): 2.387(6), U(1)–O(8): 2.463, U(1)–N(1): 2.540(8), U(1)–N(2): 2.540(8), U(2)–O(5): 1.779(7), U(2)–O(6): 1.784(7), U(2)–O(7): 2.217(6), U(2)–O(8): 2.400(6), U(2)–O(4): 2.475, U(2)–N(3): 2.546(7), U(2)–N(4): 2.495(8), U(3)–O(9): 1.771(7), U(3)–O(10): 1.773(7), U(3)–O(11): 2.389(7), U(3)–O(12): 2.202(6), U(3)–O(15): 2.491(6), U(3)–N(5): 2.560(8), U(3)–N(6): 2.535(8), U(4)–O(13): 1.779(7), U(4)–O(14): 1.784(6), U(4)–O(15): 2.392(7), U(4)–O(16): 2.207(7), U(4)–N(7): 2.512(7), U(4)–N(8): 2.524(9), U(1)...U(2): 3.8807(14), U(3)...U(4): 3.8718(19).

enantiomeric pair of the units of $[UO_2(saloph)]_2$ as shown in Figure 2.8. The crystal lattice contains same number of the enantiomers of $[UO_2(saloph)]_2$, *i.e.*, the racemic compound. The distance between the uranium atoms in each unit are 3.87 or 3.88 Å, which are too far to interact the uranium atoms each other. It was found that there is a solvent-accessible void in the crystal lattice of $[UO_2(saloph)]_2$. In fact, some crystals of $[UO_2(saloph)]_2$ involving the dichloromethane molecules in such a void were obtained with the identical cell parameters as shown in Table 2.2. The ORTEP view of the crystal lattice of $[UO_2(saloph)]_2 \cdot 0.5CH_2Cl_2$ is depicted in Figure 2.9. It is obvious that $[UO_2(saloph)]_2$ is one of the candidates of the DMF dissociated uranyl(VI) species observed in Figure 2.7, because $[UO_2(saloph)]_2$ is produced from the dichloromethane solution.

For the reactions of UO_2(saloph)DMF accompanied by the dissociation of DMF in dichloromethane and chloroform observed in the ^{1}H NMR spectra (Figure 2.7), the following dimerization and dissociation equilibria can be proposed.

Dimerization of UO_2(saloph)DMF:

$$2UO_2(saloph)DMF \rightleftarrows [UO_2(saloph)]_2 + 2DMF \tag{2.1}$$

$$K_{dim} = \frac{[[UO_2(saloph)]_2]\,[DMF]^2}{[UO_2(saloph)DMF]^2} \tag{2.2}$$

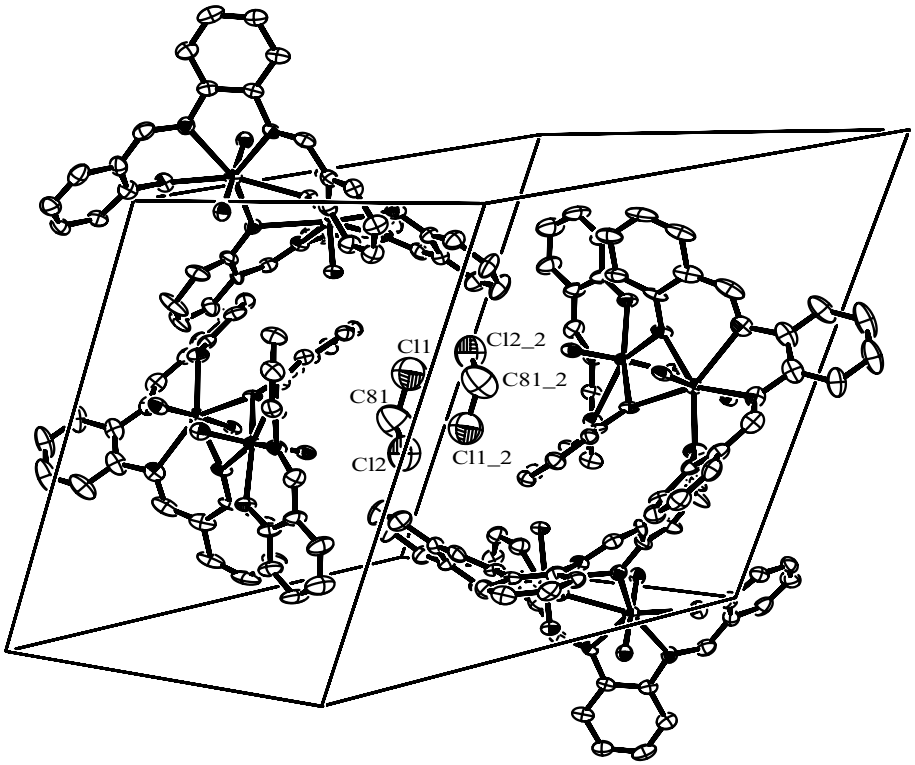

Figure 2.9. ORTEP view of crystal lattice of $[UO_2(saloph)]_2 \cdot 0.5CH_2Cl_2$.

Dissociation of DMF from UO_2(saloph)DMF:

$$UO_2(saloph)DMF \rightleftarrows UO_2(saloph) + DMF \tag{2.3}$$

$$K_{dis} = \frac{[[UO_2(saloph)]_2]\,[DMF]}{[UO_2(saloph)DMF]} \tag{2.4}$$

To determine which reaction is correct, the dependence of UV-visible absorption spectra on the DMF concentration was examined. As initial conditions, the crystals of $[UO_2(saloph)]_2$ (*ca.* 10^{-5} M) were dissolved in dichlromethane or chloroform solvents. Then, DMF diluted by the corresponding solvent was added stepwise into the sample solution dissolving $[UO_2$-(saloph)$]_2$. The resulting spectra of the dichloromethane and chloroform solutions at 298 K are shown in Figures 2.10(a) and (b), respectively. In these figures, isosbestic points were observed at 293, 392, and 518 nm in Figure 2.10(a) and 287 and 385 nm in Figure 2.10(b). The equilibrium constants assuming Eq. 2.1 (K_{dim}) and Eq. 2.3 (K_{dis}) were calculated from the absorbancies at 430 nm in Figures 2.10(a) and (b). As a result, in the dichloromethane system, the K_{dim} value at 298 K was evaluated as $(3.00 \pm 0.08) \times 10^{-3}$ M ($\log K_{dim} = -2.52 \pm 0.01$) in average and almost constant within 3% error, while K_{dis} varied from 3.49×10^{-4} M to 1.63×10^{-4} M with the increase in the DMF concentration. This result concludes that the dimerization reaction of UO_2(saloph)DMF (Eq. 2.1) occurs in the dichloromethane solution, *i.e.*, the DMF dissociated uranyl(VI) species is $[UO_2(saloph)]_2$. In the chloroform system (Figure 2.10(b)), the calculated K_{dim} values also agreed with $(1.80 \pm 0.06) \times 10^{-2}$ M ($\log K_{dim} = -1.74 \pm 0.01$) within 3% error. Therefore, the azomethine signal at 9.66 ppm in the ^{1}H NMR spectra (Figure 2.7) is assigned to that of $[UO_2(saloph)]_2$.

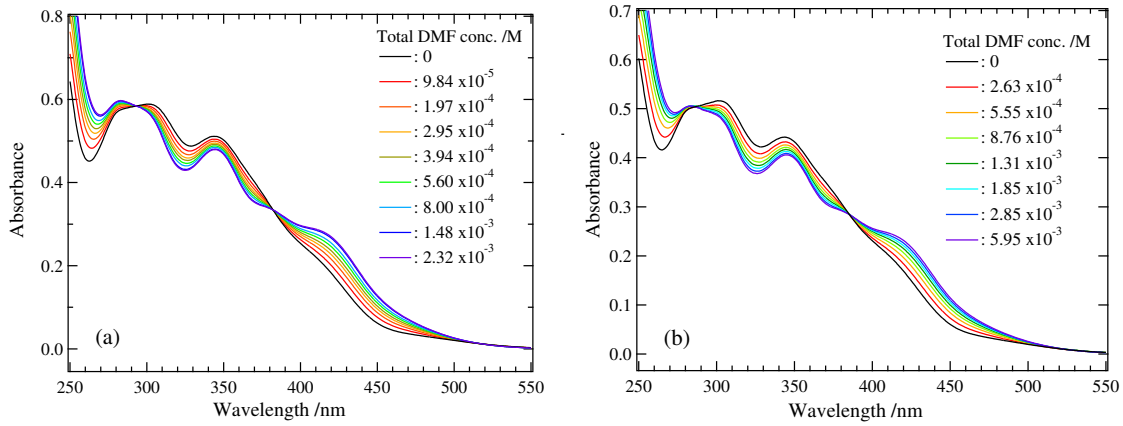

Figure 2.10. UV-visible absorption spectra of (a) dichloromethane and (b) chloroform solutions containing $[UO_2(saloph)]_2$ ((a): 1.26×10^{-5} M, (b): 1.19×10^{-5} M) and various total concentration of DMF ((a): 0 ~ 2.32×10^{-3} M, (b): 0 ~ 5.95×10^{-3} M) at 298 K.

In Figure 2.7, the temperature dependence of the intensities of the ^{1}H NMR signals at 9.39 and 9.66 ppm was observed. Hence, the thermodynamic parameters of Eq. 2.1 can be estimated by using the K_{dim} values at different temperatures and the van't Hoff relationship (Eq. 2.5).

$$K_{dim} = \exp\left(-\frac{\Delta H_{dim}}{R} \cdot \frac{1}{T} + \frac{\Delta S_{dim}}{R}\right) \tag{2.5}$$

where ΔH_{dim}, ΔS_{dim}, R, and T are the formation enthalpy and the formation entropy in Eq. 2.1, the gas constant (8.314 J·mol^{-1}·K^{-1}), and the absolute temperature (K), respectively. The resulting van't Hoff plot for Eq. 2.1 in the dichloromethane-d_2 and chloroform-d solutions are shown in Figure 2.11. The values of ΔH_{dim}, ΔS_{dim}, and $\log K_{dim}$ at 298 K were calculated as 33.0 ± 0.7 kJ·mol^{-1}, 68 ± 3 J·mol^{-1}·K^{-1}, and -2.21 ± 0.03 for the dichloromethane system and 11.3 ± 0.6 kJ·mol^{-1}, 8.0 ± 2.4 J·mol^{-1}·K^{-1}, and -1.56 ± 0.02 for the chloroform

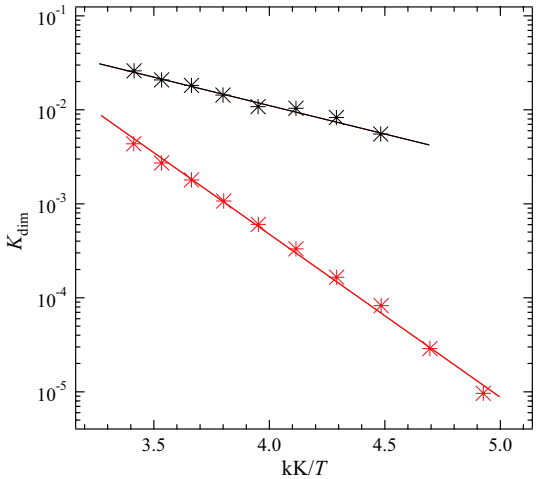

Figure 2.11. Semi-logarithmic plots of K_{dim} *vs.* the reciprocal temperature for dimerization of UO_2(saloph)-DMF (Eq. 2.1) in dichloromethane-d_2 (red) and chloroform-d (black).

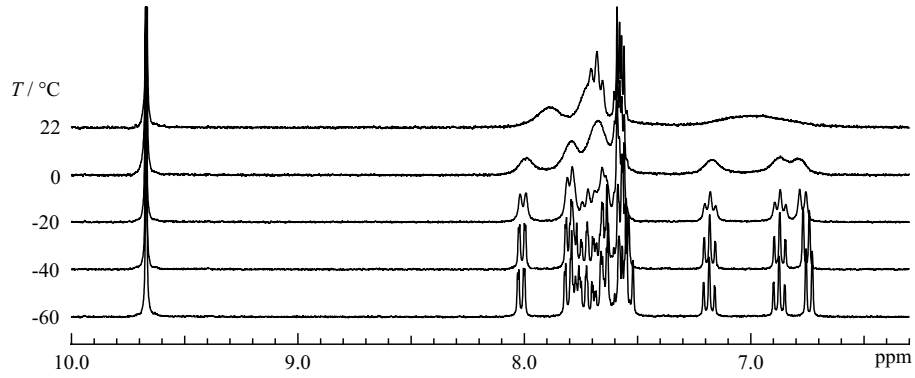

Figure 2.12. ^{1}H NMR spectra of $[UO_2(saloph)]_2$ in dichloromethane-d_2 at different temperatures.

system, respectively. The log K_{dim} values of both systems at 298 K from the ^{1}H NMR data are consistent with those from the UV-visible absorption spectral data in Figure 2.10.

The ^{1}H NMR spectra of $[UO_2(saloph)]_2$ in dichloromethane-d_2 were measured at different temperatures. The results are shown in Figure 2.12. The peak attributable to the azomethine group in $[UO_2(saloph)]_2$ appears at 9.67 ppm, which is much close to that at 9.66 ppm in Figure 2.7. Thus, it was confirmed that the assignment for the signal at 9.66 ppm to the azomethine group in $[UO_2(saloph)]_2$ described above is correct. The phenyl signals in the range from 6.7 to 8.0 ppm are well-resolved at −60°C. With elevating temperature, such signals are broadened and finally coalesced. This phenomenon means occurrence of the intramolecular exchange reaction between the enantiomers of $[UO_2(saloph)]_2$ as shown in Figure 2.13. According to Cort *et al.*,[175] it has been suggested that the monomeric UO_2(saloph) and its derivatives, which have not been identified in both solid and solution states, show the intramolecular exchange reactions through a flipping of the distorted saloph ligand. If such a flipping model is also true in the case of $[UO_2(saloph)]_2$, the bridged and non-bridged phenoxide groups in $[UO_2(saloph)]_2$ do not exchange each other as shown in Figure 2.14, *i.e.*, no aspects of the chemical exchange of the phenyl groups in $[UO_2(saloph)]_2$ should be observed in ^{1}H NMR spectra. Therefore, the flipping model cannot explain the experimental result observed in Figure 2.12. Another candidate for the exchange mechanism is the sliding model as shown in Figure 2.15. In this model, the bridged and non-bridged phenoxide groups exchange each other. As a result, the line-broadening of the phenyl signals as found in Figure 2.12 will be observed. Hence, the intramolecular exchange reaction of $[UO_2(saloph)]_2$

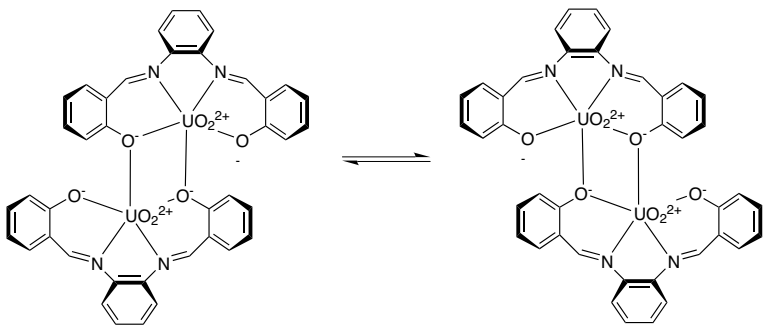

Figure 2.13. Scheme of intramolecular exchange between enantiomers of $[UO_2(saloph)]_2$.

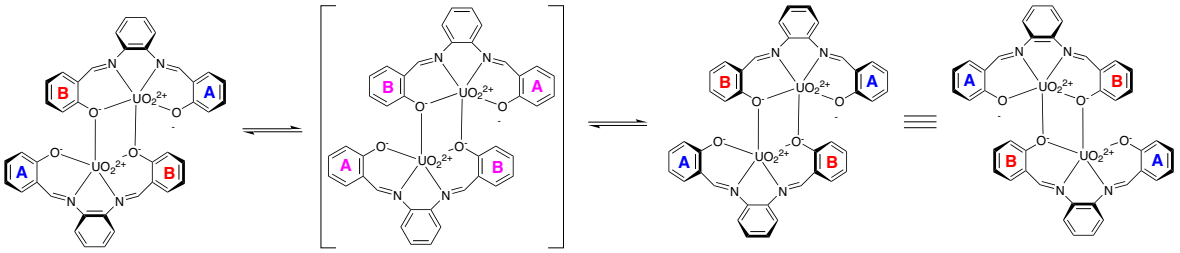

Figure 2.14. Scheme of flipping model for the intramolecular exchange in $[UO_2(saloph)]_2$. Red, blue, and purple colors of capital letters "A" and "B" mean bridged and non-bridged phenoxide groups and that in intermediate, respectively.

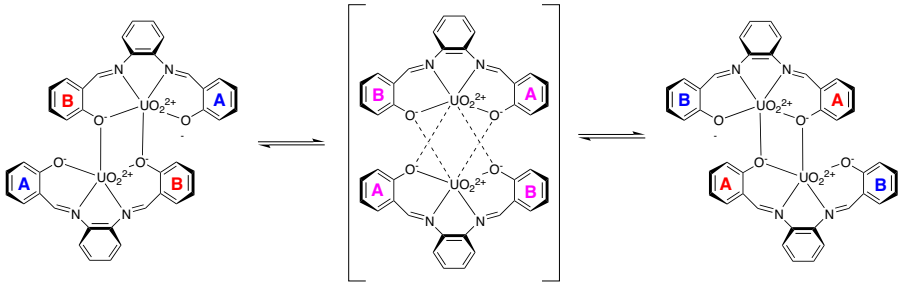

Figure 2.15. Scheme of sliding model for the intramolecular exchange in $[UO_2(saloph)]_2$. Red, blue, and purple colors of capital letters "A" and "B" mean bridged and non-bridged phenoxide groups and that in intermediate, respectively.

can be considered to proceed through the sliding model.

If the $UO_2(saloph)$ fragments in $[UO_2(saloph)]_2$ completely dissociate at the intermediate in the sliding mechanism, the competition between DMF and $UO_2(saloph)$ to enter another $UO_2(saloph)$ should take place. In this case, the azomethine signals of $UO_2(saloph)DMF$ and $[UO_2(saloph)]_2$ are no longer independent of the DMF exchange reaction in $UO_2(saloph)$-DMF. However, the NMR line-widths of the azomethine signals due to $UO_2(saloph)DMF$ and $[UO_2(saloph)]_2$ did not show any dependences on the DMF exchange reaction in UO_2-(saloph)DMF. Thus, the $UO_2(saloph)$ fragments in $[UO_2(saloph)]_2$ should bind each other even at the intermediate in Figure 2.15. The kinetic analysis for the intramolecular exchange reaction of $[UO_2(saloph)]_2$ observed in Figure 2.12 could not be performed, because the multiplet phenyl signals of $[UO_2(saloph)]_2$ are too complicated and it is undistinguishable which sites exchange each other.

Determining the mechanism of the DMF exchange reaction in $UO_2(saloph)DMF$ (Eq. 2.6) may also be a probe to valid this matter.

$$UO_2(saloph)DMF + DMF^* \overset{k_{ex}}{\rightleftharpoons} UO_2(saloph)DMF^* + DMF \tag{2.6}$$

where k_{ex} is the apparent first-order rate constant and the asterisk is a typographical distinction only. If this DMF exchange reaction in $UO_2(saloph)DMF$ proceeds through the dissociative mechanism and the $UO_2(saloph)$ fragments in $[UO_2(saloph)]_2$ are completely divided at the intermediate of its sliding intramolecular exchange (Figure 2.15), the azomethine signals at 9.39 and 9.66 ppm are no longer independent of the DMF exchange reaction.

To estimate the rate constant of the DMF exchange reaction in $UO_2(saloph)DMF$ (Eq. 2.6),

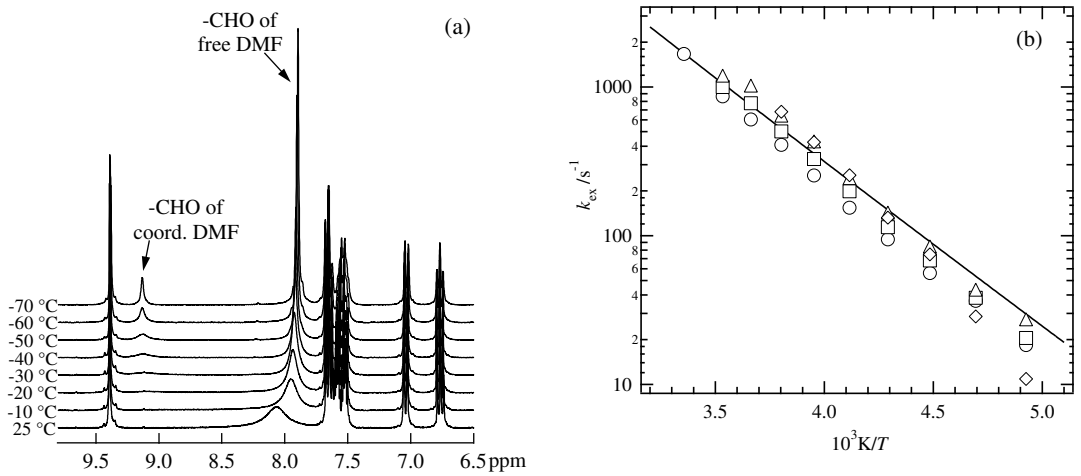

Figure 2.16. (a) ^{1}H NMR spectra of dichloromethane-d_2 solution containing UO_2(saloph)DMF (1.6×10^{-2} M) and DMF (1.02×10^{-1} M) measured at various temperatures and (b) temperature dependence of k_{ex}. Symbols; circle: [UO_2(saloph)DMF] = 1.37×10^{-2} M, [DMF] = 7.49×10^{-2} M; square: [UO_2(saloph)DMF] = 1.37×10^{-2} M, [DMF] = 1.12×10^{-1} M; triangle: [UO_2(saloph)DMF] = 1.37×10^{-2} M, [DMF] = 1.56×10^{-1} M; and diamond: [UO_2(saloph)DMF] = 1.6×10^{-2} M, [DMF] = 1.02×10^{-1} M. Smooth line is the best fit of Eq. 2.8 for the experimental data.

the NMR line-broadening method was utilized. The temperature dependences of the ^{1}H NMR spectra of the dichloromethane-d_2 solution containing UO_2(saloph)DMF (1.6×10^{-2} M) and free DMF (1.02×10^{-1} M) are shown in Figure 2.16(a). From the K_{dim} value of UO_2-(saloph)DMF in the dichloromethane system, the presence of [UO_2(saloph)]$_2$ in this system is negligible. To determine the mechanism of Eq. 2.6, the dependence of the NMR line-broadening on the DMF concentration was tested. The experimental NMR spectra involving the DMF exchange reaction in UO_2(saloph)DMF at the different temperatures were simulated by using *gNMR* program.[3] The resulting k_{ex} values from the NMR spectrum simulation are plotted in Figure 2.16(b). As can be seen from these plots, it seems likely that there are no remarkable dependences of k_{ex} on [DMF]. This indicates that Eq. 2.6 proceeds through a dissociative mechanism as shown in Eq. 2.7.

$$UO_2(saloph)DMF + DMF^* \xrightarrow{slow} UO_2(saloph) + DMF + DMF^* \xrightarrow{fast} UO_2(saloph)DMF^* + DMF \tag{2.7}$$

This fact also suggests that the UO_2(saloph) fragments in [UO_2(saloph)]$_2$ are not dissociated completely even at the intermediate in the sliding intramolecular exchange reaction of [UO_2-(saloph)]$_2$ (Figure 2.15) as described above. In the next section, the similar dissociative ligand exchange reaction was also observed in the system of the analogous uranyl(VI) saloph complex which contains dimethyl sulfoxide (DMSO) instead of DMF, UO_2(saloph)DMSO. The details of UO_2(saloph)DMSO will be discussed later.

The k_{ex} value of Eq. 2.7 is expressed by Eyring equation (Eq. 2.8).

$$k_{ex} = \frac{k_B T}{h} \exp\left(-\frac{\Delta H^{\ddagger}}{R} \cdot \frac{1}{T} + \frac{\Delta S^{\ddagger}}{R}\right) \tag{2.8}$$

[3]The program, *gNMR*,[176] uses the standard Liouville representation of quantum mechanics to evaluate dynamic NMR spectra, as described by Binsch.[177] This formalism easily lends itself to treatment of general inter- and intra-molecular permutations of nuclei.

where k_B, h, $\Delta H^{\ddagger}$, and $\Delta S^{\ddagger}$ are the Boltzmann constant (1.3807×10^{-23} J·K^{-1}), the Planck constant (6.6261×10^{-34} J·s), the activation enthalpy, and the activation entropy, respectively. The least-squares fit of Eq. 2.8 to the experimental plots shown in Figure 2.16(b) gave the activation parameters of Eq. 2.7 as $\Delta H^{\ddagger} = 19 \pm 1$ kJ·mol^{-1} and $\Delta S^{\ddagger} = -118 \pm 4$ J·mol^{-1}·K^{-1}. The large negative value of $\Delta S^{\ddagger}$ of Eq. 2.7 might be caused by a rearrangement of solvent molecules around UO_2(saloph) and the dissociated DMF. The k_{ex} value at 298 K for the DMF exchange reaction in UO_2(saloph)DMF was calculated as 1.68×10^3 s^{-1}.

Consequently, the whole reaction mechanisms starting from UO_2(saloph)DMF in dichloromethane and chloroform solutions are depicted in Figure 2.17.

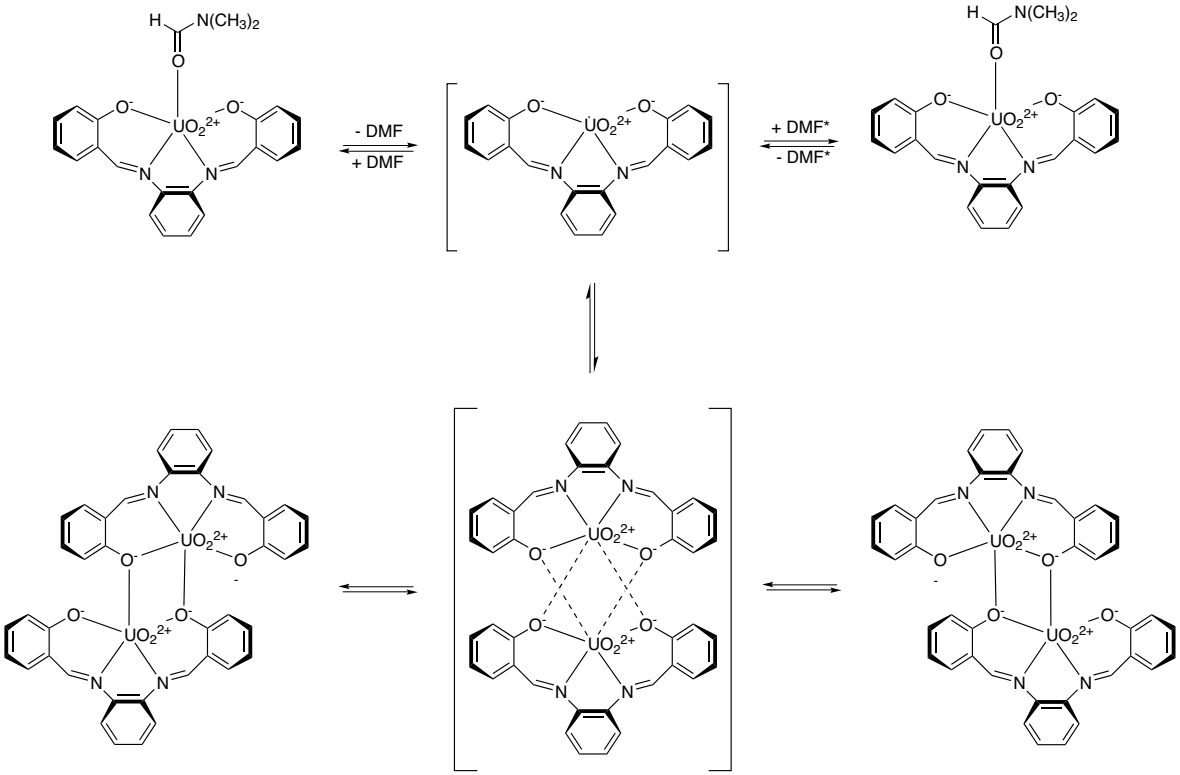

Figure 2.17. Whole reaction mechanism starting from UO_2(saloph)DMF including the DMF exchange (Eq. 2.7), the dimerization (Eq. 2.1), and the intramolecular exchange between the enantiomers of [UO_2-(saloph)]$_2$ (Figure 2.15) in dichloromethane and chloroform solutions.

2.3 UO_2(saloph)DMSO

2.3.1 Experimental Details

Synthesis of UO_2(saloph)DMSO. This uranyl(VI) complex was synthesized by the same procedure as that of UO_2(saloph)DMF, in which DMF was replaced by dimethyl sulfoxide (DMSO, Wako Pure Chemical Ind., Ltd.). Single crystals of UO_2(saloph)DMSO for X-ray crystallography were obtained from a DMSO solution containing UO_2(saloph)DMSO.

Other Materials. Dichloromethane-d_2 (ACROS, 99.8 atom% D) and chloroform-*d* (ACROS, 99.8 atom% D) were used for NMR measurements without further purification. All other chemicals used in this section were of reagent grade.

Methods. Characterization of UO_2(saloph)DMSO was performed by using the IR spectrophotometer, the NMR spectrometer, and the single crystal X-ray diffractmeter in the similar manners to Section 2.2.

In the X-ray crystallography, the weighing scheme for the refinement of UO_2(saloph)-DMSO by SHELXL-97[166] was $w = 1/[\sigma^2 F_o^2 + (0.0356P)^2 + 4.8982P]$ ($P = F_o^2 + 2F_c^2)/3$). The maximum (minimum) peaks on the final difference Fourier maps for UO_2(saloph)DMSO corresponded to 0.955 (−0.918) $e^- \cdot Å^{-3}$. Crystal data and other data collection parameters are summarized in Tables 2.3. The crystallographic information of UO_2(saloph)DMSO is in Appendix D.

2.3.2 Results and Discussion

The IR spectrum of UO_2(saloph)DMSO in KBr (Figure 2.18) showed the characteristic peaks at 897, 999, and 1605 cm^{-1}, which were assigned to the ν_3 of the uranyl(VI) moiety, S=O stretching of DMSO, and the C=N stretching of saloph, respectively. The C=N stretching of saloph indicates its coordination to uranyl(VI) ion as well as UO_2(saloph)DMF. It is known that the DMSO molecule is an ambidentate ligand. According to Nakamoto,[160] the

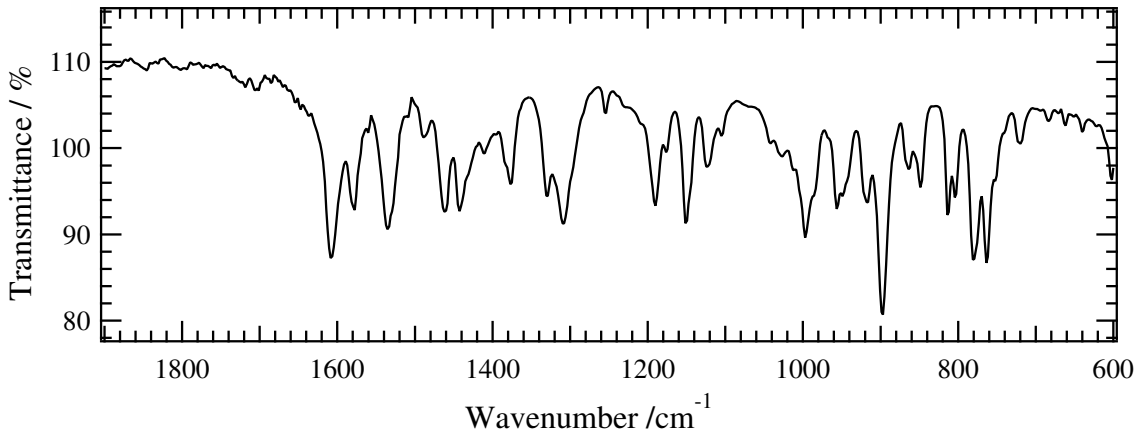

Figure 2.18. IR spectrum of UO_2(saloph)DMSO in KBr.

Table 2.3. Crystallographic data of UO_2(saloph)DMSO

Empirical formula	$C_{22}H_{20}N_2O_5SU$	Temparature (°C)	−160.0
Formula weight	662.50	D_{calc} (g·cm^{-3})	2.047
Crystal system	monoclinic	Crystal size (mm)	0.27 × 0.15 × 0.07
Space group	$P2_1$ (#4)	Crystal color and shape	yellow, block
a (Å)	13.303(7)	F_{000}	1256
b (Å)	9.422(4)	$2\theta_{max}$ (°)	55.0
c (Å)	17.205(8)	Observed data	9110
β (°)	94.45(5)	R [a]	0.0267
V (Å^3)	2149.9(17)	wR [b]	0.0677
Z	4	S (Goodness of fit) [c]	1.088

[a] $R = \Sigma||F_o| - |F_c||/\Sigma|F_o|$, [b] $wR = [\Sigma(w(F_o^2 - F_c^2)^2)/\Sigma w(F_o^2)^2]^{1/2}$, [c] $S = [\Sigma w(F_o^2 - F_c^2)^2/(N_o - N_v)]^{1/2}$, $w = 1/[\sigma^2 F_o^2 + (0.0356P)^2 + 4.8982P)]$ where $P = (F_o^2 + 2F_c^2)/3)$

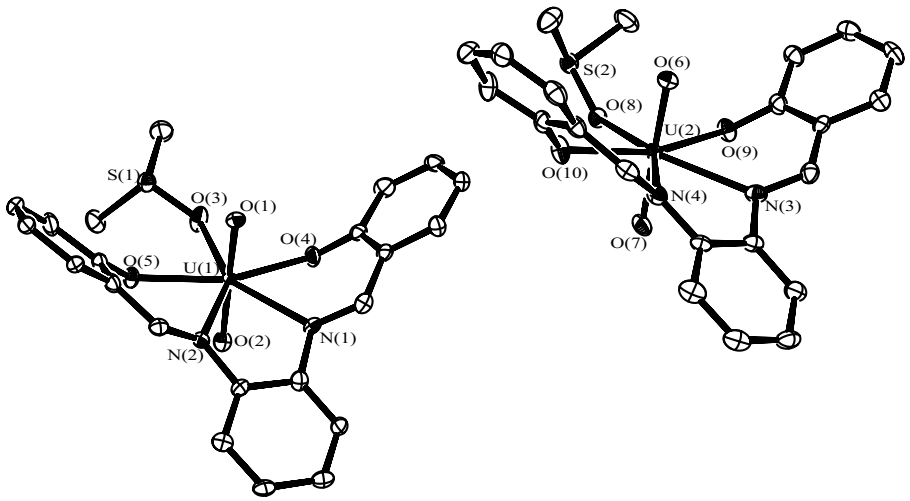

Figure 2.19. ORTEP view of asymmetric unit of UO_2(saloph)DMSO. Probability: 50%. Bond distances (Å); U(1)–O(1), 1.780(4), U(1)–O(2), 1.788(5), U(1)–O(3), 2.416(4), U(1)–O(4), 2.255(4), U(1)–O(5), 2.274(4), U(1)–N(1), 2.541(5), U(1)–N(2), 2.545(5), U(2)–O(6), 1.781(4), U(2)–O(7), 1.784(5), U(2)–O(8), 2.408(4), U(2)–O(9), 2.270(4), U(2)–O(10), 2.276(4), U(2)–N(3), 2.580(5), U(2)–N(4), 2.551(5).

coordination of DMSO through its oxygen atom to a metal ion shows the S=O stretching at lower frequency than that of the free DMSO at 1055~1100 cm^{-1}. Therefore, the observed S=O stretching of DMSO at 999 cm^{-1} indicates its coordination through the oxygen atom to the uranyl(VI) ion.

The single crystal X-ray analysis for UO_2(saloph)DMSO was performed to obtain its molecular structure. The crystallographic data and ORTEP view of UO_2(saloph)DMSO are shown in Table 2.3 and Figure 2.19, respectively. The geometry around the uranium atom in UO_2(saloph)DMSO is also pentagonal bipyramidal. The U=O bond lengths in the axial O=U=O moiety, U(1)–O(1): 1.780(4), U(1)–O(2): 1.788(5), U(2)–O(6): 1.781(4), and U(2)–O(7): 1.784(5) Å, are usual. Furthermore, the bond distances between the donor atoms in saloph and the center uranium and the distortion of saloph in UO_2(saloph)DMSO are quite similar to those in UO_2(saloph)DMF. The bond distance between the oxygen atom in the unidentate ligand (DMSO) and the uranium is 2.416(4) or 2.408(4) Å, which is comparable with that in UO_2(saloph)DMF. It is likely that there are no remarkable differences

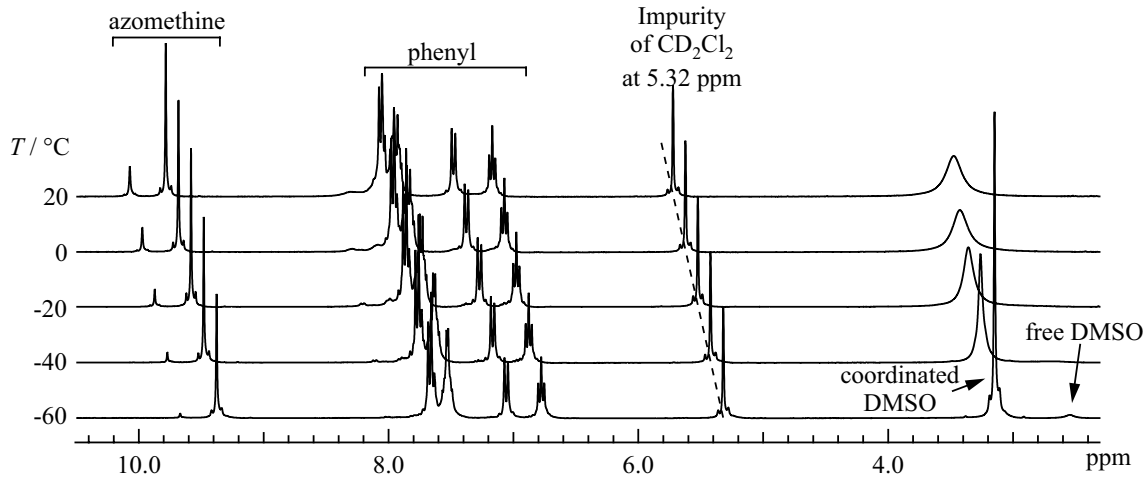

Figure 2.20. ^{1}H NMR spectra of dichloromethane-d_2 solution dissolving UO_2(saloph)DMSO at various temperatures.

between the coordination strengths of DMSO and DMF to the UO_2(saloph) fragment from a viewpoint of the bond length.

To examine whether the dimerization of UO_2(saloph)DMSO preceded by the DMSO dissociation also occurs in dichloromethane and chloroform systems, the ^{1}H NMR spectra of solutions dissolving UO_2(saloph)DMSO were measured at various temperatures. The results for the dichloromethane-d_2 solution are shown in Figure 2.20. As a result, the quite similar spectral features to Figure 2.7 were observed, *i.e.*, the presence of the DMSO dissociated uranyl(VI) species and the DMSO exchange reaction in UO_2(saloph)DMSO. The methyl signals of the free and coordinated DMSO were detected at 2.54 and 3.14 ppm, respectively. Two signals due to the azomethine group in the coordinated saloph appeared at 9.38 and 9.67 ppm. Because of the consistencies of the peak area ratios, the former corresponds to UO_2(saloph)DMSO, and the latter can be assigned to the DMSO dissociated uranyl(VI) species. The intensities of the azomethine signals depend on the temperature. Whereas, their line-widths do not change remarkably in spite of the DMSO exchange reaction in UO_2-(saloph)DMSO. Furthermore, the red crystals of $[UO_2(saloph)]_2$ were also obtained from the dichloromethane solution dissolving UO_2(saloph)DMSO. The same phenomena were also confirmed in the chloroform system dissolving UO_2(saloph)DMSO. Needless to say, the most probable candidate of the DMSO dissociated uranyl(VI) species is $[UO_2(saloph)]_2$. This is supported by the chemical shift of its azomethine signal at 9.67 ppm which agrees with that of $[UO_2(saloph)]_2$ shown in Figure 2.12. Hence, the following equilibrium should be presented in this system.

$$2UO_2(saloph)DMSO \rightleftarrows [UO_2(saloph)]_2 + 2DMSO \tag{2.9}$$

$$K_{dim} = \frac{[[UO_2(saloph)]_2]\,[DMSO]^2}{[UO_2(saloph)DMSO]^2} \tag{2.10}$$

The dependence of the UV-visible absorption spectra on the free DMSO concentration were measured in a similar manner to Figure 2.10. The resulting spectra of the dichloromethane and chloroform solutions are shown in Figure 2.21. The isosbestic points were confirmed at 297 and 382 nm in Figure 2.10(a), and 295 and 383 nm in Figure 2.10(b). The

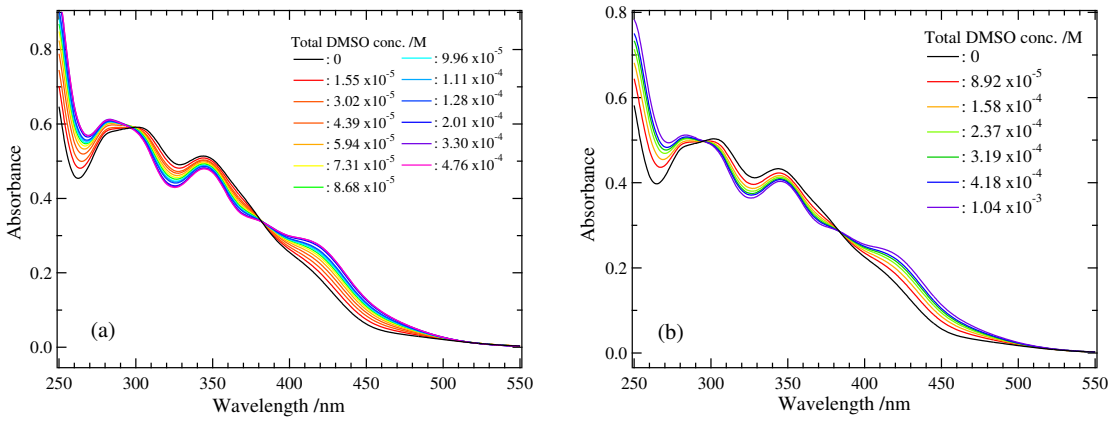

Figure 2.21. UV-visible absorption spectra of (a) dichloromethane and (b) chloroform solutions containing $[UO_2(saloph)]_2$ ((a): 1.26×10^{-5} M, (b): 1.15×10^{-5} M) and various total concentration of DMSO ((a): $0 \sim 4.76 \times 10^{-4}$ M, (b): $0 \sim 1.04 \times 10^{-3}$ M) at 298 K.

K_{dim} values in Eq. 2.10 were evaluated by using the absorbancies at 430 nm in Figure 2.21. The resulting K_{dim} ($\log K_{dim}$) values at 298 K were $(5.3 \pm 0.8) \times 10^{-5}$ M (-4.28 ± 0.06) for the dichloromethane system and $(8.2 \pm 1.4) \times 10^{-4}$ M (-3.09 ± 0.08) for the chloroform one.

The thermodynamic parameters for Eq. 2.9 were estimated by using Eq. 2.5 and the concentrations of UO_2(saloph)DMSO, $[UO_2(saloph)]_2$, and the free DMSO derived from the peak areas in Figure 2.20. The van't Hoff plots for the dimerization of UO_2(saloph)DMSO in dichloromethane-d_2 and chloroform-d are shown in Figure 2.22. Consequently, the values of ΔH_{dim}, ΔS_{dim}, and $\log K_{dim}$ at 298 K for Eq. 2.9 were calculated as 39 ± 1 kJ·mol^{-1}, 52 ± 6 J·mol^{-1}·K^{-1}, and -4.0 ± 0.5 for the dichloromethane system and 22 ± 1 kJ·mol^{-1}, 14 ± 4 J·mol^{-1}·K^{-1}, and -3.1 ± 0.3 for the chloroform system, respectively. The $\log K_{dim}$ values of both systems at 298 K showed the agreements with those obtained from the UV-visible absorption spectra.

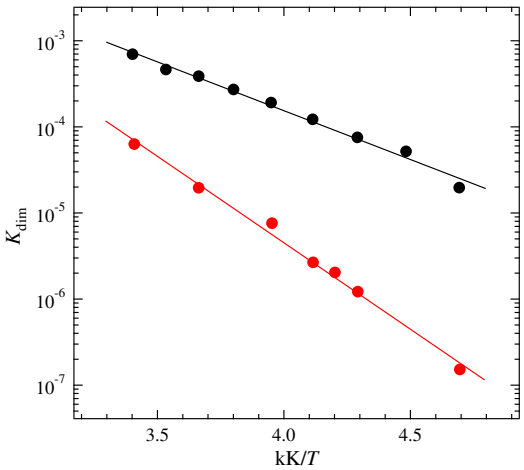

Figure 2.22. Semi-logarighmic plots of K_{dim} *vs.* reciprocal temperature for dimerization of UO_2(saloph)DMSO (Eq. 2.9) in dichloromethane-d_2 (red) and chloroform-d (black).

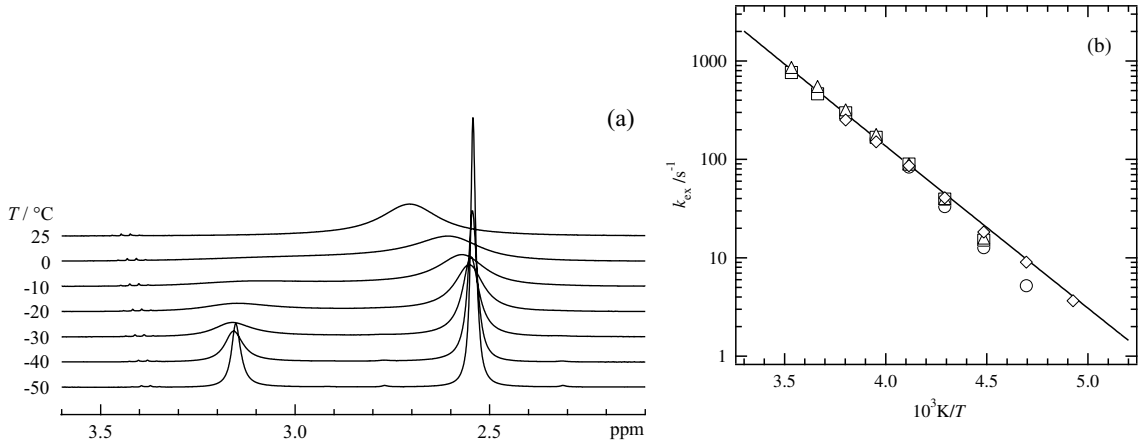

Figure 2.23. (a) ^{1}H NMR spectra of dichloromethane-d_2 solution containing UO_2(saloph)DMSO (1.37×10^{-2} M) and DMSO (3.29×10^{-2} M) measured at various temperatures and (b) temperature dependences of k_{ex}. [UO_2(saloph)DMSO] = 1.37×10^{-2} M (fixed). Symbols; circle: [DMSO] = 3.29×10^{-2} M; square: [DMSO] = 5.89×10^{-2} M; diamond: [DMSO] = 7.30×10^{-2} M; and triangle: [DMSO] = 8.77×10^{-2} M. Smooth line is the best fit of Eq. 2.8 for the experimental data.

Further support for validity of Eq. 2.9 can be obtained by determining the mechanism of the DMSO exchange reaction in UO_2(saloph)DMSO (Eq. 2.11) observed in Figure 2.20.

$$UO_2(\text{saloph})\text{DMSO} + \text{DMSO}^* \overset{k_{ex}}{\rightleftharpoons} UO_2(\text{saloph})\text{DMSO}^* + \text{DMSO} \qquad (2.11)$$

where the asterisk is a typographical distinction only. If the exchange reaction of DMSO in UO_2(saloph)DMSO proceeds through the dissociative mechanism and the DMSO dissociated uranyl(VI) species is the monomeric one, UO_2(saloph), the azomethine signals at 9.38 and 9.67 ppm are no longer independent of the DMSO exchange reaction. Thus, to determine the mechanism of Eq. 2.11, dependences of the k_{ex} value on the temperature and DMSO concentration were examined. The typical ^{1}H NMR spectra of the dichloromethane-d_2 solution containing UO_2(saloph)DMSO (1.37×10^{-2} M) and DMSO (3.29×10^{-2} M) at various temperatures are shown in Figure 2.23(a). The resulting NMR spectra at the different DMSO concentration (3.29×10^{-2}, 5.89×10^{-2}, 7.30×10^{-2}, and 8.77×10^{-2} M) were analyzed by using *gNMR* computer program.[176] The temperature dependence of k_{ex} at the different DMSO concentrations are plotted in Figure 2.23(b). As can be seen from these plots, it is obvious that there are no dependences of k_{ex} in Eq. 2.11 on the DMSO concentration. This result indicates that the DMSO exchange reaction in UO_2(saloph)DMSO proceeds through the dissociative mechanism as follows (Eq. 2.12).

$$\begin{aligned} UO_2(\text{saloph})\text{DMSO} + \text{DMSO}^* &\overset{\text{slow}}{\longrightarrow} \\ UO_2(\text{saloph}) + \text{DMSO} + \text{DMSO}^* &\overset{\text{fast}}{\longrightarrow} \\ UO_2(\text{saloph})\text{DMSO}^* + \text{DMSO} \end{aligned} \qquad (2.12)$$

Therefore, the possibility of the monomeric UO_2(saloph) as the DMSO dissociated uranyl(VI) species has been neglected completely, and the validity of Eq. 2.9 has been confirmed consequently. By using the Eyring equation (Eq. 2.8) and the data in Figure 2.23(b), the activation parameters, $\Delta H^{\ddagger}$ and $\Delta S^{\ddagger}$, of Eq. 2.12 were evaluated as 29.7 ± 0.8 kJ·mol^{-1} and

-83 ± 3 J·mol^{-1}·K^{-1}, respectively. The negative value of $\Delta S^{\ddagger}$ of Eq. 2.12 might be caused by a rearrangement of solvent molecules around UO_2(saloph) and the dissociated DMSO at the transition state. The k_{ex} at 298 K was calculated as 1.63×10^3 s^{-1} by using Eq. 2.8.

In a comparison between the k_{ex} values in both systems of UO_2(saloph)DMSO (1.63×10^3 s^{-1}) and UO_2(saloph)DMF (1.68×10^3 s^{-1}), no significant difference is found. However, the $\Delta H^{\ddagger}$ value of Eq. 2.12 (29.7 ± 0.8 kJ·mol^{-1}) is larger than that of Eq. 2.7 (19 ± 1 kJ·mol^{-1}). Furthermore, the equilibrium constants (K_{dim}) of the dimerization of UO_2(saloph)DMSO (Eq. 2.9) were found to be smaller than those of UO_2(saloph)DMF (Eq. 2.1) in both dichloromethane and chloroform systems. Such differences in $\Delta H^{\ddagger}$ and K_{dim} indicate that DMSO coordinates to the UO_2(saloph) fragment more strongly than DMF.

2.4 $UO_2(dbm)_2DMSO$

2.4.1 Experimental Details

Synthesis of $UO_2(dbm)_2DMSO$. Dibenzoylmethane (0.5 g, Hdbm, Kanto, see Figure 2.24) and $UO_2(NO_3)_2{\cdot}nH_2O$ were mixed in EtOH (20 ml) with vigorous stirring and heating. After refluxing for 3 h in the dark, water (40 ml) was added into this reaction mixture. The resulting orange precipitate was collected by filtration. This orange powder was dissolved in hot EtOH, and then DMSO (1 ml) was added with stirring. Water was mixed with this solution until precipitate was produced. The golden yellow powder of $UO_2(dbm)_2DMSO$ was filtered off, washed by EtOH and ether, and dried under vacuum. The product was recrystallized from dichloromethane and *n*-pentane. Single crystals of $UO_2(dbm)_2DMSO$ for X-ray crystallography were obtained from its dichloromethane solution with slow evaporation at 0°C.

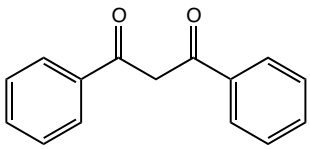

Figure 2.24. Schematic structure of *keto*-form of dibenzoylmethane (Hdbm).

Other Materials. Dichloromethane-d_2 (ACROS, 99.8 atom% D) was used for NMR measurements without further purification. All other chemicals used in this section were of reagent grade.

Methods. Characterization of $UO_2(dbm)_2DMSO$ was performed by using the IR spectrophotometer, the NMR spectrometer, and the single crystal X-ray diffractmeter in the similar manners to Section 2.2.

In the X-ray crystallography, the weighing scheme for the refinement of $UO_2(dbm)_2DMSO$ by SHELXL-97[166] was $w = 1/[\sigma^2F_o^2 + (0.0312P)^2 + 38.5857P]$ ($P = F_o^2 + 2F_c^2)/3$). The maximum (minimum) peaks on the final difference Fourier maps for $UO_2(dbm)_2DMSO$ corresponded to 1.481 (−1.404) $e^-{\cdot}Å^{-3}$. Crystal data and other data collection parameters are summarized in Tables 2.4. The crystallographic information of $UO_2(dbm)_2DMSO$ is in Appendix E.

2.4.2 Results and Discussion

The IR spectrum of $UO_2(dbm)_2DMSO$ in KBr is shown in Figure 2.25. The characteristic peaks due to the ν_3 in the uranyl(VI) moiety, S=O stretching in DMSO, C=O and C=C stretchings in dbm were observed at 906, 1000, 1537, and 1590 cm^{-1}, respectively.[160] These IR peaks suggest the coordination of dbm and DMSO through its oxygen atom to the uranyl(VI) ion.

The crystallographic data of $UO_2(dbm)_2DMSO$ were summarized in Table 2.4. Figure 2.26 shows the ORTEP view of the asymmetric unit of $UO_2(dbm)_2DMSO$. From this figure, it was found that $UO_2(dbm)_2DMSO$ also has the pentagonal bipyramidal geometry

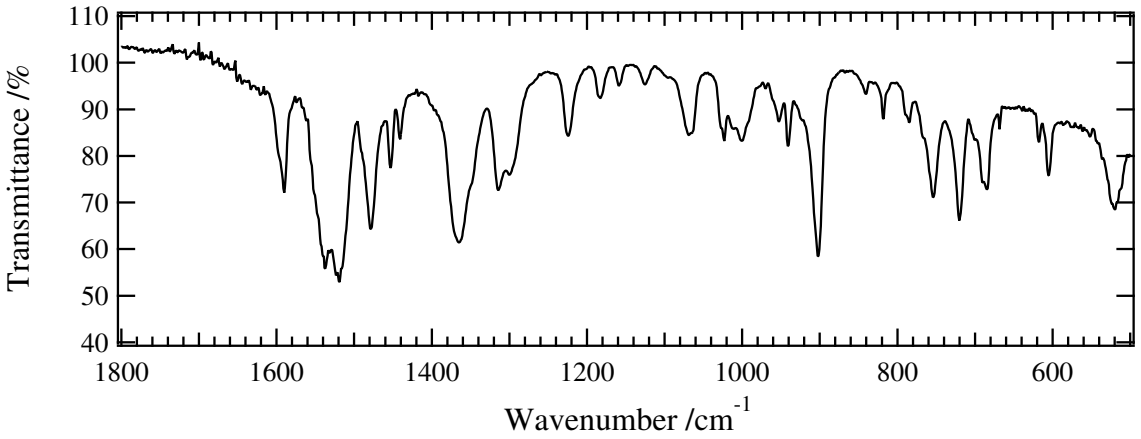

Figure 2.25. IR spectrum of $UO_2(dbm)_2DMSO$ in KBr.

which consists of two molecules of dibenzoylmethanate (dbm) and one molecule of DMSO around the axial uranyl(VI) ion. Such a structure is quite similar to the analogous complexes ($UO_2(dbm)_2L$, L = benzylmethyl sulfoxide, dibenzyl sulfoxide, diphenyl sulfoxide, and (±)camphor) reported by Kannan *et al.*[19, 21] The U=O bond lengths in the uranyl(VI) moiety are U(1)–O(1): 1.789(5), U(1)–O(2): 1.791(5), U(2)–O(8): 1.768(5), and U(2)–O(9): 1.788(6) Å, which are the usual values. In the equatorial plane, the bond distances between the oxygen atoms in dbm and the center uranium (U(1)–O(4), U(1)–O(5), U(1)–O(6), U(1)–O(7), U(2)–O(11), U(2)–O(12), U(2)–O(13), and U(2)–O(14)) are quite similar each other, 2.34–2.36 Å. The bond distance between the oxygen atom in DMSO and the uranium atom is U(1)–O(3): 2.435(6) or U(2)–O(10): 2.440(5) Å, which is slightly longer than that in UO_2(saloph)DMSO (2.41–2.42 Å).

It is necessary to confirm whether $UO_2(dbm)_2DMSO$ in solution also shows some reactions in a similar manner to UO_2(saloph)DMF and UO_2(saloph)DMSO or not. Thus, the ^1H NMR spectra of the dichloromethane-d_2 solution dissolving $UO_2(dbm)_2DMSO$ were measured at various temperatures. The results are shown in Figure 2.27. The sharp singlet signal due to the methyl group of DMSO was observed at 3.12 ppm (6H). Since the free DMSO

Table 2.4. Crystallographic data of $UO_2(dbm)_2DMSO$

Empirical formula	$C_{32}H_{28}O_7SU$	D_{calc} (g·cm^{-3})	1.835
Formula weight	794.63	Crystal size (mm)	0.10 × 0.10 × 0.10
Crystal system	orthorhombic	Crystal color and shape	yellow, block
Space group	$Pna2_1$ (#33)	F_{000}	3072.00
a (Å)	16.090(6)	$2\theta_{max}$ (°)	55.0
b (Å)	9.975(3	Observed data	13170
c (Å)	35.845(8)	R [a]	0.0340
V (Å^3)	5753(3)	wR [b]	0.0776
Z	8	S (Goodness of fit) [c]	1.024
Temparature (°C)	−180.0		

[a] $R = \Sigma||F_o| - |F_c||/\Sigma|F_o|$, [b] $wR = [\Sigma(w(F_o^2 - F_c^2)^2)/\Sigma w(F_o^2)^2]^{1/2}$, [c] $S = [\Sigma w(F_o^2 - F_c^2)^2/(N_o - N_v)]^{1/2}$, $w = 1/[\sigma^2 F_o^2 + (0.0312P)^2 + 38.5857P)]$ where $P = (F_o^2 + 2F_c^2)/3)$

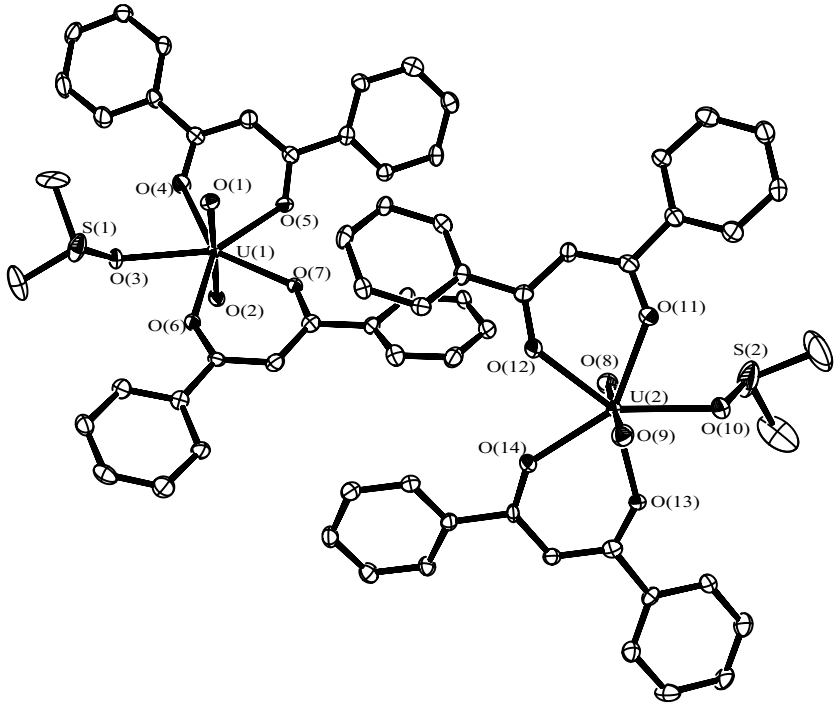

Figure 2.26. ORTEP view of asymmetric unit of $UO_2(dbm)_2DMSO$. Probability: 50%. Bond distances (Å); U(1)–O(1): 1.789(5), U(1)–O(2): 1.791(5), U(1)–O(3): 2.435(6), U(1)–O(4): 2.350(6), U(1)–O(5): 2.337(5), U(1)–O(6): 2.348(5), U(1)–O(7): 2.346(5), U(2)–O(8): 1.768(5), U(2)–O(9): 1.788(6), U(2)–O(10): 2.440(5), U(2)–O(11): 2.340(6), U(2)–O(12): 2.361(5), U(2)–O(13): 2.351(5), U(2)–O(14): 2.346(5).

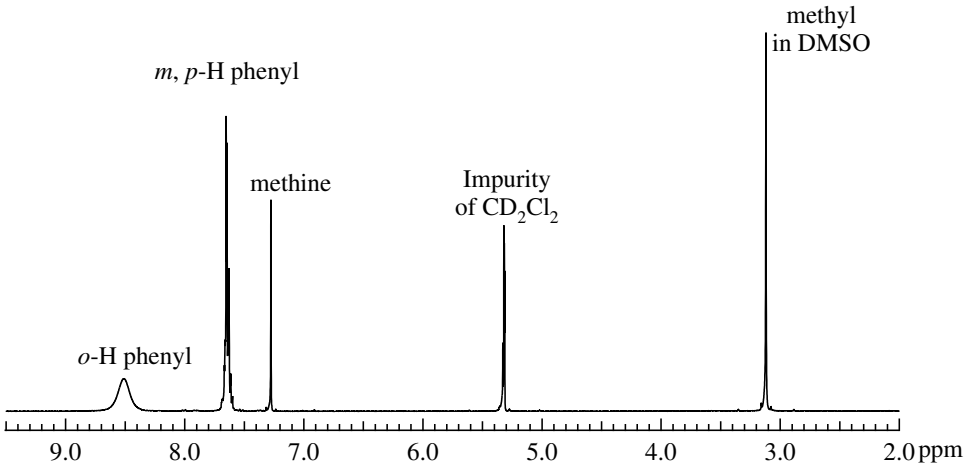

Figure 2.27. ^1H NMR spectra of dichloromethane-d_2 solution dissolving $UO_2(dbm)_2DMSO$ at room temperature.

shows its signal at 2.54 ppm and the broad peak in Figure 2.20 of Section 2.3 is the result of the DMSO exchange reaction in UO_2(saloph)DMSO, a sharp signal of DMSO at 3.12 ppm indicates that the DMSO molecule coordinates to the $UO_2(dbm)_2$ fragment strongly even in the dichloromethane solution.

For the dbm ligands in $UO_2(dbm)_2DMSO$, the methine group showed the sharp singlet

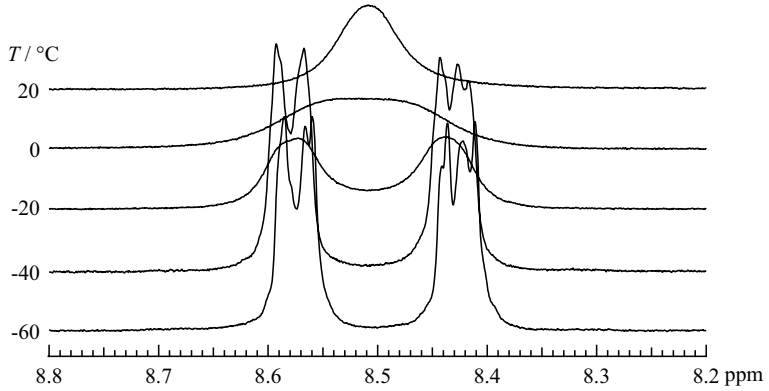

Figure 2.28. ^{1}H NMR spectra of $UO_2(dbm)_2DMSO$ in dichloromethane-d_2 focused on the signals due to the *o*-proton in dbm.

signal at 7.28 ppm (2H). Furthermore, the sharp signals due to the protons of the phenyl groups at *m*- and *p*-positions also appeared at in the range of 7.60–7.70 ppm as multiplet peaks (12H). On the other hand, the *o*-protons of the phenyl groups were observed at 8.51 ppm (8H) as a broad signal. Such features may suggest the dynamic behavior of dbm, especially concerning the *o*-protons, in $UO_2(dbm)_2DMSO$. Thus, the temperature dependence of the ^{1}H NMR spectra was measured. The results are shown in Figure 2.28. Since there were no remarkable changes of the signals except for that of *o*-proton with the temperature variation, this figure focuses on the *o*-proton signals in the region from 8.2 to 8.8 ppm. With a decrease in the temperautre from 20 to −20°C, the signal of *o*-protons was split into two peaks, and in the temperature below −20°C, these two signals were further split into the multiplet peaks. The first splitting shows that there are two distinguishable sites in this temperature range (20 ∼ −20°C). The second splitting below −20°C indicates that the multiplet signals are involved in the two signals at −20°C. From the splitting schemes, the reaction mechanism corresponding to the first step may be the intramolecular exchange reaction of the phenyl ring position nearer to and further from the coordinated DMSO. Presence of such a reaction has already been confirmed in the systems of the analogous uranyl(VI) bis(*β*-diketonato) complexes, $UO_2(acac)_2L$ (acac = acetylacetonato, L = DMSO, DMF, and *N*,*N*-diethylformamide) and UO_2(1,1,1-trifluoroacetylacetonato)$_2$THF (THF = tetrahydrofuran).[79, 80] The intramolecular reactions of these uranyl(VI) complexes are proposed to be initiated by the L dissociation. For the reaction mechanism of the second step (−20 ∼ −60°C), the phenyl ring rotation will be most probable. The schematic mechanisms of $UO_2(dbm)_2DMSO$ are shown in Figure 2.29. Unfortunately, it was difficult to perform the kinetic analysis for the behavior of the *o*-protons themselves in dbm, because their NMR signals are essentially complicated multiplets as shown in Figure 2.28 at −60°C. Limiting the first step in Figure 2.28, the apparent first-order rate constant of the intramolecular exchange reaction (k_{intra}) at the coalescence temperature (0°C) was evaluated as 9.2×10^1 s^{-1} by Eq. 2.13.

$$k_{intra} = \frac{\pi \delta \nu}{\sqrt{2}} \tag{2.13}$$

where $\delta\nu$ is the peak separation between two sites in s^{-1}.

Ikeda *et al.*[80] have determined the reaction mechanism of such an intramolecular exchange in $UO_2(acac)_2L$ by relating it with the L exchange reactions. According to them, the

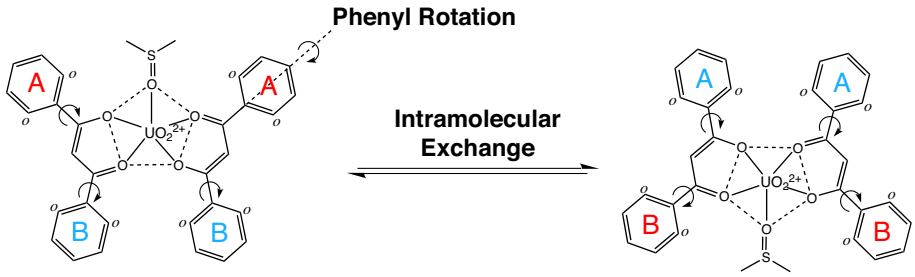

Figure 2.29. Scheme of intramolecular exchange of the phenyl ring positions and the rotation of the phenyl ring. Red and blue colors of the capital letters "A" and "B" indicate the phenyl groups nearer to and further from the coordination site for DMSO, respectively.

L exchange reaction proceed through the dissociative mechanism and the uranyl(VI) species at the intermediate of the intramolecular exchange should also be the L dissociated one such as $UO_2(acac)_2$. In that case, the free L molecule can coordinate to both sides of $UO_2(acac)_2$ at the transition state. Since the coordination sites for L in $UO_2(acac)_2$ should be equivalent, the probabilities of the re-coordination of L to either vacant sites in the intermediate must be equal. Therefore, the rate constant of the intramolecular exchange in $UO_2(acac)_2L$ should be one half of that of the L exchange reaction. Actually, their proposal has been evidenced in the experiments. This theory can also be applied to the present system of $UO_2(dbm)_2DMSO$.

To confirm the reaction mechanism shown in Figure 2.29, the following DMSO exchange reaction in $UO_2(dbm)_2DMSO$ were studied.

$$U^{VI}O_2(dbm)_2DMSO + DMSO^* \overset{k_{ex}}{\rightleftharpoons} U^{VI}O_2(dbm)_2DMSO^* + DMSO \qquad (2.14)$$

where the asterisk is a typographical distinction only. If the rate-determining step of the intramolecular exchange in $UO_2(dbm)_2DMSO$ is the dissociation of the coordinated DMSO and the DMSO exchange reaction in $UO_2(dbm)_2DMSO$ occurs in the dissociative mechanism, one half of the k_{ex} value at 273 K will equals to k_{intra} (9.2×10^1 s^{-1}). Thus, the dependences of the ^1H NMR spectrum of $UO_2(dbm)_2DMSO$ (1.3×10^{-2} M) on the temperature and concentration of the free DMSO (2.8×10^{-2}, 4.6×10^{-2}, and 6.7×10^{-2} M)

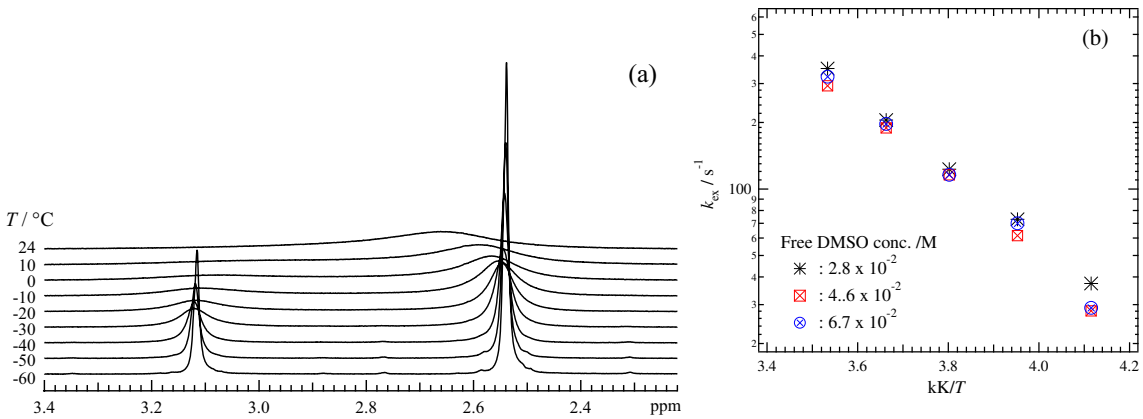

Figure 2.30. (a) ^1H NMR spectra of dichloromethane-d_2 solution containing $UO_2(dbm)_2DMSO$ (1.3×10^{-2} M) and DMSO (2.8×10^{-2} M) measured at different temperatures and (b) temperature dependence of k_{ex}.

were measured for $UO_2(dbm)_2DMSO$ in dichloromethane-d_2. The typical NMR spectra are shown in Figure 2.30(a). The k_{ex} values were obtained by simulating the spectra using *gNMR* program[176] and plotted against the reciprocal temperatures. The results are shown in Figure 2.30(b). The k_{ex} value at each temperature was found to be independent of the DMSO conccentration, indicating the dissociative mechanism of the DMSO exchange reaction in $UO_2(dbm)_2DMSO$ as follows.

$$\begin{aligned} UO_2(dbm)_2DMSO + DMSO^* &\xrightarrow{\text{slow}} \\ UO_2(dbm)_2 + DMSO + DMSO^* &\xrightarrow{\text{fast}} \\ UO_2(dbm)_2DMSO^* + DMSO & \end{aligned} \qquad (2.15)$$

By using Eq. 2.8, the activation parameters, $\Delta H^{\ddagger}$ and $\Delta S^{\ddagger}$, for Eq. 2.15 were evaluated as 30 ± 2 kJ·mol^{-1} and -88 ± 5 J·mol^{-1}·K^{-1}, respectively. The k_{ex} values at 273 K was calculated as 2.0×10^2 s^{-1}. As a result, one half of k_{ex} at 273 K is almost comparable with k_{intra} at the same temperature (9.2×10^1 s^{-1}). Therefore, it can be suggested that the intramolecular exchange reaction in $UO_2(dbm)_2DMSO$ occurs through the formation of the intermediate such as $UO_2(dbm)_2$.

Interestingly, with addition of the free DMSO into the dichloromethane-d_2 solution containing $UO_2(dbm)_2DMSO$, both of the phenyl rotation and the intramolecular exchange reaction of $UO_2(dbm)_2DMSO$ in Figure 2.29 become slower than those in the system without the free DMSO. Such a feature was confirmed in the ^{1}H NMR spectra of the sample solutions containing free DMSO shown in Figure 2.31. In the system without free DMSO (Figure 2.28), the *o*-proton signals are coalesced at 273 K because of the intramolecular exchange of $UO_2(dbm)_2DMSO$. On the other hand, in the case of the presence of the free DMSO (2.8×10^{-2} M, Figure 2.31), such signals are still split into the essential multiplets of the *o*-proton at the same temperature.

To explain such a slowdown of the intramolecular exchange reaction in $UO_2(dbm)_2$-DMSO caused by the addition of the free DMSO, a mechanism shown in Figure 2.32 may be proposed. At the intermediate of the intramolecular exchange reaction in $UO_2(dbm)_2$-DMSO, the geometry in $UO_2(dbm)_2$ just after the dissociation of the coordinated DMSO should not be regularly tetragonal bipyramidal, but a bipyramid with a trapezoidal equatorial plane, because the $UO_2(dbm)_2$ fragment also has such a structure at the initial state.

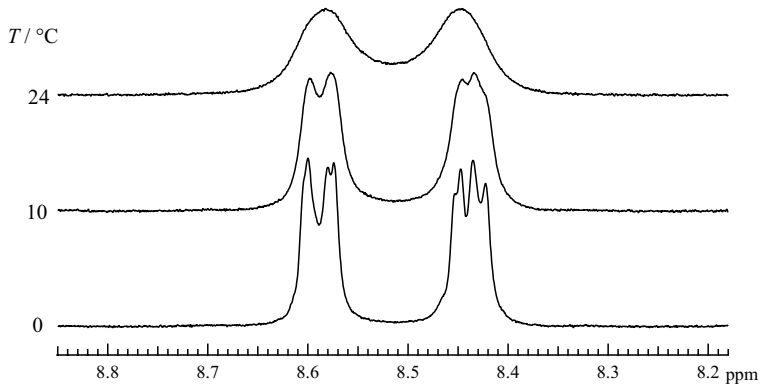

Figure 2.31. ^{1}H NMR spectra of dichloromethane-d_2 solution containing $UO_2(dbm)_2DMSO$ (1.3×10^{-2} M) and free DMSO (2.8×10^{-2} M).

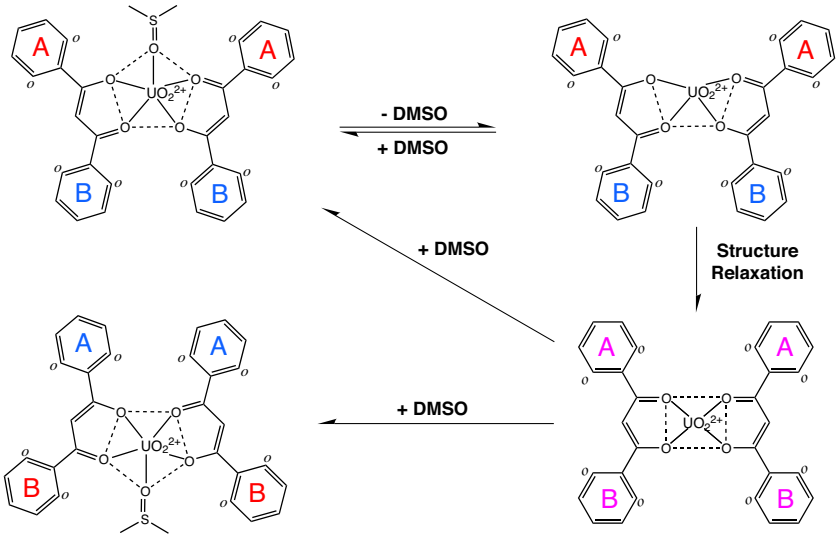

Figure 2.32. Schematic mechanism of the intramolecular exchange reaction in $UO_2(dbm)_2DMSO$. Red and blue colors of the capital letters "A" and "B" indicate the phenyl groups nearer to and further from the coordination site for DMSO, respectively. The letters in purple means the equivalent phenyl groups.

To occur the intramolecular exchange in $UO_2(dbm)_2DMSO$, a structure relaxation process from the distorted $UO_2(dbm)_2$ to the regularly tetragonal bipyramidal one must take place, because of the steric hindrance in the approach of entering DMSO to either vacant sites in $UO_2(dbm)_2$. Therefore, the slower intramolecular exchange reaction of $UO_2(dbm)_2DMSO$ in the presence of the free DMSO observed in Figure 2.31 can be considered to be a result that the re-coordination of DMSO occurs before the achievement of the structure relaxation at the intermediate. The rate constant of the structure relaxation should be twice larger than k_{intra} under the presence of the free DMSO, because the product in the relaxation will be re-coordinated by DMSO from either sides in 50% probability, respectively. Unfortunately, the kinetic analyses for k_{intra} and the structure relaxation at the transition state could not be performed for the complexity of the experimental spectra as shown in Figure 2.31. Furthermore, it can be postulated that the additional free DMSO interacts with $UO_2(dbm)_2DMSO$ in some manners and hence the slow phenyl rotation results. However, the details why the phenyl rotation also becomes slower with the addition of the free DMSO are still uncertain.

For the system of $UO_2(dbm)_2DMSO$, it was found that the DMSO molecule coordinates to the $UO_2(dbm)_2$ fragment even in the dichloromethane solution. Furthermore, the calculated k_{ex} value of the dissociative DMSO exchange reaction in $UO_2(dbm)_2DMSO$ at 298 K is 6.8×10^2 s^{-1}, which is one-order smaller than that in UO_2(saloph)DMSO (1.63×10^3 s^{-1}). These results imply that the coordination of DMSO to $UO_2(dbm)_2$ is stronger than that to UO_2(saloph).

Chapter 3

Uranyl(V) Carbonate Complex in Aqueous System

Uranyl(V) carbonate is known as only one stable uranyl(V) complex in the aqueous system, which exists as $[U^{V}O_2(CO_3)_3]^{5-}$. Thus, it can be expected to obtain useful information concerning chemical properties of $[U^{V}O_2(CO_3)_3]^{5-}$. In fact, some researchers have already studied its spectroscopic,[147, 148] electrochemical,[148, 150] thermodynamic,[149] structural properties,[151, 153] and so on. One of the most important properties to prepare $[U^{V}O_2(CO_3)_3]^{5-}$ is its electrochemical data, especially the standard redox potential (E°) of the $[U^{V}O_2(CO_3)_3]^{5-}$/ $[U^{VI}O_2(CO_3)_3]^{4-}$ couple. However, various E° values of this redox couple were reported such as −0.714, −0.730, −0.7459, −0.749, −0.815, and −0.859 V *vs.* Ag/AgCl as summarized by Grenthe *et al.*[12] Therefore, it was necessary to know the correct E° value of the $[U^{V}O_2(CO_3)_3]^{5-}$/$[U^{VI}O_2(CO_3)_3]^{4-}$ couple under the experimental condition in the present study.

The advantages of study on properties of $[U^{V}O_2(CO_3)_3]^{5-}$ in aqueous system are the stability of the simple ligand like CO_3^{2-} to redox reaction and the high conductivity of the sample solution. These will make it possible to prepare $[U^{V}O_2(CO_3)_3]^{5-}$ with a bulk electrolysis. The bulk solution of $[U^{V}O_2(CO_3)_3]^{5-}$ allows to investigate its kinetics such as the ligand exchange reaction. The study on the reactivity of the uranyl(V) complex is also the important issue in this study.

3.1 Spectroelectrochemistry of $[U^{VI}O_2(CO_3)_3]^{4-}$ in Aqueous Solution

3.1.1 Experimental Details

UV-visible Spectroelectrochemical Measurements. In this study, spectroelectrochemical techniques[178, 179] were used to study electrochemical processes of the uranyl(VI) complexes and to obtain data concerning properties of the uranyl(V) complexes. To observe absorption spectra in UV and visible regions, quartz cells with optical transparent Pt minigrid working electrodes were designed according to the previous articles[180, 181] and mounted on the cell holder of SHIMADZU UV-3150 spectrophotometer. The schematic view of this optical transparent thin layer electrode (OTTLE) cell is shown in Figure 3.1. The effective optical path length of the OTTLE cell was spectrophotometrically calibrated as 1.89×10^{-2} cm. The three-electrode system was utilized, which consisted of the Pt minigrid OTTLE as a working electrode, a Pt wire counter electrode (BAS 002222), and an Ag/AgCl reference electrode (BAS 002020 RE-1B, sat. NaCl aq.) with a liquid junction of glass flit filled by a blank solution (1 M Na_2CO_3aq.). The potential applied on the OTTLE was controlled by BAS CV-50W voltammetric analyzer. The absorption spectra at various applied potentials were measured after reaching equilibrium of the electrochemical reaction on the OTTLE at 298 K, which required 2 min. The sample solutions in the OTTLE cells were deoxygenated by passing dry argon gas at least 1 h prior to starting the measurements.

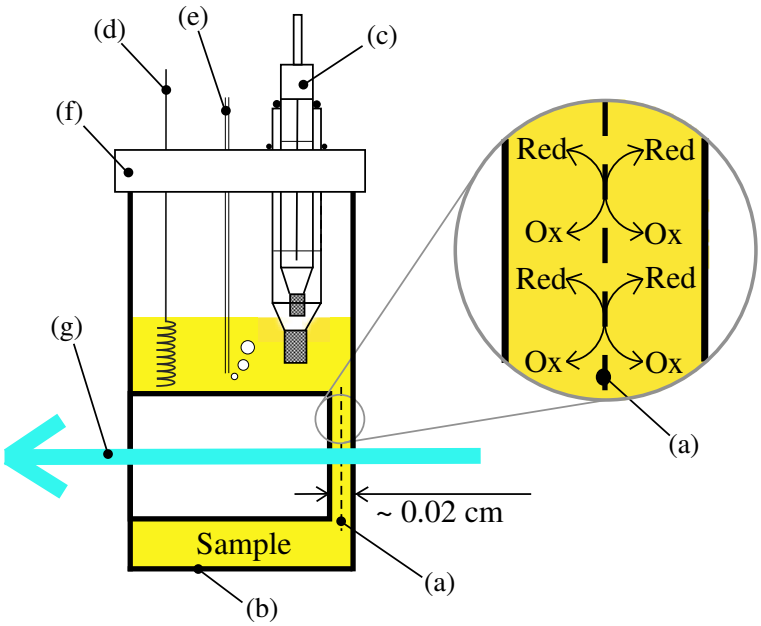

Figure 3.1. Schematic view of OTTLE cell. (a) Pt minigrid working electrode, (b) quartz cell body, (c) reference electrode with a liquid junction of glass flit filled by a blank solution, (d) Pt wire counter electrode, (e) argon gas inlet, (f) PTFE cap, (g) optical path of the spectrophotometer.

3.1.2 Results and Discussion

According to the previous reports,[150] the electrochemical reduction of $[U^{VI}O_2(CO_3)_3]^{4-}$ to $[U^{V}O_2(CO_3)_3]^{5-}$ should occur at around −0.8 V *vs.* Ag/AgCl. Thus, the UV-visible spectroelectrochemical measurements for the $[U^{V}O_2(CO_3)_3]^{5-}/[U^{VI}O_2(CO_3)_3]^{4-}$ redox couple were carried out in the range from 0 to −0.900 V *vs.* Ag/AgCl. The resulting UV-visible absorption spectra at different potentials are shown in Figure 3.2. The absorbancies at around 450 nm corresponding to the LMCT transition in $[U^{VI}O_2(CO_3)_3]^{4-}$ (Figure 2.2) decreased with a decrease in the potential and converged at −0.900 V *vs.* Ag/AgCl. In Figure 3.2, clear isosbestic points were observed at 367 and 387 nm, indicating that only one equilibrium, *i.e.*, $[U^{V}O_2(CO_3)_3]^{5-}/[U^{VI}O_2(CO_3)_3]^{4-}$ redox reaction, occurs in this system. The absorbance of each spectrum in Figure 3.2 is reflecting the concentration profile between the oxidant and reductant at each potential. Such a concentration profile is determined by the Nernstian equation (Eq. 3.1)

$$E = E^{\circ\prime} + \frac{RT}{nF} \ln \frac{C_O}{C_R} \qquad (3.1)$$
$$= E^{\circ\prime} + \frac{RT}{nF} \ln \frac{A - A_R}{A_O - A}$$

E: Potential applied on the OTTLE
$E^{\circ\prime}$: Formal potential
n: Electron stoichiometry
F: Faraday constant (96485 C)
C_O, C_R: Concentrations of oxidant and reductant (M)
A: Absorbance at each potential value
A_O, A_R: Absorbance of oxidant and reductant, respectively

The Nernstian plot from the absorbancies at 447 nm in Figure 3.2 is shown in Figure 3.3. In the least-squares fit for the experimental plot to Eq. 3.1, the slope and the intercept were

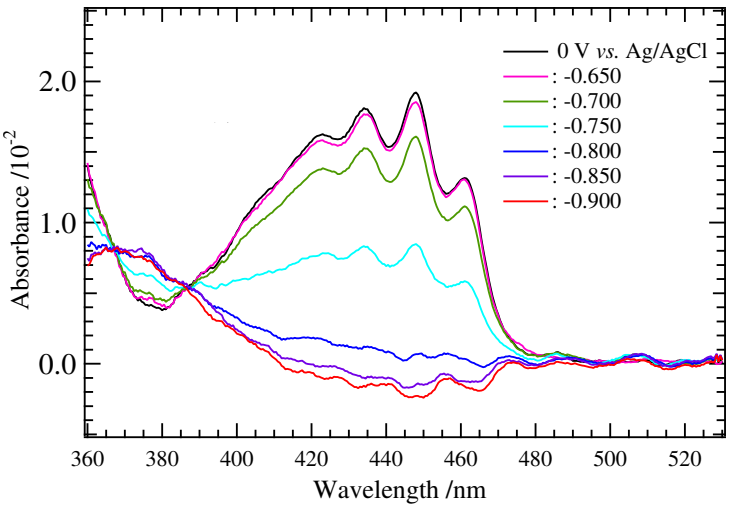

Figure 3.2. UV-visible absorption spectra measured at the applied potentials in the range from 0 to −0.900 V *vs.* Ag/AgCl for the $[U^{V}O_2(CO_3)_3]^{5-}/[U^{VI}O_2(CO_3)_3]^{4-}$ redox couple (total concentration: 4.38×10^{-2} M) in aqueous solution containing Na_2CO_3 (1.0 M). Optical path length: 1.89×10^{-2} cm.

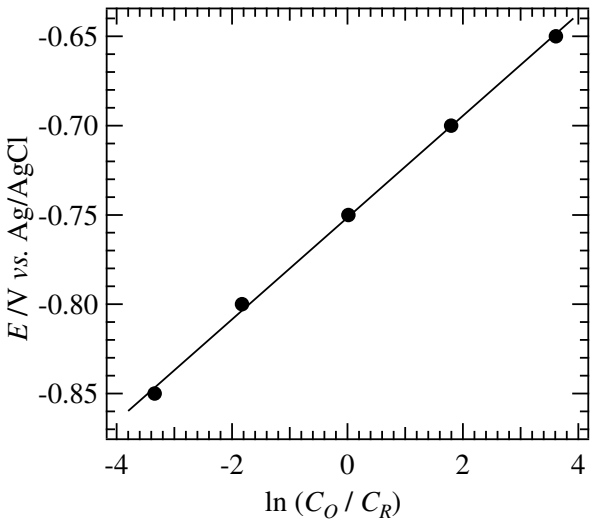

Figure 3.3. A Nernstian plot for the absorbancies at 447 nm in Figure 3.2.

calculated as 0.028 ± 0.001 and −0.751 ± 0.001, respectively. It is obvious that these parameters are corresponding to RT/nF and $E^{\circ\prime}$ in Eq. 3.1, respectively. Thus, the electron stoichiometry (n) and the formal potential ($E^{\circ\prime}$) at 298 K in the electrochemical reduction of $[U^{VI}O_2(CO_3)_3]^{4-}$ were evaluated as 0.90 ± 0.02 and −0.751 ± 0.001 V *vs.* Ag/AgCl, respectively. Consequently, it was confirmed that the electrochemical reaction observed in Figure 3.2 is that between $[U^{V}O_2(CO_3)_3]^{5-}$ and $[U^{VI}O_2(CO_3)_3]^{4-}$ as follows.

$$[U^{VI}O_2(CO_3)_]^{4-} + e^- \rightleftarrows [U^{V}O_2(CO_3)_]^{5-} \tag{3.2}$$

Furthermore, the $E^{\circ\prime}$ value under the present experimental condition was determined. This electrochemical data were used to prepare sample solutions of $[U^{V}O_2(CO_3)_3]^{5-}$ in Section 3.2 (^{13}C NMR) and Chapter 6 (electronic spectrum).

From the reviews reported previously,[12, 13] the thermodynamic data of $[U^{V}O_2(CO_3)_3]^{5-}$ and related species are available. Here, the stability of $[U^{V}O_2(CO_3)_3]^{5-}$ towards its disproportionation is examined from the thermodynamic view. In the disproportionation of the uranyl(V) species, a proton source to remove the axial oxygen atoms from the resulting uranium(IV) is required. In basic carbonate system, the most probable proton source should be HCO_3^-. Therefore, the disproportionation equilibrium of $[U^{V}O_2(CO_3)_3]^{5-}$ to $[U^{VI}O_2(CO_3)_3]^{4-}$ and $[U^{IV}(CO_3)_5]^{6-}$ can be written as,

$$2[U^{V}O_2(CO_3)_3]^{5-} + 4HCO_3^- \rightleftarrows [U^{VI}O_2(CO_3)_3]^{4-} + [U^{IV}(CO_3)_5]^{6-} + 2CO_3^{2-} + 2H_2O. \tag{3.3}$$

To obtain Eq. 3.3, the following equilibria are combined.

$$2U^{V}O_2^+ + 4H^+ \rightleftarrows U^{VI}O_2^{2+} + U^{4+} + 2H_2O \tag{3.4}$$
$$\log K^{\circ}_{3.4} = 6.070 \pm 0.047$$

$$U^{V}O_2^+ + 3CO_3^{2-} \rightleftarrows [U^{V}O_2(CO_3)_3]^{5-} \tag{3.5}$$
$$\log K^{\circ}_{3.5} = 6.950 \pm 0.360$$

$$U^{VI}O_2^{2+} + 3CO_3^{2-} \rightleftarrows [U^{VI}O_2(CO_3)_3]^{4-} \tag{3.6}$$
$$\log K^\circ_{3.6} = 21.840 \pm 0.040$$

$$U^{4+} + 5CO_3^{2-} \rightleftarrows [U^{IV}(CO_3)_5]^{6-} \tag{3.7}$$
$$\log K^\circ_{3.7} = 34.000 \pm 0.900$$

$$CO_3^{2-} + H^+ \rightleftarrows HCO_3^- \tag{3.8}$$
$$\log K^\circ_{3.8} = 10.329 \pm 0.020$$

where $\log K_{3.n}$ ($n = 3 \sim 8$) is the logarithmic equilibrium constant of Eq. 3.*n* at 298.15 K, 0.1 MPa, and zero ionic strength.[13] Thus,

Factor						$\log K^\circ_{3.n}$
+	(	$2U^{V}O_2^+ + 4H^+$	$\rightleftarrows$	$U^{VI}O_2^{2+} + U^{4+} + 2H_2O$	)	6.070 ± 0.047
−2	(	$U^{V}O_2^+ + 3CO_3^{2-}$	$\rightleftarrows$	$[U^{V}O_2(CO_3)_3]^{5-}$	)	6.950 ± 0.360
+	(	$U^{VI}O_2^{2+} + 3CO_3^{2-}$	$\rightleftarrows$	$[U^{VI}O_2(CO_3)_3]^{4-}$	)	21.840 ± 0.040
+	(	$U^{4+} + 5CO_3^{2-}$	$\rightleftarrows$	$[U^{IV}(CO_3)_5]^{6-}$	)	34.000 ± 0.900
−4	(	$CO_3^{2-} + H^+$	$\rightleftarrows$	HCO_3^-	)	10.329 ± 0.020

$$2[U^{V}O_2(CO_3)_3]^{5-} + 4HCO_3^- \rightleftarrows [U^{VI}O_2(CO_3)_3]^{4-} + [U^{IV}(CO_3)_5]^{6-} + 2CO_3^{2-} + 2H_2O$$
$$\log K^\circ_{3.3} = 6.694 \pm 0.017.$$

The resulting value of $\log K^\circ_{3.3}$ is at zero ionic strength.[1] On the other hand, the present system of $[U^{V}O_2(CO_3)_3]^{5-}$ contains 1 M Na_2CO_3. To apply the result of the equilibrium calculation to the system of interest, the ionic strength correction must be performed for $\log K^\circ_{3.3}$. According to the theory of the ionic strength correction described in "*Update on the Chemical Thermodynamics of Uranium, Neptunium, Plutonium, Americium and Technetium*",[13] the equilibrium constant of Eq. 3.3 at ionic strength I_m ($K^{I_m}_{3.3}$) can be given as,

$$\log K^{I_m}_{3.3} = \log K^\circ_{3.3} + \Delta z^2 \cdot D - \Delta\epsilon \cdot m_{Na^+} \tag{3.9}$$

where,

$$\Delta z^2 = [z^2_{U(VI)} + z^2_{U(IV)} + 2z^2_{CO_3^{2-}}] - [2z^2_{U(V)} + 4z^2_{HCO_3^-}] = 6 \tag{3.10}$$

$$D = \frac{0.509\sqrt{I_m}}{1 + 1.5\sqrt{I_m}} \tag{3.11}$$

$$\Delta\epsilon = [\epsilon_{U(VI),Na^+} + \epsilon_{U(IV),Na^+} + 2\epsilon_{CO_3^-,Na^+}] - [2\epsilon_{U(V),Na^+} + 4\epsilon_{HCO_3^-,Na^+}]. \tag{3.12}$$

Here, D is the Debye–Hückel term, m_{Na^+} is the concentration of Na^+ in molality (mol·kg^{-1}, m), and z_i is the charge of ion i (U(VI), U(IV), and U(V) as i correspond to $[U^{VI}O_2(CO_3)_3]^{4-}$, $[U^{IV}(CO_3)_5]^{6-}$, and $[U^{V}O_2(CO_3)_3]^{5-}$, respectively). The notation, ϵ_{i,Na^+}, is the specific ion interaction coefficient between ion i and Na^+. To calculate $\Delta\epsilon$ in Eq. 3.9, the reported ϵ_{i,Na^+}

[1] In the definition, the standard state for a solute B in a solution is hypothetical solution, at the standard state pressure, in which $m_B = m^\circ = 1$ mol·kg^{-1}, and in which the activity coefficient γ_B is unity. However, the usual experimental system is not such hypothetical one. Hence, correction of an equilibrium constant in an ionic medium of interest is required. The details have been presented by Grenthe *et al.*[12, 13]

values are available; $\epsilon_{U(VI),Na^+} = -0.01 \pm 0.11$, $\epsilon_{U(IV),Na^+} = -0.30 \pm 0.15$, $\epsilon_{CO_3^{2-},Na^+} = -0.08 \pm 0.03$, $\epsilon_{U(V),Na^+} = -0.62 \pm 0.15$, and $\epsilon_{HCO_3^-,Na^+} = 0.00 \pm 0.02$.[13] As a result, the following equation (Eq. 3.13) was obtained from Eq. 3.9.

$$\log K_{3.3}^{I_m} = (6.694 \pm 0.017) + 6D - (0.77 \pm 0.02)m_{Na^+} \tag{3.13}$$

The value of I_m in an aqueous medium is calculated by Eq. 3.14.

$$I_m = \frac{1}{2}\sum z_i^2 m_i \tag{3.14}$$

The result in 1 M Na_2CO_3 aq. is $I_m = 3.03$ m with a conversion factor from molarity (mol·dm^{-3}, M) to molality (m), 1.0094 for 1 M Na_2CO_3.[13] Thus, the D value in Eq. 3.11 is calculated as 0.245. Further, the m_{Na^+} value in 1 M Na_2CO_3 is evaluated as 2.02 m. Hence, in 1 M Na_2CO_3 aqueous solution,

$$\log K_{3.3}^{3.03m} = 6.61 \pm 0.01$$

was obtained from Eq. 3.13.

At $[[U^{V}O_2(CO_3)_3]^{5-}] = 5 \times 10^{-2}$ m, $I_m = 3.03$ m (1 M = 1.01 m Na_2CO_3), and pH = 12 ($[HCO_3^-] = 1.56 \times 10^{-3}$ m),[2] which is the typical experimental condition to prepare $[U^{V}O_2(CO_3)_3]^{5-}$ in this study, the mass action law for Eq. 3.3 is expressed as,

$$10^{(6.61\pm0.01)} = \frac{\left[[U^{VI}O_2(CO_3)_3]^{4-}\right]\left[[U^{IV}(CO_3)_5]^{6-}\right] \cdot 1.01^2}{(5 \times 10^{-2})^2 \cdot (1.56 \times 10^{-3})^4}$$

The stoichiometry of $[U^{VI}O_2(CO_3)_3]^{4-}$ in Eq. 3.3 is same as $[U^{IV}(CO_3)_5]^{6-}$. Thus, the concentrations of these U(VI) and -(IV) species were evaluated as $(2.46\pm0.02)\times10^{-4}$ m, respectively. Consequently, the mole fraction of $[U^{V}O_2(CO_3)_3]^{5-}$ in Eq. 3.3 at 1 M (= 1.01 m) Na_2CO_3 system at pH = 12 can be estimated as 99%. Therefore, the stability of $[U^{V}O_2(CO_3)_3]^{5-}$ towards its disproportionation to $[U^{VI}O_2(CO_3)_3]^{4-}$ and $[U^{IV}(CO_3)_5]^{6-}$ in the present experimental condition has been confirmed thermodynamically. As seen from Eq. 3.3, the total concentration of Na_2CO_3 and the balance between CO_3^{2-} and HCO_3^-, which depends on the pH value, are the most important factors for the stability of $[U^{V}O_2(CO_3)_3]^{5-}$ in the aqueous system.

[2] Concentration of HCO_3^- ($[HCO_3^-]$) was obtained by the ionic strength correction for Eq. 3.8 in a similar manner to Eq. 3.9 as follows.

$$\begin{aligned}\log K_{3.8}^{I_m} &= \log K_{3.8}^{\circ} + [z_{HCO_3^-}^2 - (z_{CO_3^{2-}}^2 + z_{H^+}^2)] - [\epsilon_{HCO_3^-,Na^+} - \epsilon_{CO_3^{2-},Na^+}]m_{Na^+} \\ &= (10.329 \pm 0.020) - 4D - (0.08 \pm 0.02)m_{Na^+}\end{aligned}$$

At $I_m = 3.03$ m ($D = 0.245$) and $m_{Na^+} = 2.02$ m, $\log K_{3.8}^{3.03m}$ equals to 9.19 ± 0.01. Since the pH value is expressed by $pH = \log K_{3.8}^{I_m} + \log[CO_3^{2-}]/[HCO_3^-]$, $[HCO_3^-]$ is calculated as 1.56×10^{-3} m at pH = 12 and total $[Na_2CO_3] = 1.01$ m (= 1 M).

3.2 Kinetics of Ligand Exchange Reaction in $[U^{V}O_2(CO_3)_3]^{5-}$

Little information is available concerning kinetics of ligand exchange and substitution reactions in uranyl(V) complexes, in spite of many data for uranyl(VI) complexes.[66, 67, 69–74, 77–82] Here, the ligand exchange reaction in $[U^{V}O_2(CO_3)_3]^{5-}$ was studied by using ^{13}C NMR spectroscopy.

3.2.1 Experimental Details

Preparation of $[U^{V}O_2(CO_3)_3]^{5-}$. All operations were performed under argon atmosphere in a glove-box. A D_2O (99.8 atom% D, ACROS) solution containing $[U^{V}O_2(CO_3)_3]^{5-}$ (4.598×10^{-2} M) and $Na_2{}^{13}CO_3$ (1.003 M, 99 atom% ^{13}C, ISOTEC) was prepared by potentiostatic electrochemical reduction of $[U^{VI}O_2(CO_3)_3]^{4-}$ on a Pt-plate working electrode at −0.950 V *vs.* Ag/AgCl. The potential applied on the working electrode was controlled by BAS CV-50W voltammetric analyzer. The sample solution was deoxygenated by passing argon gas through the solution for at least 3 h prior to the preparation of $[U^{V}O_2(CO_3)_3]^{5-}$. The completeness of the reduction from $[U^{VI}O_2(CO_3)_3]^{4-}$ to $[U^{V}O_2(CO_3)_3]^{5-}$ was confirmed by spectroscopic techniques (UV-visible absorption and ^{13}C NMR spectroscopies). The pD ($-\log[D^+]$) value of the sample solution was 11.96. After the preparation of $[U^{V}O_2(CO_3)_3]^{5-}$, the solution was immediately transfered into an NMR sample tube filled by argon gas. The solution in this sample tube was cooled by ice-NaCl mixture, and then the gases over the solution was replaced by argon gas again.

Methods. UV-visible absorption and ^{13}C NMR spectra were measured by using SHIMADZU UV-3150 spectrophotometer and JEOL JNM-LA300WB NMR spectrometer (^1H: 300.4 MHz, ^{13}C: 75.45 MHz), respectively.

3.2.2 Results and Discussion

The D_2O solution of the uranyl(V) carbonate prepared by the electrochemical reduction of $[U^{VI}O_2(CO_3)_3]^{4-}$ was colorless as reported by Cohen[147] and Wester *et al.*[148] The ^{13}C NMR spectra of D_2O solution containing the uranyl(V) carbonate (4.598×10^{-2} M) and Na_2CO_3 (1.003 M) were measured at different temperatures. The resulting NMR spectra in the range from 273 to 313 K are shown in Figure 3.4. At 273 K, two sharp singlet peaks were observed at 169.13 and 106.70 ppm. As reported previously,[71, 72, 162] the peak at 169.13 ppm is the result of fast exchange reaction between free CO_3^{2-} and DCO_3^- (bicarbonate). Another singlet peak at 106.70 ppm can be assigned to the coordinated CO_3^{2-} in $[U^{V}O_2(CO_3)_3]^{5-}$. Such a singlet peak indicates that the coordinated CO_3^{2-} ligands are immersed in the equivalent chemical environment. From the areas of the peaks of the free and coordinated CO_3^{2-}, the coordination number of CO_3^{2-} was evaluated 2.8 ± 0.1. This result agrees with the stoichiometry of $[U^{V}O_2(CO_3)_3]^{5-}$ reported previously.[149, 153] If the sample solution is mixture of the uranyl(V) carbonate, $[U^{VI}O_2(CO_3)_3]^{4-}$, and CO_3^{2-}, another signal due to the uranyl(VI) complex must be observed at 168.22 ppm as shown in Figure 3.5. However, even in the end of the ^{13}C NMR measurement for Figure 3.4, the signal of $[U^{VI}O_2(CO_3)_3]^{4-}$ (168.22 ppm) was not observed.

As can be seen from Figure 3.4, the line-widths of the two signals corresponding to the free and coordinated CO_3^{2-} increase with increasing temperature. This is the result of an

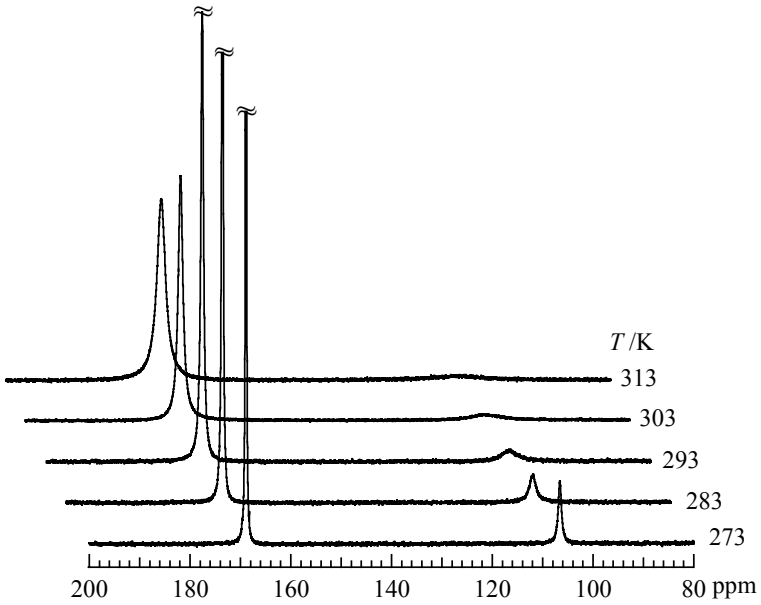

Figure 3.4. ^{13}C NMR spectra of D_2O solution containing $[U^{V}O_2(CO_3)_3]^{5-}$ (4.598×10^{-2} M) and Na_2CO_3 (1.003 M, pD = 11.96).

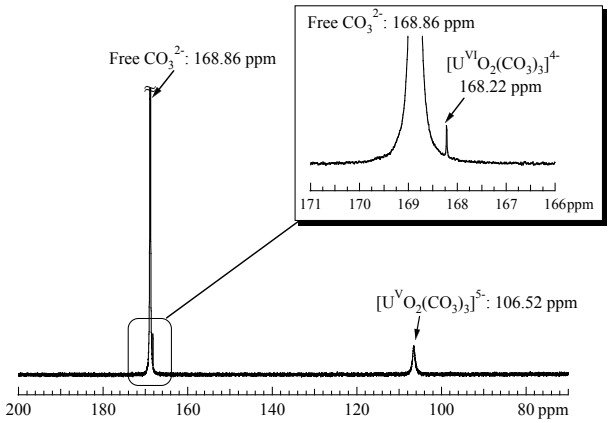

Figure 3.5. ^{13}C NMR spectrum of D_2O solution containing $[U^{V}O_2(CO_3)_3]^{5-}$, $[U^{VI}O_2(CO_3)_3]^{4-}$, and 1 M Na_2CO_3 at 273 K. Inset shows the spectrum magnified in the range from 166 to 171 ppm.

increase in the rate of the following ligand exchange reaction:

$$[U^{V}O_2(CO_3)_3]^{5-} + *CO_3^{2-} \rightleftarrows [U^{V}O_2(CO_3)_2(*CO_3)]^{5-} + CO_3^{2-} \tag{3.15}$$

where the asterisk is a typographical distinction only. To analyze the rate of the CO_3^{2-} exchange by using the NMR line-broadening method, line-widths at half-height of the free CO_3^{2-} signal in the presence and absence of $[U^{V}O_2(CO_3)_3]^{5-}$ in the range from 273 to 333 K were measured. Figure 3.6 shows a semilogarithmic plot of $(T_{2obs}^{-1} - T_{2n}^{-1})P_L/P_M$ against the reciprocal temperature. T_{2obs} and T_{2n} are the transverse relaxation times of free CO_3^{2-} in the presence and absence of $[U^{V}O_2(CO_3)_3]^{5-}$, respectively, and are related with the line-width ($\Delta\nu$) at half-height by $T_{2obs}^{-1} = \pi\Delta\nu_{obs}$ and $T_{2n}^{-1} = \pi\Delta\nu_n$ (subscriptions of $\Delta\nu$ are same with those of the respective T_2). P_L and P_M are molar fractions of the free and coordinated CO_3^{2-}, respectively. Since the uranyl(V) ion has one unpaired electron in the 5f-orbital of uranium

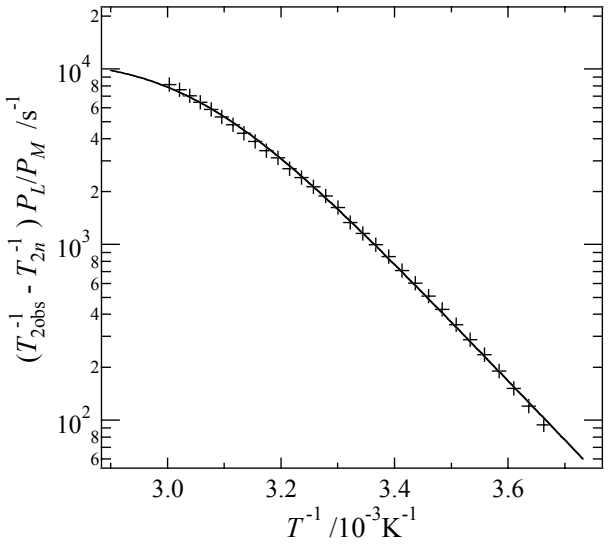

Figure 3.6. Plot of $(T_{2\mathrm{obs}}^{-1} - T_{2n}^{-1})P_L/P_M$ *vs.* $1/T$ for the exchange of CO_3^{2-} in $[U^{V}O_2(CO_3)_3]^{5-}$. Experimental results are shown by +; solid line: best fit of Eq. 3.16

(*i.e.*, $5f^1$ configuration), $[U^{V}O_2(CO_3)_3]^{5-}$ is paramagnetic. Hence, the temperature dependence of $(T_{2\mathrm{obs}}^{-1} - T_{2n}^{-1})P_L/P_M$ for the present system can be described by Eq. 3.16.[65, 182, 183)]

$$(T_{2\mathrm{obs}}^{-1} - T_{2n}^{-1})\frac{P_L}{P_M} = \tau_M^{-1}\left[\frac{T_{2M}^{-2} + T_{2M}^{-1}\tau_M^{-1} + \Delta\omega_M^2}{(T_{2M}^{-1} + \tau_M^{-1})^2 + \Delta\omega_M^2}\right] \tag{3.16}$$

where T_{2M}, τ_M, and $\Delta\omega_M$ are the transverse relaxation time of coordinated CO_3^{2-}, mean lifetime of coordinated CO_3^{2-}, and the difference between chemical shifts of the free and coordinated CO_3^{2-}, respectively. According to a review by Stengle and Langford,[183)] it is reasonable to conclude that the transverse relaxation time of the free CO_3^{2-} in the temperature range from 273 to 303 K (*i.e.*, $3.66 \sim 3.30\times10^{-3}$ K^{-1}) is mainly controlled by a mean lifetime of coordinated CO_3^{2-} (τ_M).[3] The relationship between τ_M and the first-order exchange rate constant (k_{ex}) with temperature is

$$\tau_M^{-1} = k_{\mathrm{ex}} = \frac{k_{\mathrm{B}}T}{h}\exp\left[-\frac{\Delta H^{\ddagger}}{R}\cdot\frac{1}{T} + \frac{\Delta S^{\ddagger}}{R}\right]. \tag{3.17}$$

Therefore, from the Eyring plot in this temperature range, the activation enthalpy ($\Delta H^{\ddagger}$) and entropy ($\Delta S^{\ddagger}$) in Eq. 3.15 could be estimated as 61.8 kJ·mol^{-1} and 20 J·mol^{-1}·K^{-1}, respectively.

For more precise evaluation of the activation parameters in Eq. 3.15, the nonlinear least-square fit of Eq. 3.16 to the experimental results in Figure 3.6 were performed by the following process. The temperature dependence of T_{2M} and $\Delta\omega_M$ is assumed to be given by Eqs. 3.18 and 3.19, respectively.[184, 185)]

$$T_{2M}^{-1} = C_M \exp\left(\frac{E_M}{RT}\right) \tag{3.18}$$

$$\Delta\omega_M = \frac{C_\omega}{T} \tag{3.19}$$

[3]Details are described in Appendix F, “NMR relaxation times in paramagnetic solutions”.

The kinetic parameters were determined by the nonlinear least-squares fit of $(T_{2\mathrm{obs}}^{-1} - T_{2n}^{-1})P_L/P_M$ data to the equation obtained by substitution of Eqs. 3.17–3.19 into Eq. 3.16. The C_M, E_M, and C_ω values were roughly estimated as 2.57×10^3 s^{-1}, 4.80 kJ·mol^{-1}, and 2.51×10^5 rad·s^{-1}·K^{-1}, respectively. When the values of C_M and E_M were fixed to 2.57×10^3 s^{-1} and 4.80 kJ·mol^{-1}, respectively, the nonlinear least-squares fit to Eq. 3.16 gave a minimum error. The $\Delta\omega_M$ value was found to have no influence on the fit even in $\Delta\omega_M = 0$. This means that the line-widths in the range from 273 to 333 K in Figure 3.6 are independent of $\Delta\omega_M$. Subsequently, the activation parameters in Eq. 3.15 were calculated as $\Delta H^\ddagger = 62.0 \pm 0.7$ kJ·mol^{-1} and $\Delta S^\ddagger = 22 \pm 3$ J·mol^{-1}·K^{-1}. The standard deviation in this fitting process was 0.03.

The resulting activation parameters are consistent with those obtained by the Eyring plot in the range from 273 to 303 K ($\Delta H^\ddagger = 61.8$ kJ·mol^{-1} and $\Delta S^\ddagger = 20$ J·mol^{-1}·K^{-1}, previous paragraph). Using these values and Eq. 3.17, the k_{ex} value of Eq. 3.15 at 298 K was evaluated as 1.13×10^3 s^{-1}. This is the first report of a rate constant for ligand exchange reaction in uranyl(V) complexes.

It should be noted that the exchange reaction between the free and coordinated CO_3^{2-} in $[U^{V}O_2(CO_3)_3]^{5-}$ is about 10^2 times faster and 10^5 times slower than those in $[U^{VI}O_2(CO_3)_3]^{4-}$ and $[Pu^{VI}O_2(CO_3)_3]^{4-}$, in which the exchange reactions follow dissociative mechanisms.[71, 186] Their activation parameters ($\Delta H^\ddagger$/kJ·mol^{-1} and $\Delta S^\ddagger$/J·mol^{-1}·K^{-1}) are 82 and 50 for $[U^{VI}O_2(CO_3)_3]^{4-}$, and 34 and 31 for $[Pu^{VI}O_2(CO_3)_3]^{4-}$, respectively. To clarify the mechanism *i.e.*, the rate-determining step of Eq. 3.15, the dependence of k_{ex} on free CO_3^{2-} concentration should be examined. For this requirement, the preparation of $[U^{V}O_2(CO_3)_3]^{5-}$ was attempted in D_2O solutions containing Na_2CO_3 (0.2 M, 0.5 M) by using same electrochemical technique. Unfortunately, black precipitate was formed during the bulk electrolysis of $[U^{VI}O_2(CO_3)_3]^{4-}$ in such conditions. Consequently the pure solution of $[U^{V}O_2(CO_3)_3]^{5-}$ has not been obtained in the lower concentrations of Na_2CO_3. Therefore, the dependence of k_{ex} on free CO_3^{2-} could not be studied. However, the positive value of $\Delta S^\ddagger$ (22 ± 3 J·mol^{-1}·K^{-1}) in Eq. 3.15 suggests that the CO_3^{2-} exchange reaction in $[U^{V}O_2(CO_3)_3]^{5-}$ also occurs through the dissociative mechanism. This suggestion should be supported by the saturated coordination sites in the equatorial plane of $[U^{V}O_2(CO_3)_3]^{5-}$, *i.e.*, there is no space for the additional CO_3^{2-} to $[U^{V}O_2(CO_3)_3]^{5-}$. Hence, it seems reasonable to assume that Eq. 3.15 proceeds through the dissociative mechanism.

It is likely that the difference in the dissociation rates (k_{ex} at 298 K) in $[U^{V}O_2(CO_3)_3]^{5-}$ (1.13×10^3 s^{-1}) and $[U^{VI}O_2(CO_3)_3]^{4-}$ (13 s^{-1}) is related to the bond strength between U and CO_3^{2-}. This can be supported by the third stepwise formation constant ($\log K_3$) of the following reaction:

$$[UO_2(CO_3)_2]^{n-4} + CO_3^{2-} \rightleftarrows [UO_2(CO_3)_3]^{n-6} \tag{3.20}$$

where n is equal to 1 and 2 for uranyl(V) and -(VI), respectively. According to the comprehensive study by Grenthe *et al.*,[12] the second and third gross formation constants of the uranyl(VI) carbonate ($\log\beta_2$ and $\log\beta_3$) in $I = \frac{1}{2}\sum m_i z_i^2 = 3.0$ (m_i: molality of ion i, z_i: charge of ion i; this value of the ionic strength (I) corresponds to 1.0 M Na_2CO_3) are 16.20 and 22.61, respectively. Therefore, the $\log K_3$ values of uranyl(VI) ($n = 2$) in 1.0 M Na_2CO_3 ($I = 3.0$) is 6.41. On the other hand, there are no direct references for uranyl(V) ($n = 1$). However, assuming that the $\log K_3$ value is similar to that of the isovalent neptunyl(V) carbonate in $I = 3.0$ ($\log\beta_2 = 8.15$, $\log\beta_3 = 10.46$), the $\log K_3$ value of the uranyl(V) carbonate might be near to 2.3, which is 10^4 times smaller than that of uranyl(VI). Furthermore, the EXAFS study reported by Docrat *et al.*[153] shows that the bond distance

between U and O of coordinated CO_3^{2-} in $[U^{V}O_2(CO_3)_3]^{5-}$ (2.50 ± 0.02 Å) is 0.07 Å longer than that in $[U^{VI}O_2(CO_3)_3]^{4-}$ (2.43 ± 0.02 Å). These data suggest that the dissociation of CO_3^{2-} from $[U^{V}O_2(CO_3)_3]^{5-}$ occurs more readily than from $[U^{VI}O_2(CO_3)_3]^{4-}$. In fact, the $\Delta H^{\ddagger}$ value of Eq. 3.15 (62.0 ± 0.7 kJ·mol^{-1}) is much smaller than the corresponding reaction in $[U^{VI}O_2(CO_3)_3]^{4-}$ (82 kJ·mol^{-1}), indicating a weaker bonding of the leaving CO_3^{2-} in $[U^{V}O_2(CO_3)_3]^{5-}$ than $[U^{VI}O_2(CO_3)_3]^{4-}$. It is likely that such a relationship between the metal–ligand bond strengths in uranyl(V) and -(VI) complexes is also true for the nonaqueous systems of uranyl(V) and -(VI) complexes. In Sections 4.1 and 4.2, the unidentate ligand (L = DMSO, DMF) in $[U^{V}O_2(saloph)L]^{-}$ dissociates more easily than that in $U^{VI}O_2(saloph)L$ in the non-aqueous system. The proposed dissociative mechanism for Eq. 3.15 is also consistent with the result of a quantum chemical study on the mechanism of water exchange reactions in $[U^{V}O_2(H_2O)_5]^{+}$ and $[U^{VI}O_2(H_2O)_5]^{2+}$ by Vallet *et al.*[83, 187] In such studies, the authors suggested that the dissociative mechanism is favored in the uranyl(V) aqua ions as a result of the weaker metal–ligand bond strength.

Chapter 4

Electrochemical and Spectroelectrochemical Studies on Uranyl(VI) Complexes in Nonaqueous Systems

Since one of the goals in this study is to observe pure uranyl(V) complexes in aqueous and nonaqueous systems by using electrochemical reduction of corresponding uranyl(VI) ones, their electrochemical properties must be studied. For the aqueous system, the UV-visible spectroelectrochemical study on $[U^{V}O_2(CO_3)_3]^{5-}/[U^{VI}O_2(CO_3)_3]^{4-}$ has been performed and the formal potential of this redox couple was determined. On the other hand, there are no reports for stable uranyl(V) species in nonaqueous systems still now. However, an insight how to produce the stable uranyl(V) species in such systems has been proposed in the previous study by Ikeda *et al.*[140–142] According to them, the uranyl(VI) complexes coordinated with multidentate ligand(s) have a tendency to form the more stable uranyl(V) complexes through their electrochemical reductions than those with unidentate ligands such as $[U^{VI}O_2L_5]^{2+}$ (L = dimethyl sulfoxide, *N*,*N*-dimethylformamide). In this study, *N*,*N'*-disalicylidene-*o*-phenylenediaminate (saloph) and dibenzoylmethanate (dbm) were selected as the multidentate ligands. The uranyl(VI) complexes coordinated by these ligands in the nonaqueous media ($U^{VI}O_2$(saloph)DMF, $U^{VI}O_2$(saloph)DMSO, and $U^{VI}O_2(dbm)_2$DMSO) have already been characterized in Chapter 2.

4.1 $U^{VI}O_2$(saloph)DMF in *N*,*N*-Dimethylformamide

4.1.1 Experimental Details

Electrochemical Measurements. Cyclic voltammetry (CV) was used for electrochemical investigations. The CV measurements were carried out at 25°C under dry argon atmosphere using BAS CV-50W voltammetric analyzer. The three-electrode system, which consisted of a Pt working electrode (BAS 002013, electrode surface area: 0.020 cm^2), a Pt wire counter electrode (BAS 002222) and an Ag/Ag^+ (BAS 002025 RE-5, 0.01 M $AgNO_3$ + 0.1 M tetra-*n*-ammonium perchlorate in acetonitrile) reference electrode, was utilized. As an internal potential standard for nonaqueous systems, a ferrocene/ferrocenium ion redox couple (Fc/Fc^+) was used.[188] The solvents for CV mesumrements (DMF and dichloromethane) were distilled (*in vacuo* for DMF) after drying with CaH_2 and then stored over molecular sieves 4A (Wako). Tetra-*n*-butylammonium perchlorate (TBAP, Fluka, electrochemical grade) was used as a supporting electrolyte without further purification. To remove the dissolved oxygen, argon gas dried by passing through a $CaCl_2$ tube was purged through all sample solutions for at least 30 min prior to starting all electrochemical measurements. In the case that dichloromethane was used as solvent, the argon gas was soaked with dichloromethane by using a gas bubbler to prevent change of solution composition.

UV-visible Spectroelectrochemical Measurements. The UV-visible spectroelectrochemical measurements were also performed for $U^{VI}O_2$(saloph)DMF in a similar manner to those for $[U^{VI}O_2(CO_3)_3]^{4-}$ (Section 3.1.1). The spectrophotometer used here was Agilent 8453 diode-array spectrophotometer. The Ag/Ag^+ (BAS 002025 RE-5) reference electrode was connected to the sample solution without the liquid junction filled by a blank solution (*cf.* Figure 3.1). The effective optical path length of the OTTLE cell was spectrophotometrically calibrated as 2.76×10^{-2} cm. Other details were same as those described in Section 3.1.1.

4.1.2 Results and Discussion

Cyclic voltammograms of $U^{VI}O_2$(saloph)DMF (8.71×10^{-4} M) in DMF containing TBAP (0.10 M) are shown in Figure 4.1. Peaks (P_{cf} and P_{af1}) of one redox couple and an uncoupled oxidation peak (P_{af2}) are observed at around −1.69 (E_{pcf}), −1.56 (E_{paf1}), and −1.00 (E_{paf2}) V *vs.* Fc/Fc^+, respectively. Ratios of peak currents at P_{af1} and P_{cf} (i_{paf1}/i_{pcf}) were calculated from the semiempirical equation, Eq. 4.1, derived by Nicholson.[189]

$$\frac{i_{pa}}{i_{pc}} = \frac{i_{pa0}}{i_{pc0}} + \frac{0.485 \times i_{sp0}}{i_{pc0}} + 0.086 \tag{4.1}$$

where i_{pa0}, i_{pc0}, and i_{sp0} are currents measured with respect to the zero current axis at anodic peak potential, cathodic peak potential, and switching potential, respectively. To evaluate the ratio, i_{paf1}/i_{pcf}, the variables i_{pa} and i_{pc} in Eq. 4.1 were replaced by i_{paf1} and i_{pcf}, respectively. The electrochemical data from the cyclic voltammograms for various scan rates (v, $V \cdot s^{-1}$) are summarized in Table 4.1. The peak separation ($\Delta E_p = |E_{pcf} - E_{paf1}|$) increases from 0.101 to 0.168 V with an increase in v. The formal potential $E^{\circ\prime}$ ($(E_{paf1} + E_{pcf})/2$) were constant at -1.626 ± 0.005 *vs.* Fc/Fc^+. The i_{paf1}/i_{pcf} values are smaller than 1 and increase with an increase in v. Furthermore, any other redox waves except for P_{cf1}, P_{af1}, and P_{af2} were not observed even in the multiple scanned cyclic voltammogram of $U^{VI}O_2$(saloph)DMF under the

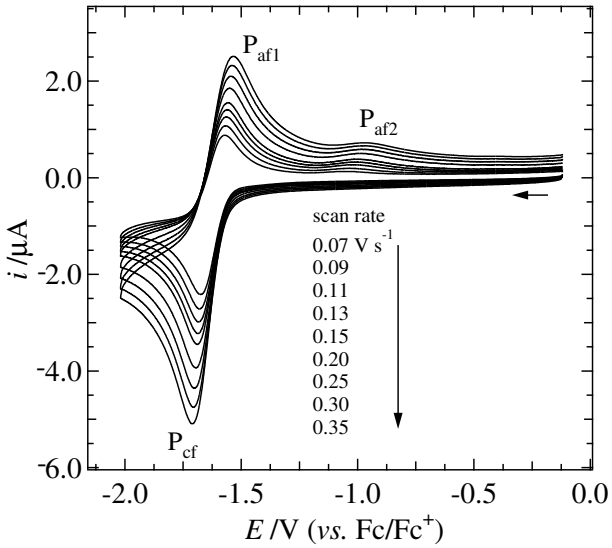

Figure 4.1. Cyclic voltammograms of $U^{VI}O_2$(saloph)DMF (8.71×10^{-4} M) in DMF containing TBAP (0.10 M) measured in the potential range from −0.119 to −2.019 V at different scan rates (v = 0.07 − 0.35 V·s^{-1}). Initial scan direction: cathodic.

same condition with Figure 4.1. From these results, it is suggested that the electrochemical reaction of $U^{VI}O_2$(saloph)DMF in DMF is a quasi-reversible system accompanied by a successive reaction of reductant at E_{pcf}. If the electrochemical reduction of $U^{VI}O_2$(saloph)DMF observed in Figure 4.1 is two-electron process, the reductant must be U(IV) species, which forms an U^{4+} complex or $U^{IV}O_2$ precipitate. In both cases, the cyclic voltammogram should show a quite irreversible aspect, because the reduction from $U^{VI}O_2^{2+}$ to U^{4+} is accompanied by a dissociation of the axial oxygen atoms from uranium and the solubility of $U^{IV}O_2$ is very low. Therefore, the reductant at E_{cf} in Figure 4.1 should be $[U^{V}O_2(saloph)DMF]^{-}$. This uranyl(V) complex produces an electrochemical active substance oxidized at E_{paf2}.

The UV-visible spectroelectrochemical measurements were carried out for the DMF solution containing $U^{VI}O_2$(saloph)DMF (9.33×10^{-4} M) and TBAP (0.30 M) to examine the electrochemical reaction mechanism. The UV-visible absorption spectra measured at the applied potentials in the range from 0 to −1.785 V *vs.* Fc/Fc$^+$ are shown in Figure 4.2. The spectral changes with a stepwise decrease in the applied potential converged at −1.785 V *vs.*

Table 4.1. Electrochemical data of $U^{VI}O_2$(saloph)DMF in DMF

v/V·s^{-1}	E_{pcf}/V	E_{paf1}/V	E_{paf2}/V	$E_{pcf/2}$/V	i_{pcf}/μA	i_{pc0}/μA	i_{pa0}/μA	i_{sp0}/μA	i_{paf1}/i_{pcf}
0.07	−1.673	−1.572	−1.058	−1.607	2.130	2.415	0.879	1.249	0.70
0.09	−1.679	−1.569	−1.037	−1.611	2.412	2.717	1.075	1.337	0.72
0.11	−1.682	−1.569	−1.020	−1.613	2.662	2.984	1.256	1.413	0.74
0.13	−1.687	−1.565	−1.012	−1.616	2.871	3.227	1.406	1.528	0.75
0.15	−1.689	−1.559	−1.002	−1.617	3.078	3.452	1.553	1.627	0.76
0.20	−1.695	−1.554	−0.987	−1.621	3.513	3.936	1.855	1.847	0.78
0.25	−1.698	−1.552	−0.981	−1.625	3.861	4.362	2.104	2.083	0.80
0.30	−1.703	−1.546	−0.975	−1.628	4.209	4.750	2.325	2.284	0.81
0.35	−1.710	−1.542	−0.968	−1.631	4.498	5.094	2.516	2.478	0.82

All potentials are versus Fc/Fc$^+$.

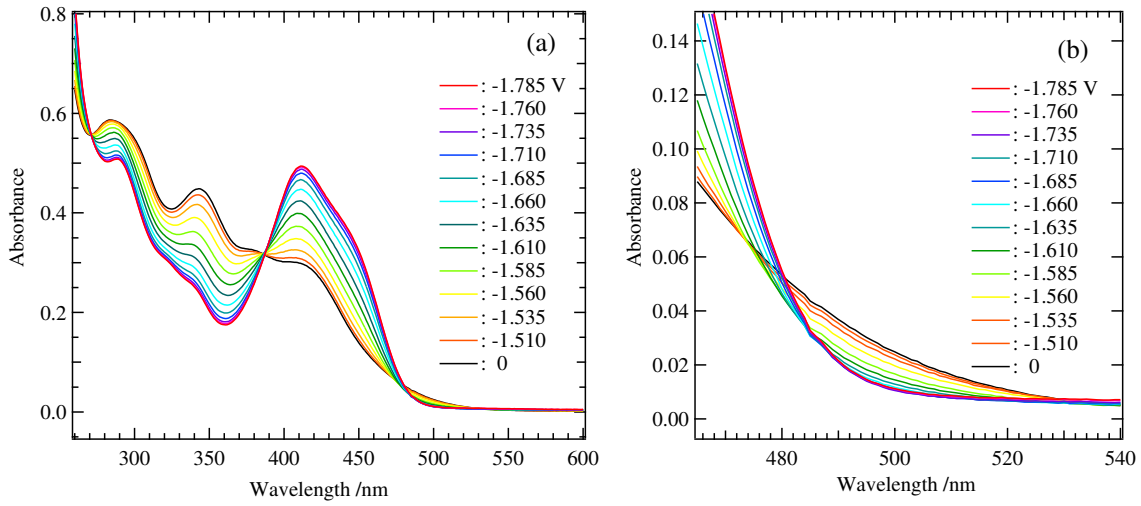

Figure 4.2. UV-visible absorption spectra measured at the applied potentials in the range from 0 to −1.785 V *vs.* Fc/Fc^+ for $U^{VI}O_2$(saloph)DMF (9.33×10^{-4} M) in DMF solution containing TBAP (0.30 M). Wavelength range: (a) 260–600 nm, (b) 465–540 nm. Optical path length: 2.76×10^{-2} cm.

Fc/Fc^+. As seen from this figure, any clear isosbestic points are not observed. This is the evidence that the reduction of $U^{VI}O_2$(saloph)DMF is followed by a successive reaction. When the potential applied on the OTTLE returned to 0 V *vs.* Fc/Fc^+, the UV-visible absorption spectrum of the sample solution almost completely reproduced the initial one. This phenomenon is consistent with the result of multiple-scanned cyclic voltammograms for $U^{VI}O_2$-(saloph)DMF in DMF. Thus, the possibility of the two-electron reduction of $U^{VI}O_2$(saloph)-DMF can be neglected, and the oxidant at E_{paf2} in Figure 4.1 returns to $U^{VI}O_2$(saloph)DMF. Consequently, the following reaction mechanism should be reasonable to the coupled peaks of E_{pcf}/E_{paf1} in Figure 4.1.

$$U^{VI}O_2(\text{saloph})\text{DMF} + e^- \rightleftarrows [U^{V}O_2(\text{saloph})\text{DMF}]^- \tag{4.2}$$

The kinetic analysis was carried out for Eq. 4.2. According to Nicholson,[190–192] a standard rate constant (k°) in an electrochemical reaction is calculated by the following equation on the basis of the assumption that diffusion coefficients of an oxidant (D_O) and the corresponding reductant (D_R) are equal.

$$\psi = \frac{k^\circ}{[D_O \pi (nF/RT)v]^{\frac{1}{2}}} \tag{4.3}$$

where ψ is the kinetic parameter defined by Nicholson.[190] Since Eq. 4.2 is followed by a successive reaction, this electrochemical process is not reversible in the definition.[192] Thus, the D_O value was estimated by a theoretical equation (Eq. 4.4) for the cathodic peak current (i_{pc}) in an irreversible system.[191, 192]

$$i_{pc} = 2.985 \times 10^2 n A C_O^\circ (\alpha n_B)^{\frac{1}{2}} v^{\frac{1}{2}} D_O^{\frac{1}{2}} \tag{4.4}$$

In Eq. 4.4, A, C_O°, α, and n_B are the surface area of a working electrode, the bulk concentration of the oxidant, the transfer coefficient, and the electron stoichiometry in a rate-determining

process, respectively. The αn_B value was obtained as 0.67 in average from Eq. 4.5.[193)]

$$\alpha n_B = \frac{0.04768}{E_{p/2} - E_p} \tag{4.5}$$

where $E_{p/2}$ and E_p are half and full peak potentials and corresponding to $E_{pcf/2}$ and E_{pcf} in Table 4.1, respectively. Hence, the D_O value of $U^{VI}O_2$(saloph)DMF in DMF was estimated as 3.4×10^{-6} cm^2s^{-1} by Eq. 4.4. According to the previous articles,[190, 191)] the ψ values for the present system are in the range from 0.55 (v = 0.07 $V{\cdot}s^{-1}$, ΔE_p = 0.101) to 0.17 (v = 0.35 $V{\cdot}s^{-1}$, ΔE_p = 0.168). Therefore, the k° value for the electrochemical reaction 4.2 is estimated as 2.5×10^{-3} $cm{\cdot}s^{-1}$ by using Eq. 4.3.

For the overall reaction mechanism initiated by the electrochemical reaction of $U^{VI}O_2$-(saloph)DMF in DMF, there are two candidates as follows.

Mechanism 1

$$U^{VI}O_2(\text{saloph})\text{DMF} + e^- \rightleftarrows [U^{V}O_2(\text{saloph})\text{DMF}]^- \quad (E_{pcf}/E_{paf1}) \tag{4.6}$$

$$[U^{V}O_2(\text{saloph})\text{DMF}]^- \rightleftarrows [U^{V}O_2(\text{saloph})]^- + \text{DMF} \tag{4.7}$$

$$[U^{V}O_2(\text{saloph})]^- \longrightarrow U^{VI}O_2(\text{saloph}) + e^- \quad (E_{paf2}) \tag{4.8}$$

$$U^{VI}O_2(\text{saloph}) + \text{DMF} \longrightarrow U^{VI}O_2(\text{saloph})\text{DMF} \tag{4.9}$$

Mechanism 2

$$U^{VI}O_2(\text{saloph})\text{DMF} + e^- \rightleftarrows [U^{V}O_2(\text{saloph})\text{DMF}]^- \quad (E_{pcf}/E_{paf1}) \tag{4.10}$$

$$[U^{V}O_2(\text{saloph})\text{DMF}]^- \rightleftarrows [U^{V}O_2(\text{tri-saloph})\text{DMF}]^- \tag{4.11}$$

$$[U^{V}O_2(\text{tri-saloph})\text{DMF}]^- \longrightarrow U^{VI}O_2(\text{tri-saloph})\text{DMF} + e^- \quad (E_{paf2}) \tag{4.12}$$

$$U^{VI}O_2(\text{tri-saloph})\text{DMF} \longrightarrow U^{VI}O_2(\text{saloph})\text{DMF} \tag{4.13}$$

In **Mechanism 1**, the successive reaction of $[U^{V}O_2(\text{saloph})\text{DMF}]^-$ is the DMF dissociation (Eq. 4.7). The product in this chemical reaction is $[U^{V}O_2(\text{saloph})]^-$, which is oxidized to $U^{VI}O_2$(saloph) at E_{paf2} (Eq. 4.8) and then coordinated by DMF again (Eq. 4.9). In **Mechanism 2**, the successive reaction is dissociation of one part of saloph from $U^{V}O_2^+$ moiety (tri-saloph means tridentate saloph). The similar reaction mechanisms have been proposed in the electrochemical reactions of $U^{VI}O_2$(β-diketonato)$_2$DMF systems.[140–142)]

In all systems of electrochemical reactions (reversible, quasi-reversible, and irreversible), it is theoretically clarified that the reduction (oxidation) peak current (i_p) is proportional to the initial concentration (C°) of oxidant (reductant).[191, 192)] In **Mechanism 1**, the equilibrium of Eq. 4.7 will shift to right with a decrease in the concentration of free DMF in the solution, and hence the peak current values at E_{paf1} and E_{paf2} will decrease and increase, respectively. On the other hand, such phenomena should not be observed in **Mechanism 2**. Therefore, the CV measurements for $U^{VI}O_2$(saloph)DMF in DMF and dichloromethane (DM) mixed solvent systems (DMF + DM) should be a probe to determine the correct mechanism. In this study, the cyclic voltammograms of $U^{VI}O_2$(saloph)DMF (1×10^{-3} M) in DMF + DM (free DMF concentration: 2.95 M, 0.854 M) were measured (*cf.* neat DMF: 12.9 M). In these conditions, the dimerization of $U^{VI}O_2$(saloph)DMF can be neglected from the value of K_{dim} for Eq. 2.1 described in Chapter 2. The resulting cyclic voltammograms are shown in Figure 4.3.

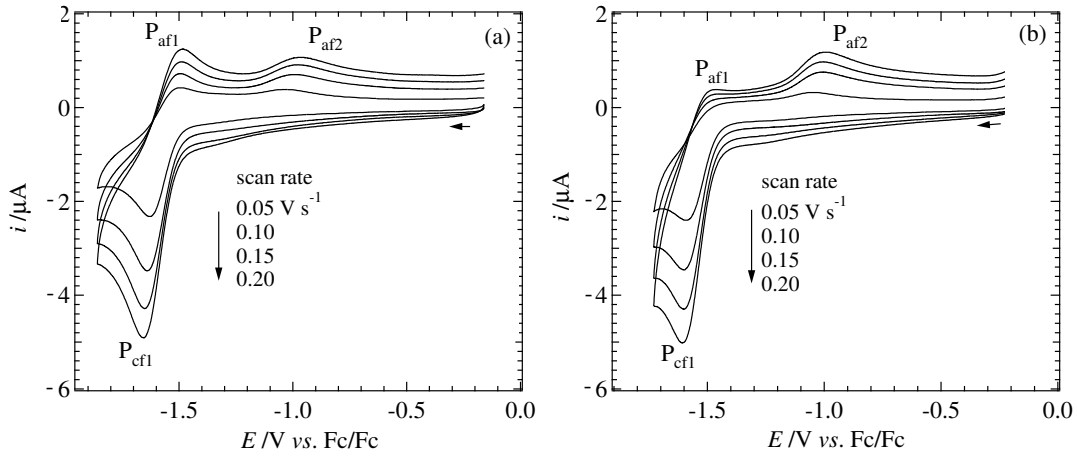

Figure 4.3. Cyclic voltammograms of $U^{VI}O_2$(saloph)DMF (a: 9.87×10^{-4} M, b: 9.49×10^{-4} M) in DMF + DM containing TBAP (0.10 M). DMF concentration, a: 2.95 M, b: 0.854 M.

The reduction and oxidation peaks were observed at the same potentials in Figure 4.1. The peak current values at E_{paf1} and E_{paf2} showed the dependence on the concentration of free DMF as predicted from **Mechanism 1**. Hence, it is concluded that the reaction mechanism of $U^{VI}O_2$(saloph)DMF in the present system is **Mechanism 1**.

After the DMF dissociation in Eq. 4.7, the possibility of the formation of the dinuclear complex containing uranyl(V) ion (*e.g.*, $[U^{V}O_2(saloph)]_2^{2-}$ or $[U^{VI}O_2(saloph)U^{V}O_2(saloph)]^{-}$) must be discussed, because the dimerization was actually observed in the case of the corresponding uranyl(VI) complex (see Section 2.2). If this is true, the electrochemical reaction of $[U^{VI}O_2(saloph)]_2$ will be in a reversible or quasi-reversible system without any successive reactions. Thus, the CV measurements for $[U^{VI}O_2(saloph)]_2$ in dichloromethane were carried out. The results are shown in Figure 4.4. As can be seen from this figure, the electrochemical reaction of $[U^{VI}O_2(saloph)]_2$ is completely irreversible. This indicates that $[U^{V}O_2(saloph)]^{-}$ produced in Eq. 4.7 remains as the monomeric form rather than the dimer.

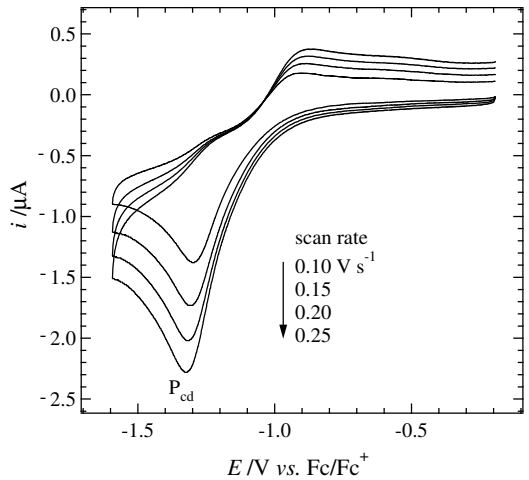

Figure 4.4. Cyclic voltammograms of $[U^{VI}O_2(saloph)]_2$ (4.02×10^{-4} M) in dichloromethane containing TBAP (0.10 M). Initial scan direction: cathodic.

The reduction (oxidation) peak currents (i_p) are corresponding to the initial concentration (C°) of oxidant (reductant) as shown in Eq. 4.4. Thus, the DMF dissociation constant (K_{disV}) in Eq. 4.7 was roughly estimated from the current values at E_{paf1} and E_{paf2} by the following equation.

$$K_{disV} = \frac{\left[[U^{V}O_2(saloph)]^-\right][DMF]}{[[U^{V}O_2(saloph)DMF]^-]} \tag{4.14}$$

$$= \frac{C^\circ_U \times (1 - i_{paf1}/i_{pcf}) \times [DMF]}{C^\circ_U \times i_{paf1}/i_{pcf}} \tag{4.15}$$

where C°_U is the initial concentration of the uranyl(VI) complex. From the peak currents and free DMF concentration in Figures 4.1 and 4.3, the K_{disV} value for Eq. 4.7 was estimated as 5 M in average.

Furthermore, even in the multiple-scanned cyclic voltammograms in all condition with the various concentration of free DMF (12.9 M (neat), 2.95 M, and 0.854 M; Figures 4.1 and 4.3), the reduction peak coupled with P_{af2} was not observed and the respective peak current values at E_{pcf}, E_{paf1}, and E_{paf2} were almost constant. These results suggest that the $U^{VI}O_2$(saloph) produced at P_{af2} is rapidly recombined by free DMF in solution. In Section 2.2, it was suggested that the DMF exchange reaction in $U^{VI}O_2$(saloph)DMF proceeds through the dissociative mechanism, *i.e.*, the rate-determining step of this reaction is the dissociation of DMF from $U^{VI}O_2$(saloph)DMF. Thus, the intermediate of the DMF exchange reaction in $U^{VI}O_2$(saloph)DMF is $U^{VI}O_2$(saloph) and the re-coordination of free DMF to $U^{VI}O_2$(saloph) is much faster than the dissociation of the coordinated DMF from $U^{VI}O_2$(saloph)DMF ($k_{ex} = 1.68 \times 10^3$ s^{-1} at 298 K). This makes the reduction peak coupled with P_{af2} in Figures 4.1 and 4.3 unobservable. Here, overall consistency of the mechanisms including the electrochemical reaction, the dimerization, and the DMF exchange reaction of $[U^{V}O_2(saloph)DMF]^-$ and/or $U^{VI}O_2$(saloph)DMF were confirmed. A scheme of the whole reaction mechanisms starting from $U^{VI}O_2$(saloph)DMF is shown in Figure 4.5.

It is obvious that the coordination ability of DMF to the $[U^{V}O_2(saloph)]^-$ fragment is much weaker than that to $U^{VI}O_2$(saloph) one, because the coordinated DMF dissociates from $[U^{V}O_2(saloph)DMF]^-$ even in neat DMF solvent. This phenomenon can be considered to be a result of the lower positive charge on the center uranium in $[U^{V}O_2(saloph)]^-$ than that in $U^{VI}O_2$(saloph). Moreover, it can be predicted that the ligand exchange reaction in a uranyl(V) complex is about 10^2 times faster than that in the corresponding uranyl(VI) complex according to the result for $[U^{V}O_2(CO_3)_3]^{5-}$ described in Section 3.2. Hence, the first-order rate constant of the DMF exchange reaction in $[U^{V}O_2(saloph)DMF]^-$ may be estimated as $\sim 10^5$ s^{-1}.

In this section, it has been found out that $[U^{V}O_2(saloph)DMF]^-$ is not stable even in neat DMF solvent. However, no aspects of the disproportionation of this uranyl(V) complex has also been confirmed. This should be due to the effects of (1) the aprotic solvent DMF (no active proton in the system) and (2) the tetradentate saloph ligand (its strong coordination to the uranyl(V) ion). It can be expected easily that the former prevents the proton-assisted disproportionation of uranyl(V) species such as Eq. 3.3 described in Chapter 3. The latter has also been proposed by Ikeda *et al.*[140–142] Indeed, as introduced in Chapter 1, the colloidal precipitate expected as $U^{IV}O_2$ which is the result of the disproportionation of uranyl(V) species coordinated only with unidentate ligands was confirmed even in the similar aprotic solvent DMSO.[129] Although the mechanism of the disproportionation of the uranyl(V) species in

aprotic nonaqueous systems have not been clarified, it is clear that the multidentate ligand such as saloph stabilizes its uranyl(V) complex.

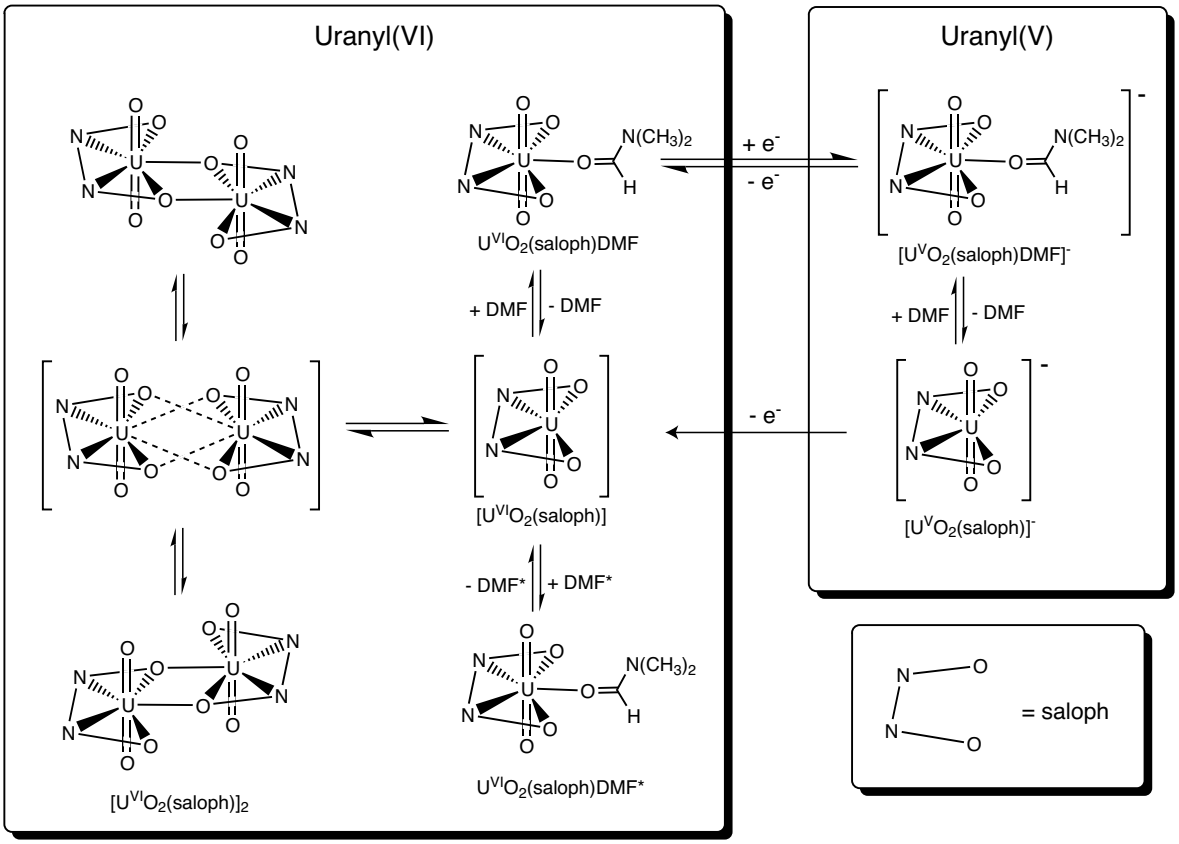

Figure 4.5. Scheme of whole reaction mechanisms of $U^{VI}O_2$(saloph)DMF. The asterisk on DMF is typographical distinction only.

4.2 $U^{VI}O_2$(saloph)DMSO in Dimethyl Sulfoxide

In Section 4.1, the DMF dissociation from the electrochemically produced uranyl(V) complex, $[U^{V}O_2(\text{saloph})\text{DMF}]^-$, was observed. On the other hand, the disproportionation of the uranyl(V) species has not been detected in such a system. Therefore, the preparation of the stable uranyl(V) complexes with saloph can be expected by using a unidentate ligand more strongly binding to $[U^{V}O_2(\text{saloph})]^-$ than DMF. One of the most potential unidentate ligands instead of DMF is dimethyl sulfoxide (DMSO), because DMSO molecule is also known as the usual unidentate ligand strongly coordinating to $U^{VI}O_2^{2+}$ ion. Actually, the stronger coordination ability of DMSO to $U^{VI}O_2$(saloph) than DMF has been evidenced in Chapter 2.

4.2.1 Experimental Details

Electrochemical Measurements. The CV measurements for $U^{VI}O_2$(saloph)DMSO in non-aqueous systems were carried out in a similar manner to those for $U^{VI}O_2$(saloph)DMF. Dimethyl sulfoxide and dichloromethane as the solvents for CV measurements were distilled (*in vacuo* for DMSO) after the drying with CaH_2 and then stored over molecular sieves 4A (Wako).

UV-visible Spectroelectrochemical Measurements. The UV-visible spectroelectrochemical measurements were also performed for $U^{VI}O_2$(saloph)DMSO. The effective optical path length of the OTTLE cell was spectrophotometrically calibrated as 2.90×10^{-2} cm. Other details were same as those described in Section 4.1.1

4.2.2 Results and Discussion

Cyclic voltammograms of $U^{VI}O_2$(saloph)DMSO (9.55×10^{-4} M) in DMSO containing TBAP (0.10 M) are shown in Figure 4.6. Coupled peaks (P_{cs} and P_{as}) were observed at around -1.60 (E_{pcs}) and -1.50 V (E_{pas}) *vs.* Fc/Fc^+. In this system, no other redox waves such as P_{af2} in Figure 4.1 were observed. The ratios of peak currents (i_{pas}/i_{pcs}) were calculated by Eq. 4.1. The electrochemical data of $U^{VI}O_2$(saloph)DMSO are collected in Table 4.2. The ΔE_p between E_{pcs} and E_{pas} increased from 0.093 to 0.108 with an increase in v. The $E^{\circ\prime}$ value, $E^{\circ\prime} = (E_{pcs}+E_{pas})/2$, is constant, -1.550 ± 0.002 V *vs.* Fc/Fc^+. As can be seen from Table 4.2, the estimated i_{pas}/i_{pcs} values are almost unity without dependence on v. From these results, it is suggested that the electrochemical reaction of $U^{VI}O_2$(saloph)DMSO is a quasi-reversible

Table 4.2. Electrochemical data of $U^{VI}O_2$(saloph)DMSO in DMSO

v /V·s^{-1}	E_{pcs} /V	E_{pas} /V	$E_{pcs/2}$ /V	i_{pcs}/μA	i_{pc0}/μA	i_{pa0}/μA	i_{sp0}/μA	i_{pas}/i_{pcs}
0.05	−1.594	−1.501	−1.530	1.596	1.733	0.986	0.967	0.93
0.07	−1.593	−1.502	−1.530	1.857	2.030	1.154	1.116	0.92
0.09	−1.597	−1.501	−1.532	2.092	2.283	1.289	1.295	0.93
0.11	−1.600	−1.498	−1.533	2.295	2.511	1.404	1.420	0.95
0.13	−1.604	−1.496	−1.535	2.482	2.716	1.511	1.569	0.92
0.15	−1.606	−1.498	−1.536	2.649	2.908	1.608	1.678	0.92

All potentials are versus Fc/Fc^+.

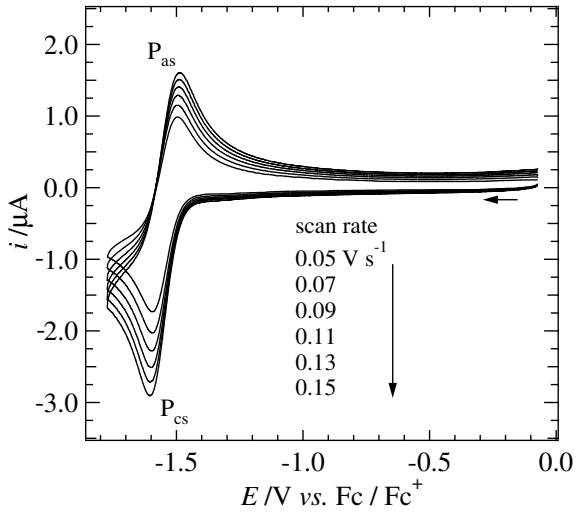

Figure 4.6. Cyclic voltammograms of $U^{VI}O_2$(saloph)DMSO (9.55×10^{-4} M) in DMSO containing TBAP (0.10 M) measured in the potential range from −0.073 to −1.773 V *vs.* Fc/Fc^+ at different scan rates (v = 0.05 – 0.15 $V{\cdot}s^{-1}$). Initial scan direction: cathodic.

system and has no successive reactions to produce electrochemically active substance in this potential range. The possibility of the two-electron reduction of $U^{VI}O_2$(saloph)DMSO at E_{pcs} can be ruled out, because of the reversibility of the cyclic voltammograms in Figure 4.6 and the same discussion as Section 4.1. Therefore, the electrochemical reaction in the potential range from −0.073 to −1.773 V *vs.* Fc/Fc^+ should be

$$U^{VI}O_2(\text{saloph})\text{DMSO} + e^- \rightleftarrows [U^{V}O_2(\text{saloph})\text{DMSO}]^-. \tag{4.16}$$

For a more quantitative discussion on the electrochemical reaction mechanism in this system, the UV-visible spectroelectrochemical measurements were carried out for the $U^{VI}O_2$-(saloph)DMSO (8.56×10^{-4} M) in DMSO containing TBAP (0.30 M). The UV-visible absorption spectra of this sample solution were measured at various applied potentials in the range from 0 to −1.650 V *vs.* Fc/Fc^+. The results are shown in Figure 4.7. As can be seen from this figure, the spectral feature changed with a stepwise decrease in the applied potential and converged at −1.650 V *vs.* Fc/Fc^+. The clear isosbestic points were observed at 271, 387, 479 and 535 nm. This indicates that only one equilibrium exists in this system. Such an equilibrium should be the redox reaction of $U^{VI}O_2$(saloph)DMSO at E_{pcs}/E_{pas} in Figure 4.6.

To determine the electron stoichiometry (n) for the redox couple corresponding to E_{pcs}/E_{pas} in Figure 4.6, the Nernstian plot (Eq. 3.1) was applied for the absorbancies at 344 nm in Figure 4.7. The resulting plot is shown in Figure 4.8. From the intercept and slope of this plot, the values of $E^{\circ\prime}$ and n in the present system were calculated as -1.550 ± 0.001 V *vs.* Fc/Fc^+ and 1.09 ± 0.02, respectively. Therefore, it is concluded that the redox couple at E_{pcs}/E_{pas} corresponds to Eq. 4.16 and that the uranyl(V) complex, $[U^{V}O_2(\text{saloph})\text{DMSO}]^-$ stably exists in the DMSO solution.

The kinetic analyses for the electrochemical reaction (Eq. 4.16) were also performed by the same procedure as explained in Section 4.1. The αn_B value was evaluated to be 0.72 in average by Eq. 4.5, and hence, the D_O value for $U^{VI}O_2$(saloph)DMSO in DMSO

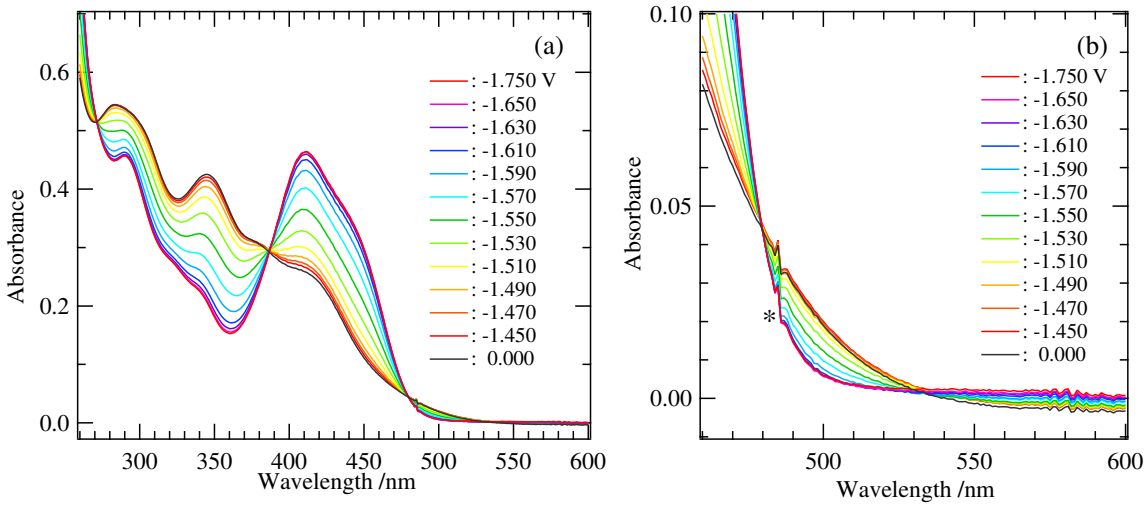

Figure 4.7. UV-visible absorption spectra measured at the applied potentials in the range from 0 to −1.650 V *vs.* Fc/Fc$^+$ for $U^{VI}O_2$(saloph)DMSO (8.56×10^{-4} M) in DMSO containing TBAP (0.30 M). Wavelength range, a: 260–600, b: 460–600 nm. Asterisk indicates noise of Agilent 8453 diode-allay spectrophotometer. Optical path length: 2.90×10^{-2} cm.

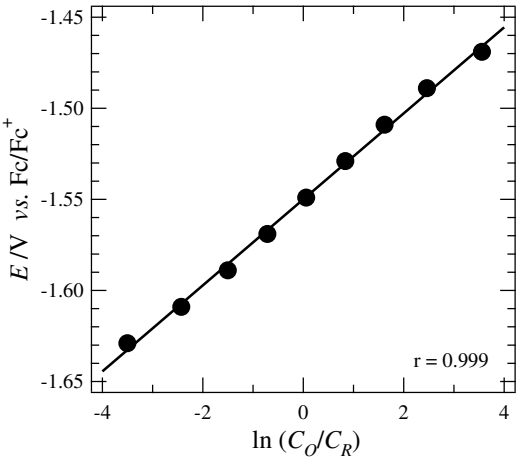

Figure 4.8. Nernstian plot for the absorbancies at 344 nm in Figure 4.7.

was estimated as 2.1×10^{-6} cm^2·s^{-1} by Eq. 4.4. The ψ values are in the range from 0.70 (v = 0.05 V·s^{-1}, ΔE_p = 0.093 V) to 0.46 (v = 0.15 V·s^{-1}, ΔE_p = 0.108 V).[190, 191] As a result, the k° value of Eq. 4.16 is estimated as 2.9×10^{-3} cm·s^{-1} by using Eq. 4.3.

To examine whether the DMSO dissociation from $[U^VO_2$(saloph)DMSO$]^-$ is also observed in the redox couple of $[U^VO_2$(saloph)DMSO$]^-$/$U^{VI}O_2$(saloph)DMSO, the CV experiments of this couple in the mixed solvent systems of DMSO and dichloromethane (DMSO + DM) were carried out. The resulting cyclic voltammograms are shown in Figure 4.9. From the K_{dim} value of Eq. 2.9, the dimerization of $U^{VI}O_2$(saloph)DMSO is negligible in all solutions. An uncoupled second oxidation peak (P_{as2}) was newly observed at *ca.* −1.1 V *vs.* Fc/Fc$^+$, which is similar to E_{paf2} in Figures 4.1 and 4.3. The relative current values at E_{pas} and E_{pas2} decrease and increase with a decrease in the concentration of the free DMSO, re-

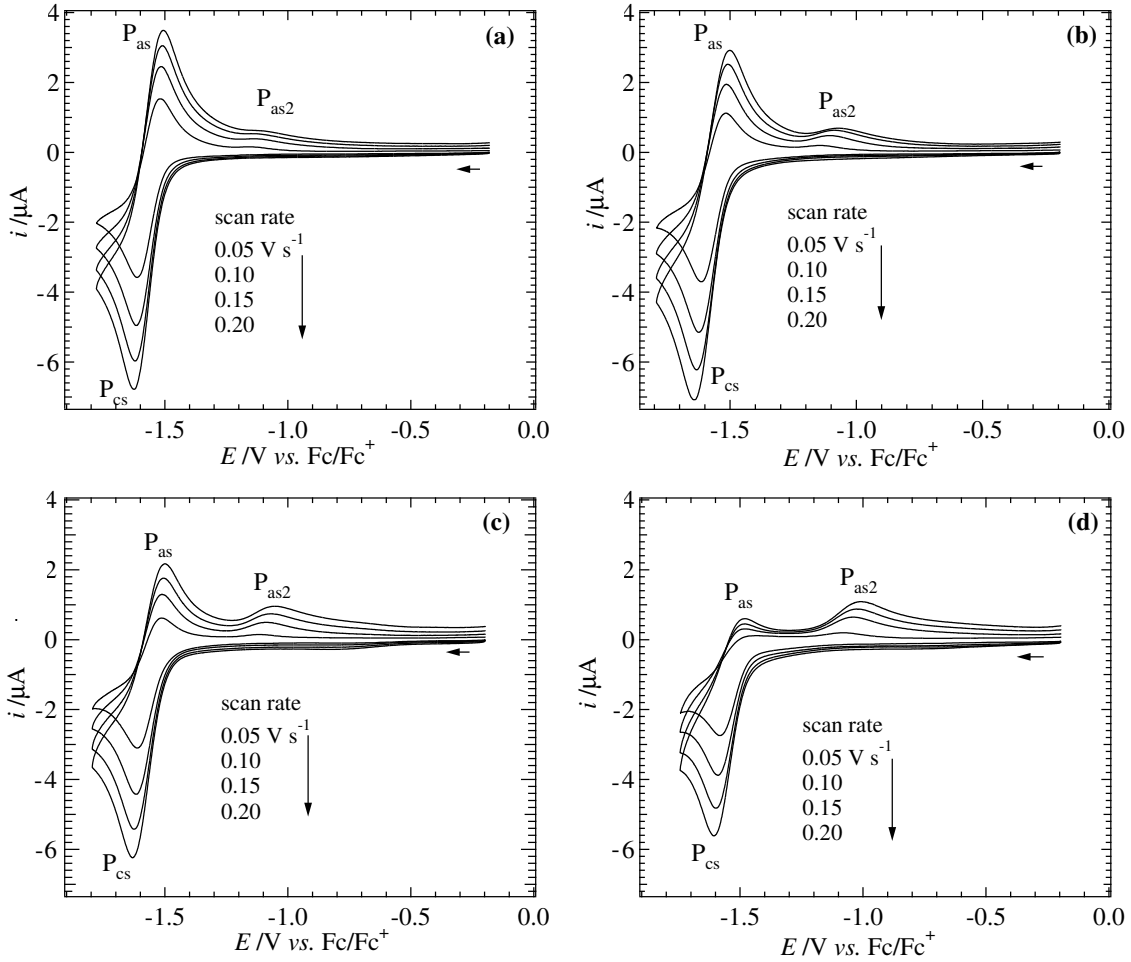

Figure 4.9. Cyclic voltammograms of $U^{VI}O_2$(saloph)DMSO (a: 1.11×10^{-3} M, b: 1.09×10^{-3} M, c: 1.08×10^{-3} M, and d: 1.14×10^{-3} M) in DMSO + DM containing TBAP (0.10 M). DMSO concentration, a: 1.67 M, b: 0.818 M, c: 0.486 M, and d: 0.182 M.

spectively. Even in the multiple-scanned cyclic voltammograms for the same solutions in Figure 4.9, no peak other than P_{cs}, P_{as}, and P_{as2} appeared. Therefore, it is clarified that the electrochemical reduction of $U^{VI}O_2$(saloph)DMSO can also be accompanied by the dissociation of the coordinated DMSO from $[U^{V}O_2(saloph)DMSO]^-$ as follows.

$$U^{VI}O_2(saloph)DMSO + e^- \rightleftarrows [U^{V}O_2(saloph)DMSO]^- \quad (E_{pcs}/E_{pas}) \tag{4.17}$$

$$[U^{V}O_2(saloph)DMSO]^- \rightleftarrows [U^{V}O_2(saloph)]^- + DMSO \tag{4.18}$$

$$[U^{V}O_2(saloph)]^- \longrightarrow U^{VI}O_2(saloph) + e^- \quad (E_{pas2}) \tag{4.19}$$

$$U^{VI}O_2(saloph) + DMSO \longrightarrow U^{VI}O_2(saloph)DMSO \tag{4.20}$$

The dissociation constant (K_{disV}) of Eq. 4.18 was estimated by the peak current values in Figure 4.9 and Eq. 4.15, in which i_{paf1}/i_{pcf1} and [DMF] were replaced by i_{pas}/i_{pcs} and [DMSO], respectively. The resulting K_{disV} value was 0.5 M in average, which is smaller than that for $[U^{V}O_2(saloph)DMF]^-$ (5 M). Such a difference in K_{disV} means that the coordination ability of DMSO to $[U^{V}O_2(saloph)]^-$ is stronger than that of DMF. Consequently, the overall mechanisms including the electrochemical reaction, the dimerization, and the DMSO exchange

reaction of $U^{VI}O_2$(saloph)DMSO are same as those of $U^{VI}O_2$(saloph)DMF (Figure 4.5) in which DMF was displaced by DMSO. In a similar manner to $[U^{V}O_2(saloph)DMF]^-$, the first-order rate constant of the DMSO exchange reaction in $[U^{V}O_2(saloph)DMSO]^-$ can be estimated about 10^5 s^{-1}, which is two-order lager than that in $U^{VI}O_2$(saloph)DMSO ($k_{ex} = 1.63 \times 10^3$ s^{-1} at 298 K).

In this section, $[U^{V}O_2(saloph)DMSO]^-$ was found to exist stably in DMSO. This is the first example of the stable uranyl(V) species in nonaqueous solvents.

4.3 $U^{VI}O_2(dbm)_2DMSO$ in Dimethyl Sulfoxide

In Sections 4.1 and 4.2, it was found that the DMSO molecule can coordinate to uranium more strongly than DMF even in the uranyl(V) complexes and that the uranyl complexes with DMSO and multidentate ligand like as saloph have a possibility to form the stable uranyl(V) complex in DMSO solution. Therefore, for another candidate for the system of the stable uranyl(V) species, dibenzoylmethanate (dbm) and DMSO was selected as ligands to $U^{V}O_2^+$.

4.3.1 Experimental Details

Electrochemical Measurements. The CV measurements for $U^{VI}O_2$(saloph)DMSO in DMSO were carried out in a similar manner to those for $U^{VI}O_2$(saloph)DMF. Dimethyl sulfoxide as the solvent was distilled under vacuum after the drying with CaH_2, and then stored over molecular sieves 4A (Wako).

UV-visible Spectroelectrochemical Measurements. The UV-visible spectroelectrochemical measurements were performed for $U^{VI}O_2(dbm)_2DMSO$. The effective optical path length of the OTTLE cell was spectrophotometrically calibrated as 2.80×10^{-2} cm. Other details were same as those described in Section 4.1.1

4.3.2 Results and Discussion

In order to investigate the redox behavior of $U^{VI}O_2(dbm)_2DMSO$ in DMSO, the CV measurements were carried out. The resulting cyclic voltammograms of $U^{VI}O_2(dbm)_2DMSO$ (1.04×10^{-3} M) in DMSO containing TBAP (0.10 M) are shown in Fig. 4.10. In this figure, reduction and oxidation peaks, P_{cd} and P_{ad}, were observed at around -1.40 (E_{pcd}) and

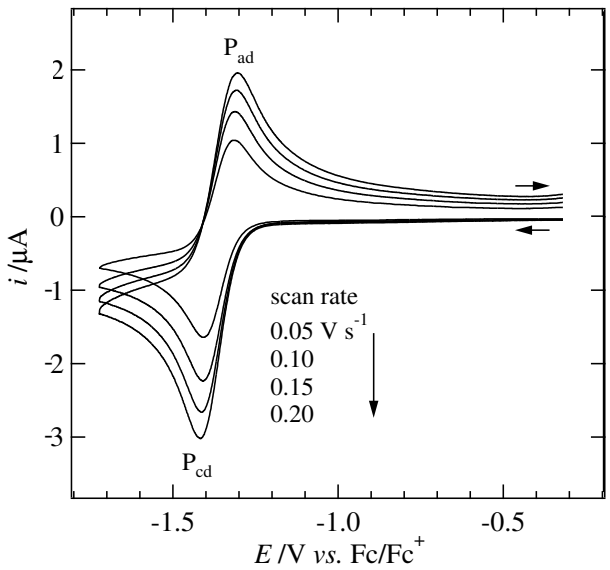

Figure 4.10. Cyclic voltammograms for $U^{VI}O_2(dbm)_2DMSO$ (1.04×10^{-3} M) in DMSO containing TBAP (0.10 M) in the potential range from -0.323 to -1.723 V. Initial scan direction: Cathodic.

Table 4.3. Electrochemical data of $U^{VI}O_2(dbm)_2$DMSO in DMSO

v /V·s^{-1}	E_{pcd} /V	E_{pad} /V	$E_{pcd/2}$ /V	i_{pcd}/μA	i_{pc0}/μA	i_{pa0}/μA	i_{sp0}/μA	i_{pad}/i_{pcd}
0.05	−1.407	−1.317	−1.346	1.525	1.043	1.640	0.698	0.93
0.10	−1.408	−1.317	−1.345	2.120	1.426	2.235	0.966	0.93
0.15	−1.413	−1.308	−1.348	2.523	1.719	2.660	1.147	0.94
0.20	−1.418	−1.307	−1.350	2.963	1.954	3.017	1.327	0.95

All potentials are versus Fc/Fc^+.

−1.30 (E_{pad}) V *vs.* Fc/Fc^+, respectively. The i_{pad}/i_{pcd} values at the various scan rates v were calculated by Eq. 4.1. The electrochemical data of $U^{VI}O_2(dbm)_2$DMSO are summarized in Table 4.3. The ΔE_p values increased from 0.090 to 0.111 V with an increase in v. These results indicate that the electrochemical reaction of $U^{VI}O_2(dbm)_2$DMSO is a quasi-reversible system. The i_{pad}/i_{pcd} values close to unity suggest that the reduction product of $U^{VI}O_2(dbm)_2$-DMSO is almost completely reoxidized to $U^{VI}O_2(dbm)_2$DMSO without any successive reactions such as the DMSO dissociation (*cf.* Eqs. 4.7 and 4.18) observed in the systems of $U^{VI}O_2$(saloph)DMF and $U^{VI}O_2$(saloph)DMSO. This is supported by the fact that any other redox waves except for P_{cd} and P_{ad} were not observed even in the multiple scanned cyclic voltammograms of $U^{VI}O_2(dbm)_2$DMSO. Therefore, the electrochemical reaction of $U^{VI}O_2$-$(dbm)_2$DMSO in DMSO observed in Figure 4.10 is considered to be,

$$U^{VI}O_2(dbm)_2DMSO + e^- \rightleftarrows [U^{V}O_2(dbm)_2DMSO]^-. \quad (4.21)$$

The formal potential $E^{\circ\prime}$ (= $(E_{pcd} + E_{pad})/2$) of the redox couple P_{cd}/P_{ad} was constant at −1.362 ± 0.002 V *vs.* Fc/Fc^+.

To confirm the validity of Eq. 4.21 quantitatively, the UV-visible spectroelectrochemical measurements were performed for the DMSO solution containing $U^{VI}O_2(dbm)_2$DMSO (1.04×10^{-3} M) and TBAP (0.30 M) by using the OTTLE cell (optical path length: 2.80 ×

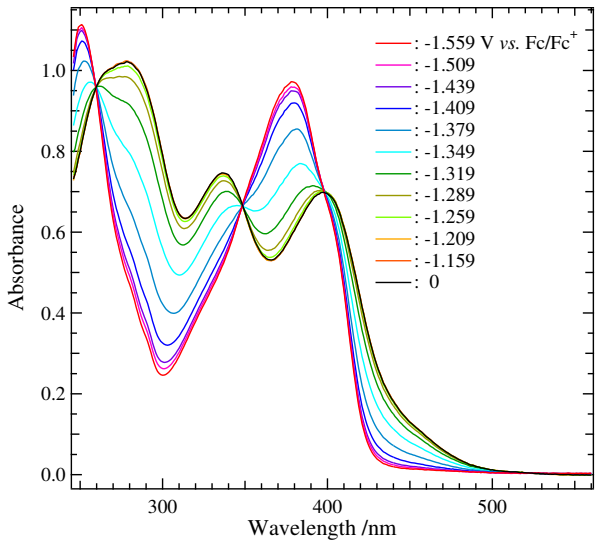

Figure 4.11. UV-visible absorption spectra measured at the applied potentials in the range from 0 to −1.559 V *vs.* Fc/Fc^+ for $U^{VI}O_2(dbm)_2$DMSO (1.04×10^{-3} M) in DMSO containing TBAP (0.30 M). Optical path length: 2.80×10^{-2} cm.

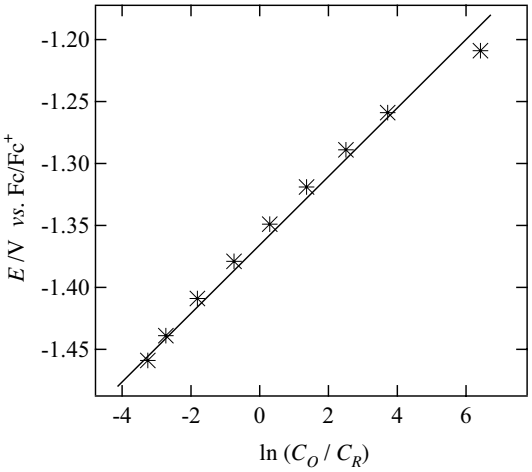

Figure 4.12. Nernstian plot for the absorbancies at 379 nm in Figure 4.11.

10^{-2} cm). The potential applied on the OTTLE were changed stepwise in the range from 0 to −1.559 V *vs.* Fc/Fc^+. The results are shown in Figure 4.11. The isosbestic points were clearly observed at 260, 348, 398, and 524 nm, indicating that only one equilibrium exists in this system. The applied potential values were plotted against the corresponding logarithmical concentration profiles according to the Nernstian Eq. 3.1 as shown in Figure 4.12. The slope and intercept of the least-square line for these plot were 0.028 ± 0.001 and −1.366 ± 0.004. From these data, the electron stoichiometry n and the formal potential $E^{\circ\prime}$ were evaluated as 0.92 ± 0.03 and −1.366 ± 0.004 V *vs.* Fc/Fc^+, respectively. The $E^{\circ\prime}$ value obtained in the UV-visible spectroelectrochemical measurements was comparable with that from the cyclic voltammograms. As a consequence, the validity of Eq. 4.21 was confirmed by the almost unity value of n. Thus, it was concluded that $[U^{V}O_2(dbm)_2DMSO]^-$ is purely produced as the stable uranyl(V) complex in DMSO. The absorption spectrum measured at −1.550 V *vs.* Fc/Fc^+ in Figure 4.11 is assigned to pure $[U^{V}O_2(dbm)_2DMSO]^-$ in DMSO.

Since the electrochemical reaction of $U^{VI}O_2(dbm)_2DMSO$ is quasi-reversible, the diffusion coefficient (D_O) of $U^{VI}O_2(dbm)_2DMSO$ and the standard rate constant k° in Eq. 4.21 were evaluated in a similar manner to Sections 4.1 and 4.2. The αn_B value in Eq. 4.4 was calculated as 0.74 in average by using Eq. 4.5. Therefore, the D_O value of $U^{VI}O_2(dbm)_2$-DMSO was estimated as 1.5×10^{-6} $cm^2 \cdot s^{-1}$ by Eq. 4.4. According to Nicholson,[190,191] the ψ values corresponding to the various v were 0.77 (v = 0.05 $V \cdot s^{-1}$) 0.75 (v = 0.10 $V \cdot s^{-1}$), 0.50 (v = 0.15 $V \cdot s^{-1}$), and 0.43 (v = 0.20 $V \cdot s^{-1}$). Thus, the k° value was estimated as 2.7×10^{-3} $cm \cdot s^{-1}$ in average by using Eq. 4.3.

The DMSO dissociation from $[U^{V}O_2(dbm)_2DMSO]^-$ was not examined by using the mixed solvent systems. However, it is reasonable to consider that the DMSO exchange reaction in $[U^{V}O_2(dbm)_2DMSO]^-$ should occurs in the solution through the dissociative mechanism because of the quite similar structure of $[U^{V}O_2(dbm)_2DMSO]^-$ to $U^{VI}O_2(dbm)_2$-DMSO (see Chapter 5). If the same discussion as $[U^{V}O_2(saloph)DMF]^-$ and $[U^{V}O_2(saloph)$-$DMSO]^-$ is also applicable to the present system, the first-order rate constant of the DMSO exchange reaction in $[U^{V}O_2(dbm)_2DMSO]^-$ may be estimated *ca.* 10^4 s^{-1}. The difference between the estimated rate constants of the DMSO exchange reactions in $[U^{V}O_2(saloph)$-$DMSO]^-$ (10^5 s^{-1}) and $[U^{V}O_2(dbm)_2DMSO]^-$ (10^4 s^{-1}) might imply the difference between

the coordination strengths of DMSO to $[U^{V}O_2(saloph)]^-$ and $U^{V}O_2(dbm)_2$ fragments.

In this section, it was clarified that $[U^{V}O_2(dbm)_2DMSO]^-$ stably exists in the DMSO solution. This is the second system of a stable uranyl(V) complex in nonaqueous system.

Chapter 5

Structural Changes of Uranyl Moiety with Reduction from U(VI) to U(V)

Molecular structure of the uranyl(V) complex is one of the most important issue in this thesis. Infrared (IR) spectroscopy is a good method to investigate the molecular structures of objective complexes. Furthermore, the spectroelectrochemical technique can also be combined with the IR spectroscopy. Unfortunately, it is difficult to apply the IR spectroscopy to the aqueous system, because of the strong absorption due to water in IR region. However, the structural properties of $[U^{V}O_2(CO_3)_3]^{5-}$, which is only one stable uranyl(V) species in the aqueous system, has been already analyzed in Section 3.2 (coordination number of CO_3^{2-}), and the previous Raman[151)] and EXAFS[153)] studies (symmetric stretching frequency (ν_1) and bond distances, respectively). Therefore, the IR spectroscopy for the redox couples of $[U^{V}O_2(\text{saloph})\text{DMSO}]^{-}$/$U^{VI}O_2(\text{saloph})\text{DMSO}$ and $[U^{V}O_2(\text{dbm})_2\text{DMSO}]^{-}$/$U^{VI}O_2(\text{dbm})_2$-DMSO in DMSO solutions using the spectroelectrochemical method have been performed to examine the vibrational and structural properties of the present uranyl(V/VI) complexes. The results are discussed with the previous theoretical and experimental data of actinyl(V/VI) couples, not only uranyl(V/VI) ones.

5.1 Experimental Details

IR Spectroelectrochemical Measurements. The spectroelectrochemical technique was combined with IR spectroscopy. An IR spectroelectrochemical thin layer electrode cell (IRTLE cell) was produced as shown in Figure 5.1. The IR spectra were measured after achievement of equilibrium at each applied potential on the working electrode in the IRTLE cell, which requires 2 min. To improve a ratio of signal-to-noise in this technique, each IR spectrum was accumulated 500 times. Other conditions were same as those of the CV measurements, *e.g.* Section 4.1.

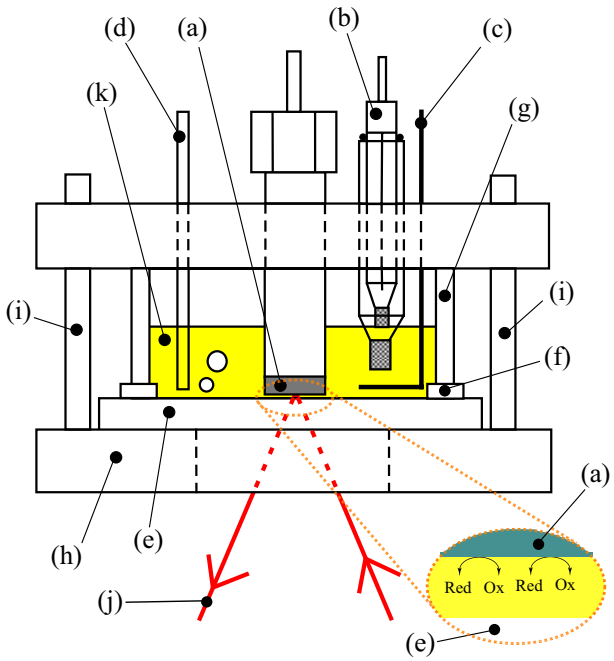

Figure 5.1. Schematic view of IRTLE cell. (a) Pt working electrod, (b) Ag/AgCl reference electrode with a liquid junction filled by 0.1 M TBAP/DMSO, (c) Pt counter electrode, (d) argon gas inlet, (e) NaCl window, (f) PTFE rubber packing, (g) glass cell, (h) PTFE frames, (i) PTFE screws, (j) He-Ne laser from SHIMADZU FTIR-8400S, and (k) sample solution.

5.2 Results

5.2.1 $[U^{V}O_2(saloph)DMSO]^-/U^{VI}O_2(saloph)DMSO$ in Dimethyl Sulfoxide

To confirm that the IR spectroelectrochemical thin layer electrode (IRTLE) cell functions properly, the IR spectrum of $U^{VI}O_2$(saloph)DMSO (8.0×10^{-3} M) in DMSO containing TBAP (0.10 M) was measured by using the standard liquid (SL) and IRTLE cells. The results are shown in Figure 5.2. These FTIR spectra by using SL and IRTLE cells required 40 and 500 times accumulation to obtain them with acceptable signal-to-noise (S/N) ratio, respectively. In the IR spectrum measured with the SL cell (black line, Figure 5.2), the characteristic peaks for azomethine stretching ($\nu_{C=N}$) and asymmetric stretching of uranyl moiety (ν_3) of $U^{VI}O_2$(saloph)DMSO are observed at 1605 and 895 cm^{-1}, respectively, being consistent with those of the solid state of $U^{VI}O_2$(saloph)DMSO in KBr (Section 2.3). These peaks are also obseved in the IR spectrum measured with the IRTLE cell (red line, Figure 5.2). Therefore, it was confirmed that the IRTLE cell functions as well as the SL cell. Since the S/N ratio of the IR spectra with the IRTLE cell is somewhat poor, the ν_3 peak of $U^{VI}O_2$(saloph)DMSO at 895 cm^{-1} is split by noise.

In order to examine the vibrational changes with the reduction of $U^{VI}O_2$(saloph)DMSO to $[U^{V}O_2(saloph)DMSO]^-$, the IR spectra at various potentials were measured. The applied potential was changed stepwise from 0 to −1.73 V *vs.* Fc/Fc^+. The results are shown in Figure 5.3, where two regions of the IR spectra due to saloph (1700–1420 cm^{-1}) and uranyl (950–700 cm^{-1}) moieties are displayed in parts (a) and (b), separately. The clear isosbestic points are observed at 1577 and 1531 cm^{-1} in Figure 5.3(a), indicating that only the redox equilibrium of $[U^{V}O_2(saloph)DMSO]^-/U^{VI}O_2$(saloph)DMSO (Eq. 4.16) exists in this system. From the Nernstian equation (Eq. 3.1) and the potential data in Section 4.2, the IR spectrum measured at −1.73 V *vs.* Fc/Fc^+ was assigned to that of pure $[U^{V}O_2(saloph)DMSO]^-$. The reproducibility of the IR spectrum in the reverse reaction ($[U^{V}O_2(saloph)DMSO]^- \rightarrow U^{VI}O_2$(saloph)DMSO + e^-) was confirmed by application of the potential at −1.33 V *vs.* Fc/Fc^+, which is sufficient to oxidize $[U^{V}O_2(saloph)DMSO]^-$ to $U^{VI}O_2$(saloph)DMSO completely. This is the first observation of the IR spectrum of pure uranyl(V) complex.

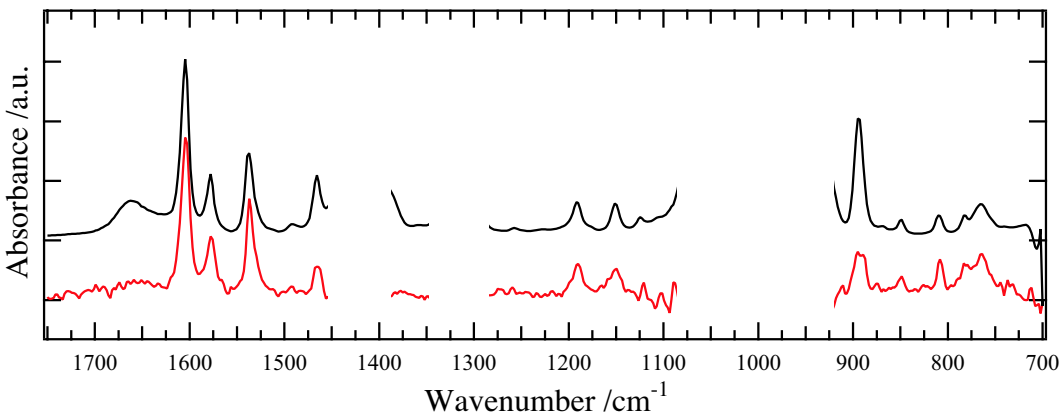

Figure 5.2. IR spectra of $U^{VI}O_2$(saloph)DMSO (8.0×10^{-3} M) in DMSO containing TBAP (0.10 M) measured with SL (black) and IRTLE (red) cells.

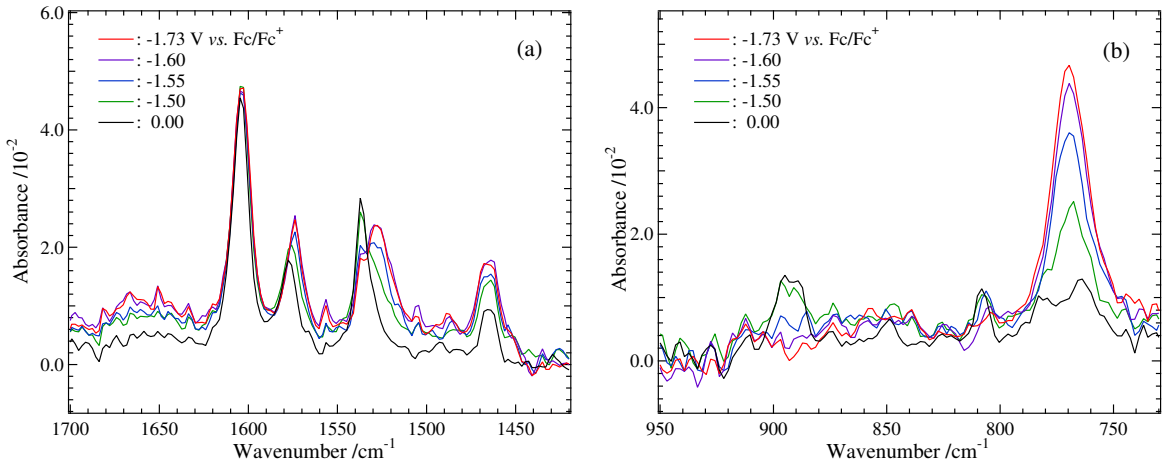

Figure 5.3. IR spectra of $[U^{V}O_2(saloph)DMSO]^-$/$U^{VI}O_2(saloph)DMSO$ (8.0×10^{-3} M) in DMSO containing TBAP (0.10 M) at various applied potentials. Wavenumber range: (a) 1700–1420 cm^{-1}, (b) 950–700 cm^{-1}. Peak at 895 cm^{-1} is split by noise.

In Figure 5.3(a), the IR peaks due to the coordinated saloph showed slight changes with the isosbestic points at 1577 and 1531 cm^{-1}. However, any significant changes in the IR spectra of the coordinated saloph were not observed in spite of the reduction from $U^{VI}O_2$-(saloph)DMSO to $[U^{V}O_2(saloph)DMSO]^-$. This result indicates that the structure of the coordinated saloph in $[U^{V}O_2(saloph)DMSO]^-$ is similar to that in $U^{VI}O_2(saloph)DMSO$.

In Figure 5.3(b), with the reduction from $U^{VI}O_2(saloph)DMSO$ to $[U^{V}O_2(saloph)DMSO]^-$, the ν_3 peak of $U^{VI}O_2(saloph)DMSO$ at 895 cm^{-1} disappeared and a new peak appeared at 770 cm^{-1}. Since the electron density on U^{5+} is larger than that on U^{6+}, the electrostatic attraction between U^{n+} (n = 5, 6) and O^{2-} in $U^{V}O_2^+$ should be smaller than that in $U^{VI}O_2^{2+}$. Thus, it is considered that the U=O bond strength in $U^{V}O_2^+$ is weaker than that in $U^{VI}O_2^{2+}$. This leads to the shift of the ν_3 peak to lower energy region with the reduction from $U^{VI}O_2^{2+}$ to $U^{V}O_2^+$. Hence, the peak at 770 cm^{-1} in the IR spectrum of $[U^{V}O_2(saloph)DMSO]^-$ can be assigned to the ν_3 peak of this uranyl(V) complex. The difference ($\Delta\nu_3$) between the ν_3 peaks of $[U^{V}O_2(saloph)DMSO]^-$ and $U^{VI}O_2(saloph)DMSO$ is 125 cm^{-1}.

5.2.2 $[U^{V}O_2(dbm)_2DMSO]^-$/$U^{VI}O_2(dbm)_2DMSO$ in Dimethyl Sulfoxide

The IR spectroelectrochemical measurements for the redox couple of $[U^{V}O_2(dbm)_2$-$DMSO]^-$/ $U^{VI}O_2(dbm)_2DMSO$ were performed to obtain the data concerning the vibrational properties of $[U^{V}O_2(dbm)_2DMSO]^-$ by using the same technique. The potential applied on the IRTLE was changed from 0 to −1.56 V *vs.* Fc/Fc^+. The resulting spectra are shown in Figure 5.4. The peak heights are not reflecting the concentrations of $[U^{V}O_2(dbm)_2DMSO]^-$ and $U^{VI}O_2(dbm)_2DMSO$ directly, because the normalization of the spectral intensities has not been performed. Since the fraction of $[U^{V}O_2(dbm)_2DMSO]^-$ at −1.56 V *vs.* Fc/Fc^+ was evaluated as 99.9% from Eq. 3.1 and $E^{\circ\prime}$ value of $[U^{V}O_2(dbm)_2DMSO]^-$/$U^{VI}O_2(dbm)_2$-DMSO (−1.366 V *vs.* Fc/Fc^+), the IR spectrum measured at the most negative potential in Figure 5.4 is attributable to that of pure $[U^{V}O_2(dbm)_2DMSO]^-$.

In Figure 5.4(a), the IR peaks due to the coordinated dbm show small shifts in the re-

gion from 0 to 12 cm^{-1} with the reduction of $U^{VI}O_2(dbm)_2DMSO$ to $[U^{V}O_2(dbm)_2DMSO]^-$, indicating that the structural changes of the coordinated dbm itself are small. This is the same phenomenon as that observed in the $[U^{V}O_2(saloph)DMSO]^-/U^{VI}O_2(saloph)DMSO$ redox system.

In Figure 5.4(b), the disappearance of the ν_3 peak of $U^{VI}O_2(dbm)_2DMSO$ at 906 cm^{-1} and the appearance of a new peak at 775 cm^{-1} were observed with the reduction from $U^{VI}O_2(dbm)_2DMSO$ to $[U^{V}O_2(dbm)_2DMSO]^-$. From the same consideration as the case of $[U^{V}O_2(saloph)DMSO]^-$, the new peak at 775 cm^{-1} can be assigned to the ν_3 peak of $[U^{V}O_2(dbm)_2DMSO]^-$. The $\Delta\nu_3$ value between $[U^{V}O_2(dbm)_2DMSO]^-$ and $U^{VI}O_2(dbm)_2DMSO$ is 131 cm^{-1}, which is the quite similar value to that of the $[U^{V}O_2(saloph)DMSO]^-/U^{VI}O_2(saloph)DMSO$ system. This red shift of the ν_3 peak also means the weakening of the U=O bond strength with the reduction from $U^{VI}O_2(dbm)_2DMSO$ to $[U^{V}O_2(dbm)_2DMSO]^-$.

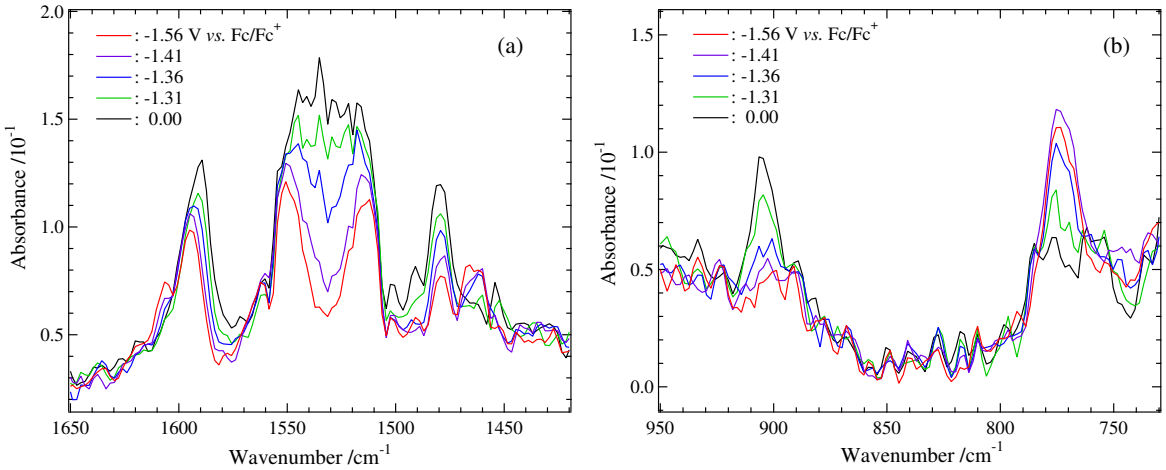

Figure 5.4. IR spectra of $[U^{V}O_2(dbm)_2DMSO]^-/U^{VI}O_2(dbm)_2DMSO$($6.0 \times 10^{-3}$ M) in DMSO containing TBAP (0.10 M) at various applied potentials. Wavenumber range: (a) 1650–1420 cm^{-1}, (b) 950–730 cm^{-1}. Peaks at 1538 and 1522 cm^{-1} are split by noise.

5.3 Discussion

Because of no significant spectral changes in Figures 5.3(a) and 5.4(a), it was found that the structures of the ligands themselves (saloph and dbm) coordinated in the equatorial plane of the uranyl moieties are not largely influenced by the changes in the oxidation states of the center uranium. On the other hand, in Figures 5.3(b) and 5.4(b), it was clarified that the ν_3 peaks due to the axial uranyl moiety show the remarkable red shifts about 130 cm^{-1} with the reduction from $U^{VI}O_2^{2+}$ to $U^{V}O_2^{+}$. The similar phenomenon was also confirmed in the system of $[U^{V}O_2(CO_3)_3]^{5-}$/$[U^{VI}O_2(CO_3)_3]^{4-}$. Madic *et al.* studied the Raman spectra of this aqueous system, and reported the red shift of the symmetric stretching (ν_1) peak of the uranyl moiety with the reduction from $[U^{VI}O_2(CO_3)_3]^{4-}$ (812 cm^{-1}) to $[U^{V}O_2(CO_3)_3]^{5-}$ (759 cm^{-1}).[151] Therefore, it is concluded that the weakening of the U=O bond strength with the reduction from $U^{VI}O_2^{2+}$ to $U^{V}O_2^{+}$ is the common property of the uranyl(V/VI) redox systems.

According to Jones,[8] the force constant of the U=O bond in the uranyl moiety (F_{UO}) can be related to its bond distance (R_{UO}) by Badger's rule[9] as follows.

$$R_{UO} = \beta \cdot F_{UO}^{-\frac{1}{3}} + d_{UO} \tag{5.1}$$

where β and d_{UO} are constants defined by Badger.[9] In the definition,[8] the value of β is about 1.08 for all pairs of elements if one element has atomic number greater than 18, *i.e.*, $_{92}$U. The F_{UO} values of the U=O bonds of $[U^{V}O_2(saloph)DMSO]^{-}$, $U^{VI}O_2(saloph)DMSO$, $[U^{V}O_2(dbm)_2DMSO]^{-}$, and $U^{VI}O_2(dbm)_2DMSO$ were roughly estimated as 5.31, 7.17, 5.31, 7.25 mdyne·$Å^{-1}$, respectively, by Eq. 5.2.

$$\nu_3 = (2\pi c)^{-1} \sqrt{\frac{F_{UO}(m_U + m_O)}{(m_U m_O)}} \tag{5.2}$$

where c, m_U, and m_O are light velocity (3.00×10^{10} cm·s^{-1}), mass of U ($238/N_A$; N_A: Avogadro number, 6.02×10^{23}) and, mass of O ($16/N_A$). The d_{UO} values for $U^{VI}O_2(saloph)DMSO$ and $U^{VI}O_2(dbm)_2DMSO$ were calculated as 1.22 and 1.23 Å, respectively, by using Eq. 5.1 together with the average R_{UO} values in these uranyl(VI) complexes (1.783 Å and 1.784 Å, respectively) from the single crystal X-ray analyses (see Sections 2.3 and 2.4) and their F_{UO}values. As a result of Eq. 5.1 with F_{UO} of the uranyl(V) complexes and d_{UO} of the corresponding uranyl(VI) ones, both R_{UO} values of $[U^{V}O_2(saloph)DMSO]^{-}$ and $[U^{V}O_2(dbm)_2$-$DMSO]^{-}$ were estimated as 1.84 Å. The difference between R_{UO} (ΔR_{UO}) of the uranyl(V) and uranyl(VI) complexes were 0.06 Å for both $[U^{V}O_2(saloph)DMSO]^{-}$/$U^{VI}O_2(saloph)DMSO$ and $[U^{V}O_2(dbm)_2DMSO]^{-}$/$U^{VI}O_2(dbm)_2DMSO$ systems.

The results obtained for the present uranyl(V/VI) complexes can be compared with the experimental and theoretical data concerning the stretching frequencies in the actinyl(V/VI) moieties and U=O bond distances in other systems, which are summarized in Table 5.1. In this table, the values of $\Delta\nu_3$ for $[U^{V}O_2(saloph)DMSO]^{-}$/ $U^{VI}O_2(saloph)DMSO$ and $[U^{V}O_2$-$(dbm)_2DMSO]^{-}$/ $U^{VI}O_2(dbm)_2DMSO$ are comparable with the experimental results for $Np^{V}O_2^{+}$/ $Np^{VI}O_2^{2+}$ (145 ± 5 cm^{-1}) and $Am^{V}O_2^{+}$/ $Am^{VI}O_2^{2+}$ (107 ± 3 cm^{-1}) by Jones and Penneman[155] and the theoretical prediction for $U^{V}O_2(H_2O)_5^{+}$ /$U^{VI}O_2(H_2O)_5^{2+}$ (92 cm^{-1}) by Hay *et al.*[108] Such a consistency of $\Delta\nu_3$ indicates the validity of the assignments for the peaks at 770 cm^{-1} in Figure 5.3(b) and 775 cm^{-1} in Figure 5.4(b) to the ν_3 ones of $[U^{V}O_2(saloph)DMSO]^{-}$ and $[U^{V}O_2(dbm)_2DMSO]^{-}$, respectively.

Table 5.1. Vibrational and structural properties of AnO_2^{n+} (n = 1 or 2) species

An(V), (VI)	ν_3 /cm^{-1}	$\Delta\nu_3$ /cm^{-1} [a]	F_{AnO} /mdyne·Å^{-1} [b]	R_{UO} /Å	ΔR_{UO} /Å[c]	Reference
$[U^{V}O_2(saloph)DMSO]^-$	770	125	5.31[d]	1.84	0.06	This work
$U^{VI}O_2(saloph)DMSO$	895		7.17[d]	1.783[e]		This work
$[U^{V}O_2(dbm)_2DMSO]^-$	775	131	5.31[d]	1.84	0.06	This work
$U^{VI}O_2(dbm)_2DMSO$	906		7.25[d]	1.784[e]		This work
$Np^{V}O_2^+$ [f]	824 ± 4	145 ± 5	5.65 ± 0.06	–	–	[155]
$Np^{VI}O_2^{2+}$ [f]	969 ± 1		7.81 ± 0.02	–		[155]
$Am^{V}O_2^+$ [f]	832 ± 2	107 ± 3	5.77 ± 0.03	–	–	[155]
$Am^{VI}O_2^{2+}$ [f]	939 ± 1		7.35 ± 0.02	–		[155]
$U^{V}O_2(H_2O)_5^+$ [g]	909	92	–	1.810	0.054	[108]
$U^{VI}O_2(H_2O)_5^{2+}$ [g]	1001		–	1.756		[108]
$[U^{V}O_2(CO_3)_3]^{5-}$ [h]	759 (ν_1)	53 ($\Delta\nu_1$)	–	–	–	[151]
$[U^{VI}O_2(CO_3)_3]^{4-}$ [h]	812 (ν_1)		–	–		[151]
$[U^{V}O_2(CO_3)_3]^{5-}$ [i]	–	–	–	1.90 ± 0.02	0.10 ± 0.04	[153]
$[U^{VI}O_2(CO_3)_3]^{4-}$ [i]	–		–	1.80 ± 0.02		[153]
$[U^{V}O_2(CO_3)_3]^{5-}$ [j]	–	–	–	1.929	0.083	[110]
$[U^{VI}O_2(CO_3)_3]^{4-}$ [j]	–		–	1.845		[110]
$[U^{V}O_2(OPPh_3)_4](CF_3SO_3)$ [k]	–	–	–	1.821	0.059	[194]
$[U^{VI}O_2(OPPh_3)_4](CF_3SO_3)_2$ [k]	–		–	1.762		[194]

[a] Difference between the ν_3 peaks of $An^{VI}O_2^{2+}$ and $An^{V}O_2^+$. [b] Force constants of An=O bond. [c] Difference between R_{UO} of $U^{V}O_2^+$ and $U^{VI}O_2^{2+}$. [d] Roughly estimated by the equation: $\nu_3 = (2\pi c)^{-1}\sqrt{F_{UO}(m_U + m_O)/(m_U m_O)}$ (c, light velocity; m_U, mass of U; m_O, mass of O). [e] Average of the R_{UO} values in the single crystal X-ray analysis in Sections 2.3 and 2.4. [f] Experimental data by Jones and Penneman[155] [g] Theoretical data by Hay *et al.*[108] [h] Experimental data by Madic *et al.*[151] [i] Experimental data by Docrat *et al.*[153] [j] Theoretical data by Gagliardi *et al.*[110] [k] Experimental data by Berthet *et al.*[194]

In the theoretical calculations, the R_{UO} values of the uranyl(V) species were simulated as 1.810 Å for in $U^{V}O_2(H_2O)_5^+$ by Hay *et al.*[108] and 1.929 Å for $[U^{V}O_2(CO_3)_3]^{5-}$ by Gagliardi *et al.*,[110] which are 0.054 and 0.083 Å longer than those in the corresponding uranyl(VI) species, respectively. Furthermore, only two data are available as experimental references for uranyl(V) species, one is the EXAFS study for $[U^{V}O_2(CO_3)_3]^{5-}$ by Docrat *et al.*[153] (R_{UO} = 1.90 ± 0.02 Å) and the other is the X-ray crystallographic study for the uranyl(V) complex with triphenylphosphine oxide ($OPPh_3$), $U^{V}O_2(OPPh_3)_4(CF_3SO_3)$, by Berthet *et al.*[194] (R_{UO} = 1.821 Å).[1] In the comparison with these data, the values of R_{UO} of $[U^{V}O_2$-(saloph)DMSO]$^-$ and $[U^{V}O_2(dbm)_2DMSO]^-$ and ΔR_{UO} of $[U^{V}O_2(saloph)DMSO]^-/U^{VI}O_2$-(saloph)DMSO and $[U^{V}O_2(dbm)_2DMSO]^-/ U^{VI}O_2(dbm)_2DMSO$ estimated in this study are concluded to be reasonable.

[1] According to Berthet and co-workers,[194] a few orange-colored crystals of $U^{V}O_2(OPPh_3)_4(CF_3SO_3)$ were serendipitously obtained from acetonitrile solution containing $U^{VI}O_2(CF_3SO_3)_2$ and $OPPh_3$ (1:4 molar ratio) under inert N_2 atmosphere. Thus, the acetonitrile solution containing $U^{V}O_2(OPPh_3)_4^+$ could be expected as the alternative system of the stable uranyl(V) complex. However, no data of $U^{V}O_2(OPPh_3)_4(CF_3SO_3)$ except for its molecular structure are reported. In this study, I have attempted the cyclic voltammetric measurement for $U^{VI}O_2(OPPh_3)_4^{2+}$ in acetonitrile. As a result, irreversible cyclic voltammograms of the acetonitrile solution containing $U^{VI}O_2(OPPh_3)_4^{2+}$ were recorded. This means that $U^{V}O_2(OPPh_3)_4^+$ is not stable in this system.

Chapter 6

Electronic Spectra of Uranyl(V) Complexes

Uranyl(V) has one unpaired electron in its 5f orbital, which is the simplest electronic configuration in the actinyl species. Thus, electronic structure of the uranyl(V) complex is the most essential issue to explore the coordination chemistry of not only uranyl, but also all actinyl ions. In spite of many attempts, there are no reports concerning the observation of the uranyl(V) complexes with identified structure as described in Chapter 1. As the exception, $[U^{V}O_2(CO_3)_3]^{5-}$ is traditionally known as the stable uranyl(V) complex in solution. However, even its spectroscopic properties is still uncertain.

In the previous chapters, it was found that two kinds of the uranyl(V) complexes are also stable in the nonaqueous systems and that they exist as $[U^{V}O_2(saloph)DMSO]^{-}$ and $[U^{V}O_2(dbm)_2DMSO]^{-}$. Here, the electronic spectra of three types of the pure uranyl(V) complexes, $[U^{V}O_2(CO_3)_3]^{5-}$, $[U^{V}O_2(saloph)DMSO]^{-}$, and $[U^{V}O_2(dbm)_2DMSO]^{-}$, have been measured and discussed their spectroscopic properties in a comparison each other.

6.1 Experimental Details

Visible-NIR Absorption Spectrum of $[U^{V}O_2(CO_3)_3]^{5-}$ in D_2O. The preparation of D_2O solution containing $[U^{V}O_2(CO_3)_3]^{5-}$ was performed according to the procedure described in Section 3.2.1. The resulting solution of $[U^{V}O_2(CO_3)_3]^{5-}$ was transfered immediately to a conventional quartz cell (optical path length: 1 cm) filled by argon gas preliminarily, and sealed with a cap tightly. The visible-NIR absorption spectrum of $[U^{V}O_2(CO_3)_3]^{5-}$ in D_2O was measured by using SHIMADZU UV-3150 spectrophotometer.

Visible-NIR Spectroelectrochemical Measurements. Visible-NIR spectroelectrochemical measurements were performed for the redox couples of $[U^{V}O_2(saloph)DMSO]^{-}/U^{VI}O_2$-(saloph)DMSO and $[U^{V}O_2(dbm)_2DMSO]^{-}/U^{VI}O_2(dbm)_2DMSO$ in a similar manner to those for the UV-visible spectroelectrochemical ones in Sections 4.2.1 and 4.3.1, respectively. To keep the potential on the working electrode stably during the measurements of the absorption spectra, the Ag/AgCl aqueous reference electrode (BAS 002020 RE-1B) with a glass-flit liquid junction filled by 0.3 M TBAP/DMSO was used instead of Ag/Ag^{+}. In the visible-NIR spectroelectrochemical measurements, the absorption spectra were recorded by SHIMADZU UV-3150 spectrophotometer. The effective optical path length of the OTTLE cell was spectrophotometrically calibrated as 1.89×10^{-2} cm.

6.2 Results

6.2.1 $[U^{V}O_2(CO_3)_3]^{5-}$ in D_2O

Uranyl(V) carbonate, $[U^{V}O_2(CO_3)_3]^{5-}$, is traditionally known as a stable uranyl(V) species in basic aqueous system containing CO_3^{2-}. Previously, Cohen has reported its characteristic absorption bands at 765, 990, and 1120 nm in the visible-NIR absorption spectrum.[147] However, there are no informations in the wavelength region longer than 1350 nm, because the large interferences of the absorption due to H_2O as solvent. To solve this problem, the use of D_2O as solvent instead of H_2O is effective. In Section 3.2, the D_2O solution containing $[U^{V}O_2(CO_3)_3]^{5-}$ and Na_2CO_3 has already been obtained by the bulk electrolysis of $[U^{VI}O_2$-$(CO_3)_3]^{4-}$. Therefore, by using the same technique, $[U^{V}O_2(CO_3)_3]^{5-}$ (5.5×10^{-2} M) was also prepared in D_2O containing Na_2CO_3 (1 M) here. The electronic spectrum of the resulting solution was measured in the range from 260 to 1870 nm with a conventional quartz cell (optical path length: 1 cm). The result is drawn with a solid line in Figure 6.1. To confirm the completeness of the electrolysis from $[U^{VI}O_2(CO_3)_3]^{4-}$ to $[U^{V}O_2(CO_3)_3]^{5-}$, the spectrum of the initial solution of $[U^{VI}O_2(CO_3)_3]^{4-}$ is also depicted by a dotted line in Figure 6.1. In the resulting spectrum for the D_2O solution containing $[U^{V}O_2(CO_3)_3]^{5-}$ (5.5×10^{-2} M) and Na_2CO_3 (1.0 M), the spectrum of HDO was also involved. The HDO was given by the contamination of atmospheric H_2O into the D_2O solution during the bulk electrolysis from $[U^{VI}O_2(CO_3)_3]^{4-}$ to $[U^{V}O_2(CO_3)_3]^{5-}$. Therefore, the spectrum of HDO was subtracted from the observed spectrum. The broken arrows in Figure 6.1 indicate the residuals of the absorption due to HDO.

In the UV-visible region, the disappearance of the LMCT absorption bands of $[U^{VI}O_2$-$(CO_3)_3]^{4-}$ at *ca.* 450 nm with its reduction to $[U^{V}O_2(CO_3)_3]^{5-}$, which was observed in Figure 3.2, was reproduced, *i.e.*, such absorption bands on the dotted line ($[U^{VI}O_2(CO_3)_3]^{4-}$)

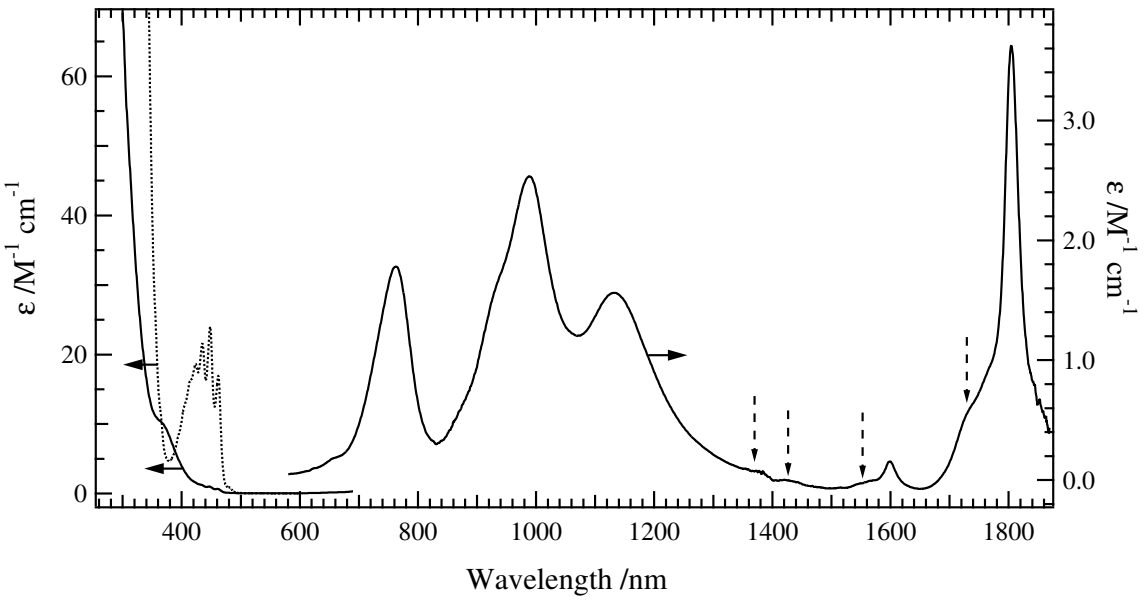

Figure 6.1. Electronic spectra of $[U^{V}O_2(CO_3)_3]^{5-}$ (5.5×10^{-2} M, solid line) and $[U^{VI}O_2(CO_3)_3]^{4-}$ (5.5×10^{-2} M, dotted line) in D_2O containing Na_2CO_3 (1.0 M). Broken arrows indicate residuals after subtraction of the spectrum due to HDO from the resulting spectrum (Details are in text). Optical path length: 1 cm.

are not observed on the solid line ($[U^{V}O_2(CO_3)_3]^{5-}$). This means that $[U^{VI}O_2(CO_3)_3]^{4-}$ in the starting solution was completely reduced to $[U^{V}O_2(CO_3)_3]^{5-}$. For the sample solution of $[U^{V}O_2(CO_3)_3]^{5-}$ in the tightly sealed quartz cell, any spectral changes from the solid line in Figure 6.1 were not observed over the course of several months.

In the visible-NIR region, the characteristic absorption bands of $[U^{V}O_2(CO_3)_3]^{5-}$ were observed at around 760, 990, 1140, 1600, and 1800 nm. The absorption bands at 760, 990, and 1140 nm are consistent with the results of Cohen.[147] On the other hand, the absorption peaks at 1600 and 1800 nm, which are in the strong absorption region of H_2O, are the first observation for $[U^{V}O_2(CO_3)_3]^{5-}$. The molar absorptivities (ϵ) of these absorption bands are in the range from 0.2 to 3.6 $M^{-1}\cdot cm^{-1}$.

6.2.2 $[U^{V}O_2(saloph)DMSO]^-$ in Dimethyl Sulfoxide

In Section 4.2, $[U^{V}O_2(saloph)DMSO]^-$ can exist stably in DMSO solution. To obtain details concerning the spectroscopic properties of $[U^{V}O_2(saloph)DMSO]^-$ in visible-NIR region, the visible-NIR absorption spectra for the redox couple of $[U^{V}O_2(saloph)DMSO]^-/U^{VI}O_2(saloph)DMSO$ in DMSO were measured at various applied potentials by using the same method as the UV-visible spectroelectrochemical technique. In this measurement, the effective optical path length was spectrophotometrically evaluated as 1.89×10^{-2} cm. The resulting spectra for the $[U^{V}O_2(saloph)DMSO]^-/U^{VI}O_2(saloph)DMSO$ (total concentration: 5.28×10^{-3} M) redox couple in DMSO containing TBAP (0.30 M) are shown in Figure 6.2. The applied potential on the OTTLE was varied stepwise from 0 to -1.814 V *vs.* Fc/Fc^+. The absorption bands were observed at around 650, 750, 900, 1400, and 1875 nm with a decrease in the potential, and then the spectral changes converged at -1.814 V *vs.* Fc/Fc^+, which is consistent with the result observed in Figure 4.7. Therefore, it is concluded that the spectrum at -1.814 V *vs.* Fc/Fc^+ is attributed to that of $[U^{V}O_2(saloph)DMSO]^-$ in DMSO and that the absorption bands in Figure 6.2 are intrinsic ones of $[U^{V}O_2(saloph)DMSO]^-$. The ϵ values of these absorption bands are in the range from 100 to 300 $M^{-1}\cdot cm^{-1}$.

6.2.3 $[U^{V}O_2(dbm)_2DMSO]^-$ in Dimethyl Sulfoxide

As the alternative system of the stable uranyl(V) complex in nonaqueous solvent, $[U^{V}O_2(dbm)_2DMSO]^-$ in DMSO was found in Section 4.3. To examine whether the characteristic absorption bands of $[U^{V}O_2(saloph)DMSO]^-$ in the visible-NIR region are a common property of the uranyl(V) complexes, the visible-NIR absorption spectra for the redox couple of $[U^{V}O_2(dbm)_2DMSO]^-/U^{VI}O_2(dbm)_2DMSO$ (4.11×10^{-3} M) in DMSO containing TBAP (0.30 M) were also measured at various applied potentials from 0 to -1.664 V *vs.* Fc/Fc^+. The resulting spectra are shown in Figure 6.3. The absorbancies at around 640, 740, 860, 1470, and 1890 nm increased with the reduction of $U^{VI}O_2(dbm)_2DMSO$ to $[U^{V}O_2(dbm)_2DMSO]^-$, and such spectral changes converged at -1.564 V *vs.* Fc/Fc^+. The potential value of the convergence is consistent with the result in Figure 4.11, Section 4.3. Thus, the absorption spectrum measured at -1.564 V *vs.* Fc/Fc^+ is assigned to $[U^{V}O_2(dbm)_2DMSO]^-$. It is clear that the absorption bands in Figure 6.3 are the characteristic ones of $[U^{V}O_2(dbm)_2DMSO]^-$. The ϵ values of these absorption bands are in the range from 150 to 900 $M^{-1}\cdot cm^{-1}$.

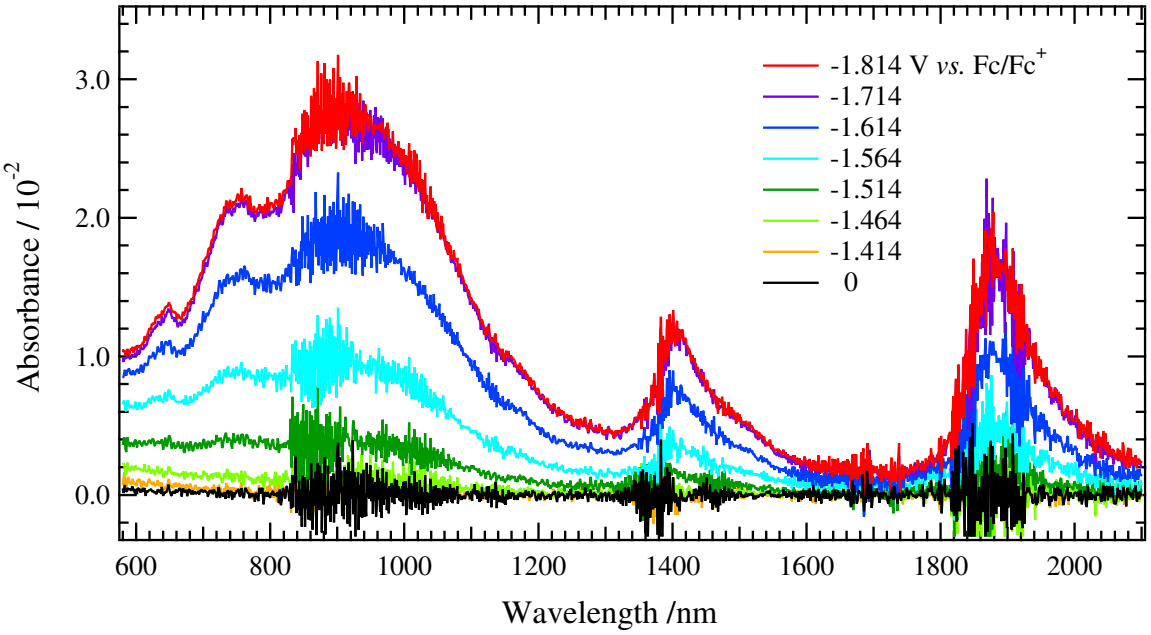

Figure 6.2. Visible-NIR absorption spectra measured at the applied potentials in the range from 0 to −1.814 V *vs.* Fc/Fc^+ for $[U^{V}O_2(saloph)DMSO]^-/U^{VI}O_2(saloph)DMSO$ (5.28×10^{-3} M) in DMSO solution containing TBAP (0.30 M). Noises are due to detectors (photomultiplier and PbS detector) in the spectrophtometer and/or absorption of DMSO in the OTTLE cell. Optical path length: 1.89×10^{-2} cm.

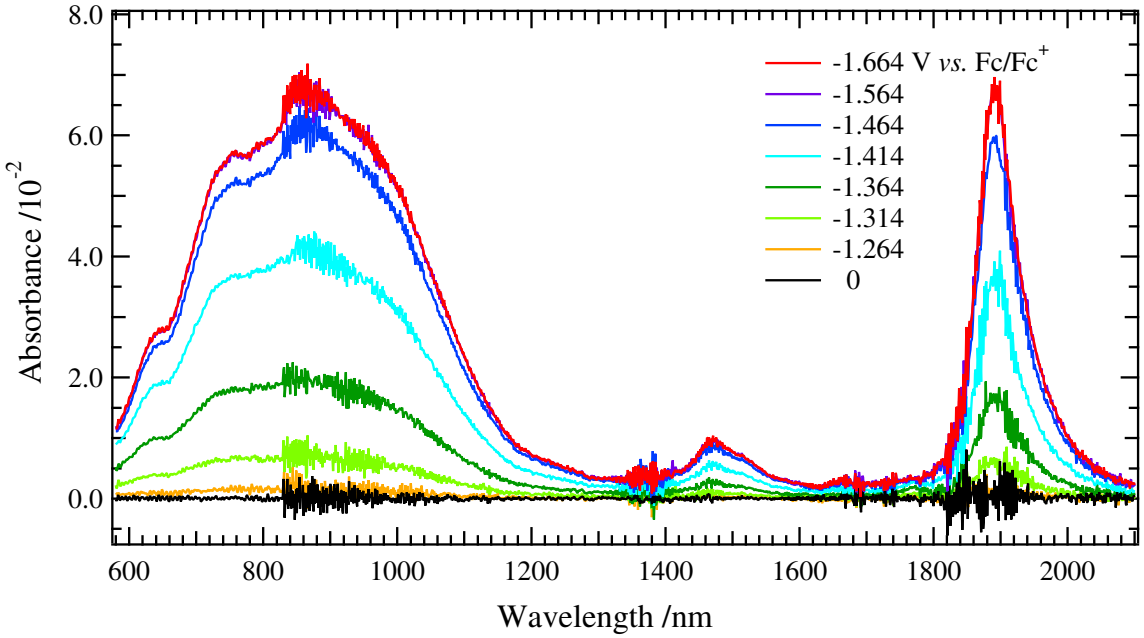

Figure 6.3. Visible-NIR absorption spectra measured at the applied potentials in the range from 0 to −1.664 V *vs.* Fc/Fc^+ for $[U^{V}O_2(dbm)_2DMSO]^-/U^{VI}O_2(dbm)_2DMSO$ (4.11×10^{-3} M) in DMSO solution containing TBAP (0.30 M). Noises are due to detectors (photomultiplier and PbS detector) in the spectrophtometer and/or absorption of DMSO in the OTTLE cell. Optical path length: 1.89×10^{-2} cm.

6.3 Discussion

In a comparison between Figures 6.1, 6.2, and 6.3, the electronic spectra of $[U^{V}O_2(CO_3)_3]^{5-}$, $[U^{V}O_2(saloph)DMSO]^{-}$, and $[U^{V}O_2(dbm)_2DMSO]^{-}$ resemble each other despite the difference in the ligands coordinated to the equatorial plane of the uranyl(V) moiety, especially the middle and latter are quite similar. Such a similarity implies that the spectral changes in Figures 6.1, 6.2, and 6.3 do not correspond to the reduction of the ligands (CO_3^{2-}, saloph, dbm, and DMSO) but do the uranyl core ($U^{VI}O_2^{2+} + e^- \rightarrow U^{V}O_2^{+}$) and strongly suggests that the characteristic absorption bands of these uranyl(V) complexes in the visible-NIR region are primarily due to the electronic transtions in the $U^{V}O_2^{+}$ core.

To examine the spectral features of the uranyl(V) complexes in the visible-NIR region from the viewpoint of energy, the electronic spectra of $[U^{V}O_2(CO_3)_3]^{5-}$, $[U^{V}O_2(saloph)DMSO]^{-}$, and $[U^{V}O_2(dbm)_2DMSO]^{-}$ were replotted in wavenumbers (cm^{-1}), as shown in parts (a)–(c) of Figure 6.4, respectively. The peak positions of the characteristic absorption bands of these uranyl(V) complexes are listed in Table 6.1 in cm^{-1} (the corresponding wavelength are in parentheses).

Interestingly, the ϵ values of the characteristic absorption bands of $[U^{V}O_2(CO_3)_3]^{5-}$ are in the range from 0.2 to 3.6 $M^{-1}\cdot cm^{-1}$, while those of $[U^{V}O_2(saloph)DMSO]^{-}$ and $[U^{V}O_2(dbm)_2DMSO]^{-}$ are from 10^2 close to 10^3 $M^{-1}\cdot cm^{-1}$. The small ϵ values of $[U^{V}O_2(CO_3)_3]^{5-}$ indicate that the characteristic absorption bands of the uranyl(V) complexes in visible-NIR region are due to the essentially forbidden electronic transitions in the $U^{V}O_2^{+}$ core. As can be seen from Figure 6.4 and the molecular structures of these uranyl(V) complexes (see Chapter 5), it is likely that the differences in the ϵ values and the spectral shapes of these uranyl(V) complexes depend on the arrangement of the atoms directly bonded to the center uranium.

It is well accepted that the most important electronic transition scheme is the electric-dipole one. Other transition schemes such as magnetic-dipole, electric-quadrupole and so on

Table 6.1. Transition energy values of f–f transitions in actinyl species with $5f^1$ configuration

$U^{V}O_2^{+}$ complexes		Transition energy / cm^{-1} (nm)					Reference
$[U^{V}O_2(CO_3)_3]^{5-}$	–	5560 (1800)	6250 (1600)	8770 (1140)	10100 (990)	13200 (760)	This work
$[U^{V}O_2(saloph)DMSO]^{-}$	–	5330 (1875)	7140 (1400)	11100 (900)	13300 (750)	15400 (650)	This work
$[U^{V}O_2(dbm)_2DMSO]^{-}$	–	5290 (1890)	6800 (1470)	11600 (860)	13500 (740)	15600 (640)	This work
$Np^{VI}O_2^{2+}$ species		Transition energy / cm^{-1} (Term symbol in $D_{\infty h}$)					
$Np^{VI}O_2^{2+}$(aq)	*ca.* 2000	6752	8168	18180	21100	*ca.* 24000	[89]
$(^2\Phi_{\frac{5}{2}u})^a$	$(^2\Delta_{\frac{3}{2}u})$	$(^2\Phi_{\frac{7}{2}u})$	$(^2\Delta_{\frac{5}{2}u})$	$(^2\Pi_{\frac{1}{2}u})$	$(^2\Pi_{\frac{3}{2}u})$	$(^2\Sigma_u^+)$	
$[Np^{VI}O_2Cl_4]^{2-}$	*ca.* 1000	6880.4	7990	17241.4	20080.8	–	[101]
$(^2\Delta_{\frac{3}{2}u} + {}^2\Phi_{\frac{5}{2}u})^a$	$(^2\Delta_{\frac{3}{2}u} + {}^2\Phi_{\frac{5}{2}u})$	$(^2\Delta_{\frac{5}{2}u})$	$(^2\Phi_{\frac{7}{2}u})$	$(^2\Pi_{\frac{1}{2}u})$	$(^2\Pi_{\frac{3}{2}u})$		
$[Np^{VI}O_2(NO_3)_3]^{-}$	–	6459.0	9420.2	17843.6	20816.3	–	[101]
$(^2\Phi_{\frac{5}{2}u})^a$		$(^2\Delta_{\frac{5}{2}u})$	$(^2\Phi_{\frac{7}{2}u})$	$(^2\Pi_{\frac{1}{2}u})$	$(^2\Pi_{\frac{3}{2}u})$		
bare $Np^{VI}O_2^{2+}$	447	5515	6565	25844	28909	–	[107]
$(^2\Phi_{\frac{5}{2}u} + {}^2\Delta_{\frac{5}{2}u})^a$	$(^2\Delta_{\frac{3}{2}u})$	$(^2\Delta_{\frac{5}{2}u} + {}^2\Phi_{\frac{5}{2}u})$	$(^2\Phi_{\frac{7}{2}u})$	$(^2\Pi_{\frac{1}{2}u})$	$(^2\Pi_{\frac{3}{2}u})$		

[a] Ground state.

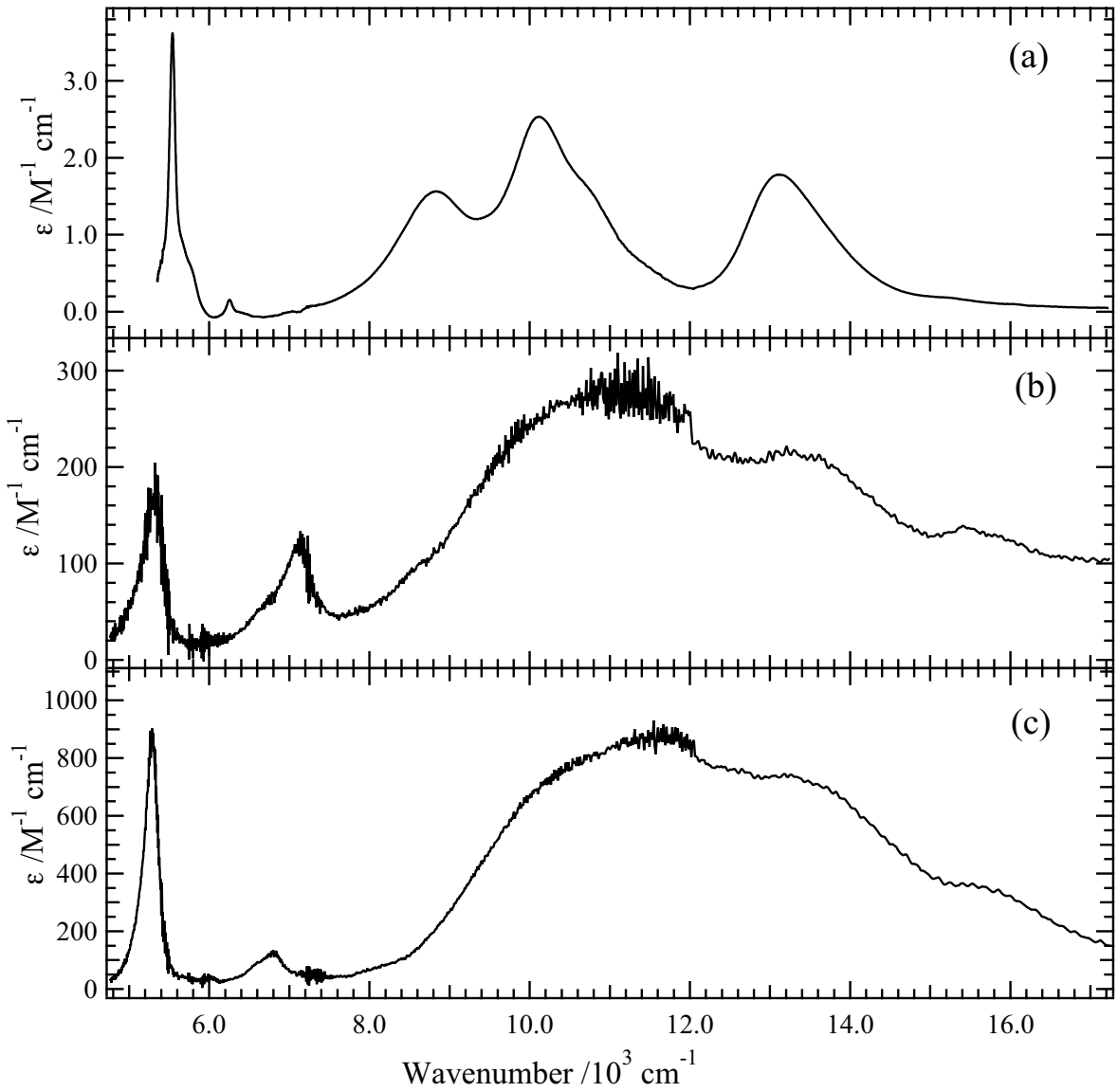

Figure 6.4. Electronic spectra of uranyl(V) complexes in visible-NIR region: (a) $[U^{V}O_2(CO_3)_3]^{5-}$(5.5×10^{-2} M) in D_2O containing Na_2CO_3 (1.0 M); (b) $[U^{V}O_2(saloph)DMSO]^{-}$ (5.28×10^{-3} M) in DMSO containing TBAP (0.30 M); (c) $[U^{V}O_2(dbm)_2DMSO]^{-}$ (4.11×10^{-3} M) in DMSO containing TBAP (0.30 M). Noises in parts (b) and (c) are due to detectors (photomultiplier and PbS detector) in the spectrophotometer and/or absorption of DMSO in the OTTLE cell. Optical path length: 1 cm for part (a) and 1.89×10^{-2} cm for parts (b) and (c).

can also be considered. However, it is generally known that the magnitudes of these transition schemes are much smaller than the electric-dipole one. Hence, the discussion performed here was limited mainly in the electric-dipole transition. A bare $U^{V}O_2^+$ ion has a linear geometry, *i.e.*, O=U=O ($D_{\infty h}$). Thus, there is an inversion center in the $U^{V}O_2^+$ ion. In this case, electronic transitions between energy states with the same parities ($g \rightarrow g$, $u \rightarrow u$) in the $U^{V}O_2^+$ ion are forbidden.[195] This selection rule is so-called "Laporte forbidden". Even for the uranyl(V) complexes with equatorial ligands, such a selection rule holds in a centrosymmetric system. Assuming that a coordination environment experienced by the center uranium is approximated by the arrangement of the atoms bonded to the center uranium directly, that in $[U^{V}O_2(CO_3)_3]^{5-}$ can be regarded as being in a pseudocentrosymmetric hexagonal bipyramidal field (D_{6h}), while those in $[U^{V}O_2(\text{saloph})\text{DMSO}]^-$ and $[U^{V}O_2(\text{dbm})_2\text{DMSO}]^-$ are in noncentrosymmetric pentagonal bipyramidal ones (D_{5h}). Thus, it is predicted that the essentially forbidden electronic transitions in the $U^{V}O_2^+$ core of $[U^{V}O_2(\text{saloph})\text{DMSO}]^-$ and $[U^{V}O_2(\text{dbm})_2\text{DMSO}]^-$ are partially allowed by the disappearance of the inversion center and that the absorption bands due to such transitions in $[U^{V}O_2(\text{saloph})\text{DMSO}]^-$ and $[U^{V}O_2(\text{dbm})_2\text{DMSO}]^-$ are observed more strongly than those of $[U^{V}O_2(CO_3)_3]^{5-}$. This interpretation well explains the differences in the ϵ values in Figure 6.4. A similar effect of the lack of centrosymmetricity on the intensities of electronic transitions between states with same parities is also predicted by the theoretical calculations for neptunyl(V) ($Np^{V}O_2^+$, $5f^2$) complexes with chloride ligands.[109]

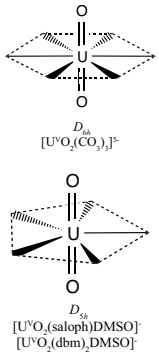

For the transition scheme between the electronic states with same parities in the $U^{V}O_2^+$ core, there are two candidates; one is the charge transfer from the axial oxygen to the center uranium (LMCT, *e.g.*, $\sigma_u^2(\delta_u \text{ or } \phi_u) \rightarrow \sigma_u(\delta_u \text{ and/or } \sigma_u\phi_u)^2$), and another is a f–f transition ($u \rightarrow u$, u: ungerade) in the $5f^1$ electronic configuration of U^{5+}. Normally, the uranyl(VI) species ($5f^0$) show the LMCT absorption bands at around 22000 cm^{-1} (*e.g.*, the dotted line in Figure 6.1 for $[U^{VI}O_2(CO_3)_3]^{4-}$). With the reduction to $[U^{V}O_2(CO_3)_3]^{5-}$, the disappearance of such LMCT bands of $[U^{VI}O_2(CO_3)_3]^{4-}$ was observed (Section 2.1). Because of the lower positive charge on U^{5+} than U^{6+}, it is expected that the LMCT transition in the $U^{V}O_2^+$ core requires a higher energy (> 22000 cm^{-1}) than that in $U^{VI}O_2^{2+}$; *i.e.*, a blue shift of the LMCT bands should be observed with the reduction from uranyl(VI) to uranyl(V). Unfortunately, the LMCT bands of $[U^{V}O_2(CO_3)_3]^{5-}$ could not be detected in Figure 6.1. However, such a blue shift with the reduction from uranyl(VI) species to uranyl(V) one has been observed in the CsCl–NaCl melt by Khokhryakov (uranyl(VI): 25000, 31250, and 33300 cm^{-1} → uranyl(V): 27770, 31764, and 33300 cm^{-1}).[145] Furthermore, according to the quantum chemical calculations for analogous actinyl(V/VI) couple, bare $Np^{V}O_2^+/Np^{VI}O_2^{2+}$, by Matsika and Pitzer,[107] it was predicted that the LMCT bands in $Np^{V}O_2^+$ appear at a much higher energy region (the lowest transition: 23079 cm^{-1}) than those in $Np^{VI}O_2^{2+}$ (the lowest one: 12622 cm^{-1}). Consequently, the characteristic absorption bands of $[U^{V}O_2(CO_3)_3]^{5-}$, $[U^{V}O_2(\text{saloph})\text{DMSO}]^-$, and $[U^{V}O_2(\text{dbm})_2\text{DMSO}]^-$ in visible-NIR region can be assigned to the f–f transitions in the $U^{V}O_2^+$ core.

It is likely that the electronic spectra in Figure 6.4 is classified into two regions by the widths of the absorption bands; *Region I*: two narrower absorption peaks in the lower energy side (4800–7600 cm^{-1}), and *Region II*: the others with the larger widths (7600–17200 cm^{-1}). According to the previous papers,[3, 4, 84, 89, 108] it is well-understood for bare actinyl ions that the $5f\sigma_u$ and $5f\pi_u$ orbitals are involved in the axial An=O bonds and hence have antibonding characters. On the other hand, the $5f\delta_u$ and $5f\phi_u$ orbitals in the bare actinyl ion are nonbonding ones, which can interact with ligands in the equatorial plane. Thus, the typical energy

order of the 5f orbitals in the actinyl ion is,

$$5f\delta_u \approx 5f\phi_u < 5f\pi_u \ll 5f\sigma_u$$

Such a relationship should be kept even in the actinyl complexes with ligands in the equatorial plane, because of the generally accepted perturbation order, $V_{ax} \gg e^2/r_{ij} \geq H_{SO} > V_{eq}$ (Eq. 1.17, Chapter 1). Considering the less participation of the $5f\delta_u$ and $5f\phi_u$ orbitals in the axial U=O bonding, the narrower absorption peaks in *Region I* are understandable as the electronic transitions from the $5f(\delta_u$ or $\phi_u)$ orbital to other $5f\delta_u$ and/or $5f\phi_u$ ones. The absorption bands in *Region II* might be attributed to the transitions to the $5f\pi_u$ and $5f\sigma_u$ orbitals, because the larger participation of these 5f orbitals in the axial U=O bonding should cause broadening of the spectra by a vibronic coupling. According to the usual energy order of the 5f orbitals, the lower two absorption bands in *Region II* are attributable to the electronic transitions to the $5f\pi_u$ orbitals and the highest one should be that to the $5f\sigma_u$.

Since neptunyl(VI) species ($Np^{VI}O_2^{2+}$) are isoelectronic with the uranyl(V) ones, $5f^1$, it is interesting to compare the electronic spectra of the uranyl(V) complexes observed in this study with those of the neptunyl(VI) species. Actually, the neptunyl(VI) species in the acidic aqueous solutions has been reported to have the absorption bands due to f–f transition as shown in Figure 1.9, Chapter 1.[87, 89, 156–159)] The well-established work for the polarized absorption spectra of the neptunyl(VI) complexes was reported by Denning *et al.*[101)] According to them, $[Np^{VI}O_2Cl_4]^{2-}$ and $[Np^{VI}O_2(NO_3)_3]^-$ complexes also have the absorption bands due to the f–f transitions in the visible-NIR region. Furthermore, such experimental data have been compared with the recent quantum chemical calculations for $Np^{VI}O_2^{2+}$ (bare ion) by Matsika and Pitzer.[107)]

To compare the electronic spectra of the uranyl(V) complexes with those of the neptunyl(VI) species, the energy values of the f–f transitions in the neptunyl(VI) species[89, 101, 107)] are also collected in Table 6.1. In this comparison, the absorption band of each uranyl(V) complex in the range of 5290–5560 cm^{-1} should correspond to the second excited state in the f–f transitions. According to the reported data of the neptunyl(VI) species, the first excited state in the f–f transitions places in the range from 447 to 2000 cm^{-1},[89, 101, 107)] which is out of detection for the electronic spectra of the uranyl(V) complexes in this study. The transition energy values of the uranyl(V) complexes in *Region I* are very similar to those of the neptunyl(VI) species. Considering that the participation of the $5f\delta_u$ and $5f\phi_u$ orbitals in the axial Np=O bonding is also small, this similarity of the energy values supports our assignment that the absorption peaks of the uranyl(V) complexes in *Region I* are due to the electronic transitions to the $5f\delta_u$ and $5f\phi_u$ orbitals. On the other hand, the transition energy values of the uranyl(V) complexes in *Region II* (corresponding to the transitions to $5f\pi_u$) are much lower than those of the neptunyl(VI) species. Such a difference of the transition energy to the $5f\pi_u$ orbitals exhibits that the anti-bonding characters of the $5f\pi_u$ orbitals in the uranyl(V) complexes are lower than those in the neptunyl(VI) ones, *i.e.*, the U=O bond strength is weaker than Np=O one. This is consistent with the data of the ν_3 peak and the force constant of An=O bond (An: U, Np) as shown in Table 5.1 in Chapter 5 (ν_3 = 770 and 775 cm^{-1}, F_{UO} = 5.31 mdyne·$Å^{-1}$ for the uranyl(V); $\nu_3 = 969 \pm 1$ cm^{-1}, $F_{NpO} = 7.81 \pm 0.02$ mdyne·$Å^{-1}$ for the neptunyl(VI)[155)]). Although the electronic transition to the $5f\sigma_u$ orbital in the neptunyl(VI) species has not been observed experimentally, McGlynn *et al.*[89)] and Denning *et al.*[101)] estimated it at 24000 or 45000~120000 cm^{-1} ($^2\Sigma_{1/2u}$), respectively. These are not comparable with the absorption bands at around 15600 cm^{-1} ($[U^VO_2(saloph)DMSO]^-$, $[U^VO_2(dbm)_2$-$DMSO]^-$) and 13200 cm^{-1} ($[U^VO_2(CO_3)_3]^{5-}$) in Figure 6.4. Thus, uncertainty remains in

the assignment for the absorption band at the highest energy in the electronic spectrum of each uranyl(V) complex. However, if it is true that the absorption bands of these uranyl(V) complexes at 13200 ($[U^{V}O_2(CO_3)_3]^{5-}$), 15400 ($[U^{V}O_2(\text{saloph})\text{DMSO}]^{-}$), and 15600 cm^{-1} ($[U^{V}O_2(\text{dbm})_2\text{DMSO}]^{-}$) are due to the transition to the $5f\sigma_u$ orbital, the unusual instability of most uranyl(V) species can be explained, because such a low anti-bonding character of the $5f\sigma_u$ orbital in each uranyl(V) complex means the unusually weak U=O bond strength.

To perform more detailed discussion for the electronic structure of the present uranyl(V) complexes, the splitting schemes of the 5f and related orbitals of the center uranium were examined by using the group theory. For the D_{6h} symmetric ligand filed, which is corresponding to $[U^{V}O_2(CO_3)_3]^{5-}$, the splitting scheme of the 5f orbitals and the hybridization of 5f, 6d and 7s orbitals were simulated by using a character table of D_{6h} point group shown in Table 6.2. Firstly, each 5f orbital must be assigned to the appropriate representation in D_{6h}, because normally the reported character tables do not contain the assignments for the f orbitals. The representation corresponding to each f orbital is given simply by multiplication of the characters in proper representations. For example, the representation of f_{z^3} orbital ($f\sigma_u$, $m = 0$) can be obtained as $A_{2u} \times A_{2u} \times A_{2u}$ (A_{2u} corresponds to z), resulting A_{2u} for f_{z^3}. Using the same procedure, other f orbitals were assigned as follows.

$$m = \pm 1,\ f_{xz^2}, f_{yz^2}(\pi_u) :\ A_{2u} \times E_{1g} = E_{1u} \tag{6.1}$$

$$m = \pm 2,\ f_{xyz}, f_{z(x^2-y^2)}(\delta_u) :\ A_{2u} \times E_{2g} = E_{2u} \tag{6.2}$$

$$m = \pm 3,\ f_{x(x^2-3y^2)}, f_{y(3x^2-y^2)}(\phi_u) :\ E_{2g} \times E_{1u} = \Gamma_{f\phi_u} \tag{6.3}$$

where m is the magnetic quantum number. The representation $\Gamma_{f\phi_u}$ for ϕ_u ($m = \pm 3$, Eq. 6.3) can be reduced by the following usual treatment.[196] The characters of $\Gamma_{f\phi_u}$ for 24 symmetric operations in D_{6h} are,

D_{6h}	E	$2C_6$	$2C_3$	C_2	$3C_2'$	$3C_2''$	i	$2S_3$	$2S_6$	σ_h	$3\sigma_d$	$3\sigma_v$
$\Gamma_{f\phi_u}$	4	−1	1	−4	0	0	−4	1	−1	4	0	0

Table 6.2. Character table of D_{6h}

D_{6h}	E	$2C_6$	$2C_3$	C_2	$3C_2'$	$3C_2''$	i	$2S_3$	$2S_6$	σ_h	$3\sigma_d$	$3\sigma_v$			
A_{1g}	1	1	1	1	1	1	1	1	1	1	1	1		x^2+y^2, z^2	
A_{2g}	1	1	1	1	−1	−1	1	1	1	1	−1	−1	R_z		
B_{1g}	1	−1	1	−1	1	−1	1	−1	1	−1	1	−1	R_z		
B_{2g}	1	−1	1	−1	−1	1	1	−1	1	−1	−1	1			
E_{1g}	2	1	−1	−2	0	0	2	1	−1	−2	0	0	(R_x, R_y)	(xy, yz)	
E_{2g}	2	−1	−1	2	0	0	2	−1	−1	2	0	0		(x^2-y^2, xy)	
A_{1u}	1	1	1	1	1	1	−1	−1	−1	−1	−1	−1			
A_{2u}	1	1	1	1	−1	−1	−1	−1	−1	−1	1	1	z		z^3
B_{1u}	1	−1	1	−1	1	−1	−1	1	−1	1	−1	1			$x(x^2-3y^2)$
B_{2u}	1	−1	1	−1	−1	1	−1	1	−1	1	1	−1			$y(3x^2-y^2)$
E_{1u}	2	1	−1	−2	0	0	−2	−1	1	2	0	0	(x, y)		(xz^2, yz^2)
E_{2u}	2	−1	−1	2	0	0	−2	1	1	−2	0	0			$(xyz, z(x^2-y^2))$

Therefore, the irreducible representation of $\Gamma_{f\phi_u}$ is calculated as,

$$\frac{1}{24}\begin{pmatrix} 1 & 1 & 1 & 1 & 1 & 1 & 1 & 1 & 1 & 1 & 1 & 1 \\ 1 & 1 & 1 & 1 & -1 & -1 & 1 & 1 & 1 & 1 & -1 & -1 \\ 1 & -1 & 1 & -1 & 1 & -1 & 1 & -1 & 1 & -1 & 1 & -1 \\ 1 & -1 & 1 & -1 & -1 & 1 & 1 & -1 & 1 & -1 & -1 & 1 \\ 2 & 1 & -1 & -2 & 0 & 0 & 2 & 1 & -1 & -2 & 0 & 0 \\ 2 & -1 & -1 & 2 & 0 & 0 & 2 & -1 & -1 & 2 & 0 & 0 \\ 1 & 1 & 1 & 1 & 1 & 1 & -1 & -1 & -1 & -1 & -1 & -1 \\ 1 & 1 & 1 & 1 & -1 & -1 & -1 & -1 & -1 & -1 & 1 & 1 \\ 1 & -1 & 1 & -1 & 1 & -1 & -1 & 1 & -1 & 1 & -1 & 1 \\ 1 & -1 & 1 & -1 & -1 & 1 & -1 & 1 & -1 & 1 & 1 & -1 \\ 2 & 1 & -1 & -2 & 0 & 0 & -2 & -1 & 1 & 2 & 0 & 0 \\ 2 & -1 & -1 & 2 & 0 & 0 & -2 & 1 & 1 & -2 & 0 & 0 \end{pmatrix}\begin{pmatrix} 4 \\ -1\times 2 \\ 1\times 2 \\ -4 \\ 0\times 3 \\ 0\times 3 \\ -4 \\ 1\times 2 \\ -1\times 2 \\ 4 \\ 0\times 3 \\ 0\times 3 \end{pmatrix} = \begin{pmatrix} 0 \\ 0 \\ 0 \\ 0 \\ 0 \\ 0 \\ 0 \\ 0 \\ 1 \\ 1 \\ 1 \\ 0 \end{pmatrix} \tag{6.4}$$

Thus,

$$\Gamma_{f\phi_u} = B_{1u} + B_{2u} + E_{1u}(\pi_u) \tag{6.5}$$

where E_{1u} representation has already been used for f_{xz^2} and f_{yz^2} (π_u) (Eq. 6.1). Hence, the $f_{x(x^2-3y^2)}$ and $f_{y(3x^2-y^2)}$ (ϕ_u) orbitals are assigned to $B_{1u} + B_{2u}$ irreducible representation. The results of the assignments for f orbitals are also listed to the right-hand side of Table 6.2. In summary, each f orbital in the D_{6h} ligand field is assigned as;

$f_{z^3}(\sigma_u)$: a_{2u}
f_{xz^2}, $f_{yz^2}(\pi_u)$: e_{1u}
f_{xyz}, $f_{z(x^2-y^2)}(\delta_u)$: e_{2u}
$f_{x(x^2-3y^2)}$, $f_{y(3x^2-y^2)}(\phi_u)$: $b_{1u} + b_{2u}$.

For σ bonding between the ligand atoms and the center uranium, the hybridization of the 5f, 6d, and 7s orbitals in the uranium atom was considered. The characters of the reducible representation for the hybrid orbitals of the σ bonding ($\Gamma_{\sigma\text{hyb}}$) in D_{6h} is,

D_{6h}	E	$2C_6$	$2C_3$	C_2	$3C_2'$	$3C_2''$	i	$2S_3$	$2S_6$	σ_h	$3\sigma_d$	$3\sigma_v$
$\Gamma_{\sigma\text{hyb}}$	8	2	2	2	2	0	0	0	0	6	2	4

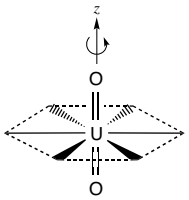

The $\Gamma_{\sigma\text{hyb}}$ can be separated into the axial ($\Gamma_{\sigma\text{ax}}$) and equatorial ($\Gamma_{\sigma\text{eq}}$) components as follows.

D_{6h}	E	$2C_6$	$2C_3$	C_2	$3C_2'$	$3C_2''$	i	$2S_3$	$2S_6$	σ_h	$3\sigma_d$	$3\sigma_v$
$\Gamma_{\sigma\text{hyb}}$	8	2	2	2	2	0	0	0	0	6	2	4
$\Gamma_{\sigma\text{ax}}$	2	2	2	2	0	0	0	0	0	0	2	2
$\Gamma_{\sigma\text{eq}}$	6	0	0	0	2	0	0	0	0	6	0	2

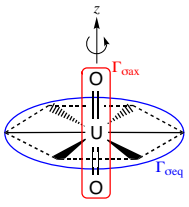

These reducible representations, $\Gamma_{\sigma\text{ax}}$ and $\Gamma_{\sigma\text{eq}}$, are reduced to the irreducible representations by the same procedure as Eq. 6.4. Consequently,

$$\Gamma_{\sigma\text{ax}} = A_{1g} + A_{2u} \tag{6.6}$$
$$\Gamma_{\sigma\text{eq}} = A_{1g} + E_{2g} + B_{1u} + E_{1u} \tag{6.7}$$

where each representation corresponds to 5f, 6d, or 7s orbitals as,

a_{1g}: s, d_{z^2}
a_{2u}: f_{z^3}
e_{2g}: ($d_{x^2-y^2}$, d_{xy})
b_{1u}: $f_{x(x^2-3y^2)}$ or $f_{y(3x^2-y^2)}$
e_{1u}: (f_{xz^2}, f_{yz^2}).

The A_{1g} and A_{2u} representations in $\Gamma_{\sigma\mathrm{ax}}$ (Eq. 6.6) corresponds to $6d_{z^2}$ and $5f_{z^3}$, respectively, because it is well-known that these orbitals form the axial σ bonding as shown in Figure 1.2. For $\Gamma_{\sigma\mathrm{eq}}$, it is reasonable to consider the combination of 7s (A_{1g}), ($6d_{x^2-y^2}$, $6d_{xy}$) (E_{2g}), and ($5f_{xz^2}$, $5f_{yz^2}$) (E_{1u}). The inclusion of B_{1u} in $\Gamma_{\sigma\mathrm{eq}}$ means that either $5f_{x(x^2-3y^2)}$ or $5f_{y(3x^2-y^2)}$ orbital is participated in the formation of the D_{6h} hybrid orbital to interact with the equatorial ligand, *i.e.*, one of the $5f\phi_u$ orbitals becomes anti-bonding character. This is consistent with the splitting of the doubly degenerated $f_{x(x^2-3y^2)}$ and $f_{y(3x^2-y^2)}$ orbitals into b_{1u} and b_{2u} ones in D_{6h} symmetry described above. Thus, in this symmetry, it can be understood that the b_{1u} orbital is higher in energy than b_{2u} one. As a result, the energy order of the 5f orbitals in D_{6h} is summarized as;

$$e_{2u}\,(5f\delta_u) \approx b_{2u}\,(5f\phi_u) < b_{1u}\,(5f\phi_u) < e_{1u}\,(5f\pi_u) < a_{2u}\,(5f\sigma_u).$$

Here, it must be noted that the $5f\pi_u$ and $5f\phi_u$ orbitals are independent of other 6d and 7s ones even in the participation of these 5f orbitals into the hybrid orbitals to form the σ bonding between the center uranium and ligand atoms in D_{6h} symmetry, *i.e.*, any mixing of the 5f orbitals with others does not occur in D_{6h} symmetric ligand field. Therefore, the remaining schemes for the intensities of the f–f transitions in $[U^{V}O_2(CO_3)_3]^{5-}$ (Figure 6.4(a)) are the vibronic coupling between the electronic excited states and vibrational mode(s) with odd parity and/or magnetic-dipole or other multipole transitions.

In D_{5h} symmetric field for $[U^{V}O_2(\mathrm{saloph})\mathrm{DMSO}]^{-}$ and $[U^{V}O_2(\mathrm{dbm})_2\mathrm{DMSO}]^{-}$, the 5f orbitals have also been attributed to the appropriate representations. Table 6.3 shows the character table of D_{5h} point group. According to the treatment similar to Eq. 6.4, the f orbitals in D_{5h} point group can be assigned as;

$f_{z^3}(\sigma_u)$: a_2''
f_{xz^2}, $f_{yz^2}(\pi_u)$: e_1'
f_{xyz}, $f_{z(x^2-y^2)}(\delta_u)$: e_2''
$f_{x(x^2-3y^2)}$, $f_{y(3x^2-y^2)}(\phi_u)$: e_2'.

These assignments for the f orbitals are also listed at the right-hand side of Table 6.3.

Table 6.3. Character table of D_{5h}

D_{5h}	E	$2C_5$	$2C_5^2$	$5C_2$	σ_h	$2S_5$	$2S_5^3$	$5\sigma_v$			
A_1'	1	1	1	1	1	1	1	1		x^2+y^2, z^2	
A_2'	1	1	1	−1	1	1	1	−1	R_z		
E_1'	2	$2\cos 2/5\pi$	$2\cos 4/5\pi$	0	2	$2\cos 2/5\pi$	$2\cos 4/5\pi$	0	(x, y)		(xz^2, yz^2)
E_2'	2	$2\cos 4/5\pi$	$2\cos 2/5\pi$	0	2	$2\cos 4/5\pi$	$2\cos 2/5\pi$	0		(x^2-y^2, xy)	$\begin{cases} x(x^2-3y^2) \\ y(3x^2-y^2) \end{cases}$
A_1''	1	1	1	1	−1	−1	−1	−1			
A_2''	1	1	1	−1	−1	−1	−1	1	z		z^3
E_1''	2	$2\cos 2/5\pi$	$2\cos 4/5\pi$	0	−2	$-2\cos 2/5\pi$	$-2\cos 4/5\pi$	0	(R_x, R_y)	(xz, yz)	
E_2''	2	$2\cos 4/5\pi$	$2\cos 2/5\pi$	0	−2	$-2\cos 4/5\pi$	$-2\cos 2/5\pi$	0			$(xyz, z(x^2-y^2))$

The hybridization of 5f, 6d, and 7s orbitals in the center metal to form the σ bonds with ligand atoms in D_{5h} symmetry was examined. The characters of $\Gamma_{\sigma\text{hyb}}$ ($= \Gamma_{\sigma\text{ax}} + \Gamma_{\sigma\text{eq}}$) for the symmetric operations in this system are,

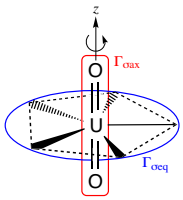

D_{5h}	E	$2C_5$	$2C_5^2$	$5C_2$	σ_h	$2S_5$	$2S_5^3$	$5\sigma_v$
$\Gamma_{\sigma\text{hyb}}$	7	2	2	1	5	0	0	3
$\Gamma_{\sigma\text{ax}}$	2	2	2	0	0	0	0	2
$\Gamma_{\sigma\text{eq}}$	5	0	0	1	5	0	0	1

As a result, the irreducible representations of $\Gamma_{\sigma\text{ax}}$ and $\Gamma_{\sigma\text{eq}}$ are obtained as,

$$\Gamma_{\sigma\text{ax}} = A_1' + A_2'' \tag{6.8}$$
$$\Gamma_{\sigma\text{eq}} = A_1' + E_1' + E_2'. \tag{6.9}$$

From Table 6.3, these representations correspond to the 5f, 6d, or 7s orbitals as follows.

a_1': s, d_{z^2}
a_2'': f_{z^3}
e_1': (f_{xz^2}, f_{yz^2})
e_2': ($d_{x^2-y^2}$, d_{xy}), ($f_{x(x^2-3y^2)}$, $f_{y(3x^2-y^2)}$)

The same assignment with the D_{6h} system can also be performed here, that is, the A_1' and A_2'' representations in $\Gamma_{\sigma\text{ax}}$ are attributable to the $6d_{z^2}$ and $5f_{z^3}$ orbitals, respectively. In $\Gamma_{\sigma\text{eq}}$, it is immediately found that the A_1' and E_1' representations correspond to 7s and ($5f_{xz^2}$, $5f_{yz^2}$), respectively. To E_2' in $\Gamma_{\sigma\text{eq}}$, both sets of ($6d_{x^2-y^2}$, $6d_{xy}$) and ($5f_{x(x^2-3y^2)}$, $5f_{y(3x^2-y^2)}$) can be assigned. This result indicates a probability that the mixing of these $6d\delta_g$ and $5f\phi_u$ orbitals occurs in the center uranium immersed into the D_{5h} ligand field. Such a phenomenon has not been observed in the D_{6h} symmetry, in other words, the $6d\delta_g$–$5f\phi_u$ mixing is intrinsic in the D_{5h} system. Furthermore, the participation of $5f\phi_u$ ($f_{x(x^2-3y^2)}$, $f_{y(3x^2-y^2)}$) orbitals in the σ bonding implies that these 5f orbitals are made to have anti-bonding character by the D_{5h} ligand field. Hence, the energy order of the 5f orbitals in D_{5h} is,

$$e_2''\ (5f\delta_u) < e_2'\ (5f\phi_u) < e_1'\ (5f\pi_u) < a_2''\ (5f\sigma_u).$$

Finding the possibility of the d–f mixing, the f–f transition in D_{5h} symmetric ligand field is no longer pure transition between 5f orbitals, may have characters of f–d or d–f transitions. Therefore, the intensities of the f–f transitions in $[U^{V}O_2(\text{saloph})\text{DMSO}]^-$ and $[U^{V}O_2(\text{dbm})_2\text{-DMSO}]^-$ can be borrowed from the f–d or d–f transitions. The selection rule of the f–f transitions in D_{5h} system were studied below. The transition probability Q is proportional to the following integration.

$$Q \propto \int \psi_e^* \mu \psi_e \, d\tau \tag{6.10}$$

where ψ_e and ψ_e^* are the electronic wave function of ground and excited states, respectively, and μ is a transition moment polarized to (x, y) or z directions. To obtain non-zero value of Q, the representation $\Gamma[\psi_e^* \mu \psi_e]$ must contain A_1' representation. From the energy order of the 5f orbitals in D_{5h}, it is likely that the unpaired electron in the uranyl(V) complex is placed in one of the e_2'' ($5f\delta_u$) orbitals, *i.e.*, the ground state is E_2'' ($^2\Delta_u$ in $D_{\infty h}$). The representations

$\Gamma^{m}_{\alpha-\beta}$ (α, β: Greek letter expression of the 5f orbitals, m: polarized axis of μ ($m = (x, y), z$)) for the possible sets are obtained as,

$$E_2'' \rightarrow E_2' \,(5\mathrm{f}\delta_u \rightarrow 5\mathrm{f}\phi_u):$$

$$\Gamma^{(x,y)}_{\delta-\phi} = E_2' \times E_1' \times E_2'' = A_1'' + A_2'' + 2E_1'' + E_2'' \tag{6.11}$$

$$\Gamma^{z}_{\delta-\phi} = E_2' \times A_2'' \times E_2'' = A_1' + A_2' + E_1' \tag{6.12}$$

$$E_2'' \rightarrow E_1' \,(5\mathrm{f}\delta_u \rightarrow 5\mathrm{f}\pi_u):$$

$$\Gamma^{(x,y)}_{\delta-\pi} = E_1' \times E_1' \times E_2'' = A_1'' + A_2'' + E_1'' + 2E_2'' \tag{6.13}$$

$$\Gamma^{z}_{\delta-\pi} = E_1' \times A_2'' \times E_2'' = E_1' + E_2' \tag{6.14}$$

$$\text{and } E_2'' \rightarrow A_2'' \,(5\mathrm{f}\delta_u \rightarrow 5\mathrm{f}\sigma_u):$$

$$\Gamma^{(x,y)}_{\delta-\sigma} = A_2'' \times E_1' \times E_2'' = E_1' + E_2' \tag{6.15}$$

$$\Gamma^{z}_{\delta-\sigma} = A_2'' \times A_2'' \times E_2'' = E_2''. \tag{6.16}$$

Thus, in the irreducible representations of these f–f transitions, only $\Gamma^{z}_{\delta-\phi}$ contains A_1'. Hence, in the D_{5h} symmetric ligand field, only the $E_2'' \rightarrow E_2'$ transition polarized in z axis in the uranyl(V) complex is allowed by the d–f mixing, and others may mainly borrow their intensities from the vibronic coupling. In this study, the polarized absorption spectra were not examined.

In the discussion about the electronic structures of actinyl species, the spin-orbit coupling must not be ruled out, because the spin-orbit coupling has important effect on them, especially for the $5f^1$ systems (no electronic repulsion). Actually, five absorption bands can be detected in each electronic spectrum of the uranyl(V) complex (Figure 6.4) in spite of the smaller numbers of the electronic transitions predicted in the D_{6h} and D_{5h} symmetric ligand fields. This fact is considered to be due to the presence of the spin-orbit coupling effect. Each uranyl(V) complex has one odd electron in its 5f orbital. This makes the value of total angular momentum (**J**) be half-integer. Therefore, to consider the spin-orbit coupling in the uranyl(V) complexes, the double group must be used instead of the simple group such as D_{6h} and D_{5h}.[1] The character tables of the double groups, D_6^* and D_5^*, corresponding to D_6 and D_5 simple groups have been reported previously,[197] and shown in Tables 6.4 and 6.5, respectively.[2]

In D_{6h} point group assumed for $[U^{V}O_2(CO_3)_3]^{5-}$, the energy order of the electronic states (configurations) was,

[1] When **J** is half-integer, the 2π rotation is no longer the identity operation E, because;

$$\chi(\alpha + 2\pi) = \frac{\sin(\mathbf{J} + \frac{1}{2})(\alpha + 2\pi)}{\sin(\alpha + 2\pi)/2} = -\chi(\alpha)$$

where $\chi(\alpha)$ is a character of α rotational operation. In this case, the 2π rotation cannot belongs to any representation of simple group. To solve such a difficulty, Bethe introduced an assumption that the 2π rotation is assigned operation R which is not E. As a result, the point group including R and its related rotational operations, so-called "double group", was created.[196]

[2] The point groups D_{6h} and D_{5h} are those added the inversion center (i) and/or horizontal mirror plane (σ_h) to the corresponding pure rotational sub-groups, D_6 and D_5, respectively. Thus, all required informations about the f orbitals are obtained only by using such pure rotational sub-groups and their double groups.

Table 6.4. Character table of D_6^*

D_6^*		E	R	$2C_6$	$2C_6R$	$2C_3$	$2C_3R$	C_2	C_2R	$3C_2'$	$3C_2'R$	$3C_2''$	$3C_2''R$
Γ_1	A_1'	1	1	1	1	1	1	1	1	1	1	1	1
Γ_2	A_2'	1	1	1	1	1	1	1	1	−1	−1	−1	−1
Γ_3	B_1'	1	1	−1	−1	1	1	−1	−1	1	1	−1	−1
Γ_4	B_2'	1	1	−1	−1	1	1	−1	−1	−1	−1	1	1
Γ_5	E_1'	2	2	1	1	−1	−1	−2	−2	0	0	0	0
Γ_6	E_2'	2	2	−1	−1	−1	−1	2	2	0	0	0	0
Γ_7	E'	2	−2	$\sqrt{3}$	$-\sqrt{3}$	1	−1	0	0	0	0	0	0
Γ_8	E''	2	−2	$-\sqrt{3}$	$\sqrt{3}$	1	−1	0	0	0	0	0	0
Γ_9	E'''	2	−2	0	0	−2	2	0	0	0	0	0	0

This character table is according to "*Theory of Transition-Metal Ions*" by Griffith.[197)]

$$E_{2u}\,(5\mathrm{f}\delta_u^1) \approx B_{2u}\,(5\mathrm{f}\phi_u^1) < B_{1u}\,(5\mathrm{f}\phi_u^1) < E_{1u}\,(5\mathrm{f}\pi_u^1) < A_{2u}\,(5\mathrm{f}\sigma_u^1).$$

These states correspond to the representations in D_6^* double group as follows.

D_{6h}	D_6^*
$A_{2u}\,(5\mathrm{f}\sigma_u^1)$	$\Gamma_2\,(A_2')$
$E_{1u}\,(5\mathrm{f}\pi_u^1)$	$\Gamma_5,\,(E_1')$
$B_{1u},\,B_{2u}\,(5\mathrm{f}\phi_u^1)$	$\Gamma_3,\,\Gamma_4,(B_1',\,B_2')$
$E_{2u},\,(5\mathrm{f}\delta_u^1)$	$\Gamma_6,\,(E_2')$

The characters (χ) of the representation of the spin component ψ_s (Γ_{ψ_s}) in the total wave function are readily obtained from the following equations.[196)]

$$\chi(E) = 2\mathbf{S} + 1 \tag{6.17}$$

$$\chi(R) = -(2\mathbf{S} + 1) \tag{6.18}$$

$$\chi(\alpha) = \frac{\sin(\mathbf{S} + \frac{1}{2})\alpha}{\sin \alpha/2} \quad (\alpha = 2m\pi/n \text{ for } C_n^m) \tag{6.19}$$

where $\mathbf{S} = \frac{1}{2}$ because of the $5\mathrm{f}^1$ configuration of the uranyl(V) species. The results are,

D_6^*	E	R	$2C_6$	$2C_6R$	$2C_3$	$2C_3R$	C_2	C_2R	$3C_2'$	$3C_2'R$	$3C_2''$	$3C_2''R$
Γ_{ψ_s}	2	−2	$\sqrt{3}$	$-\sqrt{3}$	1	−1	0	0	0	0	0	0

.

The Γ_{ψ_s} is already the irreducible representation Γ_7. The representations of the electronic states including the spin-orbit coupling are found from the direct products of their representations. That is,

$$5\mathrm{f}\sigma_u^1: \quad \Gamma_2 \times \Gamma_7 = \Gamma_7 \tag{6.20}$$

$$5\mathrm{f}\pi_u^1: \quad \Gamma_5 \times \Gamma_7 = \Gamma_7 + \Gamma_9 \tag{6.21}$$

$$5\mathrm{f}\phi_u^1: \quad \begin{cases} \Gamma_3 \times \Gamma_7 = \Gamma_8 \\ \Gamma_4 \times \Gamma_7 = \Gamma_8 \end{cases} \tag{6.22}$$

$$5\mathrm{f}\delta_u^1: \quad \Gamma_6 \times \Gamma_7 = \Gamma_8 + \Gamma_9 \tag{6.23}$$

All irreducible representations for the 5f orbitals are doublets, which are based on Kramer's theorem.

It is obvious that, in the $5f\sigma_u^1$ configuration, the representation Γ_7 corresponds to $\mathbf{J} = \frac{1}{2}$, because $\mathbf{L} = 0$ and $\mathbf{S} = \frac{1}{2}$, thus $\mathbf{J} = \mathbf{L} + \mathbf{S} = |\mathbf{L} - \mathbf{S}| = \frac{1}{2}$. Therefore, Γ_9 in $5f\pi_u^1$ (Eq. 6.21) is immediately found to be $\mathbf{J} = \frac{3}{2}$, followed by the assignment of Γ_8 in $5f\delta_u^1$ (Eq. 6.23) to $\mathbf{J} = \frac{5}{2}$. The $5f\phi_u^1$ configuration is a little problematic, because both representations of $\mathbf{J} = \frac{5}{2}$ and $\mathbf{J} = \frac{7}{2}$ are Γ_8. However, it has already been revealed that the $5f\phi_u$ orbital is split into b_{1u} and b_{2u} orbitals in the D_{6h} symmetric ligand field, and that the energy order of the corresponding states is $B_{2u}(\Gamma_4) < B_{1u}(\Gamma_3)$. Therefore, Γ_8 from $\Gamma_3 \times \Gamma_7$ may be assigned to $\mathbf{J} = \frac{7}{2}$, and the other Γ_8 from $\Gamma_4 \times \Gamma_7$ is to $\mathbf{J} = \frac{5}{2}$. The energy order from the $\mathbf{J}$ term is standing on Hunt's rule.

Table 6.5. Character table of D_5^*

D_5^*		E	R	$2C_5$	$2C_5R$	$2C_5^2$	$2C_5^2R$	$5C_2$	$5C_2R$
Γ_1	A_1'	1	1	1	1	1	1	1	1
Γ_2	A_2'	1	1	1	1	1	1	−1	−1
Γ_3	E_1'	2	2	$2\cos 2/5\pi$	$2\cos 2/5\pi$	$2\cos 4/5\pi$	$2\cos 4/5\pi$	0	0
Γ_4	E_2'	2	2	$2\cos 4/5\pi$	$2\cos 4/5\pi$	$2\cos 2/5\pi$	$2\cos 2/5\pi$	0	0
Γ_5	E'	2	−2	$-2\cos 4/5\pi$	$2\cos 4/5\pi$	$2\cos 2/5\pi$	$-2\cos 2/5\pi$	0	0
Γ_6	E''	2	−2	$-2\cos 2/5\pi$	$2\cos 2/5\pi$	$2\cos 4/5\pi$	$-2\cos 4/5\pi$	0	0
Γ_7	E''' ρ_1	1	−1	−1	1	1	−1	i	$-i$
	E''' ρ_2	1	−1	−1	1	1	−1	$-i$	i

This character table is according to "*Theory of Transition-Metal Ions*" by Griffith.[197)]

Smilarly, the D_5^* double group was applied to the systems of $[U^VO_2(saloph)DMSO]^-$ and $[U^VO_2(dbm)_2DMSO]^-$. The energy order of the electronic states (configurations) in these complexes is,

$$E_2''\ (5f\delta_u^1) < E_2'\ (5f\phi_u^1) < E_1'\ (5f\pi_u^1) < A_2''\ (5f\sigma_u^1).$$

These states correspond to the representations in D_5^* double group as follows.

D_{5h}	D_5^*
$A_2''\ (5f\sigma_u^1)$	$\Gamma_2\ (A_2')$
$E_1'\ (5f\pi_u^1)$	$\Gamma_3,\ (E_1')$
$E_2'\ (5f\phi_u^1)$	$\Gamma_4,\ (E_2')$
$E_2'',\ (5f\delta_u^1)$	$\Gamma_4,\ (E_2')$

The characters ($\chi(\Gamma_{\psi_s})$) for $\mathbf{S} = \frac{1}{2}$ in D_5^* double group are also obtained by using Eqs. 6.17–6.19. As a result,

D_5^*	E	R	$2C_5$	$2C_5R$	$2C_5^2$	$2C_5^2R$	$5C_2$	$5C_2R$
Γ_{ψ_s}	2	−2	$-2\cos 4/5\pi$	$2\cos 4/5\pi$	$2\cos 2/5\pi$	$-2\cos 2/5\pi$	0	0

.

This Γ_{ψ_s} is also irreducible, *i.e.*, $\Gamma_{\psi_s} = \Gamma_5$. Therefore, the representations of the electronic

states including the spin-orbit coupling are obtained as,

$$5f\sigma_u^1: \quad \Gamma_2 \times \Gamma_5 = \Gamma_5\left(\tfrac{1}{2}\right) \tag{6.24}$$

$$5f\pi_u^1: \quad \Gamma_3 \times \Gamma_5 = \Gamma_5\left(\tfrac{1}{2}\right) + \Gamma_6\left(\tfrac{3}{2}\right) \tag{6.25}$$

$$5f\phi_u^1: \quad \Gamma_4 \times \Gamma_5 = \Gamma_6\left(\tfrac{7}{2}\right) + \Gamma_7\left(\tfrac{5}{2}\right) \tag{6.26}$$

$$5f\delta_u^1: \quad \Gamma_4 \times \Gamma_5 = \Gamma_6\left(\tfrac{3}{2}\right) + \Gamma_7\left(\tfrac{5}{2}\right) \tag{6.27}$$

where the fractions in the parentheses are the corresponding **J** terms which were determined according to the similar discussion performed in the D_6^* double group. The presence of Kramer's doublets was also found.

In the analysis using group theory, the exact energy values of the electronic states cannot be calculated. Considering that the lowest absorption peak of each uranyl(V) complexes in Figure 6.4 is assigned to the second excited state, the first one may be expected to be at around $10^2 \sim 10^3$ cm^{-1}, because the corresponding states of the isoelectronic neptunyl(VI) species were reported at around 2000, 1000, and 447 cm^{-1} as shown in Table 6.1. Consequently, the most acceptable energy diagrams starting from the 5f atomic orbital and terminating at $[U^VO_2(CO_3)_3]^{5-}$, $[U^VO_2(\text{saloph})\text{DMSO}]^-$, and $[U^VO_2(\text{dbm})_2\text{DMSO}]^-$ through each ligand field (D_{6h}, D_{5h}) and the spin-orbit coupling effects were estimated as shown in Figure 6.5.

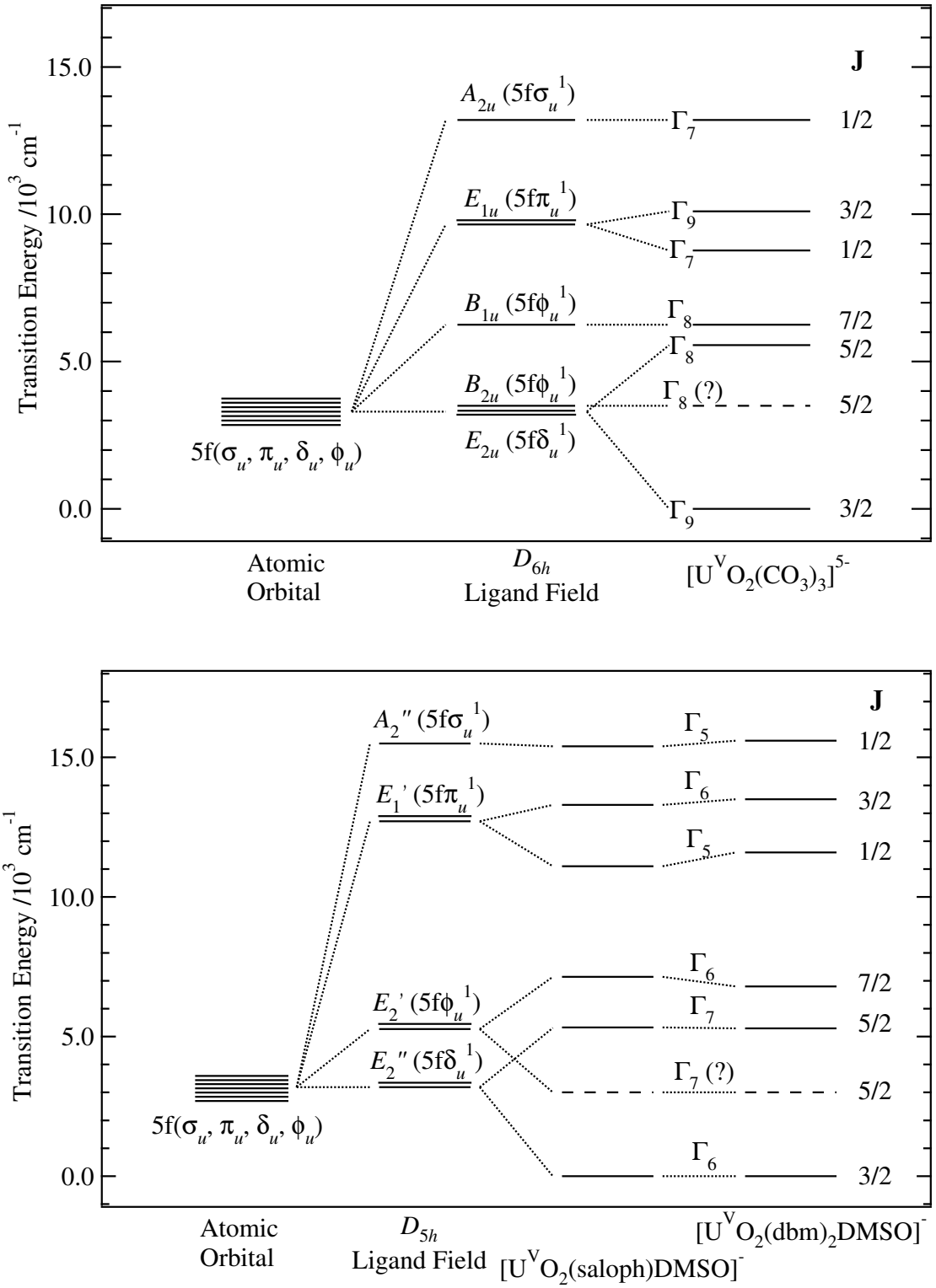

Figure 6.5. Energy diagrams of $[U^{V}O_2(CO_3)_3]^{5-}$ (upper), $[U^{V}O_2(saloph)DMSO]^{-}$, and $[U^{V}O_2(dbm)_2DMSO]^{-}$ (lower) including the D_{6h} or D_{5h} symmetric ligand field and the spin-orbit coupling effects. **J** terms are at the right-hand side of the energy states.

Chapter 7

Conclusion

I have studied the molecular structures, electronic spectra, and reactivities of uranyl(V) and -(VI) complexes by using various methods; X-ray diffractive, spectroscopic, and electrochemical measurements. Here, the results in this study are outlined and summarized as a conclusion of this doctoral thesis.

Chapter 1. As background of this doctoral thesis, the previous studies on properties of actinyl species were summarized, and the fact that little information is available concerning uranyl(V) complexes was pointed out. From this viewpoint, the objectives of this thesis was described.

Chapter 2. The uranyl(VI) complexes, $Na_4[U^{VI}O_2(CO_3)_3]$, $U^{VI}O_2$(saloph)DMF, $U^{VI}O_2$(saloph)DMSO, and $U^{VI}O_2(dbm)_2$DMSO, were selected as candidates to form stable uranyl(V) complexes. In order to discuss the properties of the uranyl(V) complexes, it was necessary to know those of the corresponding uranyl(VI) complexes firstly. Thus, in Chapter 2, syntheses and characterizations of the uranyl(VI) complexes, $Na_4[U^{VI}O_2(CO_3)_3]$, $U^{VI}O_2$(saloph)DMF, $U^{VI}O_2$(saloph)DMSO, and $U^{VI}O_2(dbm)_2$DMSO have been performed not only in the solid state, but also in the solution state by using IR, Raman, NMR spectroscopies, and/or single crystal X-ray analyses.

The sodium salt of $[U^{VI}O_2(CO_3)_3]^{4-}$ showed the symmetric (ν_1) and asymmetric stretching peaks (ν_3) in the uranyl(VI) moiety at 806 and 852 cm^{-1}, respectively. The ν_3 peak of $Na_4[U^{VI}O_2(CO_3)_3]$ is somewhat unusual, because such a peak in uranyl(VI) compounds is ranging from 900 to 950 cm^{-1} normally. Furthermore, the characteristic absorption bands of the uranyl(VI) ion in the UV-visible absorption spectrum and the coordination number of CO_3^{2-} from the ^{13}C NMR spectrum indicated that the uranyl(VI) species exists as $[U^{VI}O_2(CO_3)_3]^{4-}$ in the aqueous solution containing excess amount of Na_2CO_3.

The synthesis of $U^{VI}O_2$(saloph)DMF was confirmed by IR spectroscopy and single crystal X-ray analysis. The ν_3 peak of $U^{VI}O_2$(saloph)DMF was observed at 905 cm^{-1}, which is usual for uranyl(VI) compounds. From the red shift of the C=N stretching of saloph and C=O stretching of DMF, their coordinations to the uranyl(VI) ion were evidenced. The single crystal X-ray analysis for $U^{VI}O_2$(saloph)DMF gave the typical molecular structure of $U^{VI}O_2$(saloph)L; linear uranyl(VI) moiety, pentagonal bipyramidal geometry formed by tetradentate saloph and unidentate ligand (L = DMF), and largely distorted structure of saloph. From the ^1H NMR spectra of the dichloromethane and chloroform solutions prepared by dissolving $U^{VI}O_2$(saloph)DMF, it was found that the dimerization of $U^{VI}O_2$(saloph)DMF occurs in these solutions. This reaction produces $[U^{VI}O_2(saloph)]_2$, which is the dinuclear uranyl(VI) complex bridged by one of the oxygen atoms of saloph in each $U^{VI}O_2$(saloph) unit. Since the saloph ligand is also distorted in $[U^{VI}O_2(saloph)]_2$, this dinuclear uranyl(VI) complex is enantiomerized, and hence its crystal is racemic. By using UV-visible absorption and ^1H NMR spectroscopies, the thermodynamic parameters and the equilibrium constants at 298 K for the dimerization reaction of $U^{VI}O_2$(saloph)DMF were evaluated as $\Delta H_{dim} = 33.0 \pm 0.7$ kJ·mol^{-1}, $\Delta S_{dim} = 68 \pm 3$ J·mol^{-1}·K^{-1}, and $\log K_{dim} = -2.52 \pm 0.01$ for the dichloromethane system and $\Delta H_{dim} = 11.3 \pm 0.6$ kJ·mol^{-1}, $\Delta S_{dim} = 8.0 \pm 2.4$ J·mol^{-1}·K^{-1}, and $\log K_{dim} = -1.74 \pm 0.01$ for the chloroform system. To obtain further data for the reactivity of $U^{VI}O_2$(saloph)DMF, the DMF exchange reaction in this uranyl(VI) complex was also studied by using NMR line-broadening method. As a result, it was suggested that the DMF exchange reaction in $U^{VI}O_2$(saloph)DMF proceeds through the dissociative mechanism. The activa-

tion parameters and the first-order rate constant were estimated as $\Delta H^{\ddagger} = 19 \pm 1$ kJ·mol^{-1}, $\Delta S^{\ddagger} = -118 \pm 4$ J·mol^{-1}·K^{-1}, and $k_{ex} = 1.68 \times 10^3$ s^{-1} in the dichloromethane system.

The $U^{VI}O_2$(saloph)DMSO complex was also investigated to examine the effect of the unidentate ligand on the stability and reactivity of the uranyl(V) and -(VI) saloph complexes. The structural properties of $U^{VI}O_2$(saloph)DMSO were almost same as those of $U^{VI}O_2$(saloph)DMF; $\nu_3 = 897$ cm^{-1}, linear uranyl(VI) moikety, pentagonal bipyramidal geometry constructed from saloph and unidentate DMSO, and largely distorted saloph ligand. The reactivities of $U^{VI}O_2$(saloph)DMSO such as the dimerization to form [$U^{VI}O_2$(saloph)]$_2$ and the dissociative DMSO exchange reaction in $U^{VI}O_2$(saloph)DMSO were also confirmed. The thermodynamic parameters and the equilibrium constants at 298 K for the dimerization of $U^{VI}O_2$(saloph)DMSO were evaluated as $\Delta H_{dim} = 39 \pm 1$ kJ·mol^{-1}, $\Delta S_{dim} = 52 \pm 6$ J·mol^{-1}·K^{-1}, and $\log K_{dim} = -4.28 \pm 0.06$ for the dichloromethane system and $\Delta H_{dim} = 22 \pm 1$ kJ·mol^{-1}, $\Delta S_{dim} = 14 \pm 4$ J·mol^{-1}·K^{-1}, and $\log K_{dim} = -3.09 \pm 0.08$ for the chloroform system. Furthermore, the activation parameter and the first-order rate constant for the DMSO exchange reaction in $U^{VI}O_2$(saloph)DMSO were estimated as $\Delta H^{\ddagger} = 29.7 \pm 0.8$ kJ·mol^{-1}, $\Delta S^{\ddagger} = -83 \pm 3$ J·mol^{-1}·K^{-1}, and $k_{ex} = 1.63 \times 10^3$ s^{-1} in the dichloromethane system. In the comparison between the reactivities of $U^{VI}O_2$(saloph)DMF and $U^{VI}O_2$(saloph)DMSO, it was clarified that the coordination ability of DMSO to $U^{VI}O_2$(saloph) unit is stronger than that of DMF.

The alternative uranyl(VI) complex, $U^{VI}O_2(dbm)_2$DMSO, was also characterized by using the same methods. The ν_3 peak of $U^{VI}O_2(dbm)_2$DMSO was observed at 906 cm^{-1}. From the result of the single crystal X-ray analysis for $U^{VI}O_2(dbm)_2$DMSO, it was found that this uranyl(VI) complex also has the pentagonal bipyramidal structure consisting of two bidentate dbm ligands and one unidentate DMSO. The structural properties of $U^{VI}O_2(dbm)_2$DMSO were similar to those of $U^{VI}O_2$(saloph)DMSO in the solid state . However, $U^{VI}O_2(dbm)_2$DMSO showed different aspect from $U^{VI}O_2$(saloph)L in solutions. The intramolecular exchange reaction of the phenyl ring position of dbm nearer to and further from the coordinated DMSO and the rotation of the phenyl ring were observed as the broadening of the ^{1}H NMR signals due to *o*-protons. The first-order rate constant of the intramolecular exchange was estimated as 9.2×10^1 s^{-1} at 273 K. The DMSO exchange reaction in $U^{VI}O_2(dbm)_2$DMSO was also studied by using the NMR line-broadening method. As a result, it was proved that the coordinated DMSO in $U^{VI}O_2(dbm)_2$DMSO exchanges with free one dissociatively as well as $U^{VI}O_2$(saloph)L. The activation parameters and the first-order rate constants for the DMSO exchange reaction were calculated as $\Delta H^{\ddagger} = 30 \pm 2$ kJ·mol^{-1}, $\Delta S^{\ddagger} = -88 \pm 5$ J·mol^{-1}·K^{-1}, and $k_{ex} = 2.0 \times 10^2$ s^{-1} (273 K), 6.8×10^2 s^{-1} (298 K) in the dichloromethane system. Comparing these results for $U^{VI}O_2(dbm)_2$DMSO with those for $U^{VI}O_2$(saloph)DMSO, it was concluded that the coordination of DMSO to $U^{VI}O_2(dbm)_2$ unit is stronger than that to $U^{VI}O_2$(saloph) unit.

Chapter 3. The uranyl(V) carbonate complex, $[U^{V}O_2(CO_3)_3]^{5-}$, is traditionally know as a stable uranyl(V) species. However, the chemistry of this known uranyl(V) complex has not been established sufficiently. In this chapter, I have tried to elucidate the electrochemical and kinetic properties of $[U^{V}O_2(CO_3)_3]^{5-}$.

In the UV-visible spectroelectrochemical measurements for the redox couple of $[U^{V}O_2(CO_3)_3]^{5-}$/$[U^{VI}O_2(CO_3)_3]^{4-}$, the disappearance of the LMCT absorption bands of $[U^{VI}O_2(CO_3)_3]^{4-}$ was observed with the reduction to $[U^{V}O_2(CO_3)_3]^{5-}$. The absorbancies at different potentials were analyzed by the Nernstian equation. As a result, the electron stoichiometry

and the formal potentials the redox couple of $[U^{V}O_2(CO_3)_3]^{5-}/[U^{VI}O_2(CO_3)_3]^{4-}$ were evaluated as 0.90 ± 0.02 and −0.751 ± 0.001 V *vs.* Ag/AgCl, respectively. The electrochemical data were used for the preparation of $[U^{V}O_2(CO_3)_3]^{5-}$ in Section 3.2 and Chapter 6. Further, the discussion on the stability of $[U^{V}O_2(CO_3)_3]^{5-}$ in basic carbonate aqueous solution was performed from the reported thermodynamic data.

To examine the reactivity of $[U^{V}O_2(CO_3)_3]^{5-}$, its CO_3^{2-} exchange reaction was studied by using ^{13}C NMR spectroscopy. The NMR signals of free and coordinated CO_3^{2-} in the D_2O solution containing Na_2CO_3 (1.003 M) and $[U^{V}O_2(CO_3)_3]^{5-}$ (4.598×10^{-2} M) were observed at 169.13 and 106.70 ppm, respectively. From the peak areas, the coordination number of CO_3^{2-} was determined as 2.8 ± 0.1, indicating the existence of $[U^{V}O_2(CO_3)_3]^{5-}$. The kinetic analysis for the CO_3^{2-} exchange reaction in $[U^{V}O_2(CO_3)_3]^{5-}$ was performed by the nonlinear least-squares fit of the theoretical equation. Consequently, the activation parameters and the first-order rate constant at 298 K were evaluated as $\Delta H^{\ddagger}$ = 62.0 ± 0.7 kJ·mol^{-1}, $\Delta S^{\ddagger}$ = 22 ± 3 J·mol^{-1}·K^{-1}, and k_{ex} = 1.13×10^{3} s^{-1} in 1 M Na_2CO_3 aqueous system. It was impossible to examine the CO_3^{2-} exchange reaction of $[U^{V}O_2(CO_3)_3]^{5-}$ in the aqueous media with lower concentration of Na_2CO_3, because $[U^{V}O_2(CO_3)_3]^{5-}$ is not stable in such systems. However, the dissociative mechanism for the CO_3^{2-} exchange reaction in $[U^{V}O_2(CO_3)_3]^{5-}$ was proposed from the viewpoint of its saturated coordination sites and the positive value of $\Delta S^{\ddagger}$. Since the k_{ex} value for $[U^{V}O_2(CO_3)_3]^{5-}$ (1.13×10^{3} s^{-1}) is 10^2 times larger than that for $[U^{VI}O_2(CO_3)_3]^{4-}$ (13 s^{-1}), the bond strength between U and CO_3^{2-} in $[U^{V}O_2(CO_3)_3]^{5-}$ was considered to be weaker than that in $[U^{VI}O_2(CO_3)_3]^{4-}$. This is the first kinetic information of uranyl(V) complex.

Chapter 4. In order to find out systems of the stable uranyl(V) complexes in nonaqueous solvents, the electrochemical properties of the uranyl(VI) complexes, $U^{VI}O_2$(saloph)DMF, $U^{VI}O_2$(saloph)DMSO, and $U^{VI}O_2$(dbm)$_2$DMSO, were studied by the cyclic voltammetry and the UV-visible spectroelectrochemical measurements.

For $U^{VI}O_2$(saloph)DMF, the electrochemical reaction of $U^{VI}O_2$(saloph)DMF accompanied by the successive reaction of $[U^{V}O_2(\text{saloph})\text{DMF}]^{-}$ was observed in the cyclic voltammograms. This phenomenon was also evidenced by the UV-visible spectroelectrochemical measurement. This indicated that $[U^{V}O_2(\text{saloph})\text{DMF}]^{-}$ is not stable in DMF. From the cyclic voltammograms of $U^{VI}O_2$(saloph)DMF measured in the mixed solvent systems of DMF and dichloromethane, the successive reaction of $[U^{V}O_2(\text{saloph})\text{DMF}]^{-}$ was determined to be the dissociation of the coordinated DMF from $[U^{V}O_2(\text{saloph})\text{DMF}]^{-}$. The roughly estimated dissociation constant was 5 M. Furthermore, on the basis of the kinetic result that k_{ex} in $[U^{V}O_2(CO_3)_3]^{5-}$ is 10^2 times faster than that of $[U^{VI}O_2(CO_3)_3]^{4-}$ in Chapter 3, the DMF exchange reaction in $[U^{V}O_2(\text{saloph})\text{DMF}]^{-}$ was estimated to occur in $\sim10^5$ s^{-1}.

The electrochemical and spectroelectrochemical measurements similar to the system of $[U^{V}O_2(\text{saloph})\text{DMF}]^{-}/U^{VI}O_2$(saloph)DMF were performed for $U^{VI}O_2$(saloph)DMSO. In this system, any successive reactions of $[U^{V}O_2(\text{saloph})\text{DMSO}]^{-}$ have not been observed in the results of the cyclic voltammetry and the UV-visible spectroelectrochemical measurements. From the Nernstian analysis for the absorbancies at different potentials, the electron stoichiometry and the formal potential were evaluated as 1.09 ± 0.02 and −1.550 ± 0.001 V *vs.* Fc/Fc^{+}, respectively. In the mixed solvent systems of DMSO and dichloromethane, the DMSO dissociation from $[U^{V}O_2(\text{saloph})\text{DMSO}]^{-}$ was also observed. The roughly estimated dissociation constant was 0.5 M. This value means the stronger coordination ability of DMSO to $[U^{V}O_2(\text{saloph})]^{-}$ than that of DMF as expected in Chapter 2. The DMSO ex-

change reaction in $[U^{V}O_2(saloph)DMSO]^-$ was also estimated to occur in $\sim 10^5$ s^{-1} on the basis of the kinetic result of $[U^{V}O_2(CO_3)_3]^{5-}$. As a result, $[U^{V}O_2(saloph)DMSO]^-$ in DMSO was found to be a system of a stable uranyl(V) complex. This is the first example of the stable uranyl(V) complex in nonaqueous solvents.

For $U^{VI}O_2(dbm)_2DMSO$, the corresponding uranyl(V) complex $[U^{V}O_2(dbm)_2DMSO]^-$ did not show any successive reaction in DMSO as well as $[U^{V}O_2(saloph)DMSO]^-$. The evaluated values of the electron stoichiometry and the formal potential of the electrochemical reaction of $U^{VI}O_2(dbm)_2DMSO$ were 0.92 ± 0.03 and −1.366 ± 0.004 V *vs.* Fc/Fc^+, respectively. The DMSO exchange reaction in $[U^{V}O_2(dbm)_2DMSO]^-$ was also estimated to occur in $\sim 10^4$ s^{-1} by the same discussion. As a result, it was clarified that $[U^{V}O_2(dbm)_2$-$DMSO]^-$ stably exists in the DMSO solution. This is the second example of the stable uranyl(V) complex in nonaqueous solvents.

Chapter 5. To obtain the data of the molecular structures of the uranyl(V) complexes, the IR spectroelectrochemical measurements were performed for the redox couples of $[U^{V}O_2$-$(saloph)DMSO]^-/U^{VI}O_2(saloph)DMSO$ and $[U^{V}O_2(dbm)_2DMSO]^-/U^{VI}O_2(dbm)_2DMSO$ in DMSO found in Chapter 4. With the reduction from $U^{VI}O_2(saloph)DMSO$ to $[U^{V}O_2(saloph)$-$DMSO]^-$, the ν_3 peak of the uranyl(VI) moiety in $U^{VI}O_2(saloph)DMSO$ at 895 cm^{-1} was vanished and that of uranyl(V) moiety in $[U^{V}O_2(saloph)DMSO]^-$ appeared at 770 cm^{-1}. The difference of the ν_3 peaks of these uranyl(V) and -(VI) complexes was 125 cm^{-1}. In the system of $[U^{V}O_2(dbm)_2DMSO]^-/U^{VI}O_2(dbm)_2DMSO$, quite similar phenomenon was observed; ν_3 of $U^{VI}O_2(dbm)_2DMSO$: 906 cm^{-1}, ν_3 of $[U^{V}O_2(dbm)_2DMSO]^-$: 775 cm^{-1}, and $\Delta\nu_3$ = 131 cm^{-1}. Furthermore, it should be noted that any remarkable changes in the IR peaks due to saloph and dbm have not been observed with the reduction from uranyl(VI) to uranyl(V). By using the empirical relationship between the U=O distance (R_{UO}) and its force constant (F_{UO}) derived from ν_3, the R_{UO} values in $[U^{V}O_2(saloph)DMSO]^-$ and $[U^{V}O_2(dbm)_2DMSO]^-$ were evaluated as 1.84 Å, which are 0.06 Å longer than those of the corresponding uranyl(VI) complexes. Consequently, it was found that the ν_3 peak at around 770 cm^{-1} ($\Delta\nu_3$ = 130 cm^{-1}), similar structure of the equatorial ligands to that of the uranyl(VI) one, and the lengthening of R_{UO} about 0.06 Å from that of the uranyl(VI) one are the common structural properties of the uranyl(V) complexes

Chapter 6. The electronic spectra of three types of pure uranyl(V) complexes, $[U^{V}O_2$-$(CO_3)_3]^{5-}$, $[U^{V}O_2(saloph)DMSO]^-$, and $[U^{V}O_2(dbm)_2DMSO]^-$ were first measured. As a result, it was clarified that these uranyl(V) complexes have characteristic absorption bands in the visible-NIR region as follows.

- $[U^{V}O_2(CO_3)_3]^{5-}$: 5560, 6250, 8770, 10100, and 13200 cm^{-1} (ϵ = 0.2–3.6 $M^{-1}\cdot cm^{-1}$).
- $[U^{V}O_2(saloph)DMSO]^-$: 5330, 7140, 11100, 13300, and 15400 cm^{-1} (ϵ = 100–300 $M^{-1}\cdot cm^{-1}$).
- $[U^{V}O_2(dbm)_2DMSO]^-$: 5290, 6800, 11600, 13500, and 15600 cm^{-1} (ϵ = 150–900 $M^{-1}\cdot cm^{-1}$).

From the similarities in the electronic spectra, the differences in the ϵ values, and the coordination environments surrounding U^{5+} ion, it was proposed that these characteristic absorption bands of the uranyl(V) complexes are due to the f–f transitions in the $U^{V}O_2^+$ core.

The absorption bands due to the f–f transition in the uranyl(V) complexes could be classified into two regions, *Region I* (4800–7600 cm^{-1}) and *Region II* (7600–17200 cm^{-1}). From the discussion about the participations of the 5f orbitals in the actinyl bonding, the absorption bands in *Region I* were assigned to the transitions from the 5f(δ_u or ϕ_u) orbital to other 5fδ_u and/or 5fϕ_u, and those in *Region II* were attributed to the transitions to the 5fπ_u and 5fσ_u. In a comparison with the electronic spectral data of the isoelectronic neptunyl(VI) species, it was suggested that the absorption band of each uranyl(V) complex at the lowest wavenumber corresponds to the second excited state in the f–f transitions and that the much weaker antibonding characters of the 5fπ_u and 5fσ_u orbitals in the uranyl(V) complexes may explain their unusual instabilities.

By using the group theory, the splitting scheme of the 5f orbitals, the hybridization of the 5f, 6d and 7s orbitals, and the intensities of the f–f transitions were discussed. In D_{6h} point group corresponding to $[U^{V}O_2(CO_3)_3]^{5-}$, the energy order of the $5f^1$ electronic states were obtained as, E_{2u} ($5f\delta_u^1$) $\approx$ B_{2u} ($5f\phi_u^1$) $<$ B_{1u} ($5f\phi_u^1$) $<$ E_{1u} ($5f\pi_u^1$) $<$ A_{2u} ($5f\sigma_u^1$). Here, the splitting of the essentially doubly degenerated 5fϕ_u orbitals were observed. In the hybridization of the atomic orbitals of the center uranium in the D_{6h} point group, it was revealed that all 5f orbitals are independent of other 6d and 7s ones. This proposed that the origin of the intensities of the f–f transitions in $[U^{V}O_2(CO_3)_3]^{5-}$ is due to vibronic coupling. On the other hand, in the D_{5h} point group corresponding to $[U^{V}O_2(saloph)DMSO]^{-}$ and $[U^{V}O_2(dbm)_2$-$DMSO]^{-}$, the energy order of the $5f^1$ electronic states were determined as, E_2'' ($5f\delta_u^1$) $<$ E_2' ($5f\phi_u^1$) $<$ E_1' ($5f\pi_u^1$) $<$ A_2'' ($5f\sigma_u^1$), and the d–f mixing in the hybridization of the 5f, 6d, and 7s orbitals was predicted. As a result of the estimation for the transition probabilities, it was revealed that only the $E_2'' \rightarrow E_2'$ ($5f\delta_u \rightarrow 5f\phi_u$) transition polarized in z axis is allowed by the d–f mixing, and that others may borrows their intensities from the vibronic coupling. To examine the spin-orbit effect in $5f^1$ system ($\mathbf{S} = \frac{1}{2}$), the double groups were also involved in the discussion. Consequently, the energy diagrams including D_{6h} and D_{5h} symmetric ligand field and the spin-orbit effect were proposed for the electronic spectra of $[U^{V}O_2(CO_3)_3]^{5-}$, $[U^{V}O_2(saloph)DMSO]^{-}$, and $[U^{V}O_2(dbm)_2DMSO]^{-}$.

The properties concerning the molecular structures, electronic spectra, and reactivities of the uranyl(V) and -(VI) complexes are summarized in Table 7.1. In the present study, two systems of stable uranyl(V) complexes other than $[U^{V}O_2(CO_3)_3]^{5-}$ have been found out. This is the first observation of the pure uranyl(V) species in nonaqueous system. Furthermore, the novel experimental data concerning molecular structure, electronic spectra, and reactivities of the uranyl(V) complexes have been elucidated. These data are the first experimental evidences on the properties of a series of the uranyl(V) species, and the essential information of the actinyl species as described in Chapter 1. Not only for the progress in the basic science of the actinoid elements, such knowledges of the properties of uranyl(V) will be important also for the construction of the basis of technological developments in the nuclear engineering field; the reprocessing process of the spent nuclear fuel and the geological disposal of the high level radioactive wastes. For example, the adjustment of the oxidation states of nuclides (U, Pu, and other fission products) is most essential in both wet- and pyro-reprocessing processes. Moreover, the uranyl(V) species, especially $[U^{V}O_2(CO_3)_3]^{5-}$, may occur in the geosphere where the reductive atmosphere and carbonate-rich ground water should be presented. In conclusion, it must be noted that such elucidations of the chemistry of uranyl(V) have been established by the observation of the pure uranyl(V) complexes, which had never been achieved in the previous studies.

Table 7.1. Summary of molecular structures, electronic spectra, and reactivities of uranyl(V) and -(VI) complexes

System	Property	U(V) ($5f^1$)	U(VI) ($5f^0$)	$E^{\circ\prime}$ of U(V)/U(VI)[a]
$[U^{V/VI}O_2(CO_3)_3]^{5-/4-}$	Molecular Structure:	ν_1 = 759 cm^{-1}, R_{UO} = 1.90 Å[b]	ν_1 = 812 cm^{-1}, R_{UO} = 1.80 Å[b]	−0.751 V *vs.* Ag/AgCl
	f–f Transition:	5560, 6250, 8770, 10100, 13200 cm^{-1}	no f–f transition	(−0.529 V *vs.* SHE)[c]
	CO_3^{2-} Excahnge:	$k_{ex}^{298K} = 1.13 \times 10^3$ s^{-1}	k_{ex}^{298K} = 13 s^{-1} [d]	
		$\Delta H^{\ddagger}$ = 62.0 ± 0.7 kJ·mol^{-1}	$\Delta H^{\ddagger}$ = 82 ± 11 kJ·mol^{-1} [d]	
		$\Delta S^{\ddagger}$ = 22 ± 3 J·mol^{-1}·K^{-1}	$\Delta S^{\ddagger}$ = 50 ± 30 J·mol^{-1}·K^{-1} [d]	
$[U^{V/VI}O_2(saloph)DMF]^{-/0}$	DMF Dissociation:	$K_{disV} \approx 5$ M	–	−1.626 V *vs.* Fc/Fc^+
	DMF Exchange:	$k_{ex}^{298K} \approx 10^5$ s^{-1}	$k_{ex}^{298K} = 1.68 \times 10^3$ s^{-1}	(−0.947 V *vs.* SHE)[e]
			$\Delta H^{\ddagger}$ = 19 ± 1 kJ·mol^{-1}	
			$\Delta S^{\ddagger}$ = −118 ± 4 J·mol^{-1}·K^{-1}	
$[U^{V/VI}O_2(saloph)DMSO]^{-/0}$	Molecular Structure:	ν_3 = 770 cm^{-1}, R_{UO} = 1.84 Å	ν_3 = 895 cm^{-1}, R_{UO} = 1.783 Å	−1.550 V *vs.* Fc/Fc^+
	f–f Transition:	5330, 7140, 11100, 13300, 15400 cm^{-1}	no f–f transition	(−0.917 V *vs.* SHE)[e]
	DMSO Dissociation:	$K_{disV} \approx 0.5$ M	–	
	DMSO Exchange:	$k_{ex}^{298K} \approx 10^5$ s^{-1}	$k_{ex}^{298K} = 1.63 \times 10^3$ s^{-1}	
			$\Delta H^{\ddagger}$ = 29.7 ± 0.8 kJ·mol^{-1}	
			$\Delta S^{\ddagger}$ = −83 ± 3 J·mol^{-1}·K^{-1}	
$[U^{V/VI}O_2(dbm)_2DMSO]^{-/0}$	Molecular Structure:	ν_3 = 775 cm^{-1}, R_{UO} = 1.84 Å	ν_3 = 906 cm^{-1}, R_{UO} = 1.784 Å	−1.362 V *vs.* Fc/Fc^+
	f–f Transition:	5290, 6800, 11600, 13500, 15600 cm^{-1}	no f–f transition	(−0.729 V *vs.* SHE)[e]
	DMSO Exchange:	$k_{ex}^{298K} \approx 10^4$ s^{-1}	$k_{ex}^{298K} = 6.8 \times 10^2$ s^{-1}	
			$\Delta H^{\ddagger}$ = 30 ± 2 kJ·mol^{-1}	
			$\Delta S^{\ddagger}$ = −88 ± 5 J·mol^{-1}·K^{-1}	

[a]Formal potential of U(V)/U(VI) redox couple. [b]Reported data; ν_1: by Madic *et al.*,[151] R_{UO}: by Docrat *et al.*[153] [c]Calculated by using the known potential value of Ag/AgCl *vs.* SHE (standard hydrogen electrode), +0.222 V at 298 K. [d]Reported data by Brücher *et al.*[71] [e]Calculated by using the known potential value of Ag/Ag^+ in acetonitrile *vs.* SHE, +0.560 V, and the measured values of Fc/Fc^+ in DMSO and DMF *vs.* Ag/Ag^+ in acetonitrile, +0.073 V and +0.119 V, respectively.

Acknowledgment

It is privilege to express my sincere appreciation to **Associate Professor Yasuhisa Ikeda**, who has given me continuous supervising, guidance, and encouragement throughout my graduate research.

I wish to acknowledge gratefully to,

Dr. Masayuki Harada Assistant researcher in our laboratory, for his great help in my research and his skillful assistance.

Prof. Ingmar Grenthe Professor in Kungliga Tekniska Högskolan (KTH, Royal Institute of Technology, Sweden), for helpful discussion especially in the carbonate aqueous system and his kindness in my stay in Stockholm, Sweden from 15th November to 20th December, 2005. I would like to express my special thankfulness to him with my respect.

Prof. Satoru Tsushima Associate professor in Stockholm University, for the useful discussions concerning the electronic spectra and structural properties of the uranyl(V) complexes from a point of theoretical view. I also want to express my special appreciation to his kindness in my stay in Stockholm, Sweden.

Prof. Zoltán Szabó Associate professor in Kungliga Tekniska Högskolan (KTH, Royal Institute of Technology, Sweden), for his kindness especially in my stay in Stockholm, Sweden, and technical assistance to use the NMR and other instruments in KTH.

Prof. Toshihiko Hoshi Emeritus professor in Aoyama Gakuin University, for the helpful education and discussions, and his encouragement since my undergraduate research in Aoyama Gakuin University.

Prof. Kunio Shimizu Emeritus professor in Sophia University, for his kind and helpful advices to prepare the OTTLE cell.

Dr. Miki Hasegawa Lecturer in Aoyama Gakuin University, for the creative discussions and her encouragement since my undergraduate research in Aoyama Gakuin University.

Dr. Seong-Yun Kim Researcher in Japan Atomic Energy Agency, for his technical assistance especially for the electrochemical measurements and the creative discussion on the electrochemical properties of uranyl(VI) complexes.

Dr. Takehiko Tsukahara Assistant researcher in Tokyo University, for his helpful lecture to use the NMR instrument and his heart-warming kindness.

Dr. Noriko Asanuma Lecturer in Tokai University, for her kindness and accurate guidance to my research.

Dr. Nobuyoshi Koshino Researcher in Sumitomo Chemical, for his kindness and useful discussion in my study.

My colleagues in Ikeda Lab For the useful discussions and their heart-warming guidance, kindness, and friendships.

I would like to thank my family, **Miss Michiko Takao** (mother), **Mr. Yoshihiro Mizuoka** (brother), **Mr. Kenji Takao** (brother), **Mrs. Toshiko Takao** (grandmother), and **Mr. Keiichiro Takao** (grandfather), for their kindness and great supports in all of my student life. Finally, I want to dedicate this doctoral thesis to my beloved woman, **Dr. Shinobu Kishi**.

March, 2006

Koichiro Mizuoka

References

[1] Katz, J. J.; Seaborg, G. T.; Morss, L. R., *The Chemistry of the Actinide Elements 2nd Edition*, Chapman and Hall, London, New York, **1986**.

[2] Kaltsoyannis, N.; Scott, P., *The f elements*, OXFORD University Press Inc., New York, **1999**.

[3] Denning, R. G.; Norris, J. O. W.; Short, I. G.; Snellgrove, T. R.; Woodwark, D. R., "Electronic Structure of Actinyl Ions", *Lanthanide and Actinide Chemistry and Spectroscopy*, **1980**, *ACS Symposium Series 131*, 313–330.

[4] Matsika, S.; Zhang, Z.; Brozell, S. R.; Blaudeau, J.-P.; Wang, Q.; Pitzer, R. M., "Electronic Structure and Spectra of Actinyl Ions", *J. Phys. Chem. A*, **2001**, *105*, 3825–3828.

[5] King, R. B., "Some Aspects of Structure and Bonding in Binary and Ternary Uranium(VI) Oxides", *Chem. Mater.*, **2002**, *14*, 3628–3635.

[6] Crandall, H. W., "The Formula of Uranyl Ion", *J. Chem. Phys.*, **1949**, *17*, 602–606.

[7] Adams, D. M., *Metal-Ligand and Related Vibrations*, Edward Arnold Ltd. London, **1967**.

[8] Jones, L. H., "Determination of U–O Bond Distance in Uranyl Complexes from Thier Infrared Spectra", *Spectrochim. Acta*, **1959**, *15*, 409–411.

[9] Badger, R. M., "The Relation Between the Internuclear Distances and Force Constants of Molecules and Its Application to Polyatomic Molecules", *J. Chem. Phys.*, **1935**, *3*, 710–714.

[10] McGlynn, S. P.; Smith, J. K.; Neely, W. C., "Electronic Structure, Spectra, and Magnetic Properties of Oxycations. III. Ligation Effects on the Infrared Spectrum of the Uranyl Ion", *J. Chem. Phys.*, **1961**, *35*, 105–116.

[11] Veal, B. W.; Lam, D. J.; Carnall, W. T.; Hoekstra, H. R., "X-ray Photoemission Spectroscopy Study of Hexavalent Uranium Compoudns", *Phys. Rev.*, **1975**, *B12*, 5651–5663.

[12] Grenthe, I.; Fuger, J.; Konings, R. J. M.; Lemire, R. J.; Muller, A. B.; Hgun-Trung, C.; Wanner, H., *Chemical Thermodynamics of Uranium*, OECD/NEA and North-Holland, Amsterdam, **1992**, 2003 Updated.

[13] Guillaumont, R.; Fanghänel, T.; Neck, V.; Fuger, J.; Palmer, D. A.; Grenthe, I.; Rand, M. H., *Update on the Chemical Thermodynamics of Uranium, Neptunium, Plutonium, Americium and Technetium*, Elsevier B. V., Amsterdam, The Netherlands, **2003**.

[14] Alcock, N. W.; Esperås, S., "Crystal and Molecular Structure of Uranyl Diperchlorate Heptahydrate", *J. Chem. Soc. Dalton Trans.*, **1977** 893–896.

[15] Fischer, A., "Competitive Coordination of the Uranyl Ion by Perchlorate and Water – The Crystal Structures of $UO_2(ClO_4)_2{\cdot}3H_2O$ and $UO_2(ClO_4)_2{\cdot}5H_2O$ and a Redetermination of $UO_2(ClO_4)_2{\cdot}7H_2O$", *Z. Anorg. Allg. Chem.*, **2003**, *629*, 1012–1016.

[16] Comyns, A. E.; Gatehouse, B. M.; Wait, E., "The Chemistry of Uranyl Acetylacetone Complex", *J. Chem. Soc.*, **1958** 4655–4665.

[17] Sacconi, L.; Caroti, G.; Paoletti, P., "Investigations on the Co-ordination Power of Uranyl. Part III. Infrared Spectra of Some Complexes with β-Diketones", *J. Chem. Soc.*, **1958** 4257–4264.

[18] Haigh, J. M.; Thornton, D. A., "Ligand Substitution Effects in Uranyl β-Ketoenolates", *J. Mol. Struct.*, **1971**, *8*, 351–361.

[19] Kannan, S.; Venugopal, V.; Pillai, M. R. A.; Droege, P. A.; Barnes, C. L., "Synthesis and Characterization of Sulphoxide Adducts of Uranyl Bis(β-diketonates): The Crystal and Molecular Structure of $[UO_2(DBM)_2{\cdot}C_6H_5CH_2SOCH_3]$", *Polyhedron*, **1996**, *15*, 97–101.

[20] Kannan, S.; Venugopal, V.; Pillai, M. R. A.; Droege, P. A.; Barnes, C. L.; Schlemper, E. O., "The Dibenzylideneacetone Adducts of Uranyl Bis(β-diketonates). The Low Temperature NMR Behaviour and Molecular Structure of $[UO_2(TTA)_2{\cdot}DBA]$", *Polyhedron*, **1996**, *15*, 465–471.

[21] Kannan, S.; Pillai, M. R. A.; Venugopal, V.; Droege, P. A.; Barnes, C. L., "The Camphor Adducts of Uranyl Bis(β-diketones). The Low Temperature ^{19}F NMR Behaviour of $[UO_2(TTA)_2{\cdot}$camphor] and the Cyrstal Structure of $[UO_2(DBM)_2{\cdot}$camphor]", *Inorg. Chim. Acta*, **1997**, *254*, 113–117.

[22] Kannan, S.; Usman, A.; Fun, H. K., "Synthesis and Characterization of [Bis(β-diketonato)uranium(VI)] Nitrone Compounds. The Crystal and Molecular Structure of $[UO_2(TTA)_2{\cdot}p\text{-}NO_2\text{–}C_5H_4NO]$", *Polyhedron*, **2002**, *21*, 2403–2407.

[23] Pfeiffer, P.; Hesse, T.; Pfitzner, H.; Scholl, W.; Thielert, H., "Innere Komplexsalze der Aldimin- und Azoreihe", *J. Prakt. Chem.*, **1937**, *149*, 217–296.

[24] Bandoli, G.; Clemente, D. A.; Croatto, U.; Vidali, M.; vigato, P. A., "Preparation and Crystal and Molecular Structure of [*N,N'-o*-Phenylenebis(salicylideneiminato)UO_2(EtOH)]", *Chem. Commun.*, **1971** 1330–1331.

[25] Cattalinin, L.; Degetto, S.; Vidali, M.; Vigato, P. A., "Uranyl Complexes Containing Polydentate Schiff Bases", *Inorg. Chim. Acta*, **1972**, *6*, 173–176.

[26] Pasini, A.; Gullotti, M.; Cesarotti, E., "Schiff Base Complexes of Oxocations–I Uranyl Complexes with Tetradentate Optically Active Schiff Bases of Salicylaldehyde", *J. Inorg. Nucl. Chem.*, **1972**, *34*, 3821–3833.

[27] Bandoli, G.; Clemente, D. A.; Croatto, U.; Vidali, M.; Vigato, P. A., "Crystal and Molecular Structure of [*N,N'*Ethylene-bis(salicylideneiminato)UO_2(MeOH)]", *Inorg. Nucl. Chem. Lett.*, **1972**, *8*, 961–964.

[28] Bandoli, G.; Cattalini, L.; Clemente, D. A.; Vidali, M.; Vigato, P. A., "Preparation, Properties, and Molecular Structure of Aquoglyoxolbis-(2-hydroxyanil)dioxouranium", *J. Chem. Soc., Chem. Commun.*, **1972** 344–345.

[29] Bandoli, G.; Clemente, D. A.; Croatto, U.; Vidali, M.; Vigato, P. A., "Crystal and Molecular Structure of [*N,N'*-Ethylenebis(salicylideneiminato)](methanol)dioxouranium", *J. Chem. Soc. Dalton*, **1973** 2331–2335.

[30] Cattalini, L.; Vigato, P. A.; Vidali, M.; Degetto, S.; Casellato, U., "The Interaction of 2,2'-Bisbenzoxazoline with Uranyl Ion", *J. Inorg. Nucl. Chem.*, **1975**, *37*, 1721–1723.

[31] Bombieri, G.; Forsellini, E.; Benetollo, F.; Fenton, D. E., "Conformational Differences in Dioxouranium(VI) Coordination Compounds Crystal Structure of the Chloroform Adduct of *N,N'*-Bis-salicylidene-1,5-diamino-3-oxapentane-dioxouranium(VI)", *J. Inorg. Nucl. Chem.*, **1979**, *41*, 1437–1441.

[32] Paolucci, G.; Marangoni, G.; Bandoli, G.; Clemente, D. A., "Reactivity of Uranyl Ion with Quinquedentate Chelating Hydrazine Derivatives. Part 2. 2,6-Diacetylpyridine Bis(4-methoxybenzoylhydrazone)", *J. Chem. Soc., Dalton Trans.*, **1980** 1304–1311.

[33] Rajan, O. A.; Chakravorty, A., "New Uranyl(VI) Complexes: Binding of Mono and Bidentate Ligands to UO_2(tridentate) Species", *Inorg. Chim. Acta*, **1981**, *50*, 79–84.

[34] Fenton, D. E.; Vigato, P. A.; Casellato, U.; Graziani, R.; Vidali, M., "The Preparation and Crystal Structure of *N,N'*-bis(salicylidene)-1,5-diamino-3-thiapentane-dioxouranium(VI)", *Inorg. Chim. Acta*, **1981**, *51*, 195–199.

[35] Casellato, U.; Guerriero, P.; Tamburini, S.; Vigato, P. A.; Graziani, R., "Synthesis, Properties, and Crystal Structures of New Mono- and Homobinuclear Uranyl(VI) Complexes with Compartmental Schiff Bases", *J. Chem. Soc., Dalton Trans.*, **1990** 1533–1541.

[36] Signorini, O.; Dockal, E. R.; Castellano, G.; Oliva, G., "Synthesis and Characterization of Aquo[*N,N'*-ethylenebis(3-ethoxysalicylideneaminato)]dioxouranium(VI)", *Polyhedron*, **2996**, *15*, 245–255.

[37] Evance, D. J.; Junk, P. C.; Smith, M. K., "The Effect of Coordinated Solvent Ligands on the Solid-State Structures of Compounds Involving Uranyl Nitrate and Schiff Bases", *Polyhedron*, **2002**, *21*, 2421–2431.

[38] Kannappan, R.; Tanase, S.; Tooke, D. M.; Spek, A. L.; Mutikainen, I.; Turpeinen, U.; Reedijk, J., "Separation of Actinides and Lanthanides: Crystal and Molecular Structures of *N,N'*-Bis(3,5-di-*t*-butylsalicylidene)-4,5-dimethyl-1,2-phenylenediamine and Its Uranium Complex", *Polyhedron*, **2004**, *23*, 2285–2291.

[39] Gatto, C. C.; Lang, E. S.; Kupfer, A.; Hagenbach, A.; Wille, D.; Abram, U., "Doxouranium Complexes with Acetylpyridine Benzoylhydrazones and Related Ligands", *Z. Anor. Allog. Chem.*, **2004**, *630*, 735–741.

[40] Marks, T. J.; Stojakovic, D. R., "Large Metal Ion-Centered Template Reactions. Chemical and Spectral Studies of the 'Superphthalocyanine' Dioxocyclopentakis(1-iminoisoindolinato)uranium(VI) and Its Derivatives", *J. Am. Chem. Soc.*, **1978**, *100*, 1695–1705.

[41] Cuellar, E. A.; Marks, T. J., "Synthesis and Characterization of Metallo and Metal-Free Octaalykylphthalocyanines and Uranyl Decaalkylsuperphthalocyanines", *Inorg. Chem.*, **1981**, *20*, 3766–3770.

[42] Bauer, V. J.; Clive, D. L. J.; Dolphin, D.; Paine Ⅲ, J. B.; Harris, F. L.; King, M. M.; Loder, J.; Wang, S.-Y. C.; Woodward, R. B., "Sapphyrins: Novel Aromatic Pentapyrrolic Macrocycles", *J. Am. Chem. Soc.*, **1983**, *105*, 6429–6436.

[43] De Cola, L.; Smailes, D. L.; Vallarino, L. M., "Metal-Templated Synthesis of Novel Macrocyclic Complexes of the Uranyl Ion", *Inorg. Chim. Acta*, **1985**, *110*, L1–L2.

[44] Van Staveren, C. J.; Van Eerden, J.; Van Veggel, F. C. J. M.; Harkema, S.; Reinhoudt, D. N., "Cocomplexation of Neutral Guests and Electrophilic Metal Cations in Synthetic Macrocyclic Hosts", *J. Am. Chem. Soc.*, **1988**, *110*, 4994–5008.

[45] Benetollo, F.; Bombieri, G.; De Cola, L.; Polo, A.; Smailes, D. L.; Vallarino, L. M., "Six-Nitrogen Macrocyclic Complexes of the Dioxouranium(VI) and Praseodymium(Ⅲ)", *Inorg. Chem.*, **1989**, *28*, 3447–3452.

[46] Sessler, J. L.; Mody, T. D.; Lynch, V., "Synthesis and X-ray Characterization of a Uranyl(VI) Schiff Base Complex Derived from a 2:2 Condensation Product of 3,4-Diethylpyrrole-2,5-dicarbaldehyde and 1,2-Diamino-4,5-dimethoxybenzene", *Inorg. Chem.*, **1992**, *31*, 529–531.

[47] Sessler, J. L.; Mody, T. D.; Dulay, M. T.; Espinoza, R.; Lynch, V., "The Template synthesis and X-ray Characterization of Pyrrole-Derived Hexadentate Uranyl(VI) Schiff-Base Macrocyclic Complexes", *Inorg. Chim. Acta*, **1996**, *246*, 23–30.

[48] Casellato, U.; Tamburini, S.; Tomasin, P.; Vigato, P. A., "Uranyl(VI) Complexes with [1+1] Asymmetric Compartmental Ligands Containing a Schiff Base and a Crown Ether-Like Chamber", *Inorg. Chim. Acta*, **2002**, *341*, 118–126.

[49] Sessler, J. L.; Callaway, W. B.; Dudek, S. P.; Date, R. W.; Bruce, D. W., "Synthesis and Characterization of a Discotic Uranium-Containing Liquid Crystal", *Inorg. Chem.*, **2004**, *43*, 6650–6653.

[50] Benedict, M.; Pigford, T. H.; Levi, H. W., *Nuclear Chemical Engineering, Second Edition*, McGraw-Hill, Inc. United States, **1981**.

[51] Casellato, U.; Vigato, P. A.; Vidali, M., "Actinide Nitrate Complexes", *Cood. Chem. Rev.*, **1981**, *36*, 183–265.

[52] Burns, J. H., "Solvent-Extraction Complexes of the Uranyl Ion. 1. Crystal and Molecular Structure of Bis(nitroato)bis(tri-*n*-butylphosphine oxide)dioxouranium(VI)", *Inorg. Chem.*, **1981**, *20*, 3868–3871.

[53] Burns, J. H., "Solvent-Extraction Complexes of the Uranyl Ion. 2. Crystal and Molecular Structures of *catena*-Bis(μ-di-*n*-butyl phosphato-*O,O'*)dioxouranium(VI) and Bis(μ-di-*n*-butyl phosphato-*O,O'*)bis[(nitrato)(tri-*n*-butylphosphine oxide)dioxouranium(VI)]", *Inorg. Chem.*, **1983**, *22*, 1174–1178.

[54] Agostini, G.; Giacometti, G.; Clemente, D. A.; Vicentini, M., "Crystal and Molecular Structure of Uranyl Nitrate Trimethylphosphate", *Inorg. Chim. Acta*, **1982**, *62*, 237–240.

[55] Burns, J. H.; Brown, G. M.; Ryan, R. R., "Structure of Dinitratodioxobis(triisobutyl phosphate)uranium(VI) at 139 K", *Acta Cryst.*, **1985**, *C41*, 1446–1448.

[56] Auwer, C. D.; Revel, R.; Charbonnel, M. C.; Presson, M. T.; Conradson, S. D.; Simoni, E.; Du, J. F. L.; Madic, C., "Actinide Coordination Sphere in Various U, Np and Pu Nitrato Cooridnation Complexes", *J. Synchrotron Rad.*, **1999**, *6*, 101–104.

[57] Varga, T. R.; Sato, M.; Fazekas, Z.; Ikeda, Y.; Tomiyasu, H., "New Uranyl Nitrate Complex with *N*-Cyclohexyl-2-pyrrolidone: A Promising Candidate for Nuclear Fuel Reprocessing", *Inorg. Chem. Commun.*, **2000**, *3*, 637–639.

[58] Varga, T. R.; Bényei, A. C.; Fazekas, Z.; Tomiyasu, H.; Ikeda, Y., "Molecular and Crystal Structure of Bis(*N*-cyclohexyl-2-pyrrolidone)dioxouranium(VI) Nitrate", *Inorg. Chim. Acta*, **2003**, *342*, 291–294.

[59] Koshino, N.; Harada, M.; Morita, Y.; Kikuchi, T.; Ikeda, Y., "Development of a Simple Reprocessing Process Using Selective Precipitant for Uranyl Ions –Fundamental Studies for Evaluating the Precipitant Performance", *Prog. Nucl. Ener.*, **2005**, *47*, 406–413.

[60] Brittain, H. G.; Tsao, L.; Perry, D. L., "Photophysical Studies of Uranyl Complexes 5. Luminescence Spectrum of $K_4UO_2(CO_3)_3$", *J. Lumin.*, **1984**, *29*, 285–294.

[61] Coda, A.; Giusta, A. D.; Tazzoli, V., "The Structure of Synthetic Andersonite, $Na_2Ca[UO_2(CO_3)_3]\cdot xH_2O$ ($x \simeq 5.6$)", *Acta Cryst.*, **1981**, *B37*, 1496–1500.

[62] Mereiter, K., "Structure of Caesium Tricarbonatodioxouranate(VI) Hexahydrate", *Acta Cryst.*, **1988**, *C44*, 1175–1178.

[63] Gordon, G.; Taube, H., "The Uranium(V)-Catalysed Exchange Reaction between Uranyl Ion and Water in Perchloric Acid Solution", *J. Inorg. Nucl. Chem.*, **1961**, *16*, 272–278.

[64] Clark, D. L.; Conradson, S. D.; Donohoe, R. J.; Keogh, D. W.; Morris, D. E.; Palmer, P. D.; Rogers, R. D.; Tait, C. D., "Chemical Speciation of the Uranyl Ion under Highly Alkaline Conditions. Synthesis, Structures, and Oxo Ligand Exchange Dynamics", *Inorg. Chem.*, **1999**, *38*, 1456–1466.

[65] Lincoln, S. F., "Kinetic Applications of NMR Spectroscopy", *Prog. React. Kinetics*, **1977**, *9*, 1–91.

[66] Fratiello, A.; Kubo, V.; Lee, R. E.; Schuster, R. E., "Direct Proton Magnetic Resonance Cation Hydration Study of Uranyl Perchlorate, Nitrate, Chloride, and Bromide in Water–Acetone Mixtures", *J. Phys. Chem.*, **1970**, *74*, 3726–3730.

[67] Fratiello, A.; Kubo, V.; Schuster, R. E., "A Proton Magnetic Resonance Cation Solvation Study of Uranyl Perchlorate, Uranyl Nitrate, and Uranyl Perchlorate-Hydrochloric Acid Solutions in Water–Dimethyl Sulfoxide–Acetone Mixtures", *Inorg. Chem.*, **1971**, *10*, 744–747.

[68] Ikeda, Y.; Soya, S.; Fukutomi, H.; Tomiyasu, H., "Nuclear Magnetic Resonance Study of the Kinetics of the Water Exchange Process in the Equatorial Positions of Uranyl Complexes", *J. Inorg. Nucl. Chem.*, **1979**, *41*, 1333–1337.

[69] Bowen, R. P.; Lincoln, S. F.; Williams, E. H., "Exchange of *N,N*-Dimethylacetamide on Dioxopentakis(*N,N*-dimethylacetamide)uranium(VI) Ion. Proton Magnetic Resonance Study", *Inorg. Chem.*, **1976**, *15*, 2126–2129.

[70] Crea, J.; Digiusto, R.; Lincoln, S. F.; Williams, E. H., "A Nuclear Magnetic Resonance Study of Ligand Exchange on Dioxopentakis(trimethylphosphate)uranium(VI) Ion and Its Triethyl Phosphate Analogue", *Inorg. Chem.*, **1977**, *16*, 2825–2829.

[71] Brücher, E.; Glaser, J.; Toth, I., "Carbonate Exchange for the Complex $UO_2(CO_3)_3^{4-}$ in Aqueous Solution as Studied by ^{13}C NMR Spectroscopy", *Inorg. Chem.*, **1991**, *30*, 2239–2241.

[72] Bányai, I.; Glaser, J.; Micskei, K.; Tóth, I.; Zékány, L., "Kinetic Behavior of Carbonate Ligands with Different Coordination Modes: Equilibrium Dynamics for Uranyl(2+) Carbonato Complexes in Aqueous Solution. A ^{13}C and ^{17}O NMR Study", *Inorg. Chem.*, **1995**, *34*, 3785–3796.

[73] Szabó, Z.; Aas, W.; Grenthe, I., "Structure, Isomerism, and Ligand Dynamics in Dioxouranium(VI) Complexes", *Inorg. Chem.*, **1997**, *36*, 5369–5375.

[74] Szabó, Z.; Grenthe, I., "Mechanisms of Ligand Substitution Reactions in Ternary Dioxouranium(VI) Complexes", *Inorg. Chem.*, **1998**, *37*, 6214–6221.

[75] Bardin, N.; Rubini, P.; Madic, C., "Hydration of Actinyl(VI), MO_{2aq}^{2+} (M = U, Np, Pu). An NMR Study", *Radiochim. Acta*, **1998**, *83*, 189–194.

[76] Farkas, I.; Bányai, I.; Szabó, Z.; Wahlgren, U.; Grenthe, I., "Rates and Mechanisms of Water Exchange of UO_2^{2+}(aq) and UO_2(oxolate)F$(H_2O)_2^-$: A Variable-Temperature ^{17}O and ^{19}F NMR Study", *Inorg. Chem.*, **2000**, *39*, 799–805.

[77] Szabó, Z.; Grenthe, I., "Potentiometric and Multinuclear NMR Study of the Binary and Ternary Uranium(VI)–L–Fluoride Systems, Where L is α-Hydroxycarboxylate or Glycine", *Inorg. Chem.*, **2000**, *39*, 5036–5043.

[78] Ikeda, Y.; Tomiyasu, H.; Fukutomi, H., "Kinetics Study of the Exchange of Dimethyl Sulfoxide in Uranyl Pentakis(dimethyl suldoxide) Ion by NMR", *Bull. Res. Lab. Nucl. React. (Tokyo Inst. Technol.)*, **1979**, *4*, 47–59.

[79] Kramer, G. M.; E. T. Maas, J., "Fluxionality of Uranyl β-Diketonate-Base Complexes. Behavior of Uranyl Trifluoroacetylacetonate-Dimethyl Sulfoxide", *Inorg. Chem.*, **1981**, *20*, 3514–3516.

[80] Ikeda, Y.; Tomiyasu, H.; Fukutomi, H., "A Nuclear Magnetic Resonance Study of the Kinetics of Ligand-Exchange Reactions in Uranyl Complexes. 4. Intramolecular-Exchange Reaction of Methyl Groups of Acetylacetonate in $UO_2(acac)_2L$ with L= Me_2S=O, Me_2N=COH, Et_2N=COH", *Inorg. Chem.*, **1984**, *23*, 1356–1360.

[81] Ikeda, Y.; Tomiyasu, H.; Fukutomi, H., "Nuclear Magnetic Resonance Study of the Kinetics of Ligand-Exchange Reactions in Uranyl Complexes. 5. Exchange Reaction of Acetylacetonate in Bis(acetylacetonato)(dimethyl sulfoxide)dioxouranium(VI)", *Inorg. Chem.*, **1984**, *23*, 3197–3202.

[82] Glavincevski, B.; Brownstein, S., "Structure and Exchange of Ionic Adducts of Uranyl Bis(hexafluoroacetylacetonate)", *Inorg. Chem.*, **1983**, *22*, 221–224.

[83] Vallet, V.; Privalov, T.; Wahlgren, U.; Grenthe, I., "The Mechanism of Water Exchange in $AmO_2(H_2O)_5^{2+}$ and in the Isoelectronic $UO_2(H_2O)_5^+$ and $NpO_2(H_2O)_5^{2+}$ Complexes as Studied by Quantum Chemical Methods", *J. Am. Chem. Soc.*, **2004**, *126*, 7766–7767.

[84] McGlynn, S. P.; Smith, J. K., "The Electronic Structure, Spectra, and Magnetic Properties of Actinyl Ions. Part I. The Uranyl Ion", *J. Mol. Spectrosc.*, **1961**, *6*, 164–187.

[85] Eisenstein, J. C.; Pryce, M. H. L., "The Electronic Structure and Magnetic Properties of Uranyl-like Ions I. Uranyl and Neptunyl", *Proc. Royal Soc. London, Series A*, **1955**, *229*, 20–38.

[86] Eisenstein, J. C.; Pryce, M. H. L., "The Electronic Structure and Magnetic Properties of Uranyl-like Ions Ⅱ. Plutonyl", *Proc. Royal Soc. London, Series A*, **1956**, *238*, 31–45.

[87] Eisenstein, J. C.; Pryce, M. H. L., "Electronic Structure and Magnetic Properties of the Neptunyl Ion", *J. Res. Nat. Bur. Stand.*, **1965**, *69A*, 217–235.

[88] Eisenstein, J. C.; Pryce, M. H. L., "Interpretation of the Solution Absorption Spectra of the $(PuO_2)^{++}$ and $(NpO_2)^+$ Ions", *J. Res. Nat. Bur. Stand.*, **1966**, *70A*, 165–173.

[89] McGlynn, S. P.; Smith, J. K., "The Electronic Structure, Spectra, and Magnetic Properties of Actinyl Ions. Part Ⅱ. Neptunyl, and the Ground States of Other Actinyls", *J. Mol. Spectrosc.*, **1961**, *6*, 188–198.

[90] Bell, J. T.; Biggers, R. E., "The Absorption Spectrum of the Uranyl Ion in Perchlorate Media. Part I. Mathematical Resolution of the Overlapping Band Structure and Studies of the Environmental Effects", *J. Mol. Spectrosc.*, **1965**, *18*, 247–275.

[91] Bell, J. T.; Biggers, R. E., "The Absorption Spectrum of the Uranyl Ion in Perchlorate Media. Part Ⅱ. The Effects of Hydrolysis on the Resolved Spectral Bands", *J. Mol. Spectrosc.*, **1967**, *22*, 262–271.

[92] Bell, J. T.; Biggers, R. E., "Absorption Spectrum of the Uranyl Ion in Perchlorate Media Ⅲ. Resolution of the Ultraviolet Band Structure; Some Conclusions Concerning the Excited State of UO_2^{2+}", *J. Mol. Spectrosc.*, **1968**, *25*, 312–329.

[93] Bell, J. T., "Continuities in the Spectra and Structure of the Actinyl Ions", *J. Inorg. Nucl. Chem.*, **1969**, *31*, 703–710.

[94] Görller-Walrand, C.; Vanquickenborne, L. G., "Identification of the Lower Transitions in the Spectra of Uranyl Complexes", *J. Chem. Phys.*, **1971**, *54*, 4178–4186.

[95] Görller-Walrand, C.; De Jaegere, S., "Correlation between the Vibronic Spectra of the Uranyl Ion and the Geometry of Its Coordination", *Spectrochim. Acta*, **1972**, *28A*, 257–268.

[96] Görller-Walrand, C.; Vanquickenborne, L. G., "On the Coupling Scheme in Uranyl Complexes", *J. Chem. Phys.*, **1972**, *57*, 1436–1440.

[97] Denning, R. G.; Snellgrove, T. R.; Woodwark, D. R., "The Electronic Structure of the Uranyl Ion Part I. The Electronic Spectrum of $Cs_2UO_2Cl_4$", *Mol. Phys.*, **1976**, *32*, 419–442.

[98] Denning, R. G.; Foster, D. N. P.; Snellgrove, T. R.; Woodwark, D. R., "The Electronic Structure of the Uranyl Ion Ⅱ. The Electronic Spectra of $CsUO_2(NO_3)_3$ and $NaUO_2(CH_3COO)_3$", *Mol. Phys.*, **1979**, *37*, 1089–1107.

[99] Denning, R. G.; Snellogrove, T. R.; Woodwark, D. R., "The Electronic Structure of the Uranyl Ion Ⅲ. Theory", *Mol. Phys.*, **1979**, *37*, 1109–1143.

[100] Denning, R. G.; Short, I. G.; Woodwark, D. R., "The Electronic Structure of the Uranyl Ion Ⅳ. Nitrogen-15 Isotope Shifts in the Electronic Spectrum of $CsUO_2(NO_3)_3$", *Mol. Phys.*, **1980**, *39*, 1281–1285.

[101] Denning, R. G.; Norris, J. O. W.; Brown, D., "The Electronic Structure of Actinyl Ions V. *f–f* Transitions in $[NpO_2Cl_4]^-$ and $[NpO_2(NO_3)_2]^-$", *Mol. Phys.*, **1982**, *46*, 287–323.

[102] Denning, R. G.; Norris, J. O. W.; Brown, D., "The Electronic Structure of Actinyl Ions Ⅵ. Charge Transfer Transitions in $Cs_2NpO_2Cl_4$ and $CsNpO_2(NO_3)_3$", *Mol. Phys.*, **1982**, *46*, 325–364.

[103] Denning, R. G.; Morrison, I. D., "The Electronic Structure of Actinyl Ions: the Excited-State Absorption Spectrum of $Cs_2UO_2Cl_4$", *Chem. Phys. Lett.*, **1991**, *180*, 101–104.

[104] Hirata, M.; Monjyushiro, H.; Sekine, R.; Onoe, J.; Nkamatsu, H.; Mukoyama, T.; Adachi, H.; Tkeuchi, K., "Valence Electronic Structure of Uranyl Nitrate $UO_2(NO_3)_2{\cdot}2H_2O$", *J. Electr. Spectrosc. Relat.Phenom.*, **1997**, *83*, 59–64.

[105] De Jong, W. A.; Visscher, L.; Nieuwpoort, W. C., "On the Bonding and the Electric Field Gradient of the Uranyl Ion", *J. Mol. Struct. (Theochem)*, **1999**, *458*, 41–52.

[106] Zhang, Z.; Pitzer, R. M., "Application of Relativistic Quantum Chemistry to the Electronic Energy Levels of the Uranyl Ion", *J. Phys. Chem. A*, **1999**, *103*, 6880–6886.

[107] Matsika, S.; Pitzer, R. M., "Electronic Spectrum of the NpO_2^{2+} and NpO_2^+ Ions", *J. Phys. chem. A*, **2000**, *104*, 4064–4068.

[108] Hay, P. J.; Martin, R. L.; Schreckenbach, G., "Theoretical Studies of the Properties and Solution Chemistry of AnO_2^{2+} and AnO_2^+ Aquo Complexes for An = U, Np, and Pu", *J. Phys. Chem. A*, **2000**, *104*, 6259–6270.

[109] Matsika, S.; Pitzer, R. M.; Reed, D. T., "Intensities in the Spectra of Actinyl Ions", *J. Phys. Chem. A*, **2000**, *104*, 11983–11992.

[110] Gagliardi, L.; Grenthe, I.; Roos, B. O., "A Theoretical Study of the Structure of Tricarbonatodioxouranate", *Inorg. Chem.*, **2001**, *40*, 2976–2978.

[111] Matsika, S.; Pitzer, R. M., "Actinyl Ions in $Cs_2UO_2Cl_4$", *J. Phys. Chem. A*, **2001**, *105*, 637–645.

[112] Gagliardi, L.; Roos, B. O.; Malmqvist, P.-Å.; Dyke, J. M., "On the Electronic Structure of the UO_2 Molecule", *J. Phys. Chem. A*, **2001**, *105*, 10602–10606.

[113] Gagliardi, L.; Roos, B. O., "Coordination of the Neptunyl Ion with Carbonate Ions and Water: A Theoretical Study", *Inorg. Chem.*, **2002**, *41*, 1315–1319.

[114] Vázquez, J.; Bo, C.; Poblet, J. M.; De Pablo, J.; Bruno, J., "DFT Studies of Urany Acetate, Carbonate, and Malonate, Complexes in Solution", *Inorg. Chem.*, **2003**, *42*, 6136–6141.

[115] Majumdar, D.; Roszak, S.; Balasubramanian, K.; Nitsche, H., "Theoretical Study of Aqueous Uranyl Carbonate (UO_2CO_3) and Its Hydrated Complexes: $UO_2CO_3 \cdot nH_2O$ ($n = 1 - 3$)", *Chem. Phys. Lett.*, **2003**, *372*, 232–241.

[116] Bühl, M.; Diss, R.; Wipff, G., "Coordination Environment of Aqueous Uranyl(VI) Ion", *J. Am. Chem. Soc.*, **2005**, *127*, 13506–13507.

[117] Mizuoka, K.; Ikeda, Y., "Structural Study on Uranyl Ion in 1-Butyl-3-methylimidazolium Nonafluorobutanesulfonate Ionic Liquid", *Prog. Nucl. Ener.*, **2005**, *47*, 426–433.

[118] Kraus, K. A.; Nelson, F.; Johnson, G. L., "Chemistry of Aqueous Uranium(V) Solutions. I. Preparation and Properties. Analogy between Uranium(V), Neptunium(V) and Plutonium(V)", *J. Am. Chem. Soc.*, **1949**, *71*, 2510–2517.

[119] Kraus, K. A.; Nelson, F., "Chemistry of Aqueous Uranium(V) Solutions. II. Reaction of Uranium Pentachloride with Water. Thermodynamic Stability of UO_2^+. Potential of U(IV)/(V), U(IV)/(VI) and U(V)/(VI) Couples", *J. Am. Chem. Soc.*, **1949**, *71*, 2517–2522.

[120] Heal, H. G., "Some Observations on the Electrochemistry of Uranium", *Trans. Faraday Soc.*, **1949**, *45*, 1–11.

[121] Heal, H. G.; Thomas, J. G. N., "Unstable Ions of Quiquavalent Uranium", *Trans. Faraday Soc.*, **1949**, *45*, 11–20.

[122] Newton, T. W.; Baker, F. B., "A Uranium(V)-Uranium(VI) Complex and Its Effect on the Uranium(V) Disproportionation Rate", *Inorg. Chem.*, **1965**, *4*, 1166–1170.

[123] Ekstrom, A., "Kinetics and Mechanism of the Disproportionation of Uranium(V)", *Inorg. Chem.*, **1974**, *13*, 2237–2241.

[124] McDuffie, B.; Reilley, C. N., "Twin-Electrode Thin-Layer Electrochemistry. Kinetics of Second-Order Disproportionation of Uranium(V) by Decay of Steady-State Current", *Anal. Chem.*, **1966**, *38*, 1881–1887.

[125] Selbin, J.; Ortego, J. D., "The Chemistry of Uranium(V)", *Chem. Rev.*, **1969**, *69*, 657–671.

[126] Sipos, L.; Jeftić, L.; Branica, M.; Galus, Z., "Electrochemical Redox Mechanism of Uranium in Acidic Perchlorate Solutions", *J. Electroanal. Chem.*, **1971**, *32*, 35–47.

[127] Bell, J. T.; Fredman, H. A.; Billings, M. R., "Spectrophotometric Studies of Dioxouranium(V) in Aqueous Media–I", *J. Inorg. Nucl. Chem.*, **1974**, *36*, 2561–2567.

[128] Howes, K. R.; Bakac, A.; Espenson, J. H., "Electoron-Transfer Reactions of Uranium(V): Kinetics of the Uranium(V)-Uranium(VI) Self-Exchange Reaction", *Inorg. Chem.*, **1988**, *27*, 791–794.

[129] Gritzner, G.; Selbin, J., "Studies of Dioxouranium(V) in Dimethylsulphoxide", *J. Inorg. Nucl. Chem.*, **1968**, *30*, 1799–1804.

[130] Folcher, G.; Lambard, J.; De Villardi, G. C., "Photoreduction of UO_2(18-Crown-6)$(ClO_4)_2$. Synthesis of a U^V Crown-ether Complex", *Inorg. Chim. Acta*, **1980**, *45*, L59–L61.

[131] Miyake, C.; Yamana, Y.; Imoto, S., "Direct Evidence of Uranium(V) Intermediates by Electron Spin Resonance in Photo- and Electrolytic Reduction Processes of Uranyl Complexes in Organic Solutions", *Inorg. Chim. Acta*, **1984**, *95*, 17–21.

[132] Miyake, C.; Kondo, T.; Imoto, S., "Direct Evidence of Uranium(V) Intermediates by Electron Spin Resonance in Photo- and Electrolytic Reduction Processes of Uranyl Complexes in Organic Solutions", *J. Less-Common Met.*, **1986**, *122*, 313–317.

[133] Fukutomi, H.; Harazono, T., "Photolytic Formation of a Uranium(V)-DMSO Complex and the Paramagnetic Shift of DMSO by Uranium(V)", *Bull. Chem. Soc.Jpn.*, **1986**, *59*, 3678–3680.

[134] Monjushiro, H.; Hara, H.; Yokoyama, Y., "Identification of Uranium(V) in Photoreduced Uranyl Compounds by Photoacoustic Spectroscopy", *Polyhedron*, **1992**, *11*, 845–846.

[135] Anderson, C. J.; Choppin, G. R.; Pruett, D. J.; Costa, D.; Smith, W., "Electrochemistry and Spectroscopy of UO_2^{2+} in Acidic $AlCl_3$-EMIC", *Radiochim. Acta*, **1999**, *84*, 31–36.

[136] Kaneki, H.; Fukutomi, H., "Spectrophotometric Studies of Uranium(V) in Acidic Perchlorate Solutions", *Bull. Res. Lab. Nucl. React. (Tokyo Institute of Technology)*, **1980**, *5*, 27–39.

[137] Zanello, P.; Cinquantini, A.; Mazzocchin, G. A., "Electrochemical Behaviour of Uranyl(VI) Ion in Different Non-Aqueous Solvents", *J. Electroanal. Chem.*, **1982**, *131*, 215–227.

[138] Harazono, T.; Fukutomi, H., "Paramagnetic Shifts of DMF and DMA by Uranium(V)", *Bull. Chem. Soc. Jpn.*, **1986**, *59*, 2129–2133.

[139] Sandhu, S. S.; Singh, R. J.; Chawla, S. K., "Uranium(V) as an Intermediate in the Photochemical Reduction of the Uranyl Ion with Dicyclohexylsulphide", *J. Photochem. Photobio. A*, **1990**, *52*, 65–68.

[140] Lee, S.-H.; Mizuguchi, K.; Tomiyasu, H.; Ikeda, Y., "Electrochemical and Spectroelectrochemical Studies on Bis(acetylacetonato)(dimethyl sulfoxide)dioxouranium(VI) in Dimethyl Sulfoxide", *J. Nucl. Sci. Technol.*, **1996**, *33*, 190–192.

[141] Mizuguchi, K.; Lee, S.-H.; Ikeda, Y.; Tomiyasu, H., "Electrochemical Studies on Bis(β-diketonato)-(dimethyl sulfoxide)dioxouranium(VI) in Dimethyl Sulfoxide", *J. Alloys Compd.*, **1998**, *271-273*, 163–167.

[142] Kim, S.-Y.; Tomiyasu, H.; Ikeda, Y., "Electrochemical Studies on $[UO_2(DMF)_5](ClO_4)_2$, $UO_2(acac)_2DMF$, and UO_2(salen)DMF (DMF = *N,N*-Dimethylformaminde, acac = Acetylacetonate, salen = *N,N'*-Disalicylideneethylenediaminate) Complexes in DMF", *J. Nucl. Sci. Technol.*, **2002**, *39*, 160–165.

[143] Kim, S.-Y.; Asakura, T.; Morita, Y.; Ikeda, Y., "Electrochemical Properties of Uranium(VI) Complexes with Multidentate Ligands in *N,N*-Dimethylformamide", *J. Alloy. Compd.*, **2005**, in press.

[144] Adams, M. D.; Wenz, D. A.; Steunenberg, R. K., "Observation of a Uranium(V) Species in Molten Chloride Salt Solutions", *J. Phys. Chem.*, **1963**, *67*, 1939–1941.

[145] Khokhryakov, A. A., "Electronic Absorption Spectra of Uranyl-containing Molten Halides", *Radiochemistry*, **1998**, *40*, 413–415.

[146] Yamamura, T.; Shiokawa, Y.; Ikeda, Y.; Tomiyasu, H., "Electrochemical Investigation of Tetravalent Uranium β-Diketones for Active Materials of All-Uranium Redox Flow Battery", *J. Nucl. Sci. Technol.*, **2002**, *Supplement 3*, 445–448.

[147] Cohen, D. D., "The Preparation and Spectrum of Uranium(V) Ions in Aqueous Solutions", *J. Inorg. Nucl. Chem.*, **1970**, *32*, 3525–3530.

[148] Wester, D. W.; Sullivan, J. C., "Electrochemical and Spectroscopic Studies of Uranium(IV), -(V), and -(VI) in Carbonate-Bicarbonate Buffers", *Inorg. Chem.*, **1980**, *19*, 2838–2840.

[149] Ferri, D.; Grenthe, I.; Salvatore, F., "Studies on Metal Carbonate Equilibria. 7. Reduction of the Tris(carbonato)dioxouranate(VI) Ion, $UO_2(CO_3)_3^{4-}$, in Carbonate Solutions", *Inorg. Chem.*, **1983**, *22*, 3162–3165.

[150] Morris, D. E., "Redox Energetics and Kinetics of Uranyl Coordination Complexes in Aqueous Solution", *Inorg. Chem.*, **2002**, *41*, 3542–3547.

[151] Madic, C.; Hobart, D. E.; Begun, G. M., "Raman Spectrometric Studies of Actinide(V) and -(VI) Complexes in Aqueous Sodium Carbonate Solution and of Solid Sodium Actinide(V) Carbonate Compounds", *Inorg. Chem.*, **1983**, *22*, 1494–1503.

[152] Mizuguchi, K.; Park, Y.-Y.; Tomiyasu, H.; Ikeda, Y., "Electrochemical and Spectroelectrochemical Studies on Uranyl Carbonato and Aqua Complexes", *J. Nucl. Sci. Technol.*, **1993**, *30*, 542–548.

[153] Docrat, T. I.; Mosselmans, J. F. W.; Charnock, J. M.; Whiteley, M. W.; Collison, D.; Livens, F. R.; Jones, C.; Edmiston, M. J., "X-ray Absorption Spectroscopy of Tricarbonatodioxouranate(V), $[UO_2(CO_3)_3]^{5-}$, in Aqueous Solution", *Inorg. Chem.*, **1999**, *38*, 1879–1882.

[154] Nelson, F.; Kraus, K. A., "Chemistry of Aqueous Uranium(V) Solutions. III. The Uranium(IV)–(V)–(VI) Equilibrium in Perchlorate and Chloride Solutions", *J. Am. Chem. Soc.*, **1951**, *73*, 2157–2161.

[155] Jones, L. H.; Penneman, R. A., "Infrared Spectra and Structure of Uranyl and Transuranium (V) and (VI) Ions in Aqueous Perchloric Acid Solution", *J. Chem. Phys.*, **1953**, *21*, 542–544.

[156] Sjoblom, R.; Hindman, J. C., "Spectrophotometry of Neptunium in Perchloric Acid Solutions", *J. Am. Chem. Soc.*, **1951**, *73*, 1744–1751.

[157] Waggener, W. C., "Measurement of the Absorption Spectra of Neptunium Ions in Heavy Water Solution from 0.35 to1.85 μ", *J. Phys. Chem.*, **1958**, *62*, 382–383.

[158] Hagan, P. G.; Cleveland, J. M., "The Absorption Spectra of Neptunium Ions in Perchloric Acid Solution", *J. Inorg. Nucl. Chem.*, **1966**, *28*, 2905–2909.

[159] Friedman, H. A.; Toth, L. M., "Absorption spectra of Np(Ⅲ), (Ⅳ), (Ⅴ), (Ⅵ) in Nitric Acid Solution", *J. Inorg. Nucl. Chem.*, **1980**, *42*, 1347–1349.

[160] Nakamoto, K., *Infrared Spectra of Inorganic and Coordination Compounds*, John Wiley & Sons, Inc., New York, London, **1963**.

[161] Allen, P. G.; Bucher, J. J.; Clark, D. L.; Edelstein, N. M.; Ekberg, S. A.; Gohdes, J. W.; Hudson, E. A.; Kaltsoyannis, N.; Lukens, W. W.; Neu, M. P.; Palmer, P. D.; Reich, T.; Shuh, D. K.; Tait, C. D.; Zwick, B. D., "Multinulcear NMR, Raman, EXAFS, and X-ray Diffraction Studies of Uranyl Carbonate Complexes in Near-Neutral Aqueous Solution. X-ray Structure of $[C(NH_2)_3]_6[(UO_2)_3(CO_3)_6]\cdot 6.5H_2O$", *Inorg. Chem.*, **1995**, *34*, 4797–4807.

[162] Strom, E. T.; Woessner, D. E., "^{13}C NMR Spectra of the Uranyl Tricarbonate–bicarbonate System", *J. Am. Chem. Soc.*, **1981**, *103*, 1255–1256.

[163] Altomare, A.; Cascarano, G.; Giacovazzo, C.; Guagliardi, A., "Completion and Refinement of Crystal Structures with *SIR 92*", *J. Appl. Cryst.*, **1993**, *26*, 343–350.

[164] Beurskens, P. T.; Admiraal, G.; Beurskens, G.; Bosman, W. P.; Garcia-Granda, S.; Gould, R. O.; Smits, J. M. M.; Smykalla, C., PATTY, (1992). The DIRDIF program system, Technical Report of the Crystallography Laboratory, University of Nijmegen, The Netherlands.

[165] Beurskens, P. T.; Admiraal, G.; Beurskens, G.; Bosman, W. P.; Gelder, de R.; Israel, R.; Smits, J. M. M., DIRDIF99, (1999). the DIRDIF-99 program system, Tehcnical Report of the Crystallography Laboratory, University of Nijmegen, The Netherlands.

[166] Sheldrick, G. M., SHELXL-97, (1997). Program for Crystal Structure Refinement; University of Göttingen, Germany.

[167] Cromer, D. T.; Waber, J. T., *International Tables for X-ray Crystallography*, Vol. IV, The Kynoch Press, Birmingham, England, **1974**, Table 2.2 A.

[168] Ibers, J. A.; Hamilton, J. T., *Acta Crystallogr.*, **1964**, *17*, 781.

[169] Creagh, D. C.; McAuley, W. J., *International Tables for Crystallogryphy*, Vol. C, (A. J. C. Wilson, ed), Kluwer Academic Publishers, Boston, **1992**, pp.219-222, Table 4.2.6.8.

[170] Creagh, D. C.; Hubbell, J. H., *International Tables for Crystallogryphy*, Vol. C, (A. J. C. Wilson, ed), Kluwer Academic Publishers, Boston, **1992**, pp.200-206, Table 4.2.4.3.

[171] CrystalStructure 3.10, Crystal Structure Analysis Package, Rigaku and Rigaku/MSC (2000-2002).

[172] Thornback, J. R.; Wilkinson, G., "Schiff-Base Complexes of Ruthenium(Ⅱ)", *J. Chem. Soc., Dalton*, **1978** 110–115.

[173] Suresh, E.; Bhadbhade, M. M.; Srinivas, D., "Molecular Association, Chelate Conformation and Reactivity Correlations in Substituted *o*-Phenylenebis(salicylidenaminato)copper(Ⅱ) Complexes: UV-visible, EPR and X-ray Structural Investigations", *Polyhedron*, **1996**, *15*, 4133–4144.

[174] Zhang, K.-L.; Xu, Y.; Zheng, C.-G.; Zhang, Y.; Wang, Z.; You, X.-Z., "A Linear Polymer Manganese(Ⅲ) Complex; Syntesis, Crystal and Molecular Structure and Magnetic Properties of Catena-μ-acetato[*N,N'*-*O*-phenylenebis(salicylidenaminato)]manganese(Ⅲ)", *Inorg. Chim. Acta*, **2001**, *318*, 61–66.

[175] Cort, A. D.; Mandolini, L.; Palmieri, G.; Pasquini, C.; Schiaffino, L., "Unprecedented Detection of Inherent Chirality in Uranyl–salophen Complexes", *Chem. Commun.*, **2003** 2178–2179.

[176] *gNMR* Ver. 5.0.4.0, Adept Scientific Inc. USA.

[177] Binsch, G., "A Unified Theory of Exchange Effects on Nuclear Magnetic Resonance Line Shapes", *J. Am. Chem. Soc.*, **1969**, *91*, 1304–1309.

[178] DeAngelis, T. P.; Heineman, W. R., "An Electrochemical Experiment Using an Optically Transparent Thin Layer Electrode", *J. Chem. Edu.*, **1976**, *53*, 594–597.

[179] Heineman, W. R., "Spectroelectrochemistry The Combination of Optical and Electrochemical Techniques", *J. Chem. Edu.*, **1983**, *60*, 305–308.

[180] Lin, X. Q.; Kadish, K. M., "Vacuum-Tight Thin-Layer Spectroelectrochemical Cell with a Doublet Platinum Gauze Working Electrode", *Anal. Chem.*, **1985**, *57*, 1498–1501.

[181] Endo, A.; Mochida, I.; Shimizu, K.; Satô, G. P., "A Simple Thin-Layer Spectroelectrochemical Cell for Nonaqueous Solution Systems", *Anal. Sci.*, **1995**, *11*, 457–459.

[182] Swift, T. J.; Connick, R. E., "NMR-Relaxation Mechanisms of O^{17} in Aqueous Solutions of Paramagnetic Cations and the Lifetime of Water Molecules in the First Coordination Sphere", *J. Chem. Phys.*, **1962**, *37*, 307–320.

[183] Stengle, T. R.; Langford, C. H., "The Uses of Nuclear Magnetic Resonance in the Study of Ligand Substitution Processes", *Cood. Chem. Rev.*, **1967**, *2*, 349–370.

[184] J. E. Letter, J.; Jordan, R. B., "Nuclear Magnetic Resonance Line Broadening by a Tridendate Schiff-Base Complex of Nickel(Ⅱ), Triaquotribenzo[*b,f,j*][1,5,9]triazacylododecinenickel(Ⅱ)", *J. Am. Chem. Soc.*, **1971**, *93*, 864–867.

[185] Rusnak, L.; Jordan, R. B., "Solvent-Exchange Rates from Manganese(Ⅲ) Protoporphyrin IX Dimethyl Ester Studied by Nuclear Magnetic Resonance Line Broadening", *Inorg. Chem.*, **1972**, *11*, 196–199.

[186] Clark, D. L.; Hobart, D. E.; Neu, M. P., "Actinide Carbonate Complexes and Their Importance in Actinide Environmental Chemistry", *Chem. Rev.*, **1995**, *95*, 25–48.

[187] Vallet, V.; Wahlgren, U.; Schimmelpfennig, B.; Szabó, Z.; Grenthe, I., "The Mechanism for Water Exchange in $[UO_2(H_2O)_5]^{2+}$ and $[UO_2(oxalate)_2(H_2O)]^{2-}$, as Studied by Quantum Chemical Methods", *J. Am. Chem. Soc.*, **2001**, *123*, 11999–12008.

[188] Gritzner, G.; Kůta, J., "Recommendations on Reporting Electrode Potentials in Nonaqueous Solvents", *Pure Appl. Chem.*, **1984**, *56*, 461–466.

[189] Nicholson, R. S., "Semiempirical Procedure for Measuring with Stationary Electrode Polarography Rates of Chemical Reactions Involving the Product of Electron Transfer", *Anal. Chem.*, **1966**, *38*, 1406.

[190] Nicholson, R. S., "Theory and Application of Cyclic Voltammetry for Measurement of Electrode Reaction Kinetics", *Anal. Chem.*, **1965**, *37*, 1351–1355.

[191] Heinze, J., "Cyclic Voltammetry–Electrochemical Spectroscopy", *Angew. Chem. Int. Ed.*, **1984**, *23*, 931–947.

[192] Bard, A. J.; Faulkner, L. R., *Electrochemical Methods. Fundamentals and Applications Second Edition*, John Wiley & Sons, Inc., **2001**.

[193] Nicholson, R. S.; Shain, I., "Theory of Stationary Electrode Polarography. Single Scan and Cyclic Methods Applied to Reversible, Irreversible, and Kinetic Systems", *Anal. Chem.*, **1964**, *36*, 706–723.

[194] Berthet, J.-C.; Nierlich, M.; Ephritikhine, M., "Isolation of a Uranyl $[UO_2]^+$ Species: Crystallographic Comparison of the Dioxouranium(V) and (VI) Compounds $[UO_2(OPPh_3)_4](TfO)_n$", *Angew. Chem. Int. Ed.*, **2003**, *42*, 1952–1954.

[195] Figgis, B. N.; Hitchman, M. A., *Ligand Field Theory and Its Applications*, Wiley-VCH, New York, **2000**.

[196] Cotton, F. A., *Chemical Applications of Group Theory 2nd Edition*, John Wiley & Sons, Inc., **1971**, Japanese-translated version by Nakahara, K.

[197] Griffith, J. S., *The Theory of Transition-Metal Ions*, Cambridge University Press, **1971**.

Appendix A

Crystallographic Information of $U^{VI}O_2$(saloph)DMF·CH_2Cl_2

```
data_phdf

_audit_creation_method            SHELXL-97
_chemical_name_systematic
;
 ?
;
_chemical_name_common             ?
_chemical_melting_point           ?
_chemical_formula_moiety          'C23 H21 N3 O5 U, C H2 Cl2'
_chemical_formula_sum
 'C24 H23 Cl2 N3 O5 U'
_chemical_formula_weight          742.38

loop_
 _atom_type_symbol
 _atom_type_description
 _atom_type_scat_dispersion_real
 _atom_type_scat_dispersion_imag
 _atom_type_scat_source
 'C'  'C'   0.0033   0.0016
 'International Tables Vol C Tables 4.2.6.8 and 6.1.1.4'
 'Cl'  'Cl'   0.1484   0.1585
 'International Tables Vol C Tables 4.2.6.8 and 6.1.1.4'
 'H'  'H'   0.0000   0.0000
 'International Tables Vol C Tables 4.2.6.8 and 6.1.1.4'
 'N'  'N'   0.0061   0.0033
 'International Tables Vol C Tables 4.2.6.8 and 6.1.1.4'
 'O'  'O'   0.0106   0.0060
 'International Tables Vol C Tables 4.2.6.8 and 6.1.1.4'
 'U'  'U'  -9.6767   9.6646
 'International Tables Vol C Tables 4.2.6.8 and 6.1.1.4'

_symmetry_cell_setting            monoclinic
_symmetry_space_group_name_H-M   'P 21/n'
_symmetry_Int_Tables_number       14

loop_
 _symmetry_equiv_pos_as_xyz
 'x, y, z'
```

```
 '-x+1/2, y+1/2, -z+1/2'
 '-x, -y, -z'
 'x-1/2, -y-1/2, z-1/2'

_cell_length_a                    10.667(4)
_cell_length_b                    9.608(3)
_cell_length_c                    24.859(10)
_cell_angle_alpha                 90.00
_cell_angle_beta                  100.65(3)
_cell_angle_gamma                 90.00
_cell_volume                      2503.9(16)
_cell_formula_units_Z             4
_cell_measurement_temperature     123(2)
_cell_measurement_reflns_used     26142
_cell_measurement_theta_max       27.5

_exptl_crystal_description       'block'
_exptl_crystal_colour            'orange'
_exptl_crystal_size_max           0.30
_exptl_crystal_size_mid           0.30
_exptl_crystal_size_min           0.30
_exptl_crystal_density_meas       ?
_exptl_crystal_density_diffrn     1.969
_exptl_crystal_density_method     'not measured'
_exptl_crystal_F_000              1416
_exptl_absorpt_coefficient_mu     6.736
_exptl_absorpt_correction_type    numerical
_exptl_absorpt_correction_T_min   0.2371
_exptl_absorpt_correction_T_max   0.2371
_exptl_absorpt_process_details
;
    Higashi, T. (1999). Program for Absorption Correction.
    Rigaku Corporation, Tokyo, Japan.
;
_exptl_special_details
;
 ?
;

_diffrn_ambient_temperature       123(2)
_diffrn_radiation_wavelength      0.71075
_diffrn_radiation_type            MoK¥a
_diffrn_radiation_source          'fine-focus sealed tube'
_diffrn_radiation_monochromator   graphite
_diffrn_measurement_device_type       'Rigaku RAXIS-RAPID'
_diffrn_measurement_method            ¥w
_diffrn_detector_area_resol_mean  10.00
_diffrn_reflns_number             23518
_diffrn_reflns_av_R_equivalents   0.0402
_diffrn_reflns_av_sigmaI/netI     0.0245
_diffrn_reflns_limit_h_min        -13
_diffrn_reflns_limit_h_max        13
_diffrn_reflns_limit_k_min        -12
_diffrn_reflns_limit_k_max        12
_diffrn_reflns_limit_l_min        -27
_diffrn_reflns_limit_l_max        32
_diffrn_reflns_theta_min          3.09
_diffrn_reflns_theta_max          27.48
_reflns_number_total              5734
_reflns_number_gt                 5274
_reflns_threshold_expression      >2sigma(I)
```

```
_computing_data_collection          'PROCESS-AUTO'
_computing_cell_refinement          'PROCESS-AUTO'
_computing_data_reduction           'CrystalStructure'
_computing_structure_solution       'SIR92'
_computing_structure_refinement     'SHELXL-97 (Sheldrick, 1997)'

_refine_special_details
;
 Refinement of F^2^ against ALL reflections.  The weighted R-factor wR and
 goodness of fit S are based on F^2^, conventional R-factors R are based
 on F, with F set to zero for negative F^2^. The threshold expression of
 F^2^ > 2sigma(F^2^) is used only for calculating R-factors(gt) etc. and is
 not relevant to the choice of reflections for refinement.  R-factors based
 on F^2^ are statistically about twice as large as those based on F, and R-
 factors based on ALL data will be even larger.
;

_refine_ls_structure_factor_coef  Fsqd
_refine_ls_matrix_type            full
_refine_ls_weighting_scheme       calc
_refine_ls_weighting_details
 'calc w=1/[¥s^2^(Fo^2^)+(0.0262P)^2^+5.3741P] where P=(Fo^2^+2Fc^2^)/3'
_atom_sites_solution_primary      direct
_atom_sites_solution_secondary    difmap
_atom_sites_solution_hydrogens    geom
_refine_ls_hydrogen_treatment     mixed
_refine_ls_extinction_method      SHELXL
_refine_ls_extinction_coef        0.00272(11)
_refine_ls_extinction_expression
 'Fc^*^=kFc[1+0.001xFc^2^¥l^3^/sin(2¥q)]^-1/4^'
_refine_ls_number_reflns          5734
_refine_ls_number_parameters      317
_refine_ls_number_restraints      0
_refine_ls_R_factor_all           0.0291
_refine_ls_R_factor_gt            0.0258
_refine_ls_wR_factor_ref          0.0650
_refine_ls_wR_factor_gt           0.0633
_refine_ls_goodness_of_fit_ref    1.119
_refine_ls_restrained_S_all       1.119
_refine_ls_shift/su_max           0.002
_refine_ls_shift/su_mean          0.000

loop_
 _atom_site_label
 _atom_site_type_symbol
 _atom_site_fract_x
 _atom_site_fract_y
 _atom_site_fract_z
 _atom_site_U_iso_or_equiv
 _atom_site_adp_type
 _atom_site_occupancy
 _atom_site_symmetry_multiplicity
 _atom_site_calc_flag
 _atom_site_refinement_flags
 _atom_site_disorder_assembly
 _atom_site_disorder_group
U1 U 0.042272(11) -0.240763(11) 0.640916(5) 0.02047(6) Uani 1 1 d . . .
Cl2 Cl 0.32100(14) -0.03499(11) 0.51214(5) 0.0549(3) Uani 1 1 d . . .
Cl3 Cl 0.37658(15) 0.25791(11) 0.52559(6) 0.0528(3) Uani 1 1 d . . .
O1 O 0.1377(2) -0.3464(2) 0.69108(10) 0.0254(5) Uani 1 1 d . . .
```

```
O2 O -0.0507(2) -0.1264(3) 0.59254(10) 0.0278(5) Uani 1 1 d . . .
O3 O -0.0465(3) -0.4419(3) 0.58972(12) 0.0361(6) Uani 1 1 d . . .
O4 O -0.1270(2) -0.2799(3) 0.68169(11) 0.0284(5) Uani 1 1 d . . .
O5 O 0.1820(2) -0.2830(3) 0.58392(11) 0.0261(5) Uani 1 1 d . . .
N1 N -0.0442(3) -0.6658(3) 0.56165(13) 0.0299(7) Uani 1 1 d . . .
N2 N 0.0350(3) -0.0607(3) 0.71557(12) 0.0209(5) Uani 1 1 d . . .
N3 N 0.2223(3) -0.0641(3) 0.65781(11) 0.0210(5) Uani 1 1 d . . .
C1 C -0.1291(3) -0.2993(4) 0.73409(15) 0.0240(7) Uani 1 1 d . . .
C2 C -0.1971(3) -0.4124(4) 0.75067(17) 0.0293(8) Uani 1 1 d . . .
H2 H -0.2397 -0.4735 0.7245 0.035 Uiso 1 1 calc R . .
C3 C -0.2011(3) -0.4336(4) 0.80518(17) 0.0308(8) Uani 1 1 d . . .
H3 H -0.2470 -0.5085 0.8152 0.037 Uiso 1 1 calc R . .
C4 C -0.1376(4) -0.3445(4) 0.84558(17) 0.0316(8) Uani 1 1 d . . .
H4 H -0.1383 -0.3613 0.8824 0.038 Uiso 1 1 calc R . .
C5 C -0.0737(4) -0.2307(4) 0.82984(17) 0.0271(7) Uani 1 1 d . . .
H5 H -0.0339 -0.1689 0.8564 0.032 Uiso 1 1 calc R . .
C6 C -0.0675(3) -0.2061(3) 0.77472(15) 0.0235(7) Uani 1 1 d . . .
C7 C -0.0015(3) -0.0824(3) 0.76152(14) 0.0227(7) Uani 1 1 d . . .
H7 H 0.0157 -0.0136 0.7882 0.027 Uiso 1 1 calc R . .
C8 C 0.0893(3) 0.0703(3) 0.70618(14) 0.0217(6) Uani 1 1 d . . .
C9 C 0.0432(3) 0.1962(4) 0.72217(15) 0.0259(7) Uani 1 1 d . . .
H9 H -0.0239 0.1978 0.7414 0.031 Uiso 1 1 calc R . .
C10 C 0.0990(4) 0.3207(4) 0.70899(15) 0.0284(7) Uani 1 1 d . . .
H10 H 0.0694 0.4054 0.7198 0.034 Uiso 1 1 calc R . .
C11 C 0.1974(3) 0.3186(4) 0.68010(15) 0.0280(7) Uani 1 1 d . . .
H11 H 0.2342 0.4019 0.6719 0.034 Uiso 1 1 calc R . .
C12 C 0.2424(3) 0.1933(4) 0.66309(14) 0.0258(7) Uani 1 1 d . . .
H12 H 0.3083 0.1926 0.6432 0.031 Uiso 1 1 calc R . .
C13 C 0.1878(3) 0.0686(3) 0.67612(13) 0.0212(6) Uani 1 1 d . . .
C14 C 0.3402(3) -0.0895(3) 0.65632(13) 0.0229(7) Uani 1 1 d . . .
H14 H 0.4000 -0.0235 0.6718 0.027 Uiso 1 1 calc R . .
C15 C 0.3877(3) -0.2120(4) 0.63262(14) 0.0228(6) Uani 1 1 d . . .
C16 C 0.5202(4) -0.2355(3) 0.64224(15) 0.0251(7) Uani 1 1 d . . .
H16 H 0.5729 -0.1776 0.6666 0.030 Uiso 1 1 calc R . .
C17 C 0.5748(3) -0.3409(4) 0.61693(15) 0.0279(7) Uani 1 1 d . . .
H17 H 0.6623 -0.3566 0.6250 0.034 Uiso 1 1 calc R . .
C18 C 0.4951(4) -0.4235(4) 0.57881(16) 0.0287(7) Uani 1 1 d . . .
H18 H 0.5306 -0.4932 0.5604 0.034 Uiso 1 1 calc R . .
C19 C 0.3647(3) -0.4037(3) 0.56800(15) 0.0272(7) Uani 1 1 d . . .
H19 H 0.3141 -0.4596 0.5422 0.033 Uiso 1 1 calc R . .
C20 C 0.3067(3) -0.3000(3) 0.59539(14) 0.0230(6) Uani 1 1 d . . .
C21 C 0.0033(4) -0.5403(4) 0.56839(15) 0.0296(8) Uani 1 1 d . . .
H21 H 0.0795 -0.5229 0.5565 0.035 Uiso 1 1 calc R . .
C22 C -0.1575(5) -0.7033(5) 0.5828(2) 0.0484(12) Uani 1 1 d . . .
H22A H -0.1788 -0.7988 0.5741 0.073 Uiso 1 1 calc R . .
H22B H -0.2272 -0.6447 0.5665 0.073 Uiso 1 1 calc R . .
H22C H -0.1417 -0.6912 0.6218 0.073 Uiso 1 1 calc R . .
C23 C 0.0173(5) -0.7762(4) 0.53552(18) 0.0385(9) Uani 1 1 d . . .
H23A H -0.0321 -0.8601 0.5344 0.058 Uiso 1 1 calc R . .
H23B H 0.1014 -0.7925 0.5561 0.058 Uiso 1 1 calc R . .
H23C H 0.0229 -0.7487 0.4989 0.058 Uiso 1 1 calc R . .
C24 C 0.3392(4) 0.1214(4) 0.47818(16) 0.0327(8) Uani 1 1 d . . .
H24A H 0.2608 0.1429 0.4530 0.039 Uiso 1 1 calc R . .
H24B H 0.4068 0.1115 0.4572 0.039 Uiso 1 1 calc R . .

loop_
 _atom_site_aniso_label
 _atom_site_aniso_U_11
 _atom_site_aniso_U_22
 _atom_site_aniso_U_33
 _atom_site_aniso_U_23
```

```
 _atom_site_aniso_U_13
 _atom_site_aniso_U_12
U1 0.01927(8) 0.01873(8) 0.02214(8) -0.00071(4) 0.00046(5) -0.00324(4)
Cl2 0.0788(9) 0.0335(5) 0.0501(7) 0.0101(5) 0.0062(6) -0.0160(5)
Cl3 0.0763(9) 0.0390(6) 0.0486(7) -0.0146(5) 0.0257(6) -0.0214(5)
O1 0.0270(12) 0.0193(11) 0.0298(13) 0.0019(9) 0.0053(10) -0.0037(9)
O2 0.0264(13) 0.0318(13) 0.0249(13) 0.0038(10) 0.0039(10) 0.0021(10)
O3 0.0314(14) 0.0351(14) 0.0408(16) -0.0130(12) 0.0041(12) -0.0113(11)
O4 0.0244(13) 0.0309(12) 0.0298(14) -0.0026(11) 0.0052(10) -0.0078(10)
O5 0.0238(12) 0.0269(11) 0.0271(13) -0.0038(10) 0.0031(10) -0.0018(10)
N1 0.0346(17) 0.0294(15) 0.0263(16) -0.0075(12) 0.0077(13) -0.0124(13)
N2 0.0187(13) 0.0191(12) 0.0242(14) 0.0001(10) 0.0018(11) -0.0016(10)
N3 0.0244(14) 0.0196(12) 0.0189(13) 0.0009(10) 0.0040(11) -0.0029(10)
C1 0.0183(15) 0.0236(15) 0.0307(18) 0.0020(14) 0.0064(13) 0.0026(13)
C2 0.0226(17) 0.0223(16) 0.043(2) 0.0010(15) 0.0057(15) -0.0029(13)
C3 0.0239(17) 0.0252(17) 0.045(2) 0.0101(15) 0.0115(16) 0.0022(13)
C4 0.0328(19) 0.0271(17) 0.038(2) 0.0090(15) 0.0157(16) 0.0081(14)
C5 0.0267(18) 0.0238(16) 0.033(2) 0.0020(14) 0.0124(15) 0.0061(13)
C6 0.0205(15) 0.0199(15) 0.0315(18) 0.0023(13) 0.0082(13) 0.0017(12)
C7 0.0209(15) 0.0187(14) 0.0275(17) -0.0020(12) 0.0021(13) 0.0001(12)
C8 0.0234(16) 0.0193(15) 0.0205(16) 0.0021(12) -0.0007(13) -0.0016(12)
C9 0.0288(17) 0.0220(16) 0.0262(17) 0.0000(13) 0.0030(14) -0.0006(14)
C10 0.0354(19) 0.0187(15) 0.0284(18) -0.0014(13) -0.0015(15) -0.0005(14)
C11 0.0303(18) 0.0203(16) 0.0304(19) 0.0045(14) -0.0017(15) -0.0044(13)
C12 0.0284(17) 0.0228(16) 0.0247(17) 0.0009(13) 0.0010(14) -0.0064(13)
C13 0.0225(16) 0.0203(15) 0.0187(15) 0.0003(12) -0.0017(12) -0.0024(12)
C14 0.0245(16) 0.0227(15) 0.0207(16) 0.0006(12) 0.0022(13) -0.0066(12)
C15 0.0225(16) 0.0222(15) 0.0233(16) 0.0029(13) 0.0032(13) -0.0024(13)
C16 0.0241(17) 0.0258(17) 0.0251(18) 0.0028(13) 0.0036(14) -0.0055(12)
C17 0.0254(17) 0.0252(16) 0.033(2) 0.0059(14) 0.0062(15) -0.0010(13)
C18 0.0317(18) 0.0234(16) 0.0329(19) 0.0024(14) 0.0110(15) 0.0007(14)
C19 0.0307(18) 0.0224(16) 0.0281(18) -0.0021(13) 0.0045(15) -0.0057(13)
C20 0.0217(15) 0.0211(15) 0.0263(17) 0.0018(13) 0.0046(13) -0.0030(12)
C21 0.0303(18) 0.0300(18) 0.0273(18) -0.0029(14) 0.0027(15) -0.0105(14)
C22 0.053(3) 0.050(3) 0.046(3) -0.012(2) 0.019(2) -0.029(2)
C23 0.046(2) 0.0306(19) 0.037(2) -0.0049(17) 0.0022(19) 0.0001(17)
C24 0.042(2) 0.0280(18) 0.0267(18) 0.0012(14) 0.0020(16) -0.0046(15)

_geom_special_details
;
 All esds (except the esd in the dihedral angle between two l.s. planes)
 are estimated using the full covariance matrix.  The cell esds are taken
 into account individually in the estimation of esds in distances, angles
 and torsion angles; correlations between esds in cell parameters are only
 used when they are defined by crystal symmetry.  An approximate (isotropic)
 treatment of cell esds is used for estimating esds involving l.s. planes.
;

loop_
 _geom_bond_atom_site_label_1
 _geom_bond_atom_site_label_2
 _geom_bond_distance
 _geom_bond_site_symmetry_2
 _geom_bond_publ_flag
U1 O1 1.776(2) . ?
U1 O2 1.788(2) . ?
U1 O4 2.260(3) . ?
U1 O5 2.275(3) . ?
U1 O3 2.410(3) . ?
U1 N3 2.539(3) . ?
U1 N2 2.549(3) . ?
```

```
Cl2 C24 1.752(4) . ?
Cl3 C24 1.759(4) . ?
O3 C21 1.249(5) . ?
O4 C1 1.320(4) . ?
O5 C20 1.317(4) . ?
N1 C21 1.307(5) . ?
N1 C22 1.450(5) . ?
N1 C23 1.461(5) . ?
N2 C7 1.290(4) . ?
N2 C8 1.422(4) . ?
N3 C14 1.289(4) . ?
N3 C13 1.425(4) . ?
C1 C2 1.409(5) . ?
C1 C6 1.417(5) . ?
C2 C3 1.379(5) . ?
C2 H2 0.9300 . ?
C3 C4 1.396(6) . ?
C3 H3 0.9300 . ?
C4 C5 1.383(5) . ?
C4 H4 0.9300 . ?
C5 C6 1.404(5) . ?
C5 H5 0.9300 . ?
C6 C7 1.449(4) . ?
C7 H7 0.9300 . ?
C8 C13 1.398(5) . ?
C8 C9 1.392(5) . ?
C9 C10 1.402(5) . ?
C9 H9 0.9300 . ?
C10 C11 1.377(5) . ?
C10 H10 0.9300 . ?
C11 C12 1.390(5) . ?
C11 H11 0.9300 . ?
C12 C13 1.396(4) . ?
C12 H12 0.9300 . ?
C14 C15 1.449(5) . ?
C14 H14 0.9300 . ?
C15 C16 1.407(5) . ?
C15 C20 1.422(5) . ?
C16 C17 1.377(5) . ?
C16 H16 0.9300 . ?
C17 C18 1.398(5) . ?
C17 H17 0.9300 . ?
C18 C19 1.380(5) . ?
C18 H18 0.9300 . ?
C19 C20 1.413(5) . ?
C19 H19 0.9300 . ?
C21 H21 0.9300 . ?
C22 H22A 0.9600 . ?
C22 H22B 0.9600 . ?
C22 H22C 0.9600 . ?
C23 H23A 0.9600 . ?
C23 H23B 0.9600 . ?
C23 H23C 0.9600 . ?
C24 H24A 0.9700 . ?
C24 H24B 0.9700 . ?

loop_
 _geom_angle_atom_site_label_1
 _geom_angle_atom_site_label_2
 _geom_angle_atom_site_label_3
 _geom_angle
```

```
 _geom_angle_site_symmetry_1
 _geom_angle_site_symmetry_3
 _geom_angle_publ_flag
O1 U1 O2 176.94(11) . . ?
O1 U1 O4 89.53(11) . . ?
O2 U1 O4 90.81(11) . . ?
O1 U1 O5 88.78(11) . . ?
O2 U1 O5 92.10(11) . . ?
O4 U1 O5 156.89(10) . . ?
O1 U1 O3 91.76(11) . . ?
O2 U1 O3 91.31(11) . . ?
O4 U1 O3 80.49(10) . . ?
O5 U1 O3 76.52(9) . . ?
O1 U1 N3 87.03(10) . . ?
O2 U1 N3 90.51(11) . . ?
O4 U1 N3 132.81(9) . . ?
O5 U1 N3 70.10(9) . . ?
O3 U1 N3 146.62(9) . . ?
O1 U1 N2 88.14(10) . . ?
O2 U1 N2 89.12(11) . . ?
O4 U1 N2 69.63(9) . . ?
O5 U1 N2 133.32(9) . . ?
O3 U1 N2 150.12(9) . . ?
N3 U1 N2 63.23(9) . . ?
C21 O3 U1 132.4(2) . . ?
C1 O4 U1 128.8(2) . . ?
C20 O5 U1 129.7(2) . . ?
C21 N1 C22 120.8(4) . . ?
C21 N1 C23 122.1(3) . . ?
C22 N1 C23 117.0(3) . . ?
C7 N2 C8 119.2(3) . . ?
C7 N2 U1 126.1(2) . . ?
C8 N2 U1 114.4(2) . . ?
C14 N3 C13 119.3(3) . . ?
C14 N3 U1 125.6(2) . . ?
C13 N3 U1 114.8(2) . . ?
O4 C1 C2 120.1(3) . . ?
O4 C1 C6 121.6(3) . . ?
C2 C1 C6 118.3(3) . . ?
C3 C2 C1 120.8(3) . . ?
C3 C2 H2 119.6 . . ?
C1 C2 H2 119.6 . . ?
C2 C3 C4 121.1(3) . . ?
C2 C3 H3 119.4 . . ?
C4 C3 H3 119.4 . . ?
C5 C4 C3 118.7(4) . . ?
C5 C4 H4 120.6 . . ?
C3 C4 H4 120.6 . . ?
C4 C5 C6 121.6(4) . . ?
C4 C5 H5 119.2 . . ?
C6 C5 H5 119.2 . . ?
C5 C6 C1 119.3(3) . . ?
C5 C6 C7 118.1(3) . . ?
C1 C6 C7 122.5(3) . . ?
N2 C7 C6 124.9(3) . . ?
N2 C7 H7 117.6 . . ?
C6 C7 H7 117.6 . . ?
C13 C8 C9 120.2(3) . . ?
C13 C8 N2 116.6(3) . . ?
C9 C8 N2 123.1(3) . . ?
C8 C9 C10 119.2(3) . . ?
```

```
C8 C9 H9 120.4 . . ?
C10 C9 H9 120.4 . . ?
C11 C10 C9 120.5(3) . . ?
C11 C10 H10 119.8 . . ?
C9 C10 H10 119.8 . . ?
C10 C11 C12 120.7(3) . . ?
C10 C11 H11 119.6 . . ?
C12 C11 H11 119.6 . . ?
C11 C12 C13 119.3(3) . . ?
C11 C12 H12 120.3 . . ?
C13 C12 H12 120.3 . . ?
C8 C13 C12 120.1(3) . . ?
C8 C13 N3 116.4(3) . . ?
C12 C13 N3 123.4(3) . . ?
N3 C14 C15 125.6(3) . . ?
N3 C14 H14 117.2 . . ?
C15 C14 H14 117.2 . . ?
C16 C15 C20 119.1(3) . . ?
C16 C15 C14 118.5(3) . . ?
C20 C15 C14 122.1(3) . . ?
C17 C16 C15 122.4(3) . . ?
C17 C16 H16 118.8 . . ?
C15 C16 H16 118.8 . . ?
C16 C17 C18 118.2(3) . . ?
C16 C17 H17 120.9 . . ?
C18 C17 H17 120.9 . . ?
C19 C18 C17 121.2(3) . . ?
C19 C18 H18 119.4 . . ?
C17 C18 H18 119.4 . . ?
C18 C19 C20 121.3(3) . . ?
C18 C19 H19 119.4 . . ?
C20 C19 H19 119.4 . . ?
O5 C20 C19 119.9(3) . . ?
O5 C20 C15 122.3(3) . . ?
C19 C20 C15 117.7(3) . . ?
O3 C21 N1 124.6(4) . . ?
O3 C21 H21 117.7 . . ?
N1 C21 H21 117.7 . . ?
N1 C22 H22A 109.5 . . ?
N1 C22 H22B 109.5 . . ?
H22A C22 H22B 109.5 . . ?
N1 C22 H22C 109.5 . . ?
H22A C22 H22C 109.5 . . ?
H22B C22 H22C 109.5 . . ?
N1 C23 H23A 109.5 . . ?
N1 C23 H23B 109.5 . . ?
H23A C23 H23B 109.5 . . ?
N1 C23 H23C 109.5 . . ?
H23A C23 H23C 109.5 . . ?
H23B C23 H23C 109.5 . . ?
Cl2 C24 Cl3 110.4(2) . . ?
Cl2 C24 H24A 109.6 . . ?
Cl3 C24 H24A 109.6 . . ?
Cl2 C24 H24B 109.6 . . ?
Cl3 C24 H24B 109.6 . . ?
H24A C24 H24B 108.1 . . ?

loop_
 _geom_torsion_atom_site_label_1
 _geom_torsion_atom_site_label_2
 _geom_torsion_atom_site_label_3
```

```
 _geom_torsion_atom_site_label_4
 _geom_torsion
 _geom_torsion_site_symmetry_1
 _geom_torsion_site_symmetry_2
 _geom_torsion_site_symmetry_3
 _geom_torsion_site_symmetry_4
 _geom_torsion_publ_flag
O1 U1 O3 C21 -58.2(4) . . . . ?
O2 U1 O3 C21 121.9(4) . . . . ?
O4 U1 O3 C21 -147.5(4) . . . . ?
O5 U1 O3 C21 30.1(3) . . . . ?
N3 U1 O3 C21 29.0(4) . . . . ?
N2 U1 O3 C21 -147.6(3) . . . . ?
O1 U1 O4 C1 32.6(3) . . . . ?
O2 U1 O4 C1 -144.4(3) . . . . ?
O5 U1 O4 C1 118.4(3) . . . . ?
O3 U1 O4 C1 124.4(3) . . . . ?
N3 U1 O4 C1 -52.9(3) . . . . ?
N2 U1 O4 C1 -55.6(3) . . . . ?
O1 U1 O5 C20 -34.5(3) . . . . ?
O2 U1 O5 C20 142.6(3) . . . . ?
O4 U1 O5 C20 -120.5(3) . . . . ?
O3 U1 O5 C20 -126.6(3) . . . . ?
N3 U1 O5 C20 52.8(3) . . . . ?
N2 U1 O5 C20 51.8(3) . . . . ?
O1 U1 N2 C7 -54.6(3) . . . . ?
O2 U1 N2 C7 126.8(3) . . . . ?
O4 U1 N2 C7 35.6(3) . . . . ?
O5 U1 N2 C7 -141.2(3) . . . . ?
O3 U1 N2 C7 35.7(4) . . . . ?
N3 U1 N2 C7 -142.2(3) . . . . ?
O1 U1 N2 C8 118.7(2) . . . . ?
O2 U1 N2 C8 -60.0(2) . . . . ?
O4 U1 N2 C8 -151.2(2) . . . . ?
O5 U1 N2 C8 32.1(3) . . . . ?
O3 U1 N2 C8 -151.1(2) . . . . ?
N3 U1 N2 C8 31.0(2) . . . . ?
O1 U1 N3 C14 52.6(3) . . . . ?
O2 U1 N3 C14 -129.3(3) . . . . ?
O4 U1 N3 C14 139.2(3) . . . . ?
O5 U1 N3 C14 -37.2(3) . . . . ?
O3 U1 N3 C14 -36.1(4) . . . . ?
N2 U1 N3 C14 142.0(3) . . . . ?
O1 U1 N3 C13 -120.3(2) . . . . ?
O2 U1 N3 C13 57.9(2) . . . . ?
O4 U1 N3 C13 -33.7(3) . . . . ?
O5 U1 N3 C13 149.9(2) . . . . ?
O3 U1 N3 C13 151.0(2) . . . . ?
N2 U1 N3 C13 -30.9(2) . . . . ?
U1 O4 C1 C2 -131.0(3) . . . . ?
U1 O4 C1 C6 51.0(4) . . . . ?
O4 C1 C2 C3 -179.5(3) . . . . ?
C6 C1 C2 C3 -1.4(5) . . . . ?
C1 C2 C3 C4 -0.4(5) . . . . ?
C2 C3 C4 C5 2.3(5) . . . . ?
C3 C4 C5 C6 -2.4(5) . . . . ?
C4 C5 C6 C1 0.6(5) . . . . ?
C4 C5 C6 C7 178.3(3) . . . . ?
O4 C1 C6 C5 179.3(3) . . . . ?
C2 C1 C6 C5 1.3(5) . . . . ?
O4 C1 C6 C7 1.7(5) . . . . ?
```

```
C2 C1 C6 C7 -176.3(3) . . . . ?
C8 N2 C7 C6 174.8(3) . . . . ?
U1 N2 C7 C6 -12.3(5) . . . . ?
C5 C6 C7 N2 164.8(3) . . . . ?
C1 C6 C7 N2 -17.5(5) . . . . ?
C7 N2 C8 C13 144.2(3) . . . . ?
U1 N2 C8 C13 -29.6(3) . . . . ?
C7 N2 C8 C9 -40.2(5) . . . . ?
U1 N2 C8 C9 146.0(3) . . . . ?
C13 C8 C9 C10 -1.7(5) . . . . ?
N2 C8 C9 C10 -177.1(3) . . . . ?
C8 C9 C10 C11 0.7(5) . . . . ?
C9 C10 C11 C12 0.5(5) . . . . ?
C10 C11 C12 C13 -0.7(5) . . . . ?
C9 C8 C13 C12 1.5(5) . . . . ?
N2 C8 C13 C12 177.2(3) . . . . ?
C9 C8 C13 N3 -175.2(3) . . . . ?
N2 C8 C13 N3 0.5(4) . . . . ?
C11 C12 C13 C8 -0.3(5) . . . . ?
C11 C12 C13 N3 176.2(3) . . . . ?
C14 N3 C13 C8 -144.3(3) . . . . ?
U1 N3 C13 C8 29.0(3) . . . . ?
C14 N3 C13 C12 39.1(5) . . . . ?
U1 N3 C13 C12 -147.6(3) . . . . ?
C13 N3 C14 C15 -172.0(3) . . . . ?
U1 N3 C14 C15 15.4(5) . . . . ?
N3 C14 C15 C16 -169.6(3) . . . . ?
N3 C14 C15 C20 17.5(5) . . . . ?
C20 C15 C16 C17 0.0(5) . . . . ?
C14 C15 C16 C17 -173.2(3) . . . . ?
C15 C16 C17 C18 2.5(5) . . . . ?
C16 C17 C18 C19 -2.2(5) . . . . ?
C17 C18 C19 C20 -0.6(5) . . . . ?
U1 O5 C20 C19 139.1(3) . . . . ?
U1 O5 C20 C15 -44.6(4) . . . . ?
C18 C19 C20 O5 179.6(3) . . . . ?
C18 C19 C20 C15 3.0(5) . . . . ?
C16 C15 C20 O5 -179.1(3) . . . . ?
C14 C15 C20 O5 -6.2(5) . . . . ?
C16 C15 C20 C19 -2.7(5) . . . . ?
C14 C15 C20 C19 170.3(3) . . . . ?
U1 O3 C21 N1 150.7(3) . . . . ?
C22 N1 C21 O3 -4.6(6) . . . . ?
C23 N1 C21 O3 178.9(4) . . . . ?

_diffrn_measured_fraction_theta_max    0.997
_diffrn_reflns_theta_full              27.48
_diffrn_measured_fraction_theta_full   0.997
_refine_diff_density_max    0.964
_refine_diff_density_min   -0.740
_refine_diff_density_rms    0.112
```

Appendix B

Crystallographic Information of $[U^{VI}O_2(saloph)]_2$

```
data_shelxl

_audit_creation_method            SHELXL-97
_chemical_name_systematic
;
 ?
;
_chemical_name_common             ?
_chemical_melting_point           ?
_chemical_formula_moiety         'C40 H28 N4 O8 U2 '
_chemical_formula_sum
 'C40 H28 N4 O8 U2'
_chemical_formula_weight          1168.72

loop_
 _atom_type_symbol
 _atom_type_description
 _atom_type_scat_dispersion_real
 _atom_type_scat_dispersion_imag
 _atom_type_scat_source
 'C'  'C'   0.0033   0.0016
 'International Tables Vol C Tables 4.2.6.8 and 6.1.1.4'
 'H'  'H'   0.0000   0.0000
 'International Tables Vol C Tables 4.2.6.8 and 6.1.1.4'
 'N'  'N'   0.0061   0.0033
 'International Tables Vol C Tables 4.2.6.8 and 6.1.1.4'
 'O'  'O'   0.0106   0.0060
 'International Tables Vol C Tables 4.2.6.8 and 6.1.1.4'
 'U'  'U'  -9.6767   9.6646
 'International Tables Vol C Tables 4.2.6.8 and 6.1.1.4'

_symmetry_cell_setting             triclinic
_symmetry_space_group_name_H-M    'P -1'

loop_
 _symmetry_equiv_pos_as_xyz
 'x, y, z'
 '-x, -y, -z'

_cell_length_a                    15.689(7)
```

```
_cell_length_b                    16.044(5)
_cell_length_c                    17.642(7)
_cell_angle_alpha                 67.00(3)
_cell_angle_beta                  78.25(3)
_cell_angle_gamma                 81.72(3)
_cell_volume                      3992(3)
_cell_formula_units_Z             4
_cell_measurement_temperature     93(2)
_cell_measurement_reflns_used     37292
_cell_measurement_theta_min       3.0
_cell_measurement_theta_max       27.5

_exptl_crystal_description       'block'
_exptl_crystal_colour            'red'
_exptl_crystal_size_max           0.20
_exptl_crystal_size_mid           0.10
_exptl_crystal_size_min           0.10
_exptl_crystal_density_meas       ?
_exptl_crystal_density_diffrn     1.945
_exptl_crystal_density_method     'not measured'
_exptl_crystal_F_000              2176
_exptl_absorpt_coefficient_mu     8.158
_exptl_absorpt_correction_type    multi-scan
_exptl_absorpt_correction_T_min   0.2923
_exptl_absorpt_correction_T_max   0.4959
_exptl_absorpt_process_details
;
    Higashi, T. (1995). Program for Absorption Correction.
    Rigaku Corporation, Tokyo, Japan.
;

_diffrn_ambient_temperature       93(2)
_diffrn_radiation_wavelength      0.71075
_diffrn_radiation_type            MoK¥a
_diffrn_radiation_source          'fine-focus sealed tube'
_diffrn_radiation_monochromator   graphite
_diffrn_measurement_device_type  'Rigaku RAXIS-RAPID'
_diffrn_measurement_method        ¥w
_diffrn_detector_area_resol_mean  10.00
_diffrn_reflns_number             34895
_diffrn_reflns_av_R_equivalents   0.0687
_diffrn_reflns_av_sigmaI/netI     0.0894
_diffrn_reflns_limit_h_min        -20
_diffrn_reflns_limit_h_max        20
_diffrn_reflns_limit_k_min        -20
_diffrn_reflns_limit_k_max        20
_diffrn_reflns_limit_l_min        -22
_diffrn_reflns_limit_l_max        22
_diffrn_reflns_theta_min          3.00
_diffrn_reflns_theta_max          27.48
_reflns_number_total              17643
_reflns_number_gt                 12239
_reflns_threshold_expression      >2sigma(I)

_computing_data_collection        'PROCESS-AUTO'
_computing_cell_refinement        'PROCESS-AUTO'
_computing_data_reduction         'CrystalStructure'
_computing_structure_solution     'DIRDIF99 (PATTY)'
_computing_structure_refinement   'SHELXL-97 (Sheldrick, 1997)'
_computing_molecular_graphics     ?
_computing_publication_material   ?
```

```
_refine_special_details
;
 Refinement of F^2^ against ALL reflections.  The weighted R-factor wR and
 goodness of fit S are based on F^2^, conventional R-factors R are based
 on F, with F set to zero for negative F^2^. The threshold expression of
 F^2^ > 2sigma(F^2^) is used only for calculating R-factors(gt) etc. and is
 not relevant to the choice of reflections for refinement.  R-factors based
 on F^2^ are statistically about twice as large as those based on F, and R-
 factors based on ALL data will be even larger.
;

_refine_ls_structure_factor_coef  Fsqd
_refine_ls_matrix_type            full
_refine_ls_weighting_scheme       calc
_refine_ls_weighting_details
 'calc w=1/[¥s^2^(Fo^2^)+(0.0256P)^2^+46.5808P] where P=(Fo^2^+2Fc^2^)/3'
_atom_sites_solution_primary      direct
_atom_sites_solution_secondary    difmap
_atom_sites_solution_hydrogens    geom
_refine_ls_hydrogen_treatment     mixed
_refine_ls_extinction_method      none
_refine_ls_extinction_coef        ?
_refine_ls_number_reflns          17643
_refine_ls_number_parameters      974
_refine_ls_number_restraints      0
_refine_ls_R_factor_all           0.0983
_refine_ls_R_factor_gt            0.0578
_refine_ls_wR_factor_ref          0.1082
_refine_ls_wR_factor_gt           0.0974
_refine_ls_goodness_of_fit_ref    1.022
_refine_ls_restrained_S_all       1.022
_refine_ls_shift/su_max           0.001
_refine_ls_shift/su_mean          0.000

loop_
 _atom_site_label
 _atom_site_type_symbol
 _atom_site_fract_x
 _atom_site_fract_y
 _atom_site_fract_z
 _atom_site_U_iso_or_equiv
 _atom_site_adp_type
 _atom_site_occupancy
 _atom_site_symmetry_multiplicity
 _atom_site_calc_flag
 _atom_site_refinement_flags
 _atom_site_disorder_assembly
 _atom_site_disorder_group
U1 U 0.24047(2) 0.43472(2) 0.00772(2) 0.02418(9) Uani 1 1 d . . .
U2 U 0.28782(2) 0.17798(2) 0.04840(2) 0.02285(9) Uani 1 1 d . . .
U3 U 0.57203(2) 0.69471(2) 0.53808(2) 0.02397(9) Uani 1 1 d . . .
U4 U 0.80417(2) 0.73859(2) 0.41050(2) 0.02339(9) Uani 1 1 d . . .
O1 O 0.1316(5) 0.4471(4) 0.0563(4) 0.0294(16) Uani 1 1 d . . .
O2 O 0.3520(4) 0.4254(5) -0.0362(4) 0.0307(16) Uani 1 1 d . . .
O3 O 0.2072(4) 0.5247(4) -0.1173(4) 0.0256(15) Uani 1 1 d . . .
O4 O 0.2578(4) 0.2901(4) 0.1166(4) 0.0267(15) Uani 1 1 d . . .
O5 O 0.1845(5) 0.1309(4) 0.0875(4) 0.0309(16) Uani 1 1 d . . .
O6 O 0.3927(5) 0.2211(4) 0.0034(4) 0.0293(16) Uani 1 1 d . . .
O7 O 0.3333(4) 0.0873(4) 0.1667(4) 0.0264(15) Uani 1 1 d . . .
O8 O 0.2114(4) 0.3133(4) -0.0342(4) 0.0204(14) Uani 1 1 d . . .
```

```
O9 O 0.5014(4) 0.7804(4) 0.4782(4) 0.0285(16) Uani 1 1 d . . .
O10 O 0.6392(5) 0.6118(5) 0.6048(4) 0.0319(17) Uani 1 1 d . . .
O11 O 0.6778(4) 0.8056(4) 0.4791(4) 0.0254(15) Uani 1 1 d . . .
O12 O 0.4906(4) 0.5928(4) 0.5400(5) 0.0311(17) Uani 1 1 d . . .
O13 O 0.7909(5) 0.8120(4) 0.3071(4) 0.0287(16) Uani 1 1 d . . .
O14 O 0.8222(4) 0.6588(4) 0.5109(4) 0.0266(15) Uani 1 1 d . . .
O15 O 0.6750(4) 0.6696(4) 0.4201(4) 0.0239(14) Uani 1 1 d . . .
O16 O 0.8704(5) 0.8441(5) 0.4226(5) 0.0323(17) Uani 1 1 d . . .
N1 N 0.2422(6) 0.5995(5) -0.0103(5) 0.0292(19) Uani 1 1 d . . .
N2 N 0.2874(6) 0.4616(6) 0.1254(5) 0.031(2) Uani 1 1 d . . .
N3 N 0.3499(5) 0.0273(5) 0.0362(5) 0.0249(18) Uani 1 1 d . . .
N4 N 0.2781(5) 0.1621(5) -0.0847(5) 0.0262(18) Uani 1 1 d . . .
N5 N 0.5626(5) 0.7843(5) 0.6323(5) 0.0257(18) Uani 1 1 d . . .
N6 N 0.4476(5) 0.6645(5) 0.6601(5) 0.0263(18) Uani 1 1 d . . .
N7 N 0.8522(5) 0.6142(5) 0.3549(5) 0.0228(17) Uani 1 1 d . . .
N8 N 0.9654(6) 0.7220(5) 0.3581(5) 0.0277(19) Uani 1 1 d . . .
C1 C 0.1435(7) 0.5892(7) -0.1341(6) 0.029(2) Uani 1 1 d . . .
C2 C 0.0880(8) 0.5933(7) -0.1894(7) 0.037(3) Uani 1 1 d . . .
H2 H 0.0989 0.5518 -0.2172 0.045 Uiso 1 1 calc R . .
C3 C 0.0184(7) 0.6571(8) -0.2032(7) 0.038(3) Uani 1 1 d . . .
H3 H -0.0199 0.6564 -0.2384 0.046 Uiso 1 1 calc R . .
C4 C 0.0020(7) 0.7218(8) -0.1680(7) 0.039(3) Uani 1 1 d . . .
H4 H -0.0471 0.7646 -0.1773 0.047 Uiso 1 1 calc R . .
C5 C 0.0594(7) 0.7222(7) -0.1189(7) 0.039(3) Uani 1 1 d . . .
H5 H 0.0504 0.7680 -0.0960 0.046 Uiso 1 1 calc R . .
C6 C 0.1315(7) 0.6574(7) -0.1008(7) 0.034(3) Uani 1 1 d . . .
C7 C 0.1870(7) 0.6631(7) -0.0481(7) 0.034(3) Uani 1 1 d . . .
H7 H 0.1830 0.7188 -0.0400 0.041 Uiso 1 1 calc R . .
C8 C 0.2987(6) 0.6193(8) 0.0318(8) 0.035(3) Uani 1 1 d . . .
C9 C 0.3321(7) 0.7041(8) 0.0041(9) 0.044(3) Uani 1 1 d . . .
H9 H 0.3139 0.7527 -0.0428 0.052 Uiso 1 1 calc R . .
C10 C 0.3915(8) 0.7164(9) 0.0456(10) 0.054(4) Uani 1 1 d . . .
H10 H 0.4138 0.7743 0.0276 0.064 Uiso 1 1 calc R . .
C11 C 0.4189(8) 0.6468(10) 0.1121(10) 0.057(4) Uani 1 1 d . . .
H11 H 0.4620 0.6565 0.1380 0.069 Uiso 1 1 calc R . .
C12 C 0.3853(8) 0.5609(9) 0.1436(9) 0.055(4) Uani 1 1 d . . .
H12 H 0.4029 0.5135 0.1915 0.066 Uiso 1 1 calc R . .
C13 C 0.3247(7) 0.5481(8) 0.1012(8) 0.037(3) Uani 1 1 d . . .
C14 C 0.2763(7) 0.4106(8) 0.2024(7) 0.036(3) Uani 1 1 d . . .
H14 H 0.2939 0.4329 0.2390 0.044 Uiso 1 1 calc R . .
C15 C 0.2403(7) 0.3231(8) 0.2408(6) 0.036(3) Uani 1 1 d . . .
C16 C 0.2180(7) 0.2933(8) 0.3279(6) 0.033(2) Uani 1 1 d . . .
H16 H 0.2312 0.3284 0.3561 0.040 Uiso 1 1 calc R . .
C17 C 0.1773(8) 0.2141(9) 0.3732(7) 0.050(3) Uani 1 1 d . . .
H17 H 0.1593 0.1962 0.4318 0.060 Uiso 1 1 calc R . .
C18 C 0.1628(7) 0.1606(8) 0.3315(7) 0.042(3) Uani 1 1 d . . .
H18 H 0.1352 0.1054 0.3620 0.050 Uiso 1 1 calc R . .
C19 C 0.1881(7) 0.1868(7) 0.2465(6) 0.032(2) Uani 1 1 d . . .
H19 H 0.1783 0.1488 0.2195 0.039 Uiso 1 1 calc R . .
C20 C 0.2275(7) 0.2669(7) 0.1993(6) 0.028(2) Uani 1 1 d . . .
C21 C 0.3248(7) 0.0017(7) 0.2173(7) 0.030(2) Uani 1 1 d . . .
C22 C 0.3147(8) -0.0240(8) 0.3041(7) 0.040(3) Uani 1 1 d . . .
H22 H 0.3128 0.0212 0.3267 0.049 Uiso 1 1 calc R . .
C23 C 0.3075(9) -0.1128(9) 0.3570(7) 0.053(4) Uani 1 1 d . . .
H23 H 0.2993 -0.1276 0.4155 0.064 Uiso 1 1 calc R . .
C24 C 0.3120(11) -0.1823(9) 0.3267(8) 0.067(4) Uani 1 1 d . . .
H24 H 0.3078 -0.2439 0.3637 0.080 Uiso 1 1 calc R . .
C25 C 0.3227(9) -0.1584(7) 0.2420(8) 0.054(4) Uani 1 1 d . . .
H25 H 0.3263 -0.2048 0.2204 0.065 Uiso 1 1 calc R . .
C26 C 0.3285(8) -0.0683(7) 0.1860(7) 0.039(3) Uani 1 1 d . . .
C27 C 0.3473(8) -0.0508(7) 0.0982(7) 0.035(3) Uani 1 1 d . . .
```

```
H27 H 0.3595 -0.1028 0.0836 0.042 Uiso 1 1 calc R . .
C28 C 0.3792(6) 0.0289(6) -0.0454(6) 0.027(2) Uani 1 1 d . . .
C29 C 0.4428(6) -0.0332(6) -0.0664(7) 0.030(2) Uani 1 1 d . . .
H29 H 0.4702 -0.0797 -0.0241 0.036 Uiso 1 1 calc R . .
C30 C 0.4657(7) -0.0272(8) -0.1480(7) 0.036(3) Uani 1 1 d . . .
H30 H 0.5063 -0.0714 -0.1611 0.044 Uiso 1 1 calc R . .
C31 C 0.4295(7) 0.0432(8) -0.2108(7) 0.036(3) Uani 1 1 d . . .
H31 H 0.4460 0.0471 -0.2669 0.043 Uiso 1 1 calc R . .
C32 C 0.3690(7) 0.1083(7) -0.1926(7) 0.030(2) Uani 1 1 d . . .
H32 H 0.3454 0.1572 -0.2360 0.036 Uiso 1 1 calc R . .
C33 C 0.3438(7) 0.1006(7) -0.1102(6) 0.028(2) Uani 1 1 d . . .
C34 C 0.2132(6) 0.1918(7) -0.1250(6) 0.028(2) Uani 1 1 d . . .
H34 H 0.2126 0.1699 -0.1678 0.034 Uiso 1 1 calc R . .
C35 C 0.1409(6) 0.2550(6) -0.1123(6) 0.024(2) Uani 1 1 d . . .
C36 C 0.0678(7) 0.2602(7) -0.1491(6) 0.030(2) Uani 1 1 d . . .
H36 H 0.0684 0.2210 -0.1779 0.036 Uiso 1 1 calc R . .
C37 C -0.0039(7) 0.3188(7) -0.1455(6) 0.031(2) Uani 1 1 d . . .
H37 H -0.0527 0.3207 -0.1706 0.037 Uiso 1 1 calc R . .
C38 C -0.0018(6) 0.3763(7) -0.1026(6) 0.027(2) Uani 1 1 d . . .
H38 H -0.0502 0.4185 -0.0995 0.032 Uiso 1 1 calc R . .
C39 C 0.0672(6) 0.3732(6) -0.0658(6) 0.023(2) Uani 1 1 d . . .
H39 H 0.0652 0.4127 -0.0369 0.028 Uiso 1 1 calc R . .
C40 C 0.1413(6) 0.3134(6) -0.0691(6) 0.023(2) Uani 1 1 d . . .
C41 C 0.6605(7) 0.8966(7) 0.4628(6) 0.029(2) Uani 1 1 d . . .
C42 C 0.6846(7) 0.9607(7) 0.3845(7) 0.034(3) Uani 1 1 d . . .
H42 H 0.7116 0.9411 0.3404 0.041 Uiso 1 1 calc R . .
C43 C 0.6708(7) 1.0521(7) 0.3682(7) 0.034(3) Uani 1 1 d . . .
H43 H 0.6895 1.0943 0.3137 0.041 Uiso 1 1 calc R . .
C44 C 0.6296(7) 1.0834(7) 0.4310(7) 0.037(3) Uani 1 1 d . . .
H44 H 0.6197 1.1466 0.4200 0.045 Uiso 1 1 calc R . .
C45 C 0.6035(7) 1.0200(7) 0.5097(7) 0.031(2) Uani 1 1 d . . .
H45 H 0.5770 1.0403 0.5535 0.038 Uiso 1 1 calc R . .
C46 C 0.6152(7) 0.9258(6) 0.5265(6) 0.028(2) Uani 1 1 d . . .
C47 C 0.5789(7) 0.8664(7) 0.6100(6) 0.029(2) Uani 1 1 d . . .
H47 H 0.5662 0.8917 0.6519 0.035 Uiso 1 1 calc R . .
C48 C 0.5287(6) 0.7337(6) 0.7181(6) 0.026(2) Uani 1 1 d . . .
C49 C 0.5536(7) 0.7450(7) 0.7845(6) 0.026(2) Uani 1 1 d . . .
H49 H 0.5905 0.7914 0.7746 0.032 Uiso 1 1 calc R . .
C50 C 0.5241(7) 0.6878(7) 0.8655(7) 0.035(3) Uani 1 1 d . . .
H50 H 0.5421 0.6939 0.9113 0.042 Uiso 1 1 calc R . .
C51 C 0.4683(7) 0.6220(7) 0.8795(7) 0.039(3) Uani 1 1 d . . .
H51 H 0.4496 0.5817 0.9348 0.046 Uiso 1 1 calc R . .
C52 C 0.4396(8) 0.6146(7) 0.8134(7) 0.037(3) Uani 1 1 d . . .
H52 H 0.3989 0.5716 0.8234 0.045 Uiso 1 1 calc R . .
C53 C 0.4710(6) 0.6711(7) 0.7319(6) 0.028(2) Uani 1 1 d . . .
C54 C 0.3705(7) 0.6481(7) 0.6596(7) 0.035(3) Uani 1 1 d . . .
H54 H 0.3271 0.6484 0.7058 0.042 Uiso 1 1 calc R . .
C55 C 0.3437(7) 0.6291(7) 0.5949(7) 0.032(2) Uani 1 1 d . . .
C56 C 0.2534(7) 0.6362(7) 0.5905(7) 0.033(2) Uani 1 1 d . . .
H56 H 0.2117 0.6568 0.6277 0.040 Uiso 1 1 calc R . .
C57 C 0.2265(7) 0.6128(7) 0.5319(8) 0.040(3) Uani 1 1 d . . .
H57 H 0.1665 0.6213 0.5267 0.048 Uiso 1 1 calc R . .
C58 C 0.2865(8) 0.5769(7) 0.4803(7) 0.035(3) Uani 1 1 d . . .
H58 H 0.2670 0.5579 0.4424 0.042 Uiso 1 1 calc R . .
C59 C 0.3743(7) 0.5692(6) 0.4846(7) 0.032(2) Uani 1 1 d . . .
H59 H 0.4145 0.5439 0.4499 0.039 Uiso 1 1 calc R . .
C60 C 0.4053(7) 0.5974(6) 0.5383(6) 0.026(2) Uani 1 1 d . . .
C61 C 0.6537(7) 0.6532(7) 0.3565(6) 0.028(2) Uani 1 1 d . . .
C62 C 0.5686(7) 0.6739(8) 0.3393(7) 0.039(3) Uani 1 1 d . . .
H62 H 0.5264 0.7011 0.3711 0.047 Uiso 1 1 calc R . .
C63 C 0.5448(8) 0.6555(9) 0.2769(8) 0.049(3) Uani 1 1 d . . .
```

```
H63 H 0.4861 0.6698 0.2673 0.058 Uiso 1 1 calc R . .
C64 C 0.6036(8) 0.6168(9) 0.2275(8) 0.050(3) Uani 1 1 d . . .
H64 H 0.5865 0.6050 0.1842 0.060 Uiso 1 1 calc R . .
C65 C 0.6872(7) 0.5963(7) 0.2440(6) 0.033(2) Uani 1 1 d . . .
H65 H 0.7283 0.5689 0.2116 0.040 Uiso 1 1 calc R . .
C66 C 0.7149(6) 0.6140(6) 0.3065(6) 0.025(2) Uani 1 1 d . . .
C67 C 0.8066(6) 0.5888(6) 0.3153(6) 0.023(2) Uani 1 1 d . . .
H67 H 0.8364 0.5491 0.2887 0.028 Uiso 1 1 calc R . .
C68 C 0.9413(7) 0.5791(7) 0.3564(6) 0.028(2) Uani 1 1 d . . .
C69 C 0.9716(7) 0.4935(6) 0.3543(7) 0.035(3) Uani 1 1 d . . .
H69 H 0.9324 0.4548 0.3523 0.041 Uiso 1 1 calc R . .
C70 C 1.0590(8) 0.4659(8) 0.3550(8) 0.044(3) Uani 1 1 d . . .
H70 H 1.0795 0.4081 0.3527 0.053 Uiso 1 1 calc R . .
C71 C 1.1171(8) 0.5196(8) 0.3590(8) 0.044(3) Uani 1 1 d . . .
H71 H 1.1769 0.4993 0.3602 0.053 Uiso 1 1 calc R . .
C72 C 1.0871(7) 0.6038(7) 0.3613(6) 0.032(2) Uani 1 1 d . . .
H72 H 1.1264 0.6407 0.3659 0.038 Uiso 1 1 calc R . .
C73 C 1.0013(7) 0.6352(7) 0.3570(6) 0.030(2) Uani 1 1 d . . .
C74 C 1.0151(7) 0.7889(7) 0.3176(6) 0.031(2) Uani 1 1 d . . .
H74 H 1.0704 0.7767 0.2884 0.037 Uiso 1 1 calc R . .
C75 C 0.9918(8) 0.8818(7) 0.3138(8) 0.041(3) Uani 1 1 d . . .
C76 C 1.0457(8) 0.9498(8) 0.2565(9) 0.053(3) Uani 1 1 d . . .
H76 H 1.0949 0.9336 0.2223 0.063 Uiso 1 1 calc R . .
C77 C 1.0290(10) 1.0385(9) 0.2487(10) 0.072(5) Uani 1 1 d . . .
H77 H 1.0622 1.0847 0.2061 0.086 Uiso 1 1 calc R . .
C78 C 0.9605(9) 1.0596(9) 0.3061(9) 0.056(4) Uani 1 1 d . . .
H78 H 0.9496 1.1205 0.3034 0.068 Uiso 1 1 calc R . .
C79 C 0.9099(8) 0.9940(8) 0.3653(8) 0.048(3) Uani 1 1 d . . .
H79 H 0.8656 1.0095 0.4041 0.058 Uiso 1 1 calc R . .
C80 C 0.9228(7) 0.9040(8) 0.3694(7) 0.035(3) Uani 1 1 d . . .

loop_
 _atom_site_aniso_label
 _atom_site_aniso_U_11
 _atom_site_aniso_U_22
 _atom_site_aniso_U_33
 _atom_site_aniso_U_23
 _atom_site_aniso_U_13
 _atom_site_aniso_U_12
U1 0.0271(2) 0.02378(19) 0.0239(2) -0.01233(15) -0.00380(16) 0.00061(15)
U2 0.0269(2) 0.02145(19) 0.01957(19) -0.00791(14) -0.00305(15) 0.00001(15)
U3 0.0266(2) 0.02206(19) 0.0240(2) -0.01108(15) -0.00123(16) -0.00083(15)
U4 0.0266(2) 0.0246(2) 0.02002(19) -0.01048(15) -0.00203(15) -0.00121(15)
O1 0.038(4) 0.030(4) 0.023(4) -0.016(3) 0.001(3) 0.000(3)
O2 0.027(4) 0.033(4) 0.040(4) -0.023(3) -0.003(3) -0.003(3)
O3 0.025(4) 0.020(3) 0.031(4) -0.012(3) -0.005(3) 0.007(3)
O4 0.037(4) 0.029(4) 0.015(3) -0.010(3) -0.006(3) 0.002(3)
O5 0.036(4) 0.028(4) 0.028(4) -0.007(3) -0.013(3) 0.002(3)
O6 0.034(4) 0.019(3) 0.038(4) -0.012(3) -0.012(3) -0.002(3)
O7 0.035(4) 0.022(4) 0.021(4) -0.007(3) -0.008(3) 0.002(3)
O8 0.020(3) 0.020(3) 0.019(3) -0.007(3) -0.007(3) 0.006(3)
O9 0.029(4) 0.028(4) 0.033(4) -0.018(3) -0.004(3) 0.001(3)
O10 0.039(4) 0.030(4) 0.030(4) -0.017(3) -0.006(3) 0.002(3)
O11 0.028(4) 0.022(4) 0.028(4) -0.011(3) -0.002(3) -0.003(3)
O12 0.025(4) 0.029(4) 0.047(5) -0.022(3) -0.002(3) -0.007(3)
O13 0.039(4) 0.025(4) 0.024(4) -0.009(3) -0.012(3) 0.000(3)
O14 0.031(4) 0.030(4) 0.018(3) -0.010(3) -0.001(3) -0.001(3)
O15 0.026(4) 0.023(3) 0.027(4) -0.016(3) -0.007(3) 0.002(3)
O16 0.033(4) 0.030(4) 0.040(4) -0.021(3) 0.000(3) -0.005(3)
N1 0.029(5) 0.024(4) 0.040(5) -0.017(4) -0.008(4) 0.003(4)
N2 0.038(5) 0.033(5) 0.031(5) -0.021(4) -0.012(4) 0.007(4)
```

```
N3 0.032(5) 0.024(4) 0.023(4) -0.017(4) 0.000(4) 0.000(4)
N4 0.032(5) 0.025(4) 0.021(4) -0.009(3) 0.000(4) -0.002(4)
N5 0.027(5) 0.022(4) 0.026(5) -0.009(3) -0.004(4) 0.002(4)
N6 0.025(5) 0.021(4) 0.031(5) -0.010(4) 0.002(4) -0.001(3)
N7 0.024(4) 0.024(4) 0.026(4) -0.016(3) -0.002(4) -0.001(3)
N8 0.034(5) 0.025(4) 0.024(4) -0.009(4) -0.004(4) -0.003(4)
C1 0.026(6) 0.027(5) 0.024(5) -0.002(4) 0.004(4) -0.006(4)
C2 0.046(7) 0.037(6) 0.030(6) -0.017(5) -0.005(5) 0.003(5)
C3 0.030(6) 0.050(7) 0.034(6) -0.015(5) -0.004(5) -0.005(5)
C4 0.028(6) 0.043(7) 0.037(7) -0.007(5) -0.003(5) 0.001(5)
C5 0.036(7) 0.029(6) 0.049(7) -0.015(5) 0.000(6) 0.000(5)
C6 0.040(7) 0.020(5) 0.028(6) -0.003(4) 0.009(5) -0.003(5)
C7 0.042(7) 0.019(5) 0.038(6) -0.009(4) -0.001(5) -0.004(5)
C8 0.014(5) 0.042(7) 0.058(8) -0.033(6) -0.007(5) 0.012(5)
C9 0.026(6) 0.040(7) 0.076(9) -0.032(6) -0.008(6) -0.003(5)
C10 0.040(8) 0.039(7) 0.091(11) -0.040(8) 0.000(7) -0.001(6)
C11 0.026(7) 0.079(10) 0.094(12) -0.059(9) -0.021(7) 0.006(7)
C12 0.044(8) 0.056(8) 0.092(11) -0.049(8) -0.042(8) 0.014(6)
C13 0.026(6) 0.045(7) 0.056(8) -0.040(6) -0.007(5) 0.010(5)
C14 0.040(7) 0.042(7) 0.040(7) -0.030(6) -0.016(5) 0.020(5)
C15 0.034(6) 0.056(7) 0.024(6) -0.024(5) -0.010(5) 0.017(5)
C16 0.032(6) 0.044(7) 0.025(6) -0.017(5) -0.003(5) 0.001(5)
C17 0.040(7) 0.081(10) 0.027(6) -0.029(7) 0.000(5) 0.015(7)
C18 0.037(7) 0.052(7) 0.023(6) -0.004(5) 0.003(5) 0.002(6)
C19 0.023(6) 0.045(7) 0.024(6) -0.011(5) -0.002(4) 0.005(5)
C20 0.037(6) 0.032(6) 0.018(5) -0.012(4) -0.010(4) 0.009(5)
C21 0.028(6) 0.030(6) 0.033(6) -0.010(5) -0.004(5) -0.005(4)
C22 0.049(8) 0.038(7) 0.024(6) 0.003(5) -0.006(5) -0.011(5)
C23 0.061(9) 0.061(9) 0.021(6) 0.007(6) -0.006(6) -0.014(7)
C24 0.106(13) 0.039(8) 0.037(8) 0.003(6) 0.002(8) -0.016(8)
C25 0.079(10) 0.019(6) 0.055(9) -0.008(5) 0.005(7) -0.011(6)
C26 0.045(7) 0.027(6) 0.037(7) -0.009(5) -0.003(5) 0.002(5)
C27 0.053(8) 0.016(5) 0.037(6) -0.010(5) -0.009(6) -0.003(5)
C28 0.024(5) 0.026(5) 0.030(6) -0.010(4) -0.002(4) -0.007(4)
C29 0.021(5) 0.021(5) 0.052(7) -0.017(5) -0.015(5) 0.008(4)
C30 0.033(6) 0.045(7) 0.036(6) -0.026(5) -0.002(5) 0.005(5)
C31 0.027(6) 0.051(7) 0.036(6) -0.027(6) 0.002(5) 0.001(5)
C32 0.026(6) 0.042(6) 0.030(6) -0.021(5) -0.003(5) -0.002(5)
C33 0.028(6) 0.028(5) 0.030(6) -0.014(4) -0.007(5) 0.005(4)
C34 0.025(6) 0.036(6) 0.033(6) -0.023(5) -0.010(5) 0.006(4)
C35 0.026(6) 0.025(5) 0.023(5) -0.009(4) 0.002(4) -0.011(4)
C36 0.029(6) 0.038(6) 0.029(6) -0.018(5) 0.000(5) -0.008(5)
C37 0.021(6) 0.052(7) 0.024(5) -0.019(5) -0.002(4) -0.002(5)
C38 0.018(5) 0.032(6) 0.025(5) -0.008(4) 0.003(4) -0.004(4)
C39 0.031(6) 0.018(5) 0.022(5) -0.010(4) -0.002(4) -0.002(4)
C40 0.023(5) 0.021(5) 0.019(5) -0.003(4) -0.002(4) 0.003(4)
C41 0.034(6) 0.029(6) 0.028(6) -0.017(4) 0.000(5) -0.004(4)
C42 0.033(6) 0.027(6) 0.042(7) -0.019(5) -0.004(5) 0.009(5)
C43 0.038(7) 0.022(5) 0.038(6) -0.009(5) -0.006(5) 0.009(5)
C44 0.041(7) 0.026(6) 0.047(7) -0.017(5) -0.005(6) -0.003(5)
C45 0.032(6) 0.039(6) 0.030(6) -0.021(5) 0.001(5) -0.007(5)
C46 0.025(6) 0.026(5) 0.036(6) -0.012(4) -0.008(5) -0.007(4)
C47 0.029(6) 0.032(6) 0.030(6) -0.017(5) 0.001(5) -0.002(5)
C48 0.021(5) 0.027(5) 0.031(6) -0.016(4) 0.001(4) 0.009(4)
C49 0.029(6) 0.028(5) 0.025(5) -0.013(4) -0.011(4) 0.009(4)
C50 0.038(7) 0.039(6) 0.026(6) -0.012(5) -0.007(5) 0.004(5)
C51 0.042(7) 0.038(6) 0.029(6) -0.013(5) 0.009(5) -0.002(5)
C52 0.042(7) 0.031(6) 0.033(6) -0.012(5) 0.004(5) 0.003(5)
C53 0.023(5) 0.036(6) 0.029(6) -0.019(5) 0.005(4) -0.005(4)
C54 0.028(6) 0.031(6) 0.035(6) -0.008(5) 0.015(5) -0.007(5)
C55 0.044(7) 0.022(5) 0.031(6) -0.013(4) -0.007(5) 0.005(5)
```

```
C56 0.037(7) 0.025(6) 0.030(6) -0.005(4) 0.000(5) -0.003(5)
C57 0.028(6) 0.034(6) 0.052(8) -0.008(5) -0.008(6) -0.005(5)
C58 0.046(7) 0.027(6) 0.027(6) 0.003(4) -0.011(5) -0.010(5)
C59 0.043(7) 0.018(5) 0.032(6) -0.005(4) -0.009(5) -0.002(5)
C60 0.025(6) 0.022(5) 0.030(6) -0.006(4) 0.000(4) -0.010(4)
C61 0.033(6) 0.027(5) 0.030(6) -0.012(4) -0.011(5) -0.005(4)
C62 0.034(7) 0.051(7) 0.042(7) -0.028(6) -0.016(5) 0.013(5)
C63 0.026(6) 0.088(10) 0.050(8) -0.046(7) -0.013(6) 0.008(6)
C64 0.038(7) 0.088(10) 0.045(8) -0.047(7) -0.013(6) 0.007(7)
C65 0.032(6) 0.043(6) 0.025(6) -0.018(5) 0.005(5) -0.004(5)
C66 0.025(6) 0.025(5) 0.027(5) -0.014(4) 0.001(4) -0.002(4)
C67 0.030(6) 0.013(5) 0.019(5) -0.001(4) 0.004(4) -0.001(4)
C68 0.035(6) 0.030(6) 0.024(5) -0.015(4) -0.007(5) 0.001(5)
C69 0.042(7) 0.015(5) 0.046(7) -0.014(5) -0.010(5) 0.013(5)
C70 0.048(8) 0.033(7) 0.057(8) -0.025(6) -0.019(6) 0.018(6)
C71 0.037(7) 0.049(7) 0.052(8) -0.025(6) -0.013(6) 0.005(6)
C72 0.024(6) 0.037(6) 0.033(6) -0.009(5) -0.011(5) 0.000(5)
C73 0.041(7) 0.030(6) 0.019(5) -0.011(4) -0.005(5) 0.003(5)
C74 0.023(6) 0.038(6) 0.032(6) -0.014(5) 0.008(5) -0.012(5)
C75 0.039(7) 0.032(6) 0.050(8) -0.016(5) 0.005(6) -0.010(5)
C76 0.041(8) 0.050(8) 0.064(9) -0.022(7) 0.006(7) -0.013(6)
C77 0.086(12) 0.042(8) 0.083(11) -0.032(8) 0.034(9) -0.033(8)
C78 0.066(10) 0.038(7) 0.067(10) -0.031(7) 0.012(8) -0.012(7)
C79 0.050(8) 0.036(7) 0.056(8) -0.021(6) 0.018(6) -0.020(6)
C80 0.025(6) 0.044(7) 0.040(7) -0.021(5) 0.000(5) -0.007(5)

_geom_special_details
;
 All esds (except the esd in the dihedral angle between two l.s. planes)
 are estimated using the full covariance matrix.  The cell esds are taken
 into account individually in the estimation of esds in distances, angles
 and torsion angles; correlations between esds in cell parameters are only
 used when they are defined by crystal symmetry.  An approximate (isotropic)
 treatment of cell esds is used for estimating esds involving l.s. planes.
;

loop_
 _geom_bond_atom_site_label_1
 _geom_bond_atom_site_label_2
 _geom_bond_distance
 _geom_bond_site_symmetry_2
 _geom_bond_publ_flag
U1 O1 1.769(7) . ?
U1 O2 1.774(7) . ?
U1 O3 2.233(7) . ?
U1 O4 2.387(6) . ?
U1 O8 2.463(6) . ?
U1 N1 2.540(8) . ?
U1 N2 2.540(8) . ?
U1 U2 3.8807(14) . ?
U2 O5 1.779(7) . ?
U2 O6 1.784(7) . ?
U2 O7 2.217(6) . ?
U2 O8 2.400(6) . ?
U2 O4 2.475(6) . ?
U2 N4 2.495(8) . ?
U2 N3 2.546(7) . ?
U3 O9 1.771(7) . ?
U3 O10 1.773(7) . ?
U3 O12 2.202(6) . ?
U3 O11 2.389(7) . ?
```

```
U3 O15 2.491(6) . ?
U3 N6 2.535(8) . ?
U3 N5 2.560(8) . ?
U3 U4 3.8718(19) . ?
U4 O13 1.779(7) . ?
U4 O14 1.784(6) . ?
U4 O16 2.207(7) . ?
U4 O15 2.392(7) . ?
U4 O11 2.445(6) . ?
U4 N7 2.512(7) . ?
U4 N8 2.524(9) . ?
O3 C1 1.320(11) . ?
O4 C20 1.356(11) . ?
O7 C21 1.321(11) . ?
O8 C40 1.366(11) . ?
O11 C41 1.370(11) . ?
O12 C60 1.335(12) . ?
O15 C61 1.360(11) . ?
O16 C80 1.299(12) . ?
N1 C7 1.298(13) . ?
N1 C8 1.406(13) . ?
N2 C14 1.273(13) . ?
N2 C13 1.456(14) . ?
N3 C27 1.302(12) . ?
N3 C28 1.410(12) . ?
N4 C34 1.289(12) . ?
N4 C33 1.450(12) . ?
N5 C47 1.269(12) . ?
N5 C48 1.438(12) . ?
N6 C54 1.277(13) . ?
N6 C53 1.434(13) . ?
N7 C67 1.295(12) . ?
N7 C68 1.432(12) . ?
N8 C74 1.298(12) . ?
N8 C73 1.431(12) . ?
C1 C2 1.411(15) . ?
C1 C6 1.405(14) . ?
C2 C3 1.376(15) . ?
C2 H2 0.9500 . ?
C3 C4 1.376(15) . ?
C3 H3 0.9500 . ?
C4 C5 1.372(16) . ?
C4 H4 0.9500 . ?
C5 C6 1.418(15) . ?
C5 H5 0.9500 . ?
C6 C7 1.432(16) . ?
C7 H7 0.9500 . ?
C8 C13 1.395(16) . ?
C8 C9 1.395(15) . ?
C9 C10 1.375(17) . ?
C9 H9 0.9500 . ?
C10 C11 1.361(19) . ?
C10 H10 0.9500 . ?
C11 C12 1.406(19) . ?
C11 H11 0.9500 . ?
C12 C13 1.403(15) . ?
C12 H12 0.9500 . ?
C14 C15 1.441(16) . ?
C14 H14 0.9500 . ?
C15 C16 1.402(14) . ?
C15 C20 1.419(14) . ?
```

```
C16 C17 1.375(17) . ?
C16 H16 0.9500 . ?
C17 C18 1.397(17) . ?
C17 H17 0.9500 . ?
C18 C19 1.377(14) . ?
C18 H18 0.9500 . ?
C19 C20 1.383(15) . ?
C19 H19 0.9500 . ?
C21 C22 1.401(14) . ?
C21 C26 1.423(14) . ?
C22 C23 1.371(15) . ?
C22 H22 0.9500 . ?
C23 C24 1.400(18) . ?
C23 H23 0.9500 . ?
C24 C25 1.371(18) . ?
C24 H24 0.9500 . ?
C25 C26 1.401(15) . ?
C25 H25 0.9500 . ?
C26 C27 1.436(15) . ?
C27 H27 0.9500 . ?
C28 C29 1.406(13) . ?
C28 C33 1.409(14) . ?
C29 C30 1.377(14) . ?
C29 H29 0.9500 . ?
C30 C31 1.385(15) . ?
C30 H30 0.9500 . ?
C31 C32 1.396(13) . ?
C31 H31 0.9500 . ?
C32 C33 1.387(13) . ?
C32 H32 0.9500 . ?
C34 C35 1.453(13) . ?
C34 H34 0.9500 . ?
C35 C36 1.405(14) . ?
C35 C40 1.421(13) . ?
C36 C37 1.367(13) . ?
C36 H36 0.9500 . ?
C37 C38 1.409(14) . ?
C37 H37 0.9500 . ?
C38 C39 1.358(13) . ?
C38 H38 0.9500 . ?
C39 C40 1.404(12) . ?
C39 H39 0.9500 . ?
C41 C42 1.378(14) . ?
C41 C46 1.406(13) . ?
C42 C43 1.372(14) . ?
C42 H42 0.9500 . ?
C43 C44 1.396(14) . ?
C43 H43 0.9500 . ?
C44 C45 1.383(15) . ?
C44 H44 0.9500 . ?
C45 C46 1.413(14) . ?
C45 H45 0.9500 . ?
C46 C47 1.457(14) . ?
C47 H47 0.9500 . ?
C48 C53 1.368(14) . ?
C48 C49 1.390(13) . ?
C49 C50 1.388(14) . ?
C49 H49 0.9500 . ?
C50 C51 1.384(16) . ?
C50 H50 0.9500 . ?
C51 C52 1.383(16) . ?
```

```
C51 H51 0.9500 . ?
C52 C53 1.398(14) . ?
C52 H52 0.9500 . ?
C54 C55 1.441(15) . ?
C54 H54 0.9500 . ?
C55 C60 1.432(14) . ?
C55 C56 1.419(15) . ?
C56 C57 1.383(15) . ?
C56 H56 0.9500 . ?
C57 C58 1.398(16) . ?
C57 H57 0.9500 . ?
C58 C59 1.379(15) . ?
C58 H58 0.9500 . ?
C59 C60 1.389(14) . ?
C59 H59 0.9500 . ?
C61 C62 1.394(14) . ?
C61 C66 1.417(13) . ?
C62 C63 1.374(15) . ?
C62 H62 0.9500 . ?
C63 C64 1.388(15) . ?
C63 H63 0.9500 . ?
C64 C65 1.367(15) . ?
C64 H64 0.9500 . ?
C65 C66 1.401(14) . ?
C65 H65 0.9500 . ?
C66 C67 1.461(13) . ?
C67 H67 0.9500 . ?
C68 C69 1.399(13) . ?
C68 C73 1.397(14) . ?
C69 C70 1.380(15) . ?
C69 H69 0.9500 . ?
C70 C71 1.371(16) . ?
C70 H70 0.9500 . ?
C71 C72 1.377(15) . ?
C71 H71 0.9500 . ?
C72 C73 1.375(14) . ?
C72 H72 0.9500 . ?
C74 C75 1.462(14) . ?
C74 H74 0.9500 . ?
C75 C80 1.410(15) . ?
C75 C76 1.408(16) . ?
C76 C77 1.366(17) . ?
C76 H76 0.9500 . ?
C77 C78 1.420(18) . ?
C77 H77 0.9500 . ?
C78 C79 1.369(16) . ?
C78 H78 0.9500 . ?
C79 C80 1.405(15) . ?
C79 H79 0.9500 . ?

loop_
 _geom_angle_atom_site_label_1
 _geom_angle_atom_site_label_2
 _geom_angle_atom_site_label_3
 _geom_angle
 _geom_angle_site_symmetry_1
 _geom_angle_site_symmetry_3
 _geom_angle_publ_flag
O1 U1 O2 175.9(3) . . ?
O1 U1 O3 91.4(3) . . ?
O2 U1 O3 90.8(3) . . ?
```

```
O1 U1 O4 89.3(3) . . ?
O2 U1 O4 90.3(3) . . ?
O3 U1 O4 152.9(2) . . ?
O1 U1 O8 94.1(3) . . ?
O2 U1 O8 89.6(3) . . ?
O3 U1 O8 83.2(2) . . ?
O4 U1 O8 69.7(2) . . ?
O1 U1 N1 83.2(3) . . ?
O2 U1 N1 94.3(3) . . ?
O3 U1 N1 70.7(3) . . ?
O4 U1 N1 136.2(2) . . ?
O8 U1 N1 153.6(2) . . ?
O1 U1 N2 87.0(3) . . ?
O2 U1 N2 89.0(3) . . ?
O3 U1 N2 134.5(3) . . ?
O4 U1 N2 72.7(2) . . ?
O8 U1 N2 142.3(2) . . ?
N1 U1 N2 63.9(3) . . ?
O1 U1 U2 105.9(2) . . ?
O2 U1 U2 76.1(2) . . ?
O3 U1 U2 116.81(16) . . ?
O4 U1 U2 37.83(14) . . ?
O8 U1 U2 36.51(14) . . ?
N1 U1 U2 167.49(19) . . ?
N2 U1 U2 107.28(19) . . ?
O5 U2 O6 175.5(3) . . ?
O5 U2 O7 89.3(3) . . ?
O6 U2 O7 92.4(3) . . ?
O5 U2 O8 86.7(3) . . ?
O6 U2 O8 93.7(3) . . ?
O7 U2 O8 152.1(2) . . ?
O5 U2 O4 96.2(3) . . ?
O6 U2 O4 88.1(3) . . ?
O7 U2 O4 83.7(2) . . ?
O8 U2 O4 69.3(2) . . ?
O5 U2 N4 86.4(3) . . ?
O6 U2 N4 89.5(3) . . ?
O7 U2 N4 135.0(2) . . ?
O8 U2 N4 72.3(2) . . ?
O4 U2 N4 141.3(2) . . ?
O5 U2 N3 87.7(3) . . ?
O6 U2 N3 88.9(3) . . ?
O7 U2 N3 70.9(2) . . ?
O8 U2 N3 136.4(2) . . ?
O4 U2 N3 154.3(2) . . ?
N4 U2 N3 64.1(3) . . ?
O5 U2 U1 105.4(2) . . ?
O6 U2 U1 77.4(2) . . ?
O7 U2 U1 118.44(16) . . ?
O8 U2 U1 37.63(15) . . ?
O4 U2 U1 36.26(15) . . ?
N4 U2 U1 105.85(18) . . ?
N3 U2 U1 163.40(18) . . ?
O9 U3 O10 175.4(3) . . ?
O9 U3 O12 88.6(3) . . ?
O10 U3 O12 93.0(3) . . ?
O9 U3 O11 85.4(3) . . ?
O10 U3 O11 94.8(3) . . ?
O12 U3 O11 156.3(2) . . ?
O9 U3 O15 97.7(3) . . ?
O10 U3 O15 86.7(3) . . ?
```

```
O12 U3 O15 89.0(2) . . ?
O11 U3 O15 69.2(2) . . ?
O9 U3 N6 87.4(3) . . ?
O10 U3 N6 89.1(3) . . ?
O12 U3 N6 69.5(3) . . ?
O11 U3 N6 132.9(2) . . ?
O15 U3 N6 157.8(2) . . ?
O9 U3 N5 89.0(3) . . ?
O10 U3 N5 86.8(3) . . ?
O12 U3 N5 132.5(3) . . ?
O11 U3 N5 70.4(2) . . ?
O15 U3 N5 138.2(2) . . ?
N6 U3 N5 63.0(3) . . ?
O9 U3 U4 105.7(2) . . ?
O10 U3 U4 77.0(2) . . ?
O12 U3 U4 124.35(18) . . ?
O11 U3 U4 37.28(15) . . ?
O15 U3 U4 36.66(15) . . ?
N6 U3 U4 160.3(2) . . ?
N5 U3 U4 101.85(19) . . ?
O13 U4 O14 175.5(3) . . ?
O13 U4 O16 89.8(3) . . ?
O14 U4 O16 92.4(3) . . ?
O13 U4 O15 88.5(3) . . ?
O14 U4 O15 91.3(3) . . ?
O16 U4 O15 151.4(2) . . ?
O13 U4 O11 95.6(3) . . ?
O14 U4 O11 88.5(3) . . ?
O16 U4 O11 81.9(2) . . ?
O15 U4 O11 69.9(2) . . ?
O13 U4 N7 87.4(3) . . ?
O14 U4 N7 88.3(3) . . ?
O16 U4 N7 134.9(3) . . ?
O15 U4 N7 73.5(2) . . ?
O11 U4 N7 143.2(2) . . ?
O13 U4 N8 88.1(3) . . ?
O14 U4 N8 89.0(3) . . ?
O16 U4 N8 70.7(3) . . ?
O15 U4 N8 137.7(2) . . ?
O11 U4 N8 152.4(2) . . ?
N7 U4 N8 64.2(3) . . ?
O13 U4 U3 106.7(2) . . ?
O14 U4 U3 75.7(2) . . ?
O16 U4 U3 115.97(18) . . ?
O15 U4 U3 38.45(14) . . ?
O11 U4 U3 36.28(15) . . ?
N7 U4 U3 107.90(18) . . ?
N8 U4 U3 163.29(18) . . ?
C1 O3 U1 127.8(6) . . ?
C20 O4 U1 127.6(5) . . ?
C20 O4 U2 122.6(6) . . ?
U1 O4 U2 105.9(2) . . ?
C21 O7 U2 135.8(6) . . ?
C40 O8 U2 123.9(5) . . ?
C40 O8 U1 125.5(5) . . ?
U2 O8 U1 105.9(2) . . ?
C41 O11 U3 125.4(6) . . ?
C41 O11 U4 125.0(6) . . ?
U3 O11 U4 106.4(2) . . ?
C60 O12 U3 130.4(6) . . ?
C61 O15 U4 124.2(6) . . ?
```

```
C61 O15 U3 126.7(6) . . ?
U4 O15 U3 104.9(2) . . ?
C80 O16 U4 132.1(7) . . ?
C7 N1 C8 119.1(9) . . ?
C7 N1 U1 123.1(7) . . ?
C8 N1 U1 117.4(6) . . ?
C14 N2 C13 118.0(9) . . ?
C14 N2 U1 126.8(8) . . ?
C13 N2 U1 115.0(7) . . ?
C27 N3 C28 118.6(8) . . ?
C27 N3 U2 124.6(7) . . ?
C28 N3 U2 116.3(6) . . ?
C34 N4 C33 117.1(8) . . ?
C34 N4 U2 125.6(6) . . ?
C33 N4 U2 116.3(6) . . ?
C47 N5 C48 119.8(8) . . ?
C47 N5 U3 127.2(7) . . ?
C48 N5 U3 112.9(6) . . ?
C54 N6 C53 121.6(9) . . ?
C54 N6 U3 125.6(7) . . ?
C53 N6 U3 112.8(6) . . ?
C67 N7 C68 117.9(8) . . ?
C67 N7 U4 124.9(6) . . ?
C68 N7 U4 116.6(6) . . ?
C74 N8 C73 116.1(9) . . ?
C74 N8 U4 125.1(7) . . ?
C73 N8 U4 117.6(6) . . ?
O3 C1 C2 120.2(9) . . ?
O3 C1 C6 121.3(10) . . ?
C2 C1 C6 118.5(10) . . ?
C3 C2 C1 120.3(10) . . ?
C3 C2 H2 119.8 . . ?
C1 C2 H2 119.8 . . ?
C2 C3 C4 122.4(11) . . ?
C2 C3 H3 118.8 . . ?
C4 C3 H3 118.8 . . ?
C5 C4 C3 117.4(11) . . ?
C5 C4 H4 121.3 . . ?
C3 C4 H4 121.3 . . ?
C4 C5 C6 123.1(11) . . ?
C4 C5 H5 118.5 . . ?
C6 C5 H5 118.5 . . ?
C1 C6 C7 123.3(10) . . ?
C1 C6 C5 117.9(11) . . ?
C7 C6 C5 118.7(10) . . ?
N1 C7 C6 126.2(9) . . ?
N1 C7 H7 116.9 . . ?
C6 C7 H7 116.9 . . ?
C13 C8 N1 116.9(10) . . ?
C13 C8 C9 120.5(11) . . ?
N1 C8 C9 122.6(11) . . ?
C10 C9 C8 119.1(12) . . ?
C10 C9 H9 120.4 . . ?
C8 C9 H9 120.4 . . ?
C11 C10 C9 120.9(12) . . ?
C11 C10 H10 119.6 . . ?
C9 C10 H10 119.6 . . ?
C10 C11 C12 121.9(12) . . ?
C10 C11 H11 119.0 . . ?
C12 C11 H11 119.0 . . ?
C13 C12 C11 117.3(13) . . ?
```

```
C13 C12 H12 121.4 . . ?
C11 C12 H12 121.4 . . ?
C8 C13 C12 120.3(11) . . ?
C8 C13 N2 116.9(10) . . ?
C12 C13 N2 122.8(11) . . ?
N2 C14 C15 127.9(10) . . ?
N2 C14 H14 116.0 . . ?
C15 C14 H14 116.0 . . ?
C16 C15 C20 119.4(11) . . ?
C16 C15 C14 114.1(10) . . ?
C20 C15 C14 126.5(10) . . ?
C17 C16 C15 121.2(11) . . ?
C17 C16 H16 119.4 . . ?
C15 C16 H16 119.4 . . ?
C16 C17 C18 118.7(11) . . ?
C16 C17 H17 120.6 . . ?
C18 C17 H17 120.6 . . ?
C19 C18 C17 120.7(12) . . ?
C19 C18 H18 119.7 . . ?
C17 C18 H18 119.7 . . ?
C20 C19 C18 121.6(11) . . ?
C20 C19 H19 119.2 . . ?
C18 C19 H19 119.2 . . ?
O4 C20 C19 121.9(9) . . ?
O4 C20 C15 119.9(10) . . ?
C19 C20 C15 118.1(9) . . ?
O7 C21 C22 121.2(9) . . ?
O7 C21 C26 121.4(9) . . ?
C22 C21 C26 117.4(10) . . ?
C23 C22 C21 121.6(11) . . ?
C23 C22 H22 119.2 . . ?
C21 C22 H22 119.2 . . ?
C22 C23 C24 121.5(12) . . ?
C22 C23 H23 119.3 . . ?
C24 C23 H23 119.3 . . ?
C25 C24 C23 117.7(11) . . ?
C25 C24 H24 121.2 . . ?
C23 C24 H24 121.2 . . ?
C24 C25 C26 122.5(12) . . ?
C24 C25 H25 118.7 . . ?
C26 C25 H25 118.7 . . ?
C25 C26 C21 119.3(11) . . ?
C25 C26 C27 118.4(10) . . ?
C21 C26 C27 121.9(9) . . ?
N3 C27 C26 128.2(9) . . ?
N3 C27 H27 115.9 . . ?
C26 C27 H27 115.9 . . ?
N3 C28 C29 124.9(9) . . ?
N3 C28 C33 116.6(8) . . ?
C29 C28 C33 118.4(9) . . ?
C30 C29 C28 120.5(10) . . ?
C30 C29 H29 119.7 . . ?
C28 C29 H29 119.7 . . ?
C29 C30 C31 120.2(9) . . ?
C29 C30 H30 119.9 . . ?
C31 C30 H30 119.9 . . ?
C30 C31 C32 120.8(10) . . ?
C30 C31 H31 119.6 . . ?
C32 C31 H31 119.6 . . ?
C33 C32 C31 119.1(10) . . ?
C33 C32 H32 120.5 . . ?
```

```
C31 C32 H32 120.5 . . ?
C32 C33 C28 120.9(9) . . ?
C32 C33 N4 123.1(9) . . ?
C28 C33 N4 116.0(9) . . ?
N4 C34 C35 127.2(9) . . ?
N4 C34 H34 116.4 . . ?
C35 C34 H34 116.4 . . ?
C36 C35 C40 119.1(9) . . ?
C36 C35 C34 116.4(8) . . ?
C40 C35 C34 124.5(9) . . ?
C37 C36 C35 123.4(9) . . ?
C37 C36 H36 118.3 . . ?
C35 C36 H36 118.3 . . ?
C36 C37 C38 116.5(9) . . ?
C36 C37 H37 121.8 . . ?
C38 C37 H37 121.8 . . ?
C39 C38 C37 122.1(9) . . ?
C39 C38 H38 119.0 . . ?
C37 C38 H38 119.0 . . ?
C38 C39 C40 121.9(9) . . ?
C38 C39 H39 119.0 . . ?
C40 C39 H39 119.0 . . ?
O8 C40 C39 121.2(8) . . ?
O8 C40 C35 121.7(8) . . ?
C39 C40 C35 117.0(9) . . ?
O11 C41 C42 121.5(8) . . ?
O11 C41 C46 119.7(9) . . ?
C42 C41 C46 118.8(9) . . ?
C43 C42 C41 122.0(10) . . ?
C43 C42 H42 119.0 . . ?
C41 C42 H42 119.0 . . ?
C42 C43 C44 120.6(11) . . ?
C42 C43 H43 119.7 . . ?
C44 C43 H43 119.7 . . ?
C45 C44 C43 118.3(10) . . ?
C45 C44 H44 120.9 . . ?
C43 C44 H44 120.9 . . ?
C44 C45 C46 121.6(9) . . ?
C44 C45 H45 119.2 . . ?
C46 C45 H45 119.2 . . ?
C41 C46 C45 118.5(10) . . ?
C41 C46 C47 125.2(9) . . ?
C45 C46 C47 116.2(9) . . ?
N5 C47 C46 126.4(9) . . ?
N5 C47 H47 116.8 . . ?
C46 C47 H47 116.8 . . ?
C53 C48 C49 120.7(10) . . ?
C53 C48 N5 116.3(9) . . ?
C49 C48 N5 123.0(9) . . ?
C50 C49 C48 119.5(10) . . ?
C50 C49 H49 120.3 . . ?
C48 C49 H49 120.3 . . ?
C49 C50 C51 119.8(10) . . ?
C49 C50 H50 120.1 . . ?
C51 C50 H50 120.1 . . ?
C52 C51 C50 120.4(11) . . ?
C52 C51 H51 119.8 . . ?
C50 C51 H51 119.8 . . ?
C51 C52 C53 119.4(11) . . ?
C51 C52 H52 120.3 . . ?
C53 C52 H52 120.3 . . ?
```

```
C48 C53 C52 119.9(10) . . ?
C48 C53 N6 117.3(9) . . ?
C52 C53 N6 122.7(9) . . ?
N6 C54 C55 125.4(10) . . ?
N6 C54 H54 117.3 . . ?
C55 C54 H54 117.3 . . ?
C60 C55 C56 119.0(10) . . ?
C60 C55 C54 121.6(10) . . ?
C56 C55 C54 119.2(9) . . ?
C57 C56 C55 119.8(10) . . ?
C57 C56 H56 120.1 . . ?
C55 C56 H56 120.1 . . ?
C56 C57 C58 120.8(11) . . ?
C56 C57 H57 119.6 . . ?
C58 C57 H57 119.6 . . ?
C59 C58 C57 119.6(11) . . ?
C59 C58 H58 120.2 . . ?
C57 C58 H58 120.2 . . ?
C60 C59 C58 121.8(10) . . ?
C60 C59 H59 119.1 . . ?
C58 C59 H59 119.1 . . ?
O12 C60 C59 121.5(9) . . ?
O12 C60 C55 119.8(9) . . ?
C59 C60 C55 118.7(10) . . ?
O15 C61 C62 120.0(9) . . ?
O15 C61 C66 122.4(9) . . ?
C62 C61 C66 117.6(9) . . ?
C63 C62 C61 121.1(10) . . ?
C63 C62 H62 119.5 . . ?
C61 C62 H62 119.5 . . ?
C64 C63 C62 122.2(11) . . ?
C64 C63 H63 118.9 . . ?
C62 C63 H63 118.9 . . ?
C65 C64 C63 117.1(11) . . ?
C65 C64 H64 121.5 . . ?
C63 C64 H64 121.5 . . ?
C64 C65 C66 122.9(10) . . ?
C64 C65 H65 118.5 . . ?
C66 C65 H65 118.5 . . ?
C65 C66 C61 119.1(9) . . ?
C65 C66 C67 115.9(8) . . ?
C61 C66 C67 125.0(9) . . ?
N7 C67 C66 127.7(9) . . ?
N7 C67 H67 116.1 . . ?
C66 C67 H67 116.1 . . ?
C69 C68 C73 118.7(10) . . ?
C69 C68 N7 123.6(9) . . ?
C73 C68 N7 117.6(8) . . ?
C68 C69 C70 119.4(11) . . ?
C68 C69 H69 120.3 . . ?
C70 C69 H69 120.3 . . ?
C71 C70 C69 121.7(10) . . ?
C71 C70 H70 119.1 . . ?
C69 C70 H70 119.1 . . ?
C70 C71 C72 118.8(11) . . ?
C70 C71 H71 120.6 . . ?
C72 C71 H71 120.6 . . ?
C73 C72 C71 121.2(10) . . ?
C73 C72 H72 119.4 . . ?
C71 C72 H72 119.4 . . ?
C72 C73 C68 120.0(9) . . ?
```

```
C72 C73 N8 124.5(10) . . ?
C68 C73 N8 115.4(9) . . ?
N8 C74 C75 124.3(9) . . ?
N8 C74 H74 117.8 . . ?
C75 C74 H74 117.8 . . ?
C80 C75 C76 119.5(10) . . ?
C80 C75 C74 122.7(10) . . ?
C76 C75 C74 117.6(10) . . ?
C77 C76 C75 121.7(12) . . ?
C77 C76 H76 119.2 . . ?
C75 C76 H76 119.2 . . ?
C76 C77 C78 118.1(12) . . ?
C76 C77 H77 121.0 . . ?
C78 C77 H77 121.0 . . ?
C79 C78 C77 121.2(11) . . ?
C79 C78 H78 119.4 . . ?
C77 C78 H78 119.4 . . ?
C78 C79 C80 120.7(11) . . ?
C78 C79 H79 119.6 . . ?
C80 C79 H79 119.6 . . ?
O16 C80 C75 121.9(10) . . ?
O16 C80 C79 119.6(10) . . ?
C75 C80 C79 118.5(10) . . ?

_diffrn_measured_fraction_theta_max    0.963
_diffrn_reflns_theta_full              27.48
_diffrn_measured_fraction_theta_full   0.963
_refine_diff_density_max    1.726
_refine_diff_density_min   -2.211
_refine_diff_density_rms    0.223
```

Appendix C

Crystallographic Information of $[U^{VI}O_2(saloph)]_2 \cdot 0.5CH_2Cl_2$

```
data_shelxl

_audit_creation_method            SHELXL-97
_chemical_name_systematic
;
 ?
;
_chemical_name_common             ?
_chemical_melting_point           ?
_chemical_formula_moiety          ?
_chemical_formula_sum
 'C40.50 H29 Cl N4 O8 U2'
_chemical_formula_weight          1211.19

loop_
 _atom_type_symbol
 _atom_type_description
 _atom_type_scat_dispersion_real
 _atom_type_scat_dispersion_imag
 _atom_type_scat_source
 'C'  'C'   0.0033   0.0016
 'International Tables Vol C Tables 4.2.6.8 and 6.1.1.4'
 'H'  'H'   0.0000   0.0000
 'International Tables Vol C Tables 4.2.6.8 and 6.1.1.4'
 'Cl'  'Cl'   0.1484   0.1585
 'International Tables Vol C Tables 4.2.6.8 and 6.1.1.4'
 'N'  'N'   0.0061   0.0033
 'International Tables Vol C Tables 4.2.6.8 and 6.1.1.4'
 'O'  'O'   0.0106   0.0060
 'International Tables Vol C Tables 4.2.6.8 and 6.1.1.4'
 'U'  'U'  -9.6767   9.6646
 'International Tables Vol C Tables 4.2.6.8 and 6.1.1.4'

_symmetry_cell_setting             triclinic
_symmetry_space_group_name_H-M    'P -1'

loop_
 _symmetry_equiv_pos_as_xyz
 'x, y, z'
 '-x, -y, -z'
```

```
_cell_length_a                    15.717(5)
_cell_length_b                    15.993(7)
_cell_length_c                    17.619(5)
_cell_angle_alpha                 67.45(3)
_cell_angle_beta                  77.99(3)
_cell_angle_gamma                 81.66(3)
_cell_volume                      3990(2)
_cell_formula_units_Z             4
_cell_measurement_temperature     93(2)
_cell_measurement_reflns_used     35412
_cell_measurement_theta_min       3.0
_cell_measurement_theta_max       27.5

_exptl_crystal_description       'block'
_exptl_crystal_colour            'red'
_exptl_crystal_size_max           0.16
_exptl_crystal_size_mid           0.11
_exptl_crystal_size_min           0.06
_exptl_crystal_density_meas       ?
_exptl_crystal_density_diffrn     2.016
_exptl_crystal_density_method     'not measured'
_exptl_crystal_F_000              2260
_exptl_absorpt_coefficient_mu     8.230
_exptl_absorpt_correction_type    multi-scan
_exptl_absorpt_correction_T_min   0.3526
_exptl_absorpt_correction_T_max   0.6380
_exptl_absorpt_process_details
;
    Higashi, T. (1995). Program for Absorption Correction.
    Rigaku Corporation, Tokyo, Japan.
;

_diffrn_ambient_temperature       93(2)
_diffrn_radiation_wavelength      0.71075
_diffrn_radiation_type            MoK¥a
_diffrn_radiation_source          'fine-focus sealed tube'
_diffrn_radiation_monochromator   graphite
_diffrn_measurement_device_type  'Rigaku RAXIS-RAPID'
_diffrn_measurement_method        ¥w
_diffrn_detector_area_resol_mean  10.00
_diffrn_reflns_number             37695
_diffrn_reflns_av_R_equivalents   0.0695
_diffrn_reflns_av_sigmaI/netI     0.0811
_diffrn_reflns_limit_h_min        -20
_diffrn_reflns_limit_h_max        18
_diffrn_reflns_limit_k_min        -20
_diffrn_reflns_limit_k_max        20
_diffrn_reflns_limit_l_min        -22
_diffrn_reflns_limit_l_max        22
_diffrn_reflns_theta_min          3.01
_diffrn_reflns_theta_max          27.48
_reflns_number_total              17850
_reflns_number_gt                 12487
_reflns_threshold_expression      >2sigma(I)

_computing_data_collection        'PROCESS-AUTO'
_computing_cell_refinement        'PROCESS-AUTO'
_computing_data_reduction         'CrystalStructure'
_computing_structure_solution     'DIRDIF99 (PATTY)'
_computing_structure_refinement   'SHELXL-97 (Sheldrick, 1997)'
```

```
_computing_molecular_graphics     ?
_computing_publication_material   ?

_refine_special_details
;
 Refinement of F^2^ against ALL reflections.  The weighted R-factor wR and
 goodness of fit S are based on F^2^, conventional R-factors R are based
 on F, with F set to zero for negative F^2^. The threshold expression of
 F^2^ > 2sigma(F^2^) is used only for calculating R-factors(gt) etc. and is
 not relevant to the choice of reflections for refinement.  R-factors based
 on F^2^ are statistically about twice as large as those based on F, and R-
 factors based on ALL data will be even larger.
;

_refine_ls_structure_factor_coef  Fsqd
_refine_ls_matrix_type            full
_refine_ls_weighting_scheme       calc
_refine_ls_weighting_details
 'calc w=1/[¥s^2^(Fo^2^)+(0.0396P)^2^+60.3343P] where P=(Fo^2^+2Fc^2^)/3'
_atom_sites_solution_primary      direct
_atom_sites_solution_secondary    difmap
_atom_sites_solution_hydrogens    geom
_refine_ls_hydrogen_treatment     mixed
_refine_ls_extinction_method      none
_refine_ls_extinction_coef        ?
_refine_ls_number_reflns          17850
_refine_ls_number_parameters      1001
_refine_ls_number_restraints      0
_refine_ls_R_factor_all           0.0978
_refine_ls_R_factor_gt            0.0594
_refine_ls_wR_factor_ref          0.1297
_refine_ls_wR_factor_gt           0.1161
_refine_ls_goodness_of_fit_ref    1.031
_refine_ls_restrained_S_all       1.031
_refine_ls_shift/su_max           0.002
_refine_ls_shift/su_mean          0.000

loop_
 _atom_site_label
 _atom_site_type_symbol
 _atom_site_fract_x
 _atom_site_fract_y
 _atom_site_fract_z
 _atom_site_U_iso_or_equiv
 _atom_site_adp_type
 _atom_site_occupancy
 _atom_site_symmetry_multiplicity
 _atom_site_calc_flag
 _atom_site_refinement_flags
 _atom_site_disorder_assembly
 _atom_site_disorder_group
U1 U 0.21155(3) 0.32362(3) 0.45371(2) 0.02468(10) Uani 1 1 d . . .
U2 U 0.25921(3) 0.06733(3) 0.49028(2) 0.02631(10) Uani 1 1 d . . .
U3 U 0.92726(3) 0.80556(3) -0.03910(2) 0.02528(10) Uani 1 1 d . . .
U4 U 0.69478(3) 0.76228(3) 0.08847(2) 0.02426(10) Uani 1 1 d . . .
Cl1 Cl 0.6139(5) 0.4816(5) 0.4182(5) 0.133(2) Uani 1 1 d . . .
Cl2 Cl 0.6739(4) 0.3577(4) 0.5695(4) 0.1093(19) Uani 1 1 d . . .
O1 O 0.3146(5) 0.3708(5) 0.4166(4) 0.0295(17) Uani 1 1 d . . .
O2 O 0.1074(5) 0.2803(5) 0.4977(5) 0.0314(17) Uani 1 1 d . . .
O3 O 0.2876(5) 0.1883(5) 0.5357(4) 0.0252(16) Uani 1 1 d . . .
O4 O 0.1663(5) 0.4138(5) 0.3357(4) 0.0331(18) Uani 1 1 d . . .
```

```
O5 O 0.3684(5) 0.0555(5) 0.4424(4) 0.0310(17) Uani 1 1 d . . .
O6 O 0.1480(5) 0.0747(5) 0.5339(5) 0.0331(18) Uani 1 1 d . . .
O7 O 0.2451(5) 0.2139(5) 0.3823(4) 0.0279(17) Uani 1 1 d . . .
O8 O 0.2897(5) -0.0242(5) 0.6158(5) 0.0335(18) Uani 1 1 d . . .
O9 O 0.9974(4) 0.7198(5) 0.0215(5) 0.0284(16) Uani 1 1 d . . .
O10 O 0.8605(5) 0.8885(5) -0.1057(4) 0.0280(16) Uani 1 1 d . . .
O11 O 1.0091(5) 0.9067(5) -0.0395(5) 0.0309(17) Uani 1 1 d . . .
O12 O 0.8207(5) 0.6949(5) 0.0187(4) 0.0238(15) Uani 1 1 d . . .
O13 O 0.7076(4) 0.6888(5) 0.1917(4) 0.0251(16) Uani 1 1 d . . .
O14 O 0.6779(4) 0.8406(5) -0.0114(4) 0.0264(16) Uani 1 1 d . . .
O15 O 0.6269(5) 0.6565(5) 0.0767(4) 0.0331(18) Uani 1 1 d . . .
O16 O 0.8235(4) 0.8309(5) 0.0795(4) 0.0257(16) Uani 1 1 d . . .
N1 N 0.2194(6) 0.3410(6) 0.5875(6) 0.029(2) Uani 1 1 d . . .
N2 N 0.1487(6) 0.4743(6) 0.4665(5) 0.031(2) Uani 1 1 d . . .
N3 N 0.2131(7) 0.0426(7) 0.3710(7) 0.039(2) Uani 1 1 d . . .
N4 N 0.2573(6) -0.0964(7) 0.5048(6) 0.037(2) Uani 1 1 d . . .
N5 N 0.9384(5) 0.7167(6) -0.1337(5) 0.0237(19) Uani 1 1 d . . .
N6 N 1.0515(6) 0.8345(6) -0.1614(6) 0.029(2) Uani 1 1 d . . .
N7 N 0.5338(6) 0.7785(6) 0.1441(5) 0.027(2) Uani 1 1 d . . .
N8 N 0.6472(6) 0.8882(6) 0.1448(5) 0.0257(19) Uani 1 1 d . . .
C1 C 0.3576(7) 0.1876(7) 0.5702(6) 0.029(2) Uani 1 1 d . . .
C2 C 0.4293(7) 0.1262(7) 0.5674(6) 0.027(2) Uani 1 1 d . . .
H2 H 0.4302 0.0856 0.5395 0.033 Uiso 1 1 calc R . .
C3 C 0.4996(8) 0.1234(8) 0.6048(7) 0.034(3) Uani 1 1 d . . .
H3 H 0.5477 0.0807 0.6024 0.041 Uiso 1 1 calc R . .
C4 C 0.5010(7) 0.1828(8) 0.6465(6) 0.028(2) Uani 1 1 d . . .
H4 H 0.5499 0.1819 0.6706 0.034 Uiso 1 1 calc R . .
C5 C 0.4285(7) 0.2424(8) 0.6509(7) 0.030(2) Uani 1 1 d . . .
H5 H 0.4276 0.2818 0.6800 0.036 Uiso 1 1 calc R . .
C6 C 0.3564(7) 0.2464(8) 0.6137(7) 0.031(2) Uani 1 1 d . . .
C7 C 0.2852(7) 0.3108(7) 0.6271(6) 0.027(2) Uani 1 1 d . . .
H7 H 0.2870 0.3333 0.6693 0.033 Uiso 1 1 calc R . .
C8 C 0.1555(7) 0.4031(7) 0.6134(6) 0.027(2) Uani 1 1 d . . .
C9 C 0.1316(8) 0.3958(9) 0.6952(8) 0.039(3) Uani 1 1 d . . .
H9 H 0.1563 0.3474 0.7378 0.047 Uiso 1 1 calc R . .
C10 C 0.0717(8) 0.4593(9) 0.7148(8) 0.042(3) Uani 1 1 d . . .
H10 H 0.0554 0.4548 0.7712 0.051 Uiso 1 1 calc R . .
C11 C 0.0343(8) 0.5307(9) 0.6522(8) 0.043(3) Uani 1 1 d . . .
H11 H -0.0056 0.5754 0.6659 0.052 Uiso 1 1 calc R . .
C12 C 0.0558(8) 0.5355(8) 0.5712(7) 0.035(3) Uani 1 1 d . . .
H12 H 0.0280 0.5817 0.5294 0.042 Uiso 1 1 calc R . .
C13 C 0.1194(8) 0.4721(8) 0.5493(7) 0.034(3) Uani 1 1 d . . .
C14 C 0.1500(8) 0.5524(8) 0.4060(8) 0.038(3) Uani 1 1 d . . .
H14 H 0.1378 0.6043 0.4213 0.045 Uiso 1 1 calc R . .
C15 C 0.1679(8) 0.5696(8) 0.3178(7) 0.038(3) Uani 1 1 d . . .
C16 C 0.1743(10) 0.6597(9) 0.2640(8) 0.052(4) Uani 1 1 d . . .
H16 H 0.1712 0.7062 0.2858 0.062 Uiso 1 1 calc R . .
C17 C 0.1853(11) 0.6813(11) 0.1788(9) 0.065(4) Uani 1 1 d . . .
H17 H 0.1899 0.7428 0.1422 0.078 Uiso 1 1 calc R . .
C18 C 0.1897(10) 0.6147(10) 0.1468(8) 0.057(4) Uani 1 1 d . . .
H18 H 0.1956 0.6305 0.0883 0.068 Uiso 1 1 calc R . .
C19 C 0.1856(9) 0.5240(9) 0.1993(7) 0.045(3) Uani 1 1 d . . .
H19 H 0.1909 0.4785 0.1761 0.054 Uiso 1 1 calc R . .
C20 C 0.1739(8) 0.4991(8) 0.2853(7) 0.035(3) Uani 1 1 d . . .
C21 C 0.2750(7) 0.2357(8) 0.3002(6) 0.030(3) Uani 1 1 d . . .
C22 C 0.3155(7) 0.3167(9) 0.2548(7) 0.036(3) Uani 1 1 d . . .
H22 H 0.3252 0.3532 0.2835 0.044 Uiso 1 1 calc R . .
C23 C 0.3417(8) 0.3454(10) 0.1690(7) 0.043(3) Uani 1 1 d . . .
H23 H 0.3704 0.4000 0.1400 0.052 Uiso 1 1 calc R . .
C24 C 0.3261(9) 0.2946(12) 0.1261(8) 0.055(4) Uani 1 1 d . . .
H24 H 0.3427 0.3147 0.0672 0.066 Uiso 1 1 calc R . .
```

```
C25 C 0.2867(8) 0.2152(10) 0.1686(8) 0.044(4) Uani 1 1 d . . .
H25 H 0.2749 0.1812 0.1384 0.052 Uiso 1 1 calc R . .
C26 C 0.2627(8) 0.1817(10) 0.2573(8) 0.043(3) Uani 1 1 d . . .
C27 C 0.2264(9) 0.0954(11) 0.2931(9) 0.050(4) Uani 1 1 d . . .
H27 H 0.2099 0.0741 0.2552 0.060 Uiso 1 1 calc R . .
C28 C 0.1757(8) -0.0420(10) 0.3928(9) 0.048(3) Uani 1 1 d . . .
C29 C 0.1164(10) -0.0537(11) 0.3496(11) 0.063(5) Uani 1 1 d . . .
H29 H 0.0993 -0.0047 0.3028 0.075 Uiso 1 1 calc R . .
C30 C 0.0819(10) -0.1386(12) 0.3760(13) 0.076(6) Uani 1 1 d . . .
H30 H 0.0415 -0.1468 0.3465 0.091 Uiso 1 1 calc R . .
C31 C 0.1059(9) -0.2099(12) 0.4437(12) 0.069(5) Uani 1 1 d . . .
H31 H 0.0819 -0.2668 0.4611 0.083 Uiso 1 1 calc R . .
C32 C 0.1649(8) -0.1987(9) 0.4863(10) 0.050(4) Uani 1 1 d . . .
H32 H 0.1814 -0.2477 0.5334 0.060 Uiso 1 1 calc R . .
C33 C 0.2009(7) -0.1140(9) 0.4597(9) 0.041(3) Uani 1 1 d . . .
C34 C 0.3101(8) -0.1609(9) 0.5432(8) 0.041(3) Uani 1 1 d . . .
H34 H 0.3111 -0.2172 0.5364 0.049 Uiso 1 1 calc R . .
C35 C 0.3676(8) -0.1568(7) 0.5953(7) 0.035(3) Uani 1 1 d . . .
C36 C 0.4381(8) -0.2216(8) 0.6125(8) 0.039(3) Uani 1 1 d . . .
H36 H 0.4469 -0.2674 0.5892 0.047 Uiso 1 1 calc R . .
C37 C 0.4951(8) -0.2213(9) 0.6620(8) 0.043(3) Uani 1 1 d . . .
H37 H 0.5446 -0.2636 0.6699 0.052 Uiso 1 1 calc R . .
C38 C 0.4785(8) -0.1584(8) 0.7000(8) 0.039(3) Uani 1 1 d . . .
H38 H 0.5157 -0.1594 0.7365 0.047 Uiso 1 1 calc R . .
C39 C 0.4097(8) -0.0947(8) 0.6864(7) 0.040(3) Uani 1 1 d . . .
H39 H 0.3995 -0.0532 0.7146 0.048 Uiso 1 1 calc R . .
C40 C 0.3537(7) -0.0890(7) 0.6319(6) 0.029(2) Uani 1 1 d . . .
C41 C 0.8401(7) 0.6055(8) 0.0349(7) 0.030(2) Uani 1 1 d . . .
C42 C 0.8141(8) 0.5404(8) 0.1144(7) 0.037(3) Uani 1 1 d . . .
H42 H 0.7853 0.5598 0.1585 0.044 Uiso 1 1 calc R . .
C43 C 0.8301(8) 0.4487(8) 0.1290(8) 0.041(3) Uani 1 1 d . . .
H43 H 0.8131 0.4060 0.1835 0.049 Uiso 1 1 calc R . .
C44 C 0.8711(8) 0.4171(8) 0.0650(7) 0.037(3) Uani 1 1 d . . .
H44 H 0.8802 0.3540 0.0751 0.045 Uiso 1 1 calc R . .
C45 C 0.8975(7) 0.4801(7) -0.0121(7) 0.029(2) Uani 1 1 d . . .
H45 H 0.9261 0.4595 -0.0555 0.035 Uiso 1 1 calc R . .
C46 C 0.8842(7) 0.5733(8) -0.0298(7) 0.029(2) Uani 1 1 d . . .
C47 C 0.9208(7) 0.6332(8) -0.1122(6) 0.028(2) Uani 1 1 d . . .
H47 H 0.9331 0.6087 -0.1550 0.034 Uiso 1 1 calc R . .
C48 C 0.9714(7) 0.7652(7) -0.2198(6) 0.025(2) Uani 1 1 d . . .
C49 C 0.9451(7) 0.7558(8) -0.2861(6) 0.032(3) Uani 1 1 d . . .
H49 H 0.9058 0.7118 -0.2770 0.038 Uiso 1 1 calc R . .
C50 C 0.9780(8) 0.8131(9) -0.3673(7) 0.038(3) Uani 1 1 d . . .
H50 H 0.9610 0.8068 -0.4134 0.046 Uiso 1 1 calc R . .
C51 C 1.0343(8) 0.8783(9) -0.3819(7) 0.042(3) Uani 1 1 d . . .
H51 H 1.0535 0.9186 -0.4370 0.051 Uiso 1 1 calc R . .
C52 C 1.0621(8) 0.8832(8) -0.3142(7) 0.036(3) Uani 1 1 d . . .
H52 H 1.1034 0.9253 -0.3233 0.043 Uiso 1 1 calc R . .
C53 C 1.0308(7) 0.8281(7) -0.2334(6) 0.027(2) Uani 1 1 d . . .
C54 C 1.1314(7) 0.8527(8) -0.1615(7) 0.037(3) Uani 1 1 d . . .
H54 H 1.1751 0.8545 -0.2082 0.045 Uiso 1 1 calc R . .
C55 C 1.1549(7) 0.8698(8) -0.0946(7) 0.034(3) Uani 1 1 d . . .
C56 C 1.2446(8) 0.8639(8) -0.0898(8) 0.042(3) Uani 1 1 d . . .
H56 H 1.2865 0.8444 -0.1281 0.051 Uiso 1 1 calc R . .
C57 C 1.2728(8) 0.8858(9) -0.0305(8) 0.042(3) Uani 1 1 d . . .
H57 H 1.3326 0.8766 -0.0250 0.051 Uiso 1 1 calc R . .
C58 C 1.2125(8) 0.9211(8) 0.0200(7) 0.036(3) Uani 1 1 d . . .
H58 H 1.2319 0.9408 0.0576 0.043 Uiso 1 1 calc R . .
C59 C 1.1253(7) 0.9288(8) 0.0176(7) 0.031(2) Uani 1 1 d . . .
H59 H 1.0854 0.9532 0.0537 0.037 Uiso 1 1 calc R . .
C60 C 1.0940(8) 0.9011(7) -0.0372(7) 0.031(3) Uani 1 1 d . . .
```

```
C61 C 0.5762(7) 0.5945(7) 0.1339(7) 0.029(2) Uani 1 1 d . . .
C62 C 0.5917(9) 0.5032(9) 0.1401(8) 0.042(3) Uani 1 1 d . . .
H62 H 0.6371 0.4867 0.1024 0.050 Uiso 1 1 calc R . .
C63 C 0.5408(9) 0.4378(9) 0.2009(8) 0.048(3) Uani 1 1 d . . .
H63 H 0.5515 0.3765 0.2045 0.057 Uiso 1 1 calc R . .
C64 C 0.4737(10) 0.4606(9) 0.2572(10) 0.056(4) Uani 1 1 d . . .
H64 H 0.4407 0.4148 0.3003 0.067 Uiso 1 1 calc R . .
C65 C 0.4562(9) 0.5502(9) 0.2495(8) 0.049(3) Uani 1 1 d . . .
H65 H 0.4081 0.5662 0.2853 0.059 Uiso 1 1 calc R . .
C66 C 0.5083(7) 0.6192(8) 0.1894(7) 0.032(3) Uani 1 1 d . . .
C67 C 0.4850(7) 0.7111(8) 0.1844(7) 0.034(3) Uani 1 1 d . . .
H67 H 0.4293 0.7236 0.2129 0.040 Uiso 1 1 calc R . .
C68 C 0.4993(7) 0.8664(8) 0.1427(6) 0.029(2) Uani 1 1 d . . .
C69 C 0.4119(7) 0.8962(9) 0.1406(7) 0.038(3) Uani 1 1 d . . .
H69 H 0.3724 0.8584 0.1375 0.046 Uiso 1 1 calc R . .
C70 C 0.3827(7) 0.9810(9) 0.1430(7) 0.039(3) Uani 1 1 d . . .
H70 H 0.3227 1.0008 0.1438 0.046 Uiso 1 1 calc R . .
C71 C 0.4413(8) 1.0370(8) 0.1443(8) 0.040(3) Uani 1 1 d . . .
H71 H 0.4212 1.0960 0.1442 0.047 Uiso 1 1 calc R . .
C72 C 0.5289(8) 1.0084(8) 0.1457(7) 0.033(3) Uani 1 1 d . . .
H72 H 0.5682 1.0469 0.1478 0.040 Uiso 1 1 calc R . .
C73 C 0.5585(7) 0.9226(7) 0.1438(6) 0.029(2) Uani 1 1 d . . .
C74 C 0.6926(7) 0.9118(7) 0.1846(6) 0.027(2) Uani 1 1 d . . .
H74 H 0.6631 0.9510 0.2123 0.033 Uiso 1 1 calc R . .
C75 C 0.7825(6) 0.8865(7) 0.1924(6) 0.024(2) Uani 1 1 d . . .
C76 C 0.8101(8) 0.9049(8) 0.2557(7) 0.035(3) Uani 1 1 d . . .
H76 H 0.7697 0.9342 0.2875 0.042 Uiso 1 1 calc R . .
C77 C 0.8939(8) 0.8814(12) 0.2725(8) 0.053(4) Uani 1 1 d . . .
H77 H 0.9111 0.8928 0.3160 0.064 Uiso 1 1 calc R . .
C78 C 0.9523(8) 0.8409(12) 0.2244(9) 0.058(5) Uani 1 1 d . . .
H78 H 1.0102 0.8244 0.2358 0.070 Uiso 1 1 calc R . .
C79 C 0.9305(8) 0.8234(9) 0.1609(7) 0.037(3) Uani 1 1 d . . .
H79 H 0.9727 0.7955 0.1292 0.045 Uiso 1 1 calc R . .
C80 C 0.8468(7) 0.8464(8) 0.1432(6) 0.028(2) Uani 1 1 d . . .
C81 C 0.6266(17) 0.4636(16) 0.5177(16) 0.118(9) Uani 1 1 d . . .
H81A H 0.5686 0.4716 0.5502 0.141 Uiso 1 1 calc R . .
H81B H 0.6630 0.5103 0.5156 0.141 Uiso 1 1 calc R . .

loop_
 _atom_site_aniso_label
 _atom_site_aniso_U_11
 _atom_site_aniso_U_22
 _atom_site_aniso_U_33
 _atom_site_aniso_U_23
 _atom_site_aniso_U_13
 _atom_site_aniso_U_12
U1 0.0282(2) 0.0230(2) 0.02132(19) -0.00611(16) -0.00871(16) 0.00384(16)
U2 0.0275(2) 0.0255(2) 0.0271(2) -0.01133(17) -0.00740(16) 0.00352(16)
U3 0.0271(2) 0.0229(2) 0.0251(2) -0.00895(16) -0.00523(16) 0.00230(16)
U4 0.0272(2) 0.0243(2) 0.01979(18) -0.00665(16) -0.00649(15) 0.00257(16)
Cl1 0.155(6) 0.118(6) 0.129(6) -0.041(5) -0.034(5) -0.020(5)
Cl2 0.111(4) 0.085(4) 0.141(5) -0.055(4) -0.018(4) -0.002(3)
O1 0.027(4) 0.036(4) 0.024(4) -0.009(3) -0.009(3) 0.006(3)
O2 0.027(4) 0.031(4) 0.035(4) -0.013(4) -0.008(3) 0.008(3)
O3 0.029(4) 0.025(4) 0.017(3) -0.005(3) -0.008(3) 0.007(3)
O4 0.045(5) 0.029(4) 0.023(4) -0.006(3) -0.010(3) 0.001(4)
O5 0.041(5) 0.032(4) 0.025(4) -0.015(3) -0.013(3) 0.002(4)
O6 0.045(5) 0.026(4) 0.038(4) -0.018(4) -0.017(4) 0.003(4)
O7 0.038(4) 0.029(4) 0.021(4) -0.017(3) -0.007(3) 0.009(3)
O8 0.037(4) 0.029(4) 0.028(4) -0.007(3) -0.007(3) 0.010(3)
O9 0.021(4) 0.028(4) 0.036(4) -0.012(3) -0.005(3) 0.001(3)
```

```
O10 0.024(4) 0.030(4) 0.030(4) -0.012(3) -0.002(3) -0.002(3)
O11 0.031(4) 0.024(4) 0.040(4) -0.015(3) -0.009(3) 0.005(3)
O12 0.031(4) 0.019(4) 0.022(3) -0.012(3) 0.002(3) 0.001(3)
O13 0.026(4) 0.028(4) 0.019(3) -0.008(3) -0.005(3) 0.005(3)
O14 0.025(4) 0.029(4) 0.022(4) -0.010(3) -0.001(3) 0.005(3)
O15 0.046(5) 0.025(4) 0.026(4) -0.007(3) -0.008(4) 0.003(4)
O16 0.022(4) 0.030(4) 0.024(4) -0.010(3) 0.000(3) -0.002(3)
N1 0.030(5) 0.025(5) 0.032(5) -0.012(4) -0.009(4) 0.007(4)
N2 0.040(5) 0.025(5) 0.029(5) -0.010(4) -0.014(4) 0.004(4)
N3 0.038(6) 0.038(6) 0.045(6) -0.021(5) -0.011(5) 0.007(5)
N4 0.035(5) 0.034(6) 0.043(6) -0.020(5) 0.001(5) -0.002(4)
N5 0.027(4) 0.027(5) 0.023(4) -0.016(4) -0.005(4) 0.002(4)
N6 0.026(5) 0.031(5) 0.031(5) -0.013(4) -0.001(4) -0.004(4)
N7 0.031(5) 0.027(5) 0.016(4) -0.003(4) -0.003(4) 0.003(4)
N8 0.028(5) 0.023(5) 0.026(5) -0.010(4) -0.009(4) 0.006(4)
C1 0.038(6) 0.027(6) 0.012(4) -0.002(4) 0.001(4) 0.006(5)
C2 0.031(6) 0.024(6) 0.027(5) -0.007(4) -0.010(5) -0.001(5)
C3 0.035(6) 0.033(7) 0.035(6) -0.012(5) -0.013(5) 0.003(5)
C4 0.022(5) 0.037(6) 0.027(5) -0.014(5) -0.005(4) 0.001(5)
C5 0.035(6) 0.027(6) 0.027(6) -0.009(5) -0.007(5) 0.000(5)
C6 0.030(6) 0.032(6) 0.030(6) -0.010(5) -0.011(5) 0.002(5)
C7 0.031(6) 0.025(6) 0.025(5) -0.009(4) -0.003(4) 0.002(5)
C8 0.030(6) 0.028(6) 0.019(5) -0.009(4) 0.001(4) 0.004(5)
C9 0.034(6) 0.048(8) 0.037(7) -0.020(6) -0.010(5) 0.013(6)
C10 0.042(7) 0.055(8) 0.035(7) -0.027(6) -0.008(6) 0.012(6)
C11 0.039(7) 0.053(8) 0.044(7) -0.029(7) -0.005(6) 0.005(6)
C12 0.036(6) 0.025(6) 0.040(7) -0.005(5) -0.019(5) 0.005(5)
C13 0.046(7) 0.024(6) 0.033(6) -0.014(5) -0.013(5) 0.008(5)
C14 0.042(7) 0.021(6) 0.043(7) -0.005(5) -0.011(6) 0.006(5)
C15 0.054(8) 0.022(6) 0.029(6) 0.001(5) -0.014(5) 0.004(5)
C16 0.078(10) 0.027(7) 0.039(7) -0.004(6) -0.005(7) -0.002(7)
C17 0.088(12) 0.051(10) 0.043(8) -0.005(7) -0.013(8) 0.000(9)
C18 0.082(11) 0.049(9) 0.025(6) 0.004(6) -0.013(7) -0.001(8)
C19 0.051(8) 0.041(8) 0.029(6) 0.000(5) -0.011(6) 0.004(6)
C20 0.043(7) 0.029(6) 0.024(5) -0.003(5) -0.008(5) 0.010(5)
C21 0.039(6) 0.040(7) 0.020(5) -0.023(5) -0.013(5) 0.017(5)
C22 0.029(6) 0.054(8) 0.022(5) -0.010(5) -0.008(5) 0.004(6)
C23 0.038(7) 0.056(9) 0.031(6) -0.012(6) -0.017(5) 0.016(6)
C24 0.045(8) 0.095(13) 0.022(6) -0.026(7) -0.010(6) 0.021(8)
C25 0.044(7) 0.064(9) 0.034(7) -0.037(7) -0.018(6) 0.032(7)
C26 0.033(6) 0.061(9) 0.035(7) -0.026(6) -0.010(5) 0.029(6)
C27 0.051(8) 0.069(10) 0.050(8) -0.047(8) -0.025(7) 0.030(7)
C28 0.039(7) 0.054(9) 0.070(9) -0.047(8) -0.013(7) 0.009(6)
C29 0.064(10) 0.065(11) 0.090(12) -0.057(10) -0.042(9) 0.025(8)
C30 0.047(9) 0.075(12) 0.152(18) -0.088(13) -0.036(11) 0.017(8)
C31 0.036(8) 0.063(11) 0.136(16) -0.063(12) -0.035(9) 0.012(7)
C32 0.036(7) 0.038(8) 0.092(11) -0.044(8) -0.006(7) 0.001(6)
C33 0.022(6) 0.051(8) 0.061(8) -0.038(7) -0.004(6) 0.009(5)
C34 0.038(7) 0.032(7) 0.047(7) -0.016(6) 0.003(6) 0.004(5)
C35 0.041(7) 0.016(5) 0.036(6) -0.002(5) -0.004(5) 0.005(5)
C36 0.041(7) 0.025(6) 0.046(7) -0.013(5) 0.003(6) -0.006(5)
C37 0.037(7) 0.033(7) 0.048(8) -0.003(6) -0.007(6) 0.004(5)
C38 0.042(7) 0.030(7) 0.041(7) -0.006(5) -0.014(6) 0.000(5)
C39 0.047(7) 0.032(7) 0.025(6) 0.003(5) -0.004(5) 0.003(6)
C40 0.035(6) 0.027(6) 0.022(5) -0.009(4) 0.005(5) -0.003(5)
C41 0.028(6) 0.030(6) 0.034(6) -0.010(5) -0.013(5) 0.003(5)
C42 0.044(7) 0.027(6) 0.036(6) -0.008(5) -0.011(5) 0.004(5)
C43 0.038(7) 0.031(7) 0.044(7) -0.001(6) -0.014(6) 0.003(5)
C44 0.043(7) 0.021(6) 0.042(7) -0.007(5) -0.009(6) 0.011(5)
C45 0.028(6) 0.026(6) 0.035(6) -0.015(5) -0.006(5) 0.003(5)
C46 0.026(5) 0.035(6) 0.030(6) -0.017(5) -0.006(5) 0.000(5)
```

```
C47 0.033(6) 0.034(6) 0.025(5) -0.021(5) -0.006(5) 0.007(5)
C48 0.025(5) 0.029(6) 0.023(5) -0.013(4) -0.007(4) 0.009(4)
C49 0.029(6) 0.039(7) 0.026(5) -0.017(5) -0.006(5) 0.016(5)
C50 0.041(7) 0.042(7) 0.027(6) -0.012(5) -0.004(5) 0.001(6)
C51 0.048(8) 0.035(7) 0.029(6) -0.005(5) 0.006(6) 0.007(6)
C52 0.039(7) 0.037(7) 0.031(6) -0.018(5) 0.004(5) 0.001(5)
C53 0.035(6) 0.023(6) 0.023(5) -0.012(4) -0.002(5) 0.005(5)
C54 0.029(6) 0.040(7) 0.032(6) -0.008(5) 0.003(5) 0.001(5)
C55 0.031(6) 0.026(6) 0.043(7) -0.006(5) -0.016(5) -0.001(5)
C56 0.030(6) 0.031(7) 0.048(7) 0.004(6) -0.004(5) 0.001(5)
C57 0.033(7) 0.053(8) 0.038(7) -0.013(6) -0.010(6) -0.001(6)
C58 0.050(7) 0.026(6) 0.038(6) -0.011(5) -0.021(6) -0.004(5)
C59 0.035(6) 0.030(6) 0.029(6) -0.014(5) -0.008(5) 0.004(5)
C60 0.040(7) 0.016(5) 0.039(6) -0.011(5) -0.009(5) 0.003(5)
C61 0.032(6) 0.025(6) 0.027(5) -0.007(5) -0.003(5) -0.003(5)
C62 0.051(8) 0.038(7) 0.037(7) -0.016(6) 0.001(6) -0.006(6)
C63 0.053(8) 0.031(7) 0.055(8) -0.019(6) 0.019(7) -0.018(6)
C64 0.067(10) 0.026(7) 0.067(10) -0.014(7) 0.009(8) -0.018(7)
C65 0.047(8) 0.046(8) 0.044(8) -0.013(7) 0.004(6) -0.002(6)
C66 0.030(6) 0.035(7) 0.032(6) -0.012(5) -0.006(5) -0.005(5)
C67 0.026(6) 0.043(7) 0.036(6) -0.016(6) -0.014(5) 0.002(5)
C68 0.031(6) 0.033(6) 0.018(5) -0.005(5) -0.007(4) 0.006(5)
C69 0.028(6) 0.041(7) 0.043(7) -0.010(6) -0.012(5) 0.000(5)
C70 0.025(6) 0.055(8) 0.034(6) -0.022(6) -0.002(5) 0.015(6)
C71 0.044(7) 0.017(6) 0.045(7) 0.000(5) -0.012(6) 0.010(5)
C72 0.036(6) 0.027(6) 0.031(6) -0.005(5) -0.007(5) 0.001(5)
C73 0.028(6) 0.027(6) 0.025(5) -0.006(5) -0.002(4) 0.003(5)
C74 0.031(6) 0.027(6) 0.022(5) -0.012(4) 0.003(4) 0.002(5)
C75 0.020(5) 0.028(6) 0.032(6) -0.021(5) -0.004(4) -0.003(4)
C76 0.034(6) 0.039(7) 0.039(7) -0.024(6) -0.005(5) -0.004(5)
C77 0.031(7) 0.107(13) 0.045(8) -0.049(8) -0.011(6) -0.007(7)
C78 0.030(7) 0.116(14) 0.062(9) -0.076(10) -0.020(6) 0.028(8)
C79 0.036(6) 0.056(8) 0.028(6) -0.028(6) -0.008(5) 0.012(6)
C80 0.036(6) 0.031(6) 0.024(5) -0.013(5) -0.011(5) -0.002(5)
C81 0.13(2) 0.100(18) 0.15(2) -0.056(17) -0.068(18) 0.028(15)

_geom_special_details
;
 All esds (except the esd in the dihedral angle between two l.s. planes)
 are estimated using the full covariance matrix.  The cell esds are taken
 into account individually in the estimation of esds in distances, angles
 and torsion angles; correlations between esds in cell parameters are only
 used when they are defined by crystal symmetry.  An approximate (isotropic)
 treatment of cell esds is used for estimating esds involving l.s. planes.
;

loop_
 _geom_bond_atom_site_label_1
 _geom_bond_atom_site_label_2
 _geom_bond_distance
 _geom_bond_site_symmetry_2
 _geom_bond_publ_flag
U1 O2 1.775(8) . ?
U1 O1 1.776(8) . ?
U1 O4 2.219(7) . ?
U1 O3 2.402(7) . ?
U1 O7 2.468(7) . ?
U1 N1 2.506(9) . ?
U1 N2 2.543(9) . ?
U1 U2 3.8809(18) . ?
U2 O6 1.764(8) . ?
```

```
U2 O5 1.766(8) . ?
U2 O8 2.240(7) . ?
U2 O7 2.401(7) . ?
U2 O3 2.482(7) . ?
U2 N4 2.535(10) . ?
U2 N3 2.541(10) . ?
U3 O10 1.776(7) . ?
U3 O9 1.778(7) . ?
U3 O11 2.205(8) . ?
U3 O12 2.396(7) . ?
U3 O16 2.496(7) . ?
U3 N6 2.534(9) . ?
U3 N5 2.540(8) . ?
U3 U4 3.8735(16) . ?
U4 O14 1.774(7) . ?
U4 O13 1.782(7) . ?
U4 O15 2.220(8) . ?
U4 O16 2.387(7) . ?
U4 O12 2.445(6) . ?
U4 N8 2.528(8) . ?
U4 N7 2.531(9) . ?
Cl1 C81 1.71(2) . ?
Cl2 C81 1.73(2) . ?
O3 C1 1.362(13) . ?
O4 C20 1.319(13) . ?
O7 C21 1.346(12) . ?
O8 C40 1.326(13) . ?
O11 C60 1.332(13) . ?
O12 C41 1.347(13) . ?
O15 C61 1.327(13) . ?
O16 C80 1.366(12) . ?
N1 C7 1.299(13) . ?
N1 C8 1.438(12) . ?
N2 C14 1.295(14) . ?
N2 C13 1.424(14) . ?
N3 C27 1.297(17) . ?
N3 C28 1.436(17) . ?
N4 C34 1.289(15) . ?
N4 C33 1.427(16) . ?
N5 C47 1.296(14) . ?
N5 C48 1.435(13) . ?
N6 C54 1.328(15) . ?
N6 C53 1.418(13) . ?
N7 C67 1.296(15) . ?
N7 C68 1.424(14) . ?
N8 C74 1.277(13) . ?
N8 C73 1.423(13) . ?
C1 C2 1.390(14) . ?
C1 C6 1.418(15) . ?
C2 C3 1.386(15) . ?
C2 H2 0.9500 . ?
C3 C4 1.410(15) . ?
C3 H3 0.9500 . ?
C4 C5 1.384(14) . ?
C4 H4 0.9500 . ?
C5 C6 1.406(15) . ?
C5 H5 0.9500 . ?
C6 C7 1.452(14) . ?
C7 H7 0.9500 . ?
C8 C9 1.375(15) . ?
C8 C13 1.395(15) . ?
```

```
C9 C10 1.376(16) . ?
C9 H9 0.9500 . ?
C10 C11 1.405(17) . ?
C10 H10 0.9500 . ?
C11 C12 1.370(16) . ?
C11 H11 0.9500 . ?
C12 C13 1.422(15) . ?
C12 H12 0.9500 . ?
C14 C15 1.443(16) . ?
C14 H14 0.9500 . ?
C15 C16 1.394(16) . ?
C15 C20 1.430(17) . ?
C16 C17 1.383(19) . ?
C16 H16 0.9500 . ?
C17 C18 1.37(2) . ?
C17 H17 0.9500 . ?
C18 C19 1.391(18) . ?
C18 H18 0.9500 . ?
C19 C20 1.389(16) . ?
C19 H19 0.9500 . ?
C21 C26 1.403(17) . ?
C21 C22 1.398(17) . ?
C22 C23 1.389(15) . ?
C22 H22 0.9500 . ?
C23 C24 1.38(2) . ?
C23 H23 0.9500 . ?
C24 C25 1.37(2) . ?
C24 H24 0.9500 . ?
C25 C26 1.429(17) . ?
C25 H25 0.9500 . ?
C26 C27 1.43(2) . ?
C27 H27 0.9500 . ?
C28 C33 1.376(19) . ?
C28 C29 1.392(18) . ?
C29 C30 1.41(2) . ?
C29 H29 0.9500 . ?
C30 C31 1.37(2) . ?
C30 H30 0.9500 . ?
C31 C32 1.377(19) . ?
C31 H31 0.9500 . ?
C32 C33 1.413(18) . ?
C32 H32 0.9500 . ?
C34 C35 1.439(18) . ?
C34 H34 0.9500 . ?
C35 C36 1.400(16) . ?
C35 C40 1.431(16) . ?
C36 C37 1.375(18) . ?
C36 H36 0.9500 . ?
C37 C38 1.377(18) . ?
C37 H37 0.9500 . ?
C38 C39 1.366(16) . ?
C38 H38 0.9500 . ?
C39 C40 1.403(17) . ?
C39 H39 0.9500 . ?
C41 C42 1.407(16) . ?
C41 C46 1.435(15) . ?
C42 C43 1.383(16) . ?
C42 H42 0.9500 . ?
C43 C44 1.408(17) . ?
C43 H43 0.9500 . ?
C44 C45 1.367(16) . ?
```

```
C44 H44 0.9500 . ?
C45 C46 1.394(15) . ?
C45 H45 0.9500 . ?
C46 C47 1.451(15) . ?
C47 H47 0.9500 . ?
C48 C49 1.382(14) . ?
C48 C53 1.391(15) . ?
C49 C50 1.407(16) . ?
C49 H49 0.9500 . ?
C50 C51 1.379(18) . ?
C50 H50 0.9500 . ?
C51 C52 1.387(17) . ?
C51 H51 0.9500 . ?
C52 C53 1.384(15) . ?
C52 H52 0.9500 . ?
C54 C55 1.435(17) . ?
C54 H54 0.9500 . ?
C55 C56 1.418(16) . ?
C55 C60 1.427(16) . ?
C56 C57 1.389(18) . ?
C56 H56 0.9500 . ?
C57 C58 1.375(17) . ?
C57 H57 0.9500 . ?
C58 C59 1.366(16) . ?
C58 H58 0.9500 . ?
C59 C60 1.400(15) . ?
C59 H59 0.9500 . ?
C61 C66 1.411(15) . ?
C61 C62 1.410(16) . ?
C62 C63 1.381(17) . ?
C62 H62 0.9500 . ?
C63 C64 1.400(18) . ?
C63 H63 0.9500 . ?
C64 C65 1.379(18) . ?
C64 H64 0.9500 . ?
C65 C66 1.420(17) . ?
C65 H65 0.9500 . ?
C66 C67 1.435(16) . ?
C67 H67 0.9500 . ?
C68 C69 1.391(15) . ?
C68 C73 1.391(16) . ?
C69 C70 1.381(17) . ?
C69 H69 0.9500 . ?
C70 C71 1.383(18) . ?
C70 H70 0.9500 . ?
C71 C72 1.389(16) . ?
C71 H71 0.9500 . ?
C72 C73 1.394(15) . ?
C72 H72 0.9500 . ?
C74 C75 1.432(14) . ?
C74 H74 0.9500 . ?
C75 C76 1.417(14) . ?
C75 C80 1.435(14) . ?
C76 C77 1.377(16) . ?
C76 H76 0.9500 . ?
C77 C78 1.381(17) . ?
C77 H77 0.9500 . ?
C78 C79 1.370(15) . ?
C78 H78 0.9500 . ?
C79 C80 1.380(15) . ?
C79 H79 0.9500 . ?
```

```
C81 H81A 0.9900 . ?
C81 H81B 0.9900 . ?

loop_
 _geom_angle_atom_site_label_1
 _geom_angle_atom_site_label_2
 _geom_angle_atom_site_label_3
 _geom_angle
 _geom_angle_site_symmetry_1
 _geom_angle_site_symmetry_3
 _geom_angle_publ_flag
O2 U1 O1 175.1(3) . . ?
O2 U1 O4 92.1(3) . . ?
O1 U1 O4 90.1(3) . . ?
O2 U1 O3 93.6(3) . . ?
O1 U1 O3 86.4(3) . . ?
O4 U1 O3 152.0(3) . . ?
O2 U1 O7 89.2(3) . . ?
O1 U1 O7 95.5(3) . . ?
O4 U1 O7 83.0(3) . . ?
O3 U1 O7 69.6(2) . . ?
O2 U1 N1 89.6(3) . . ?
O1 U1 N1 85.7(3) . . ?
O4 U1 N1 134.7(3) . . ?
O3 U1 N1 72.8(3) . . ?
O7 U1 N1 142.3(3) . . ?
O2 U1 N2 89.1(3) . . ?
O1 U1 N2 87.5(3) . . ?
O4 U1 N2 70.9(3) . . ?
O3 U1 N2 136.6(3) . . ?
O7 U1 N2 153.8(3) . . ?
N1 U1 N2 63.9(3) . . ?
O2 U1 U2 77.2(2) . . ?
O1 U1 U2 105.6(2) . . ?
O4 U1 U2 117.7(2) . . ?
O3 U1 U2 38.11(17) . . ?
O7 U1 U2 36.56(17) . . ?
N1 U1 U2 106.9(2) . . ?
N2 U1 U2 163.8(2) . . ?
O6 U2 O5 175.7(3) . . ?
O6 U2 O8 89.9(3) . . ?
O5 U2 O8 91.8(3) . . ?
O6 U2 O7 91.9(3) . . ?
O5 U2 O7 88.5(3) . . ?
O8 U2 O7 152.4(3) . . ?
O6 U2 O3 90.4(3) . . ?
O5 U2 O3 93.7(3) . . ?
O8 U2 O3 83.1(3) . . ?
O7 U2 O3 69.4(2) . . ?
O6 U2 N4 93.3(3) . . ?
O5 U2 N4 83.5(3) . . ?
O8 U2 N4 70.9(3) . . ?
O7 U2 N4 136.3(3) . . ?
O3 U2 N4 153.7(3) . . ?
O6 U2 N3 88.3(3) . . ?
O5 U2 N3 87.7(3) . . ?
O8 U2 N3 134.5(3) . . ?
O7 U2 N3 73.0(3) . . ?
O3 U2 N3 142.3(3) . . ?
N4 U2 N3 63.8(3) . . ?
O6 U2 U1 77.0(2) . . ?
```

```
O5 U2 U1 105.7(3) . . ?
O8 U2 U1 116.7(2) . . ?
O7 U2 U1 37.74(15) . . ?
O3 U2 U1 36.67(15) . . ?
N4 U2 U1 167.2(2) . . ?
N3 U2 U1 107.1(2) . . ?
O10 U3 O9 175.8(3) . . ?
O10 U3 O11 93.5(3) . . ?
O9 U3 O11 87.9(3) . . ?
O10 U3 O12 94.6(3) . . ?
O9 U3 O12 85.7(3) . . ?
O11 U3 O12 156.2(2) . . ?
O10 U3 O16 86.8(3) . . ?
O9 U3 O16 97.1(3) . . ?
O11 U3 O16 89.0(3) . . ?
O12 U3 O16 69.2(2) . . ?
O10 U3 N6 88.9(3) . . ?
O9 U3 N6 87.9(3) . . ?
O11 U3 N6 70.1(3) . . ?
O12 U3 N6 132.3(3) . . ?
O16 U3 N6 158.4(3) . . ?
O10 U3 N5 86.8(3) . . ?
O9 U3 N5 89.3(3) . . ?
O11 U3 N5 132.2(3) . . ?
O12 U3 N5 70.6(3) . . ?
O16 U3 N5 138.6(3) . . ?
N6 U3 N5 62.1(3) . . ?
O10 U3 U4 77.1(2) . . ?
O9 U3 U4 105.3(2) . . ?
O11 U3 U4 124.34(19) . . ?
O12 U3 U4 37.30(15) . . ?
O16 U3 U4 36.54(17) . . ?
N6 U3 U4 160.0(2) . . ?
N5 U3 U4 102.3(2) . . ?
O14 U4 O13 176.2(3) . . ?
O14 U4 O15 92.3(3) . . ?
O13 U4 O15 89.5(3) . . ?
O14 U4 O16 91.4(3) . . ?
O13 U4 O16 88.5(3) . . ?
O15 U4 O16 152.1(3) . . ?
O14 U4 O12 87.7(3) . . ?
O13 U4 O12 95.8(3) . . ?
O15 U4 O12 82.4(3) . . ?
O16 U4 O12 70.2(2) . . ?
O14 U4 N8 88.8(3) . . ?
O13 U4 N8 87.6(3) . . ?
O15 U4 N8 134.5(3) . . ?
O16 U4 N8 73.1(3) . . ?
O12 U4 N8 143.0(3) . . ?
O14 U4 N7 90.4(3) . . ?
O13 U4 N7 87.1(3) . . ?
O15 U4 N7 70.5(3) . . ?
O16 U4 N7 137.1(3) . . ?
O12 U4 N7 152.7(3) . . ?
N8 U4 N7 64.0(3) . . ?
O14 U4 U3 75.4(2) . . ?
O13 U4 U3 106.7(2) . . ?
O15 U4 U3 116.7(2) . . ?
O16 U4 U3 38.49(16) . . ?
O12 U4 U3 36.43(17) . . ?
N8 U4 U3 107.5(2) . . ?
```

```
N7 U4 U3 163.96(19) . . ?
C1 O3 U1 124.2(6) . . ?
C1 O3 U2 125.3(6) . . ?
U1 O3 U2 105.2(3) . . ?
C20 O4 U1 136.3(7) . . ?
C21 O7 U2 126.9(6) . . ?
C21 O7 U1 124.6(7) . . ?
U2 O7 U1 105.7(2) . . ?
C40 O8 U2 127.1(6) . . ?
C60 O11 U3 130.4(6) . . ?
C41 O12 U3 123.8(6) . . ?
C41 O12 U4 125.9(6) . . ?
U3 O12 U4 106.3(2) . . ?
C61 O15 U4 130.2(7) . . ?
C80 O16 U4 125.3(6) . . ?
C80 O16 U3 125.2(6) . . ?
U4 O16 U3 105.0(3) . . ?
C7 N1 C8 117.0(9) . . ?
C7 N1 U1 124.3(7) . . ?
C8 N1 U1 117.6(6) . . ?
C14 N2 C13 118.2(10) . . ?
C14 N2 U1 125.7(8) . . ?
C13 N2 U1 115.7(7) . . ?
C27 N3 C28 118.4(12) . . ?
C27 N3 U2 126.0(9) . . ?
C28 N3 U2 115.3(8) . . ?
C34 N4 C33 119.5(11) . . ?
C34 N4 U2 123.4(9) . . ?
C33 N4 U2 116.7(8) . . ?
C47 N5 C48 117.8(8) . . ?
C47 N5 U3 127.4(7) . . ?
C48 N5 U3 114.8(6) . . ?
C54 N6 C53 120.0(9) . . ?
C54 N6 U3 125.5(7) . . ?
C53 N6 U3 114.5(7) . . ?
C67 N7 C68 118.2(9) . . ?
C67 N7 U4 124.5(7) . . ?
C68 N7 U4 116.4(7) . . ?
C74 N8 C73 118.9(9) . . ?
C74 N8 U4 124.2(7) . . ?
C73 N8 U4 116.0(7) . . ?
O3 C1 C2 120.6(10) . . ?
O3 C1 C6 120.3(9) . . ?
C2 C1 C6 119.0(10) . . ?
C1 C2 C3 120.8(11) . . ?
C1 C2 H2 119.6 . . ?
C3 C2 H2 119.6 . . ?
C2 C3 C4 121.4(10) . . ?
C2 C3 H3 119.3 . . ?
C4 C3 H3 119.3 . . ?
C5 C4 C3 117.7(10) . . ?
C5 C4 H4 121.2 . . ?
C3 C4 H4 121.2 . . ?
C4 C5 C6 122.1(11) . . ?
C4 C5 H5 119.0 . . ?
C6 C5 H5 119.0 . . ?
C5 C6 C1 119.1(10) . . ?
C5 C6 C7 114.4(10) . . ?
C1 C6 C7 126.5(10) . . ?
N1 C7 C6 127.1(10) . . ?
N1 C7 H7 116.5 . . ?
```

```
C6 C7 H7 116.5 . . ?
C9 C8 C13 121.9(10) . . ?
C9 C8 N1 122.9(10) . . ?
C13 C8 N1 115.2(9) . . ?
C8 C9 C10 119.5(11) . . ?
C8 C9 H9 120.3 . . ?
C10 C9 H9 120.3 . . ?
C9 C10 C11 120.7(11) . . ?
C9 C10 H10 119.7 . . ?
C11 C10 H10 119.7 . . ?
C12 C11 C10 119.6(11) . . ?
C12 C11 H11 120.2 . . ?
C10 C11 H11 120.2 . . ?
C11 C12 C13 120.6(10) . . ?
C11 C12 H12 119.7 . . ?
C13 C12 H12 119.7 . . ?
C8 C13 C12 117.7(10) . . ?
C8 C13 N2 117.8(9) . . ?
C12 C13 N2 124.5(10) . . ?
N2 C14 C15 127.3(11) . . ?
N2 C14 H14 116.4 . . ?
C15 C14 H14 116.4 . . ?
C16 C15 C20 120.3(11) . . ?
C16 C15 C14 117.0(11) . . ?
C20 C15 C14 122.6(10) . . ?
C15 C16 C17 119.8(14) . . ?
C15 C16 H16 120.1 . . ?
C17 C16 H16 120.1 . . ?
C18 C17 C16 120.5(14) . . ?
C18 C17 H17 119.7 . . ?
C16 C17 H17 119.7 . . ?
C17 C18 C19 120.5(13) . . ?
C17 C18 H18 119.7 . . ?
C19 C18 H18 119.7 . . ?
C20 C19 C18 121.0(13) . . ?
C20 C19 H19 119.5 . . ?
C18 C19 H19 119.5 . . ?
O4 C20 C19 121.4(11) . . ?
O4 C20 C15 120.8(10) . . ?
C19 C20 C15 117.8(11) . . ?
O7 C21 C26 121.8(12) . . ?
O7 C21 C22 119.7(9) . . ?
C26 C21 C22 118.4(10) . . ?
C21 C22 C23 121.8(12) . . ?
C21 C22 H22 119.1 . . ?
C23 C22 H22 119.1 . . ?
C24 C23 C22 119.9(14) . . ?
C24 C23 H23 120.0 . . ?
C22 C23 H23 120.0 . . ?
C25 C24 C23 119.6(12) . . ?
C25 C24 H24 120.2 . . ?
C23 C24 H24 120.2 . . ?
C24 C25 C26 121.7(12) . . ?
C24 C25 H25 119.1 . . ?
C26 C25 H25 119.1 . . ?
C21 C26 C25 118.3(14) . . ?
C21 C26 C27 126.5(11) . . ?
C25 C26 C27 115.2(12) . . ?
N3 C27 C26 128.1(12) . . ?
N3 C27 H27 116.0 . . ?
C26 C27 H27 116.0 . . ?
```

```
C33 C28 C29 119.6(14) . . ?
C33 C28 N3 117.3(12) . . ?
C29 C28 N3 123.1(14) . . ?
C28 C29 C30 119.4(16) . . ?
C28 C29 H29 120.3 . . ?
C30 C29 H29 120.3 . . ?
C31 C30 C29 120.8(15) . . ?
C31 C30 H30 119.6 . . ?
C29 C30 H30 119.6 . . ?
C32 C31 C30 119.8(16) . . ?
C32 C31 H31 120.1 . . ?
C30 C31 H31 120.1 . . ?
C31 C32 C33 119.8(15) . . ?
C31 C32 H32 120.1 . . ?
C33 C32 H32 120.1 . . ?
C28 C33 N4 117.0(12) . . ?
C28 C33 C32 120.5(13) . . ?
N4 C33 C32 122.3(13) . . ?
N4 C34 C35 126.9(12) . . ?
N4 C34 H34 116.5 . . ?
C35 C34 H34 116.5 . . ?
C36 C35 C40 118.6(12) . . ?
C36 C35 C34 119.7(11) . . ?
C40 C35 C34 121.7(10) . . ?
C37 C36 C35 122.4(12) . . ?
C37 C36 H36 118.8 . . ?
C35 C36 H36 118.8 . . ?
C38 C37 C36 118.4(11) . . ?
C38 C37 H37 120.8 . . ?
C36 C37 H37 120.8 . . ?
C39 C38 C37 121.5(12) . . ?
C39 C38 H38 119.2 . . ?
C37 C38 H38 119.2 . . ?
C38 C39 C40 121.6(12) . . ?
C38 C39 H39 119.2 . . ?
C40 C39 H39 119.2 . . ?
O8 C40 C39 121.3(10) . . ?
O8 C40 C35 121.3(10) . . ?
C39 C40 C35 117.3(10) . . ?
O12 C41 C42 121.3(10) . . ?
O12 C41 C46 120.9(10) . . ?
C42 C41 C46 117.7(10) . . ?
C43 C42 C41 120.7(11) . . ?
C43 C42 H42 119.6 . . ?
C41 C42 H42 119.6 . . ?
C42 C43 C44 121.5(11) . . ?
C42 C43 H43 119.3 . . ?
C44 C43 H43 119.3 . . ?
C45 C44 C43 118.0(11) . . ?
C45 C44 H44 121.0 . . ?
C43 C44 H44 121.0 . . ?
C44 C45 C46 122.8(10) . . ?
C44 C45 H45 118.6 . . ?
C46 C45 H45 118.6 . . ?
C45 C46 C41 119.3(10) . . ?
C45 C46 C47 117.6(10) . . ?
C41 C46 C47 123.1(10) . . ?
N5 C47 C46 126.8(9) . . ?
N5 C47 H47 116.6 . . ?
C46 C47 H47 116.6 . . ?
C49 C48 C53 120.7(10) . . ?
```

```
C49 C48 N5 124.7(10) . . ?
C53 C48 N5 114.6(9) . . ?
C48 C49 C50 118.3(12) . . ?
C48 C49 H49 120.8 . . ?
C50 C49 H49 120.8 . . ?
C51 C50 C49 121.9(12) . . ?
C51 C50 H50 119.1 . . ?
C49 C50 H50 119.1 . . ?
C50 C51 C52 118.2(11) . . ?
C50 C51 H51 120.9 . . ?
C52 C51 H51 120.9 . . ?
C53 C52 C51 121.4(12) . . ?
C53 C52 H52 119.3 . . ?
C51 C52 H52 119.3 . . ?
C48 C53 C52 119.5(10) . . ?
C48 C53 N6 116.3(9) . . ?
C52 C53 N6 124.1(11) . . ?
N6 C54 C55 123.2(10) . . ?
N6 C54 H54 118.4 . . ?
C55 C54 H54 118.4 . . ?
C56 C55 C60 117.5(11) . . ?
C56 C55 C54 118.3(11) . . ?
C60 C55 C54 123.9(10) . . ?
C57 C56 C55 121.7(12) . . ?
C57 C56 H56 119.2 . . ?
C55 C56 H56 119.2 . . ?
C58 C57 C56 118.7(12) . . ?
C58 C57 H57 120.6 . . ?
C56 C57 H57 120.6 . . ?
C59 C58 C57 121.8(11) . . ?
C59 C58 H58 119.1 . . ?
C57 C58 H58 119.1 . . ?
C58 C59 C60 120.9(11) . . ?
C58 C59 H59 119.6 . . ?
C60 C59 H59 119.6 . . ?
O11 C60 C59 121.7(10) . . ?
O11 C60 C55 119.1(10) . . ?
C59 C60 C55 119.1(11) . . ?
O15 C61 C66 120.4(10) . . ?
O15 C61 C62 119.6(10) . . ?
C66 C61 C62 120.0(11) . . ?
C63 C62 C61 120.1(12) . . ?
C63 C62 H62 120.0 . . ?
C61 C62 H62 120.0 . . ?
C62 C63 C64 121.0(12) . . ?
C62 C63 H63 119.5 . . ?
C64 C63 H63 119.5 . . ?
C65 C64 C63 119.2(13) . . ?
C65 C64 H64 120.4 . . ?
C63 C64 H64 120.4 . . ?
C64 C65 C66 121.5(12) . . ?
C64 C65 H65 119.2 . . ?
C66 C65 H65 119.2 . . ?
C61 C66 C65 118.1(11) . . ?
C61 C66 C67 123.5(11) . . ?
C65 C66 C67 118.2(11) . . ?
N7 C67 C66 125.4(11) . . ?
N7 C67 H67 117.3 . . ?
C66 C67 H67 117.3 . . ?
C69 C68 C73 120.7(11) . . ?
C69 C68 N7 123.2(11) . . ?
```

```
C73 C68 N7 116.1(9) . . ?
C68 C69 C70 119.7(12) . . ?
C68 C69 H69 120.1 . . ?
C70 C69 H69 120.1 . . ?
C71 C70 C69 119.8(10) . . ?
C71 C70 H70 120.1 . . ?
C69 C70 H70 120.1 . . ?
C70 C71 C72 121.0(11) . . ?
C70 C71 H71 119.5 . . ?
C72 C71 H71 119.5 . . ?
C73 C72 C71 119.4(11) . . ?
C73 C72 H72 120.3 . . ?
C71 C72 H72 120.3 . . ?
C72 C73 C68 119.3(10) . . ?
C72 C73 N8 122.9(10) . . ?
C68 C73 N8 117.7(9) . . ?
N8 C74 C75 128.0(9) . . ?
N8 C74 H74 116.0 . . ?
C75 C74 H74 116.0 . . ?
C76 C75 C80 117.2(9) . . ?
C76 C75 C74 115.3(9) . . ?
C80 C75 C74 127.5(9) . . ?
C77 C76 C75 121.8(11) . . ?
C77 C76 H76 119.1 . . ?
C75 C76 H76 119.1 . . ?
C76 C77 C78 118.3(11) . . ?
C76 C77 H77 120.9 . . ?
C78 C77 H77 120.9 . . ?
C79 C78 C77 122.9(11) . . ?
C79 C78 H78 118.6 . . ?
C77 C78 H78 118.6 . . ?
C80 C79 C78 119.7(10) . . ?
C80 C79 H79 120.2 . . ?
C78 C79 H79 120.2 . . ?
O16 C80 C79 120.9(10) . . ?
O16 C80 C75 119.0(9) . . ?
C79 C80 C75 120.1(9) . . ?
Cl1 C81 Cl2 114.4(14) . . ?
Cl1 C81 H81A 108.7 . . ?
Cl2 C81 H81A 108.7 . . ?
Cl1 C81 H81B 108.7 . . ?
Cl2 C81 H81B 108.7 . . ?
H81A C81 H81B 107.6 . . ?

_diffrn_measured_fraction_theta_max    0.975
_diffrn_reflns_theta_full              27.48
_diffrn_measured_fraction_theta_full   0.975
_refine_diff_density_max    2.490
_refine_diff_density_min   -2.984
_refine_diff_density_rms    0.239
```

Appendix D

Crystallographic Information of $U^{VI}O_2$(saloph)DMSO

```
data_shelxl

_audit_creation_method            SHELXL-97
_chemical_name_systematic
;
 ?
;
_chemical_name_common             ?
_chemical_melting_point           ?
_chemical_formula_moiety          'C22 H20 N2 O5 S U '
_chemical_formula_sum
 'C22 H20 N2 O5 S U'
_chemical_formula_weight          662.49

loop_
 _atom_type_symbol
 _atom_type_description
 _atom_type_scat_dispersion_real
 _atom_type_scat_dispersion_imag
 _atom_type_scat_source
 'C'  'C'   0.0033   0.0016
 'International Tables Vol C Tables 4.2.6.8 and 6.1.1.4'
 'H'  'H'   0.0000   0.0000
 'International Tables Vol C Tables 4.2.6.8 and 6.1.1.4'
 'N'  'N'   0.0061   0.0033
 'International Tables Vol C Tables 4.2.6.8 and 6.1.1.4'
 'O'  'O'   0.0106   0.0060
 'International Tables Vol C Tables 4.2.6.8 and 6.1.1.4'
 'S'  'S'   0.1246   0.1234
 'International Tables Vol C Tables 4.2.6.8 and 6.1.1.4'
 'U'  'U'  -9.6767   9.6646
 'International Tables Vol C Tables 4.2.6.8 and 6.1.1.4'

_symmetry_cell_setting            monoclinic
_symmetry_space_group_name_H-M   'P 1 21 1'
 _symmetry_Int_Tables_number      4
loop_
 _symmetry_equiv_pos_as_xyz
 'x, y, z'
 '-x, y+1/2, -z'
```

```
_cell_length_a                    13.303(7)
_cell_length_b                    9.422(4)
_cell_length_c                    17.205(8)
_cell_angle_alpha                 90.00
_cell_angle_beta                  94.45(5)
_cell_angle_gamma                 90.00
_cell_volume                      2149.9(17)
_cell_formula_units_Z             4
_cell_measurement_temperature     113(2)
_cell_measurement_reflns_used     22909
_cell_measurement_theta_min       3.1
_cell_measurement_theta_max       27.6

_exptl_crystal_description       'block'
_exptl_crystal_colour            'yellow'
_exptl_crystal_size_max           0.27
_exptl_crystal_size_mid           0.15
_exptl_crystal_size_min           0.07
_exptl_crystal_density_meas       ?
_exptl_crystal_density_diffrn     2.047
_exptl_crystal_density_method     'not measured'
_exptl_crystal_F_000              1256
_exptl_absorpt_coefficient_mu     7.684
_exptl_absorpt_correction_T_min   0.2308
_exptl_absorpt_correction_T_max   0.6153
_exptl_absorpt_correction_type    numerical
_exptl_absorpt_process_details
;
    Higashi, T. (1999). Program for Absorption Correction.
    Rigaku Corporation, Tokyo, Japan.
;

_diffrn_ambient_temperature       113(2)
_diffrn_radiation_wavelength      0.71075
_diffrn_radiation_type            MoK¥a
_diffrn_radiation_source          'fine-focus sealed tube'
_diffrn_radiation_monochromator   graphite
_diffrn_measurement_device_type  'Rigaku RAXIS-RAPID'
_diffrn_measurement_method        ¥w
_diffrn_detector_area_resol_mean  10.00
_diffrn_reflns_number             19478
_diffrn_reflns_av_R_equivalents   0.0352
_diffrn_reflns_av_sigmaI/netI     0.0295
_diffrn_reflns_limit_h_min        -15
_diffrn_reflns_limit_h_max        17
_diffrn_reflns_limit_k_min        -11
_diffrn_reflns_limit_k_max        12
_diffrn_reflns_limit_l_min        -22
_diffrn_reflns_limit_l_max        22
_diffrn_reflns_theta_min          3.07
_diffrn_reflns_theta_max          27.49
_reflns_number_total              9110
_reflns_number_gt                 8357
_reflns_threshold_expression      >2sigma(I)

_computing_data_collection        'PROCESS-AUTO'
_computing_cell_refinement        'PROCESS-AUTO'
_computing_data_reduction         'CrystalStructure'
_computing_structure_solution     'DIRDIF99 (PATTY)'
_computing_structure_refinement   'SHELXL-97 (Sheldrick, 1997)'
```

```
_computing_molecular_graphics     ?
_computing_publication_material   ?

_refine_special_details
;
 Refinement of F^2^ against ALL reflections.  The weighted R-factor wR and
 goodness of fit S are based on F^2^, conventional R-factors R are based
 on F, with F set to zero for negative F^2^. The threshold expression of
 F^2^ > 2sigma(F^2^) is used only for calculating R-factors(gt) etc. and is
 not relevant to the choice of reflections for refinement.  R-factors based
 on F^2^ are statistically about twice as large as those based on F, and R-
 factors based on ALL data will be even larger.
;

_refine_ls_structure_factor_coef  Fsqd
_refine_ls_matrix_type            full
_refine_ls_weighting_scheme       calc
_refine_ls_weighting_details
 'calc w=1/[¥s^2^(Fo^2^)+(0.0356P)^2^+4.8982P] where P=(Fo^2^+2Fc^2^)/3'
_atom_sites_solution_primary      direct
_atom_sites_solution_secondary    difmap
_atom_sites_solution_hydrogens    geom
_refine_ls_hydrogen_treatment     mixed
_refine_ls_extinction_method      SHELXL
_refine_ls_extinction_coef        0.00069(9)
_refine_ls_extinction_expression
 'Fc^*^=kFc[1+0.001xFc^2^¥l^3^/sin(2¥q)]^-1/4^'
_refine_ls_abs_structure_details
 'Flack H D (1983), Acta Cryst. A39, 876-881'
_refine_ls_abs_structure_Flack    0.012(6)
_refine_ls_number_reflns          9110
_refine_ls_number_parameters      560
_refine_ls_number_restraints      1
_refine_ls_R_factor_all           0.0313
_refine_ls_R_factor_gt            0.0267
_refine_ls_wR_factor_ref          0.0677
_refine_ls_wR_factor_gt           0.0658
_refine_ls_goodness_of_fit_ref    1.088
_refine_ls_restrained_S_all       1.088
_refine_ls_shift/su_max           0.001
_refine_ls_shift/su_mean          0.000

loop_
 _atom_site_label
 _atom_site_type_symbol
 _atom_site_fract_x
 _atom_site_fract_y
 _atom_site_fract_z
 _atom_site_U_iso_or_equiv
 _atom_site_adp_type
 _atom_site_occupancy
 _atom_site_symmetry_multiplicity
 _atom_site_calc_flag
 _atom_site_refinement_flags
 _atom_site_disorder_assembly
 _atom_site_disorder_group
U1 U -0.241447(12) -0.49750(3) -0.008426(9) 0.01257(5) Uani 1 1 d . . .
U2 U 0.233812(13) -0.50161(3) -0.469079(9) 0.01390(5) Uani 1 1 d . . .
S1 S -0.34365(12) -0.17559(16) 0.05030(9) 0.0197(3) Uani 1 1 d . . .
S2 S 0.07819(12) -0.17917(16) -0.44373(9) 0.0196(3) Uani 1 1 d . . .
O1 O -0.1289(3) -0.3944(4) -0.0015(2) 0.0179(9) Uani 1 1 d . . .
```

```
O2 O -0.3492(4) -0.6116(5) -0.0135(3) 0.0223(9) Uani 1 1 d . . .
O3 O -0.3460(4) -0.2875(5) -0.0136(2) 0.0244(10) Uani 1 1 d . . .
O4 O -0.2603(3) -0.4559(4) -0.1378(2) 0.0197(9) Uani 1 1 d . . .
O5 O -0.2584(3) -0.4552(4) 0.1200(2) 0.0167(9) Uani 1 1 d . . .
O6 O 0.3310(3) -0.3719(4) -0.4712(2) 0.0199(9) Uani 1 1 d . . .
O7 O 0.1422(4) -0.6394(5) -0.4659(3) 0.0219(10) Uani 1 1 d . . .
O8 O 0.0971(3) -0.3371(4) -0.4582(3) 0.0186(9) Uani 1 1 d . . .
O9 O 0.1952(3) -0.4489(4) -0.5966(2) 0.0201(9) Uani 1 1 d . . .
O10 O 0.2423(3) -0.4734(5) -0.3374(2) 0.0228(12) Uani 1 1 d . . .
N1 N -0.1415(4) -0.6783(5) -0.0804(3) 0.0130(9) Uani 1 1 d . . .
N2 N -0.1399(4) -0.6790(5) 0.0744(3) 0.0146(9) Uani 1 1 d . . .
N3 N 0.3271(4) -0.6719(5) -0.5562(3) 0.0184(10) Uani 1 1 d . . .
N4 N 0.3680(4) -0.6636(5) -0.4025(3) 0.0177(10) Uani 1 1 d . . .
C1 C -0.1910(5) -0.4359(6) -0.1877(3) 0.0169(12) Uani 1 1 d . . .
C2 C -0.2002(5) -0.3234(7) -0.2415(4) 0.0233(13) Uani 1 1 d . . .
H2 H -0.2550 -0.2591 -0.2401 0.028 Uiso 1 1 calc R . .
C3 C -0.1305(5) -0.3045(6) -0.2967(3) 0.0228(13) Uani 1 1 d . . .
H3 H -0.1387 -0.2280 -0.3326 0.027 Uiso 1 1 calc R . .
C4 C -0.0484(5) -0.3967(7) -0.3002(3) 0.0235(14) Uani 1 1 d . . .
H4 H -0.0002 -0.3829 -0.3375 0.028 Uiso 1 1 calc R . .
C5 C -0.0393(4) -0.5069(10) -0.2485(3) 0.0192(10) Uani 1 1 d . . .
H5 H 0.0155 -0.5710 -0.2513 0.023 Uiso 1 1 calc R . .
C6 C -0.1082(5) -0.5296(5) -0.1909(3) 0.0166(13) Uani 1 1 d . . .
C7 C -0.0946(4) -0.6562(6) -0.1423(3) 0.0163(11) Uani 1 1 d . . .
H7 H -0.0486 -0.7265 -0.1571 0.020 Uiso 1 1 calc R . .
C8 C -0.1309(5) -0.8139(6) -0.0440(3) 0.0171(11) Uani 1 1 d . . .
C9 C -0.1242(5) -0.9405(6) -0.0833(4) 0.0171(12) Uani 1 1 d . . .
H9 H -0.1268 -0.9408 -0.1387 0.020 Uiso 1 1 calc R . .
C10 C -0.1139(5) -1.0665(6) -0.0430(4) 0.0179(12) Uani 1 1 d . . .
H10 H -0.1080 -1.1532 -0.0704 0.022 Uiso 1 1 calc R . .
C11 C -0.1121(5) -1.0671(6) 0.0376(4) 0.0178(12) Uani 1 1 d . . .
H11 H -0.1053 -1.1543 0.0653 0.021 Uiso 1 1 calc R . .
C12 C -0.1201(5) -0.9409(6) 0.0780(4) 0.0178(12) Uani 1 1 d . . .
H12 H -0.1202 -0.9421 0.1332 0.021 Uiso 1 1 calc R . .
C13 C -0.1280(4) -0.8128(6) 0.0382(3) 0.0140(11) Uani 1 1 d . . .
C14 C -0.0917(4) -0.6524(6) 0.1401(3) 0.0152(11) Uani 1 1 d . . .
H14 H -0.0442 -0.7213 0.1598 0.018 Uiso 1 1 calc R . .
C15 C -0.1034(4) -0.5261(6) 0.1871(3) 0.0169(13) Uani 1 1 d . . .
C16 C -0.0287(4) -0.5009(10) 0.2492(2) 0.0175(9) Uani 1 1 d . . .
H16 H 0.0277 -0.5628 0.2556 0.021 Uiso 1 1 calc R . .
C17 C -0.0356(5) -0.3891(6) 0.3006(3) 0.0201(12) Uani 1 1 d . . .
H17 H 0.0154 -0.3723 0.3413 0.024 Uiso 1 1 calc R . .
C18 C -0.1215(5) -0.3009(6) 0.2903(3) 0.0186(12) Uani 1 1 d . . .
H18 H -0.1284 -0.2239 0.3252 0.022 Uiso 1 1 calc R . .
C19 C -0.1952(5) -0.3237(7) 0.2311(3) 0.0235(13) Uani 1 1 d . . .
H19 H -0.2526 -0.2635 0.2265 0.028 Uiso 1 1 calc R . .
C20 C -0.1871(5) -0.4353(6) 0.1770(3) 0.0153(11) Uani 1 1 d . . .
C21 C -0.4448(5) -0.2194(7) 0.1061(4) 0.0248(14) Uani 1 1 d . . .
H21A H -0.4277 -0.3047 0.1370 0.037 Uiso 1 1 calc R . .
H21B H -0.5053 -0.2374 0.0713 0.037 Uiso 1 1 calc R . .
H21C H -0.4575 -0.1405 0.1412 0.037 Uiso 1 1 calc R . .
C22 C -0.3943(5) -0.0202(8) 0.0013(4) 0.0294(16) Uani 1 1 d . . .
H22A H -0.3452 0.0173 -0.0330 0.044 Uiso 1 1 calc R . .
H22B H -0.4088 0.0519 0.0399 0.044 Uiso 1 1 calc R . .
H22C H -0.4567 -0.0450 -0.0298 0.044 Uiso 1 1 calc R . .
C23 C 0.2542(5) -0.4241(6) -0.6530(3) 0.0188(12) Uani 1 1 d . . .
C24 C 0.2426(5) -0.3003(7) -0.6989(3) 0.0214(13) Uani 1 1 d . . .
H24 H 0.1944 -0.2310 -0.6867 0.026 Uiso 1 1 calc R . .
C25 C 0.2998(5) -0.2779(7) -0.7612(3) 0.0217(13) Uani 1 1 d . . .
H25 H 0.2922 -0.1921 -0.7901 0.026 Uiso 1 1 calc R . .
C26 C 0.3695(5) -0.3804(7) -0.7827(3) 0.0222(13) Uani 1 1 d . . .
```

```
H26 H 0.4061 -0.3664 -0.8274 0.027 Uiso 1 1 calc R . .
C27 C 0.3839(4) -0.5019(11) -0.7378(3) 0.0199(10) Uani 1 1 d . . .
H27 H 0.4302 -0.5723 -0.7521 0.024 Uiso 1 1 calc R . .
C28 C 0.3305(5) -0.5218(7) -0.6713(3) 0.0183(14) Uani 1 1 d . . .
C29 C 0.3540(5) -0.6477(6) -0.6258(3) 0.0189(12) Uani 1 1 d . . .
H29 H 0.3925 -0.7190 -0.6488 0.023 Uiso 1 1 calc R . .
C30 C 0.3583(4) -0.8019(6) -0.5206(3) 0.0167(11) Uani 1 1 d . . .
C31 C 0.3639(5) -0.9310(6) -0.5597(4) 0.0218(13) Uani 1 1 d . . .
H31 H 0.3464 -0.9357 -0.6143 0.026 Uiso 1 1 calc R . .
C32 C 0.3949(5) -1.0524(7) -0.5192(5) 0.0240(14) Uani 1 1 d . . .
H32 H 0.3985 -1.1402 -0.5461 0.029 Uiso 1 1 calc R . .
C33 C 0.4208(5) -1.0463(7) -0.4393(4) 0.0230(14) Uani 1 1 d . . .
H33 H 0.4434 -1.1295 -0.4121 0.028 Uiso 1 1 calc R . .
C34 C 0.4136(5) -0.9184(7) -0.3992(4) 0.0240(14) Uani 1 1 d . . .
H34 H 0.4296 -0.9148 -0.3445 0.029 Uiso 1 1 calc R . .
C35 C 0.3832(4) -0.7974(6) -0.4394(3) 0.0151(11) Uani 1 1 d . . .
C36 C 0.4303(5) -0.6242(6) -0.3450(3) 0.0178(12) Uani 1 1 d . . .
H36 H 0.4890 -0.6804 -0.3342 0.021 Uiso 1 1 calc R . .
C37 C 0.4182(4) -0.5018(10) -0.2959(3) 0.0194(10) Uani 1 1 d . . .
C38 C 0.5017(5) -0.4575(7) -0.2458(3) 0.0231(15) Uani 1 1 d . . .
H38 H 0.5651 -0.5024 -0.2493 0.028 Uiso 1 1 calc R . .
C39 C 0.4929(5) -0.3504(7) -0.1919(4) 0.0250(14) Uani 1 1 d . . .
H39 H 0.5501 -0.3188 -0.1601 0.030 Uiso 1 1 calc R . .
C40 C 0.3975(6) -0.2892(7) -0.1852(4) 0.0274(15) Uani 1 1 d . . .
H40 H 0.3902 -0.2162 -0.1481 0.033 Uiso 1 1 calc R . .
C41 C 0.3143(6) -0.3340(8) -0.2321(4) 0.0282(15) Uani 1 1 d . . .
H41 H 0.2501 -0.2943 -0.2244 0.034 Uiso 1 1 calc R . .
C42 C 0.3219(5) -0.4369(7) -0.2908(3) 0.0192(12) Uani 1 1 d . . .
C43 C 0.1867(5) -0.1189(8) -0.3872(5) 0.0323(16) Uani 1 1 d . . .
H43A H 0.1871 -0.1583 -0.3344 0.048 Uiso 1 1 calc R . .
H43B H 0.1858 -0.0150 -0.3845 0.048 Uiso 1 1 calc R . .
H43C H 0.2473 -0.1501 -0.4113 0.048 Uiso 1 1 calc R . .
C44 C 0.0980(6) -0.0937(7) -0.5330(4) 0.0328(17) Uani 1 1 d . . .
H44A H 0.0426 -0.1170 -0.5717 0.049 Uiso 1 1 calc R . .
H44B H 0.1619 -0.1260 -0.5516 0.049 Uiso 1 1 calc R . .
H44C H 0.1005 0.0093 -0.5249 0.049 Uiso 1 1 calc R . .

loop_
 _atom_site_aniso_label
 _atom_site_aniso_U_11
 _atom_site_aniso_U_22
 _atom_site_aniso_U_33
 _atom_site_aniso_U_23
 _atom_site_aniso_U_13
 _atom_site_aniso_U_12
U1 0.01350(9) 0.01247(9) 0.01163(9) -0.00065(15) 0.00028(6) 0.00148(14)
U2 0.01401(10) 0.01555(9) 0.01213(9) 0.00260(16) 0.00096(6) 0.00093(15)
S1 0.0195(8) 0.0207(7) 0.0191(7) -0.0009(5) 0.0028(6) 0.0016(6)
S2 0.0172(8) 0.0215(7) 0.0206(7) 0.0011(5) 0.0045(6) 0.0033(6)
O1 0.021(2) 0.0119(18) 0.020(2) 0.0001(15) 0.0027(17) 0.0000(17)
O2 0.027(3) 0.023(2) 0.017(2) -0.0013(17) 0.0015(18) -0.0018(19)
O3 0.030(3) 0.027(3) 0.016(2) -0.0020(17) -0.0022(18) 0.015(2)
O4 0.028(2) 0.020(2) 0.0119(19) 0.0017(13) 0.0036(16) 0.0051(16)
O5 0.017(2) 0.020(2) 0.0126(19) -0.0007(13) -0.0001(15) 0.0050(15)
O6 0.021(2) 0.018(2) 0.021(2) 0.0013(16) 0.0037(17) -0.0039(18)
O7 0.024(3) 0.027(2) 0.015(2) 0.0047(17) 0.0025(19) -0.004(2)
O8 0.018(2) 0.017(2) 0.022(2) 0.0010(16) 0.0058(18) 0.0056(18)
O9 0.021(2) 0.025(2) 0.014(2) 0.0071(15) 0.0002(16) 0.0053(17)
O10 0.015(2) 0.039(4) 0.0144(17) 0.0023(18) -0.0001(14) 0.005(2)
N1 0.013(2) 0.012(2) 0.013(2) -0.0017(17) -0.0050(17) 0.0019(19)
N2 0.017(3) 0.013(2) 0.014(2) 0.0012(17) 0.0023(18) 0.0001(19)
```

```
N3 0.019(3) 0.017(2) 0.019(2) 0.0018(19) -0.0021(19) -0.003(2)
N4 0.018(3) 0.020(2) 0.014(2) 0.0035(18) -0.0021(19) -0.001(2)
C1 0.020(3) 0.015(3) 0.015(3) -0.002(2) -0.001(2) -0.003(2)
C2 0.029(4) 0.019(3) 0.021(3) 0.002(2) -0.004(2) 0.004(3)
C3 0.036(4) 0.017(3) 0.015(3) 0.004(2) -0.002(2) -0.005(3)
C4 0.036(4) 0.022(3) 0.014(3) -0.003(2) 0.007(3) -0.006(3)
C5 0.021(3) 0.022(3) 0.015(2) 0.001(4) 0.0027(17) 0.001(4)
C6 0.023(3) 0.015(4) 0.011(2) -0.0017(18) -0.002(2) -0.002(2)
C7 0.012(3) 0.019(3) 0.018(3) -0.003(2) -0.001(2) 0.004(2)
C8 0.017(3) 0.019(3) 0.016(3) 0.000(2) 0.001(2) 0.004(2)
C9 0.019(3) 0.018(3) 0.014(3) -0.003(2) 0.001(2) -0.005(2)
C10 0.014(3) 0.013(3) 0.026(3) 0.001(2) -0.001(3) 0.003(2)
C11 0.012(3) 0.015(3) 0.026(3) -0.001(2) 0.000(3) -0.005(2)
C12 0.014(3) 0.018(3) 0.021(3) 0.002(2) 0.000(3) 0.000(2)
C13 0.011(3) 0.014(3) 0.017(3) -0.003(2) 0.000(2) 0.000(2)
C14 0.011(3) 0.016(3) 0.019(3) 0.000(2) 0.001(2) -0.002(2)
C15 0.021(3) 0.018(4) 0.012(2) 0.003(2) 0.0019(19) 0.001(2)
C16 0.021(3) 0.016(2) 0.015(2) -0.003(4) 0.0030(17) -0.006(4)
C17 0.026(4) 0.021(3) 0.013(3) -0.002(2) 0.001(2) -0.011(3)
C18 0.027(3) 0.015(3) 0.015(3) -0.004(2) 0.003(2) -0.003(2)
C19 0.030(4) 0.027(3) 0.014(3) 0.002(2) 0.007(2) 0.002(3)
C20 0.018(3) 0.017(3) 0.011(3) 0.000(2) 0.001(2) -0.003(2)
C21 0.021(3) 0.028(3) 0.027(3) 0.003(3) 0.011(3) 0.007(3)
C22 0.035(4) 0.023(4) 0.031(3) 0.002(3) 0.005(3) 0.004(3)
C23 0.021(3) 0.023(3) 0.013(3) 0.001(2) 0.000(2) -0.001(2)
C24 0.023(3) 0.025(3) 0.016(3) 0.003(2) 0.000(2) -0.001(3)
C25 0.025(3) 0.022(3) 0.017(3) 0.008(2) -0.005(2) -0.002(3)
C26 0.018(3) 0.035(3) 0.015(3) 0.006(2) 0.002(2) -0.007(3)
C27 0.017(3) 0.024(3) 0.018(2) 0.001(4) -0.0010(18) -0.001(4)
C28 0.025(3) 0.017(4) 0.013(2) -0.005(2) 0.0005(19) -0.004(3)
C29 0.018(3) 0.023(3) 0.016(3) -0.004(2) 0.000(2) -0.002(2)
C30 0.013(3) 0.013(3) 0.024(3) 0.003(2) 0.002(2) 0.002(2)
C31 0.020(4) 0.019(3) 0.026(3) 0.003(3) 0.005(3) 0.001(3)
C32 0.020(4) 0.014(3) 0.039(4) -0.001(3) 0.008(3) 0.001(2)
C33 0.012(3) 0.020(3) 0.037(4) 0.008(2) 0.002(3) 0.004(2)
C34 0.018(4) 0.025(4) 0.028(4) 0.009(3) -0.004(3) 0.002(3)
C35 0.011(3) 0.015(3) 0.019(3) 0.003(2) -0.001(2) -0.002(2)
C36 0.013(3) 0.021(3) 0.019(3) 0.009(2) -0.003(2) 0.001(2)
C37 0.021(3) 0.024(2) 0.014(2) 0.006(4) 0.0006(17) 0.000(4)
C38 0.016(3) 0.033(4) 0.021(3) 0.005(2) 0.001(2) -0.004(2)
C39 0.030(4) 0.030(3) 0.014(3) 0.001(2) -0.003(2) -0.008(3)
C40 0.040(4) 0.021(3) 0.022(3) -0.003(2) 0.003(3) -0.003(3)
C41 0.033(4) 0.038(4) 0.013(3) -0.002(3) 0.001(3) 0.003(3)
C42 0.024(3) 0.023(3) 0.010(3) 0.002(2) 0.000(2) 0.001(2)
C43 0.023(4) 0.033(4) 0.040(4) -0.014(3) 0.002(3) -0.001(3)
C44 0.037(5) 0.028(4) 0.034(4) 0.013(3) 0.012(3) 0.001(3)

_geom_special_details
;
 All esds (except the esd in the dihedral angle between two l.s. planes)
 are estimated using the full covariance matrix.  The cell esds are taken
 into account individually in the estimation of esds in distances, angles
 and torsion angles; correlations between esds in cell parameters are only
 used when they are defined by crystal symmetry.  An approximate (isotropic)
 treatment of cell esds is used for estimating esds involving l.s. planes.
;

loop_
 _geom_bond_atom_site_label_1
 _geom_bond_atom_site_label_2
 _geom_bond_distance
```

```
 _geom_bond_site_symmetry_2
 _geom_bond_publ_flag
U1 O1 1.780(4) . ?
U1 O2 1.788(5) . ?
U1 O4 2.255(4) . ?
U1 O5 2.274(4) . ?
U1 O3 2.416(4) . ?
U1 N1 2.541(5) . ?
U1 N2 2.545(5) . ?
U2 O6 1.781(4) . ?
U2 O7 1.784(5) . ?
U2 O9 2.270(4) . ?
U2 O10 2.276(4) . ?
U2 O8 2.408(4) . ?
U2 N4 2.551(5) . ?
U2 N3 2.580(5) . ?
S1 O3 1.522(5) . ?
S1 C21 1.762(6) . ?
S1 C22 1.795(7) . ?
S2 O8 1.533(4) . ?
S2 C44 1.772(7) . ?
S2 C43 1.771(7) . ?
O4 C1 1.321(7) . ?
O5 C20 1.323(7) . ?
O9 C23 1.314(7) . ?
O10 C42 1.323(7) . ?
N1 C7 1.292(8) . ?
N1 C8 1.425(7) . ?
N2 C14 1.280(7) . ?
N2 C13 1.421(7) . ?
N3 C29 1.296(8) . ?
N3 C30 1.417(7) . ?
N4 C36 1.295(8) . ?
N4 C35 1.433(8) . ?
C1 C2 1.407(8) . ?
C1 C6 1.415(8) . ?
C2 C3 1.388(9) . ?
C2 H2 0.9500 . ?
C3 C4 1.401(10) . ?
C3 H3 0.9500 . ?
C4 C5 1.366(10) . ?
C4 H4 0.9500 . ?
C5 C6 1.419(7) . ?
C5 H5 0.9500 . ?
C6 C7 1.460(8) . ?
C7 H7 0.9500 . ?
C8 C9 1.378(8) . ?
C8 C13 1.411(8) . ?
C9 C10 1.377(8) . ?
C9 H9 0.9500 . ?
C10 C11 1.385(10) . ?
C10 H10 0.9500 . ?
C11 C12 1.385(8) . ?
C11 H11 0.9500 . ?
C12 C13 1.388(8) . ?
C12 H12 0.9500 . ?
C14 C15 1.454(8) . ?
C14 H14 0.9500 . ?
C15 C20 1.405(8) . ?
C15 C16 1.420(7) . ?
C16 C17 1.383(10) . ?
```

```
C16 H16 0.9500 . ?
C17 C18 1.412(9) . ?
C17 H17 0.9500 . ?
C18 C19 1.375(9) . ?
C18 H18 0.9500 . ?
C19 C20 1.415(8) . ?
C19 H19 0.9500 . ?
C21 H21A 0.9800 . ?
C21 H21B 0.9800 . ?
C21 H21C 0.9800 . ?
C22 H22A 0.9800 . ?
C22 H22B 0.9800 . ?
C22 H22C 0.9800 . ?
C23 C24 1.411(8) . ?
C23 C28 1.424(9) . ?
C24 C25 1.378(9) . ?
C24 H24 0.9500 . ?
C25 C26 1.407(9) . ?
C25 H25 0.9500 . ?
C26 C27 1.387(11) . ?
C26 H26 0.9500 . ?
C27 C28 1.405(7) . ?
C27 H27 0.9500 . ?
C28 C29 1.442(9) . ?
C29 H29 0.9500 . ?
C30 C31 1.396(8) . ?
C30 C35 1.410(8) . ?
C31 C32 1.386(8) . ?
C31 H31 0.9500 . ?
C32 C33 1.392(11) . ?
C32 H32 0.9500 . ?
C33 C34 1.396(9) . ?
C33 H33 0.9500 . ?
C34 C35 1.378(8) . ?
C34 H34 0.9500 . ?
C36 C37 1.446(10) . ?
C36 H36 0.9500 . ?
C37 C42 1.428(9) . ?
C37 C38 1.414(8) . ?
C38 C39 1.382(9) . ?
C38 H38 0.9500 . ?
C39 C40 1.407(10) . ?
C39 H39 0.9500 . ?
C40 C41 1.384(10) . ?
C40 H40 0.9500 . ?
C41 C42 1.410(9) . ?
C41 H41 0.9500 . ?
C43 H43A 0.9800 . ?
C43 H43B 0.9800 . ?
C43 H43C 0.9800 . ?
C44 H44A 0.9800 . ?
C44 H44B 0.9800 . ?
C44 H44C 0.9800 . ?

loop_
 _geom_angle_atom_site_label_1
 _geom_angle_atom_site_label_2
 _geom_angle_atom_site_label_3
 _geom_angle
 _geom_angle_site_symmetry_1
 _geom_angle_site_symmetry_3
```

```
 _geom_angle_publ_flag
O1 U1 O2 176.00(19) . . ?
O1 U1 O4 89.97(18) . . ?
O2 U1 O4 91.68(18) . . ?
O1 U1 O5 89.20(17) . . ?
O2 U1 O5 90.74(18) . . ?
O4 U1 O5 156.48(14) . . ?
O1 U1 O3 91.98(18) . . ?
O2 U1 O3 91.9(2) . . ?
O4 U1 O3 78.55(14) . . ?
O5 U1 O3 77.99(14) . . ?
O1 U1 N1 85.94(17) . . ?
O2 U1 N1 91.21(18) . . ?
O4 U1 N1 70.01(15) . . ?
O5 U1 N1 133.33(14) . . ?
O3 U1 N1 148.48(15) . . ?
O1 U1 N2 85.54(18) . . ?
O2 U1 N2 90.68(19) . . ?
O4 U1 N2 133.08(15) . . ?
O5 U1 N2 70.25(15) . . ?
O3 U1 N2 148.17(14) . . ?
N1 U1 N2 63.10(15) . . ?
O6 U2 O7 176.5(2) . . ?
O6 U2 O9 86.54(18) . . ?
O7 U2 O9 94.88(19) . . ?
O6 U2 O10 87.74(18) . . ?
O7 U2 O10 92.06(19) . . ?
O9 U2 O10 158.01(16) . . ?
O6 U2 O8 96.55(18) . . ?
O7 U2 O8 86.80(18) . . ?
O9 U2 O8 79.58(15) . . ?
O10 U2 O8 80.01(16) . . ?
O6 U2 N4 86.34(19) . . ?
O7 U2 N4 90.37(19) . . ?
O9 U2 N4 131.51(16) . . ?
O10 U2 N4 69.15(16) . . ?
O8 U2 N4 148.91(15) . . ?
O6 U2 N3 91.83(18) . . ?
O7 U2 N3 85.72(19) . . ?
O9 U2 N3 69.94(16) . . ?
O10 U2 N3 131.50(16) . . ?
O8 U2 N3 147.81(16) . . ?
N4 U2 N3 62.43(16) . . ?
O3 S1 C21 104.9(3) . . ?
O3 S1 C22 103.9(3) . . ?
C21 S1 C22 99.9(3) . . ?
O8 S2 C44 105.3(3) . . ?
O8 S2 C43 105.3(3) . . ?
C44 S2 C43 99.2(4) . . ?
S1 O3 U1 124.1(2) . . ?
C1 O4 U1 129.5(4) . . ?
C20 O5 U1 128.7(4) . . ?
S2 O8 U2 140.5(3) . . ?
C23 O9 U2 130.5(4) . . ?
C42 O10 U2 127.5(4) . . ?
C7 N1 C8 118.0(5) . . ?
C7 N1 U1 126.7(4) . . ?
C8 N1 U1 115.1(3) . . ?
C14 N2 C13 119.7(5) . . ?
C14 N2 U1 124.8(4) . . ?
C13 N2 U1 115.1(3) . . ?
```

```
C29 N3 C30 117.4(5) . . ?
C29 N3 U2 127.4(4) . . ?
C30 N3 U2 115.1(4) . . ?
C36 N4 C35 119.1(5) . . ?
C36 N4 U2 123.7(4) . . ?
C35 N4 U2 116.5(4) . . ?
O4 C1 C2 120.4(6) . . ?
O4 C1 C6 121.4(5) . . ?
C2 C1 C6 118.2(6) . . ?
C3 C2 C1 121.2(6) . . ?
C3 C2 H2 119.4 . . ?
C1 C2 H2 119.4 . . ?
C2 C3 C4 120.9(6) . . ?
C2 C3 H3 119.5 . . ?
C4 C3 H3 119.5 . . ?
C5 C4 C3 118.3(6) . . ?
C5 C4 H4 120.9 . . ?
C3 C4 H4 120.9 . . ?
C4 C5 C6 122.7(7) . . ?
C4 C5 H5 118.7 . . ?
C6 C5 H5 118.7 . . ?
C1 C6 C5 118.7(6) . . ?
C1 C6 C7 123.3(5) . . ?
C5 C6 C7 117.7(6) . . ?
N1 C7 C6 123.9(5) . . ?
N1 C7 H7 118.1 . . ?
C6 C7 H7 118.1 . . ?
C9 C8 N1 124.6(5) . . ?
C9 C8 C13 120.1(6) . . ?
N1 C8 C13 115.3(5) . . ?
C8 C9 C10 120.4(5) . . ?
C8 C9 H9 119.8 . . ?
C10 C9 H9 119.8 . . ?
C9 C10 C11 120.1(5) . . ?
C9 C10 H10 120.0 . . ?
C11 C10 H10 120.0 . . ?
C12 C11 C10 120.2(6) . . ?
C12 C11 H11 119.9 . . ?
C10 C11 H11 119.9 . . ?
C11 C12 C13 120.3(5) . . ?
C11 C12 H12 119.9 . . ?
C13 C12 H12 119.9 . . ?
C12 C13 N2 124.2(5) . . ?
C12 C13 C8 118.9(5) . . ?
N2 C13 C8 116.8(5) . . ?
N2 C14 C15 125.7(5) . . ?
N2 C14 H14 117.1 . . ?
C15 C14 H14 117.1 . . ?
C20 C15 C16 119.5(6) . . ?
C20 C15 C14 123.1(5) . . ?
C16 C15 C14 117.2(6) . . ?
C17 C16 C15 122.1(7) . . ?
C17 C16 H16 119.0 . . ?
C15 C16 H16 119.0 . . ?
C16 C17 C18 117.5(6) . . ?
C16 C17 H17 121.3 . . ?
C18 C17 H17 121.3 . . ?
C19 C18 C17 121.6(5) . . ?
C19 C18 H18 119.2 . . ?
C17 C18 H18 119.2 . . ?
C18 C19 C20 121.2(6) . . ?
```

```
C18 C19 H19 119.4 . . ?
C20 C19 H19 119.4 . . ?
O5 C20 C15 121.5(5) . . ?
O5 C20 C19 120.4(6) . . ?
C15 C20 C19 118.1(5) . . ?
S1 C21 H21A 109.5 . . ?
S1 C21 H21B 109.5 . . ?
H21A C21 H21B 109.5 . . ?
S1 C21 H21C 109.5 . . ?
H21A C21 H21C 109.5 . . ?
H21B C21 H21C 109.5 . . ?
S1 C22 H22A 109.5 . . ?
S1 C22 H22B 109.5 . . ?
H22A C22 H22B 109.5 . . ?
S1 C22 H22C 109.5 . . ?
H22A C22 H22C 109.5 . . ?
H22B C22 H22C 109.5 . . ?
O9 C23 C24 121.0(6) . . ?
O9 C23 C28 121.7(5) . . ?
C24 C23 C28 117.3(5) . . ?
C25 C24 C23 121.3(6) . . ?
C25 C24 H24 119.4 . . ?
C23 C24 H24 119.4 . . ?
C24 C25 C26 120.9(6) . . ?
C24 C25 H25 119.5 . . ?
C26 C25 H25 119.5 . . ?
C27 C26 C25 119.1(6) . . ?
C27 C26 H26 120.5 . . ?
C25 C26 H26 120.5 . . ?
C26 C27 C28 120.5(7) . . ?
C26 C27 H27 119.8 . . ?
C28 C27 H27 119.8 . . ?
C27 C28 C23 120.5(6) . . ?
C27 C28 C29 116.8(6) . . ?
C23 C28 C29 122.6(5) . . ?
N3 C29 C28 125.7(6) . . ?
N3 C29 H29 117.2 . . ?
C28 C29 H29 117.2 . . ?
C31 C30 C35 119.1(5) . . ?
C31 C30 N3 124.7(6) . . ?
C35 C30 N3 116.2(5) . . ?
C30 C31 C32 120.1(6) . . ?
C30 C31 H31 119.9 . . ?
C32 C31 H31 119.9 . . ?
C31 C32 C33 120.3(6) . . ?
C31 C32 H32 119.9 . . ?
C33 C32 H32 119.9 . . ?
C34 C33 C32 120.2(6) . . ?
C34 C33 H33 119.9 . . ?
C32 C33 H33 119.9 . . ?
C35 C34 C33 119.7(6) . . ?
C35 C34 H34 120.2 . . ?
C33 C34 H34 120.2 . . ?
C34 C35 C30 120.6(6) . . ?
C34 C35 N4 123.5(6) . . ?
C30 C35 N4 115.8(5) . . ?
N4 C36 C37 125.5(5) . . ?
N4 C36 H36 117.2 . . ?
C37 C36 H36 117.2 . . ?
C42 C37 C38 120.1(7) . . ?
C42 C37 C36 121.2(5) . . ?
```

```
C38 C37 C36 118.3(6) . . ?
C39 C38 C37 121.4(6) . . ?
C39 C38 H38 119.3 . . ?
C37 C38 H38 119.3 . . ?
C38 C39 C40 118.5(6) . . ?
C38 C39 H39 120.7 . . ?
C40 C39 H39 120.7 . . ?
C41 C40 C39 120.9(6) . . ?
C41 C40 H40 119.5 . . ?
C39 C40 H40 119.5 . . ?
C40 C41 C42 121.9(7) . . ?
C40 C41 H41 119.1 . . ?
C42 C41 H41 119.1 . . ?
O10 C42 C41 120.9(6) . . ?
O10 C42 C37 122.1(6) . . ?
C41 C42 C37 117.0(6) . . ?
S2 C43 H43A 109.5 . . ?
S2 C43 H43B 109.5 . . ?
H43A C43 H43B 109.5 . . ?
S2 C43 H43C 109.5 . . ?
H43A C43 H43C 109.5 . . ?
H43B C43 H43C 109.5 . . ?
S2 C44 H44A 109.5 . . ?
S2 C44 H44B 109.5 . . ?
H44A C44 H44B 109.5 . . ?
S2 C44 H44C 109.5 . . ?
H44A C44 H44C 109.5 . . ?
H44B C44 H44C 109.5 . . ?

_diffrn_measured_fraction_theta_max    0.973
_diffrn_reflns_theta_full              27.49
_diffrn_measured_fraction_theta_full   0.973
_refine_diff_density_max    0.955
_refine_diff_density_min   -0.918
_refine_diff_density_rms    0.140
```

Appendix E

Crystallographic Information of $U^{VI}O_2(dbm)_2DMSO$

```
data_shelxl

_audit_creation_method            SHELXL-97
_chemical_name_systematic
;
 ?
;
_chemical_name_common             ?
_chemical_melting_point           ?
_chemical_formula_moiety          ?
_chemical_formula_sum
 'C32 H28 O7 S U'
_chemical_formula_weight          794.63

loop_
 _atom_type_symbol
 _atom_type_description
 _atom_type_scat_dispersion_real
 _atom_type_scat_dispersion_imag
 _atom_type_scat_source
 'C'  'C'   0.0033   0.0016
 'International Tables Vol C Tables 4.2.6.8 and 6.1.1.4'
 'H'  'H'   0.0000   0.0000
 'International Tables Vol C Tables 4.2.6.8 and 6.1.1.4'
 'O'  'O'   0.0106   0.0060
 'International Tables Vol C Tables 4.2.6.8 and 6.1.1.4'
 'S'  'S'   0.1246   0.1234
 'International Tables Vol C Tables 4.2.6.8 and 6.1.1.4'
 'U'  'U'  -9.6767   9.6646
 'International Tables Vol C Tables 4.2.6.8 and 6.1.1.4'

_symmetry_cell_setting            ?
_symmetry_space_group_name_H-M    ?

loop_
 _symmetry_equiv_pos_as_xyz
 'x, y, z'
 '-x+1/2, y+1/2, z+1/2'
 'x+1/2, -y+1/2, z'
 '-x, -y, z+1/2'
```

```
_cell_length_a                    16.090(6)
_cell_length_b                    9.975(3)
_cell_length_c                    35.845(8)
_cell_angle_alpha                 90.00
_cell_angle_beta                  90.00
_cell_angle_gamma                 90.00
_cell_volume                      5753(3)
_cell_formula_units_Z             8
_cell_measurement_temperature     93(2)
_cell_measurement_reflns_used     ?
_cell_measurement_theta_min       ?
_cell_measurement_theta_max       ?

_exptl_crystal_description        ?
_exptl_crystal_colour             ?
_exptl_crystal_size_max           0.10
_exptl_crystal_size_mid           0.10
_exptl_crystal_size_min           0.10
_exptl_crystal_density_meas       ?
_exptl_crystal_density_diffrn     1.835
_exptl_crystal_density_method     'not measured'
_exptl_crystal_F_000              3072
_exptl_absorpt_coefficient_mu     5.763
_exptl_absorpt_correction_type    ?
_exptl_absorpt_correction_T_min   0.5965
_exptl_absorpt_correction_T_max   0.5965
_exptl_absorpt_process_details    ?

_exptl_special_details
;
 ?
;

_diffrn_ambient_temperature       93(2)
_diffrn_radiation_wavelength      0.71075
_diffrn_radiation_type            MoK¥a
_diffrn_radiation_source          'fine-focus sealed tube'
_diffrn_radiation_monochromator   graphite
_diffrn_measurement_device_type   ?
_diffrn_measurement_method        ?
_diffrn_detector_area_resol_mean  ?
_diffrn_standards_number          ?
_diffrn_standards_interval_count  ?
_diffrn_standards_interval_time   ?
_diffrn_standards_decay_%         ?
_diffrn_reflns_number             66370
_diffrn_reflns_av_R_equivalents   0.0427
_diffrn_reflns_av_sigmaI/netI     0.0298
_diffrn_reflns_limit_h_min        -20
_diffrn_reflns_limit_h_max        20
_diffrn_reflns_limit_k_min        -11
_diffrn_reflns_limit_k_max        12
_diffrn_reflns_limit_l_min        -46
_diffrn_reflns_limit_l_max        46
_diffrn_reflns_theta_min          3.05
_diffrn_reflns_theta_max          27.49
_reflns_number_total              13170
_reflns_number_gt                 11663
_reflns_threshold_expression      >2sigma(I)
```

```
_computing_data_collection        'PROCESS-AUTO'
_computing_cell_refinement        'PROCESS-AUTO'
_computing_data_reduction         'CrystalStructure'
_computing_structure_solution     'DIRDIF99 (PATTY)'
_computing_structure_refinement   'SHELXL-97 (Sheldrick, 1997)'
_computing_molecular_graphics     ?
_computing_publication_material   ?

_refine_special_details
;
 Refinement of F^2^ against ALL reflections.  The weighted R-factor wR and
 goodness of fit S are based on F^2^, conventional R-factors R are based
 on F, with F set to zero for negative F^2^. The threshold expression of
 F^2^ > 2sigma(F^2^) is used only for calculating R-factors(gt) etc. and is
 not relevant to the choice of reflections for refinement.  R-factors based
 on F^2^ are statistically about twice as large as those based on F, and R-
 factors based on ALL data will be even larger.
;

_refine_ls_structure_factor_coef  Fsqd
_refine_ls_matrix_type            full
_refine_ls_weighting_scheme       calc
_refine_ls_weighting_details
 'calc w=1/[¥s^2^(Fo^2^)+(0.0312P)^2^+38.5857P] where P=(Fo^2^+2Fc^2^)/3'
_atom_sites_solution_primary      direct
_atom_sites_solution_secondary    difmap
_atom_sites_solution_hydrogens    geom
_refine_ls_hydrogen_treatment     mixed
_refine_ls_extinction_method      SHELXL
_refine_ls_extinction_coef        0.00019(3)
_refine_ls_extinction_expression
 'Fc^*^=kFc[1+0.001xFc^2^¥l^3^/sin(2¥q)]^-1/4^'
_refine_ls_abs_structure_details
 'Flack H D (1983), Acta Cryst. A39, 876-881'
_refine_ls_abs_structure_Flack    0.460(6)
_refine_ls_number_reflns          13170
_refine_ls_number_parameters      740
_refine_ls_number_restraints      1
_refine_ls_R_factor_all           0.0417
_refine_ls_R_factor_gt            0.0340
_refine_ls_wR_factor_ref          0.0776
_refine_ls_wR_factor_gt           0.0743
_refine_ls_goodness_of_fit_ref    1.024
_refine_ls_restrained_S_all       1.024
_refine_ls_shift/su_max           0.001
_refine_ls_shift/su_mean          0.000

loop_
 _atom_site_label
 _atom_site_type_symbol
 _atom_site_fract_x
 _atom_site_fract_y
 _atom_site_fract_z
 _atom_site_U_iso_or_equiv
 _atom_site_adp_type
 _atom_site_occupancy
 _atom_site_symmetry_multiplicity
 _atom_site_calc_flag
 _atom_site_refinement_flags
 _atom_site_disorder_assembly
 _atom_site_disorder_group
```

```
U1 U 0.196401(13) 0.17809(2) 0.000808(5) 0.01262(5) Uani 1 1 d . . .
U2 U 0.033981(14) -0.32068(2) -0.284230(6) 0.01492(6) Uani 1 1 d . . .
S1 S 0.39606(12) 0.1669(2) 0.04166(6) 0.0324(5) Uani 1 1 d . . .
S2 S -0.1514(2) -0.2436(3) -0.33051(11) 0.0838(13) Uani 1 1 d . . .
O1 O 0.2673(3) 0.2675(5) -0.02850(14) 0.0202(10) Uani 1 1 d . . .
O2 O 0.1268(3) 0.0892(5) 0.03095(13) 0.0183(10) Uani 1 1 d . . .
O3 O 0.3029(3) 0.1627(5) 0.04887(13) 0.0207(10) Uani 1 1 d . . .
O4 O 0.1852(4) 0.3735(6) 0.03707(15) 0.0228(12) Uani 1 1 d . . .
O5 O 0.0847(3) 0.3090(5) -0.01943(14) 0.0207(10) Uani 1 1 d . . .
O6 O 0.2698(3) -0.0212(5) -0.01062(12) 0.0172(10) Uani 1 1 d . . .
O7 O 0.1420(3) 0.0716(5) -0.05220(13) 0.0178(10) Uani 1 1 d . . .
O8 O -0.0379(3) -0.2368(6) -0.25516(16) 0.0236(11) Uani 1 1 d . . .
O9 O 0.1055(4) -0.4033(6) -0.31475(15) 0.0241(11) Uani 1 1 d . . .
O10 O -0.0707(4) -0.3247(6) -0.33347(17) 0.0368(14) Uani 1 1 d . . .
O11 O 0.0489(4) -0.1259(6) -0.31997(15) 0.0253(12) Uani 1 1 d . . .
O12 O 0.1411(3) -0.1857(5) -0.25940(14) 0.0226(10) Uani 1 1 d . . .
O13 O -0.0378(3) -0.5234(5) -0.27521(12) 0.0185(10) Uani 1 1 d . . .
O14 O 0.0884(3) -0.4317(5) -0.23198(14) 0.0215(11) Uani 1 1 d . . .
C1 C 0.2595(5) 0.5584(8) 0.0814(2) 0.0330(19) Uani 1 1 d . . .
H1 H 0.2694 0.4655 0.0851 0.040 Uiso 1 1 calc R . .
C2 C 0.2936(6) 0.6506(10) 0.1059(3) 0.040(2) Uani 1 1 d . . .
H2 H 0.3242 0.6204 0.1270 0.048 Uiso 1 1 calc R . .
C3 C 0.2833(5) 0.7870(8) 0.0998(2) 0.0267(17) Uani 1 1 d . . .
H3 H 0.3085 0.8502 0.1161 0.032 Uiso 1 1 calc R . .
C4 C 0.2365(5) 0.8305(8) 0.06990(19) 0.0216(14) Uani 1 1 d . . .
H4 H 0.2285 0.9237 0.0658 0.026 Uiso 1 1 calc R . .
C5 C 0.2008(4) 0.7372(8) 0.0458(2) 0.0176(15) Uani 1 1 d . . .
H5 H 0.1690 0.7678 0.0252 0.021 Uiso 1 1 calc R . .
C6 C 0.2109(5) 0.5998(8) 0.0514(2) 0.0185(15) Uani 1 1 d . . .
C7 C 0.1751(5) 0.4945(7) 0.02667(18) 0.0171(13) Uani 1 1 d . . .
C8 C 0.1275(4) 0.5291(7) -0.0048(2) 0.0204(14) Uani 1 1 d . . .
H8 H 0.1271 0.6199 -0.0129 0.024 Uiso 1 1 calc R . .
C9 C 0.0809(4) 0.4356(7) -0.02475(18) 0.0162(13) Uani 1 1 d . . .
C10 C 0.0194(4) 0.4827(7) -0.05336(19) 0.0161(13) Uani 1 1 d . . .
C11 C 0.0271(4) 0.6053(8) -0.0712(2) 0.0194(15) Uani 1 1 d . . .
H11 H 0.0739 0.6609 -0.0664 0.023 Uiso 1 1 calc R . .
C12 C -0.0343(5) 0.6467(7) -0.0962(2) 0.0228(15) Uani 1 1 d . . .
H12 H -0.0287 0.7302 -0.1087 0.027 Uiso 1 1 calc R . .
C13 C -0.1030(5) 0.5679(8) -0.1029(2) 0.0223(15) Uani 1 1 d . . .
H13 H -0.1451 0.5982 -0.1195 0.027 Uiso 1 1 calc R . .
C14 C -0.1107(5) 0.4433(8) -0.08542(18) 0.0208(15) Uani 1 1 d . . .
H14 H -0.1579 0.3887 -0.0902 0.025 Uiso 1 1 calc R . .
C15 C -0.0492(4) 0.3991(7) -0.06094(18) 0.0175(14) Uani 1 1 d . . .
H15 H -0.0534 0.3134 -0.0495 0.021 Uiso 1 1 calc R . .
C16 C 0.3969(4) -0.2006(7) -0.0014(2) 0.0197(13) Uani 1 1 d . . .
H16 H 0.3992 -0.1168 0.0111 0.024 Uiso 1 1 calc R . .
C17 C 0.4596(4) -0.2938(8) 0.0041(2) 0.0241(16) Uani 1 1 d . . .
H17 H 0.5044 -0.2737 0.0204 0.029 Uiso 1 1 calc R . .
C18 C 0.4571(5) -0.4167(8) -0.0142(2) 0.0246(16) Uani 1 1 d . . .
H18 H 0.5012 -0.4792 -0.0113 0.030 Uiso 1 1 calc R . .
C19 C 0.3903(5) -0.4473(8) -0.0368(2) 0.0260(16) Uani 1 1 d . . .
H19 H 0.3880 -0.5322 -0.0487 0.031 Uiso 1 1 calc R . .
C20 C 0.3262(5) -0.3557(7) -0.0422(2) 0.0212(15) Uani 1 1 d . . .
H20 H 0.2799 -0.3790 -0.0573 0.025 Uiso 1 1 calc R . .
C21 C 0.3301(4) -0.2285(7) -0.02521(18) 0.0160(13) Uani 1 1 d . . .
C22 C 0.2672(4) -0.1227(7) -0.03197(19) 0.0153(13) Uani 1 1 d . . .
C23 C 0.2099(5) -0.1352(8) -0.0614(2) 0.0195(15) Uani 1 1 d . . .
H23 H 0.2094 -0.2163 -0.0753 0.023 Uiso 1 1 calc R . .
C24 C 0.1536(4) -0.0343(7) -0.07135(18) 0.0165(13) Uani 1 1 d . . .
C25 C 0.1026(4) -0.0481(7) -0.10616(19) 0.0169(13) Uani 1 1 d . . .
C26 C 0.1231(5) -0.1385(8) -0.13480(19) 0.0210(14) Uani 1 1 d . . .
```

```
H26 H 0.1717 -0.1920 -0.1328 0.025 Uiso 1 1 calc R . .
C27 C 0.0723(5) -0.1497(8) -0.1661(2) 0.0232(15) Uani 1 1 d . . .
H27 H 0.0860 -0.2121 -0.1851 0.028 Uiso 1 1 calc R . .
C28 C 0.0025(5) -0.0714(8) -0.1696(2) 0.0245(16) Uani 1 1 d . . .
H28 H -0.0319 -0.0801 -0.1910 0.029 Uiso 1 1 calc R . .
C29 C -0.0177(4) 0.0198(7) -0.1422(2) 0.0215(14) Uani 1 1 d . . .
H29 H -0.0658 0.0741 -0.1448 0.026 Uiso 1 1 calc R . .
C30 C 0.0324(4) 0.0330(8) -0.1104(2) 0.0182(15) Uani 1 1 d . . .
H30 H 0.0186 0.0970 -0.0918 0.022 Uiso 1 1 calc R . .
C31 C 0.4255(6) 0.3348(10) 0.0506(5) 0.077(5) Uani 1 1 d . . .
H31A H 0.4001 0.3938 0.0320 0.116 Uiso 1 1 calc R . .
H31B H 0.4861 0.3426 0.0493 0.116 Uiso 1 1 calc R . .
H31C H 0.4065 0.3609 0.0756 0.116 Uiso 1 1 calc R . .
C32 C 0.4465(8) 0.0883(14) 0.0767(4) 0.072(4) Uani 1 1 d . . .
H32A H 0.4361 -0.0084 0.0752 0.108 Uiso 1 1 calc R . .
H32B H 0.4264 0.1224 0.1007 0.108 Uiso 1 1 calc R . .
H32C H 0.5063 0.1052 0.0746 0.108 Uiso 1 1 calc R . .
C33 C -0.0062(5) 0.0521(8) -0.37002(19) 0.0234(15) Uani 1 1 d . . .
H33 H -0.0098 -0.0417 -0.3744 0.028 Uiso 1 1 calc R . .
C34 C -0.0373(5) 0.1402(8) -0.3964(2) 0.0287(17) Uani 1 1 d . . .
H34 H -0.0609 0.1071 -0.4189 0.034 Uiso 1 1 calc R . .
C35 C -0.0338(5) 0.2762(9) -0.3899(2) 0.0250(16) Uani 1 1 d . . .
H35 H -0.0564 0.3367 -0.4077 0.030 Uiso 1 1 calc R . .
C36 C 0.0021(5) 0.3248(8) -0.3579(2) 0.0233(15) Uani 1 1 d . . .
H36 H 0.0044 0.4188 -0.3537 0.028 Uiso 1 1 calc R . .
C37 C 0.0354(4) 0.2370(8) -0.3315(2) 0.0173(15) Uani 1 1 d . . .
H37 H 0.0616 0.2709 -0.3097 0.021 Uiso 1 1 calc R . .
C38 C 0.0298(4) 0.0978(8) -0.3374(2) 0.0184(15) Uani 1 1 d . . .
C39 C 0.0618(4) -0.0022(7) -0.31058(18) 0.0164(13) Uani 1 1 d . . .
C40 C 0.1065(4) 0.0336(7) -0.27845(18) 0.0164(13) Uani 1 1 d . . .
H40 H 0.1082 0.1255 -0.2716 0.020 Uiso 1 1 calc R . .
C41 C 0.1488(4) -0.0592(7) -0.25600(19) 0.0172(14) Uani 1 1 d . . .
C42 C 0.2121(4) -0.0129(8) -0.22940(19) 0.0168(14) Uani 1 1 d . . .
C43 C 0.2082(5) 0.1157(8) -0.2130(2) 0.0191(14) Uani 1 1 d . . .
H43 H 0.1628 0.1733 -0.2184 0.023 Uiso 1 1 calc R . .
C44 C 0.2706(5) 0.1583(7) -0.18900(18) 0.0199(14) Uani 1 1 d . . .
H44 H 0.2675 0.2446 -0.1779 0.024 Uiso 1 1 calc R . .
C45 C 0.3371(5) 0.0753(8) -0.18127(19) 0.0214(15) Uani 1 1 d . . .
H45 H 0.3802 0.1052 -0.1652 0.026 Uiso 1 1 calc R . .
C46 C 0.3411(5) -0.0519(8) -0.1970(2) 0.0219(14) Uani 1 1 d . . .
H46 H 0.3868 -0.1091 -0.1916 0.026 Uiso 1 1 calc R . .
C47 C 0.2789(4) -0.0947(7) -0.22042(19) 0.0196(14) Uani 1 1 d . . .
H47 H 0.2817 -0.1824 -0.2307 0.023 Uiso 1 1 calc R . .
C48 C -0.1608(4) -0.7064(7) -0.2879(2) 0.0218(15) Uani 1 1 d . . .
H48 H -0.1616 -0.6232 -0.3008 0.026 Uiso 1 1 calc R . .
C49 C -0.2218(5) -0.8010(8) -0.2946(2) 0.0278(18) Uani 1 1 d . . .
H49 H -0.2654 -0.7808 -0.3116 0.033 Uiso 1 1 calc R . .
C50 C -0.2205(4) -0.9233(8) -0.2773(2) 0.0251(16) Uani 1 1 d . . .
H50 H -0.2629 -0.9873 -0.2822 0.030 Uiso 1 1 calc R . .
C51 C -0.1568(5) -0.9532(8) -0.2524(2) 0.0265(17) Uani 1 1 d . . .
H51 H -0.1547 -1.0386 -0.2407 0.032 Uiso 1 1 calc R . .
C52 C -0.0958(5) -0.8577(8) -0.2448(2) 0.0214(15) Uani 1 1 d . . .
H52 H -0.0525 -0.8782 -0.2277 0.026 Uiso 1 1 calc R . .
C53 C -0.0979(4) -0.7332(7) -0.26194(18) 0.0159(13) Uani 1 1 d . . .
C54 C -0.0358(4) -0.6252(7) -0.2538(2) 0.0171(14) Uani 1 1 d . . .
C55 C 0.0200(4) -0.6382(7) -0.2238(2) 0.0164(14) Uani 1 1 d . . .
H55 H 0.0194 -0.7194 -0.2099 0.020 Uiso 1 1 calc R . .
C56 C 0.0761(4) -0.5390(7) -0.21332(17) 0.0142(12) Uani 1 1 d . . .
C57 C 0.1265(4) -0.5521(7) -0.17835(18) 0.0160(13) Uani 1 1 d . . .
C58 C 0.1064(5) -0.6445(7) -0.15018(18) 0.0189(14) Uani 1 1 d . . .
H58 H 0.0591 -0.7005 -0.1530 0.023 Uiso 1 1 calc R . .
```

```
C59 C 0.1548(5) -0.6547(7) -0.11839(19) 0.0204(14) Uani 1 1 d . . .
H59 H 0.1401 -0.7165 -0.0993 0.024 Uiso 1 1 calc R . .
C60 C 0.2249(5) -0.5747(8) -0.1143(2) 0.0230(15) Uani 1 1 d . . .
H60 H 0.2594 -0.5840 -0.0929 0.028 Uiso 1 1 calc R . .
C61 C 0.2446(5) -0.4802(7) -0.1418(2) 0.0222(14) Uani 1 1 d . . .
H61 H 0.2916 -0.4236 -0.1387 0.027 Uiso 1 1 calc R . .
C62 C 0.1957(4) -0.4691(8) -0.1736(2) 0.0195(15) Uani 1 1 d . . .
H62 H 0.2094 -0.4048 -0.1921 0.023 Uiso 1 1 calc R . .
C63 C -0.1699(9) -0.1979(16) -0.3800(4) 0.096(6) Uani 1 1 d . . .
H63A H -0.1297 -0.1293 -0.3877 0.143 Uiso 1 1 calc R . .
H63B H -0.2264 -0.1627 -0.3828 0.143 Uiso 1 1 calc R . .
H63C H -0.1632 -0.2776 -0.3958 0.143 Uiso 1 1 calc R . .
C64 C -0.2294(7) -0.3599(14) -0.3276(4) 0.069(4) Uani 1 1 d . . .
H64A H -0.2309 -0.3975 -0.3023 0.103 Uiso 1 1 calc R . .
H64B H -0.2193 -0.4319 -0.3456 0.103 Uiso 1 1 calc R . .
H64C H -0.2828 -0.3169 -0.3331 0.103 Uiso 1 1 calc R . .

loop_
 _atom_site_aniso_label
 _atom_site_aniso_U_11
 _atom_site_aniso_U_22
 _atom_site_aniso_U_33
 _atom_site_aniso_U_23
 _atom_site_aniso_U_13
 _atom_site_aniso_U_12
U1 0.01269(10) 0.01144(10) 0.01373(10) 0.00007(17) -0.00223(9) 0.00022(9)
U2 0.01566(11) 0.01253(10) 0.01658(11) 0.00155(17) -0.00500(9) -0.00137(9)
S1 0.0160(8) 0.0411(12) 0.0402(11) -0.0175(9) -0.0064(7) 0.0054(8)
S2 0.092(2) 0.0518(17) 0.108(3) -0.0404(18) -0.080(2) 0.0377(18)
O1 0.022(3) 0.017(2) 0.022(3) 0.001(2) -0.001(2) -0.004(2)
O2 0.017(2) 0.020(2) 0.018(2) 0.0043(19) -0.0013(19) -0.001(2)
O3 0.016(2) 0.024(3) 0.021(2) 0.001(2) -0.0069(19) 0.000(2)
O4 0.031(3) 0.020(3) 0.017(3) -0.005(2) -0.004(2) 0.007(2)
O5 0.020(2) 0.013(2) 0.030(3) 0.002(2) -0.006(2) -0.001(2)
O6 0.018(2) 0.014(2) 0.020(2) -0.0023(18) -0.0049(18) 0.0031(19)
O7 0.019(2) 0.012(2) 0.022(2) -0.0013(18) -0.007(2) 0.0030(19)
O8 0.024(3) 0.022(3) 0.025(3) -0.002(2) -0.002(2) 0.003(2)
O9 0.025(3) 0.024(3) 0.023(3) 0.000(2) 0.000(2) -0.002(2)
O10 0.043(3) 0.025(3) 0.042(3) 0.009(3) -0.026(3) -0.006(3)
O11 0.037(3) 0.019(3) 0.020(3) 0.005(2) -0.008(2) -0.006(2)
O12 0.022(3) 0.021(2) 0.025(2) 0.006(2) -0.009(2) -0.006(2)
O13 0.019(2) 0.013(2) 0.023(3) 0.0023(18) -0.0066(19) -0.002(2)
O14 0.026(3) 0.019(3) 0.020(2) 0.0066(19) -0.008(2) -0.006(2)
C1 0.038(5) 0.019(4) 0.042(5) -0.009(3) -0.019(4) 0.013(3)
C2 0.041(5) 0.036(5) 0.044(5) -0.003(4) -0.028(4) 0.009(4)
C3 0.025(4) 0.025(4) 0.031(4) -0.011(3) -0.009(3) -0.002(3)
C4 0.025(4) 0.019(3) 0.020(3) 0.000(3) 0.000(3) 0.000(3)
C5 0.017(3) 0.024(4) 0.011(3) 0.000(3) 0.000(2) -0.001(3)
C6 0.021(4) 0.021(4) 0.014(3) -0.001(3) -0.002(3) 0.004(3)
C7 0.019(3) 0.018(3) 0.014(3) -0.001(3) 0.003(3) 0.003(3)
C8 0.021(3) 0.019(3) 0.021(4) -0.004(3) -0.002(3) 0.003(3)
C9 0.012(3) 0.019(3) 0.018(3) 0.003(3) 0.002(2) 0.001(3)
C10 0.014(3) 0.019(3) 0.015(3) -0.007(3) 0.001(2) 0.005(3)
C11 0.020(4) 0.022(4) 0.016(3) 0.004(3) 0.002(3) -0.001(3)
C12 0.023(4) 0.023(4) 0.023(3) 0.002(3) 0.006(3) 0.003(3)
C13 0.023(4) 0.027(4) 0.017(3) 0.000(3) 0.000(3) 0.005(3)
C14 0.021(3) 0.029(4) 0.013(3) -0.003(3) -0.003(3) 0.001(3)
C15 0.019(4) 0.017(3) 0.016(3) -0.004(3) 0.000(3) 0.002(3)
C16 0.014(3) 0.022(3) 0.023(3) 0.001(3) 0.002(3) 0.000(2)
C17 0.018(3) 0.027(4) 0.027(4) 0.008(3) -0.004(3) -0.001(2)
C18 0.021(4) 0.022(4) 0.031(4) 0.005(3) 0.005(3) 0.010(3)
```

```
C19 0.023(4) 0.024(4) 0.031(4) -0.003(3) 0.000(3) 0.004(3)
C20 0.019(4) 0.015(3) 0.030(4) -0.004(3) -0.004(3) 0.003(3)
C21 0.014(3) 0.020(3) 0.014(3) -0.001(3) 0.004(2) 0.000(3)
C22 0.016(3) 0.011(3) 0.019(3) 0.002(2) 0.000(3) 0.001(3)
C23 0.021(4) 0.017(4) 0.021(4) -0.003(3) -0.001(3) -0.002(3)
C24 0.014(3) 0.019(3) 0.017(3) 0.000(3) 0.004(2) -0.002(3)
C25 0.013(3) 0.018(3) 0.020(3) 0.002(3) -0.002(2) -0.003(3)
C26 0.017(3) 0.026(4) 0.019(3) 0.002(3) 0.001(3) 0.001(3)
C27 0.026(4) 0.025(4) 0.019(3) -0.001(3) -0.002(3) -0.007(3)
C28 0.030(4) 0.022(4) 0.021(4) 0.005(3) -0.008(3) -0.006(3)
C29 0.019(3) 0.022(4) 0.024(3) 0.006(3) -0.009(3) -0.002(3)
C30 0.015(4) 0.021(4) 0.019(4) -0.001(3) -0.001(2) -0.001(3)
C31 0.017(4) 0.034(5) 0.180(15) 0.052(7) -0.021(6) -0.020(4)
C32 0.054(7) 0.074(9) 0.087(9) 0.022(7) -0.045(7) 0.011(6)
C33 0.026(4) 0.024(4) 0.021(3) 0.003(3) 0.000(3) -0.002(3)
C34 0.034(4) 0.026(4) 0.026(4) 0.001(3) -0.015(3) -0.001(3)
C35 0.024(4) 0.028(4) 0.023(4) 0.004(3) -0.005(3) 0.000(3)
C36 0.025(4) 0.019(3) 0.026(4) 0.001(3) 0.003(3) 0.005(3)
C37 0.019(3) 0.017(4) 0.016(4) 0.002(3) 0.001(2) 0.001(3)
C38 0.014(3) 0.022(4) 0.020(3) 0.006(3) 0.000(3) -0.002(3)
C39 0.013(3) 0.018(3) 0.019(3) 0.005(3) 0.004(3) -0.001(3)
C40 0.016(3) 0.018(3) 0.015(3) -0.002(3) -0.002(2) 0.002(3)
C41 0.017(3) 0.018(3) 0.017(3) 0.003(3) 0.002(3) -0.004(3)
C42 0.016(3) 0.022(4) 0.013(3) -0.002(3) 0.000(2) 0.000(3)
C43 0.020(3) 0.020(4) 0.017(3) 0.003(3) 0.000(3) 0.002(3)
C44 0.029(4) 0.019(3) 0.012(3) -0.002(2) -0.006(3) -0.004(3)
C45 0.022(4) 0.029(4) 0.013(3) -0.004(3) -0.002(3) -0.005(3)
C46 0.019(3) 0.023(4) 0.023(3) 0.002(3) -0.006(3) 0.002(3)
C47 0.022(4) 0.016(3) 0.020(3) 0.001(3) -0.001(3) 0.000(3)
C48 0.022(3) 0.019(4) 0.025(4) 0.003(3) -0.008(3) 0.000(3)
C49 0.018(3) 0.031(4) 0.035(4) -0.001(3) -0.010(3) -0.001(3)
C50 0.013(3) 0.026(4) 0.036(4) -0.004(3) -0.005(3) -0.007(3)
C51 0.025(4) 0.016(4) 0.039(4) 0.003(3) 0.003(3) -0.002(3)
C52 0.019(4) 0.023(4) 0.023(4) -0.001(3) -0.004(3) 0.000(3)
C53 0.014(3) 0.018(3) 0.016(3) -0.003(3) 0.002(2) -0.004(3)
C54 0.015(3) 0.016(3) 0.020(3) -0.003(3) 0.004(3) 0.003(3)
C55 0.016(3) 0.014(3) 0.019(3) 0.000(3) -0.001(3) 0.000(3)
C56 0.013(3) 0.017(3) 0.012(3) -0.002(2) -0.005(2) 0.003(3)
C57 0.017(3) 0.015(3) 0.016(3) -0.004(3) -0.002(2) 0.003(3)
C58 0.024(4) 0.020(3) 0.013(3) 0.000(2) -0.002(3) 0.001(3)
C59 0.024(4) 0.023(4) 0.015(3) 0.003(3) 0.001(3) 0.001(3)
C60 0.026(4) 0.023(4) 0.020(3) -0.005(3) -0.009(3) 0.006(3)
C61 0.022(4) 0.018(3) 0.027(3) -0.002(3) -0.004(3) -0.001(3)
C62 0.023(4) 0.014(4) 0.021(4) -0.002(3) -0.003(3) 0.001(3)
C63 0.072(8) 0.109(12) 0.106(11) 0.063(10) -0.061(9) -0.027(9)
C64 0.046(6) 0.082(9) 0.077(8) 0.037(7) 0.025(6) 0.019(6)

_geom_special_details
;
 All esds (except the esd in the dihedral angle between two l.s. planes)
 are estimated using the full covariance matrix.  The cell esds are taken
 into account individually in the estimation of esds in distances, angles
 and torsion angles; correlations between esds in cell parameters are only
 used when they are defined by crystal symmetry.  An approximate (isotropic)
 treatment of cell esds is used for estimating esds involving l.s. planes.
;

loop_
 _geom_bond_atom_site_label_1
 _geom_bond_atom_site_label_2
 _geom_bond_distance
```

```
 _geom_bond_site_symmetry_2
 _geom_bond_publ_flag
U1 O1 1.789(5) . ?
U1 O2 1.791(5) . ?
U1 O5 2.337(5) . ?
U1 O7 2.346(5) . ?
U1 O6 2.348(5) . ?
U1 O4 2.350(6) . ?
U1 O3 2.435(5) . ?
U2 O8 1.768(5) . ?
U2 O9 1.788(6) . ?
U2 O11 2.340(6) . ?
U2 O14 2.346(5) . ?
U2 O13 2.351(5) . ?
U2 O12 2.361(5) . ?
U2 O10 2.440(5) . ?
S1 O3 1.521(5) . ?
S1 C32 1.690(10) . ?
S1 C31 1.770(11) . ?
S2 O10 1.533(7) . ?
S2 C64 1.713(14) . ?
S2 C63 1.857(13) . ?
O4 C7 1.274(9) . ?
O5 C9 1.279(8) . ?
O6 C22 1.270(8) . ?
O7 C24 1.273(8) . ?
O11 C39 1.296(9) . ?
O12 C41 1.274(9) . ?
O13 C54 1.273(9) . ?
O14 C56 1.277(8) . ?
C1 C6 1.391(10) . ?
C1 C2 1.386(12) . ?
C1 H1 0.9500 . ?
C2 C3 1.388(12) . ?
C2 H2 0.9500 . ?
C3 C4 1.380(11) . ?
C3 H3 0.9500 . ?
C4 C5 1.392(11) . ?
C4 H4 0.9500 . ?
C5 C6 1.395(11) . ?
C5 H5 0.9500 . ?
C6 C7 1.490(10) . ?
C7 C8 1.408(10) . ?
C8 C9 1.393(10) . ?
C8 H8 0.9500 . ?
C9 C10 1.501(9) . ?
C10 C11 1.385(11) . ?
C10 C15 1.409(10) . ?
C11 C12 1.397(10) . ?
C11 H11 0.9500 . ?
C12 C13 1.377(11) . ?
C12 H12 0.9500 . ?
C13 C14 1.398(11) . ?
C13 H13 0.9500 . ?
C14 C15 1.395(10) . ?
C14 H14 0.9500 . ?
C15 H15 0.9500 . ?
C16 C17 1.386(10) . ?
C16 C21 1.400(10) . ?
C16 H16 0.9500 . ?
C17 C18 1.392(11) . ?
```

```
C17 H17 0.9500 . ?
C18 C19 1.379(11) . ?
C18 H18 0.9500 . ?
C19 C20 1.392(11) . ?
C19 H19 0.9500 . ?
C20 C21 1.409(10) . ?
C20 H20 0.9500 . ?
C21 C22 1.482(10) . ?
C22 C23 1.406(10) . ?
C23 C24 1.400(10) . ?
C23 H23 0.9500 . ?
C24 C25 1.499(9) . ?
C25 C30 1.398(10) . ?
C25 C26 1.406(10) . ?
C26 C27 1.392(10) . ?
C26 H26 0.9500 . ?
C27 C28 1.375(11) . ?
C27 H27 0.9500 . ?
C28 C29 1.379(11) . ?
C28 H28 0.9500 . ?
C29 C30 1.400(10) . ?
C29 H29 0.9500 . ?
C30 H30 0.9500 . ?
C31 H31A 0.9800 . ?
C31 H31B 0.9800 . ?
C31 H31C 0.9800 . ?
C32 H32A 0.9800 . ?
C32 H32B 0.9800 . ?
C32 H32C 0.9800 . ?
C33 C38 1.382(10) . ?
C33 C34 1.385(10) . ?
C33 H33 0.9500 . ?
C34 C35 1.377(12) . ?
C34 H34 0.9500 . ?
C35 C36 1.372(11) . ?
C35 H35 0.9500 . ?
C36 C37 1.397(11) . ?
C36 H36 0.9500 . ?
C37 C38 1.407(11) . ?
C37 H37 0.9500 . ?
C38 C39 1.478(10) . ?
C39 C40 1.404(9) . ?
C40 C41 1.403(10) . ?
C40 H40 0.9500 . ?
C41 C42 1.470(10) . ?
C42 C47 1.387(10) . ?
C42 C43 1.413(11) . ?
C43 C44 1.388(10) . ?
C43 H43 0.9500 . ?
C44 C45 1.382(10) . ?
C44 H44 0.9500 . ?
C45 C46 1.390(10) . ?
C45 H45 0.9500 . ?
C46 C47 1.374(10) . ?
C46 H46 0.9500 . ?
C47 H47 0.9500 . ?
C48 C49 1.383(10) . ?
C48 C53 1.400(10) . ?
C48 H48 0.9500 . ?
C49 C50 1.370(11) . ?
C49 H49 0.9500 . ?
```

```
C50 C51 1.390(11) . ?
C50 H50 0.9500 . ?
C51 C52 1.394(11) . ?
C51 H51 0.9500 . ?
C52 C53 1.386(10) . ?
C52 H52 0.9500 . ?
C53 C54 1.497(10) . ?
C54 C55 1.408(10) . ?
C55 C56 1.391(10) . ?
C55 H55 0.9500 . ?
C56 C57 1.499(9) . ?
C57 C62 1.399(10) . ?
C57 C58 1.405(10) . ?
C58 C59 1.384(9) . ?
C58 H58 0.9500 . ?
C59 C60 1.391(11) . ?
C59 H59 0.9500 . ?
C60 C61 1.399(11) . ?
C60 H60 0.9500 . ?
C61 C62 1.388(10) . ?
C61 H61 0.9500 . ?
C62 H62 0.9500 . ?
C63 H63A 0.9800 . ?
C63 H63B 0.9800 . ?
C63 H63C 0.9800 . ?
C64 H64A 0.9800 . ?
C64 H64B 0.9800 . ?
C64 H64C 0.9800 . ?

loop_
 _geom_angle_atom_site_label_1
 _geom_angle_atom_site_label_2
 _geom_angle_atom_site_label_3
 _geom_angle
 _geom_angle_site_symmetry_1
 _geom_angle_site_symmetry_3
 _geom_angle_publ_flag
O1 U1 O2 178.8(2) . . ?
O1 U1 O5 91.7(2) . . ?
O2 U1 O5 89.0(2) . . ?
O1 U1 O7 89.3(2) . . ?
O2 U1 O7 91.8(2) . . ?
O5 U1 O7 73.43(17) . . ?
O1 U1 O6 90.0(2) . . ?
O2 U1 O6 90.0(2) . . ?
O5 U1 O6 143.66(17) . . ?
O7 U1 O6 70.29(16) . . ?
O1 U1 O4 87.7(2) . . ?
O2 U1 O4 91.7(2) . . ?
O5 U1 O4 69.48(18) . . ?
O7 U1 O4 142.67(17) . . ?
O6 U1 O4 146.85(17) . . ?
O1 U1 O3 89.9(2) . . ?
O2 U1 O3 89.0(2) . . ?
O5 U1 O3 142.76(17) . . ?
O7 U1 O3 143.80(17) . . ?
O6 U1 O3 73.52(16) . . ?
O4 U1 O3 73.42(18) . . ?
O8 U2 O9 178.4(3) . . ?
O8 U2 O11 89.8(2) . . ?
O9 U2 O11 88.9(2) . . ?
```

```
O8 U2 O14 89.8(2) . . ?
O9 U2 O14 91.8(2) . . ?
O11 U2 O14 142.27(18) . . ?
O8 U2 O13 90.3(2) . . ?
O9 U2 O13 90.2(2) . . ?
O11 U2 O13 147.13(18) . . ?
O14 U2 O13 70.59(17) . . ?
O8 U2 O12 89.2(2) . . ?
O9 U2 O12 91.4(2) . . ?
O11 U2 O12 69.99(18) . . ?
O14 U2 O12 72.28(17) . . ?
O13 U2 O12 142.87(16) . . ?
O8 U2 O10 89.0(2) . . ?
O9 U2 O10 89.6(2) . . ?
O11 U2 O10 71.8(2) . . ?
O14 U2 O10 145.86(19) . . ?
O13 U2 O10 75.30(18) . . ?
O12 U2 O10 141.79(18) . . ?
O3 S1 C32 109.5(5) . . ?
O3 S1 C31 105.0(4) . . ?
C32 S1 C31 100.1(7) . . ?
O10 S2 C64 105.5(5) . . ?
O10 S2 C63 101.5(7) . . ?
C64 S2 C63 96.2(6) . . ?
S1 O3 U1 124.9(3) . . ?
C7 O4 U1 129.3(5) . . ?
C9 O5 U1 129.3(4) . . ?
C22 O6 U1 139.8(4) . . ?
C24 O7 U1 139.3(4) . . ?
S2 O10 U2 121.7(4) . . ?
C39 O11 U2 131.7(5) . . ?
C41 O12 U2 132.2(5) . . ?
C54 O13 U2 139.2(4) . . ?
C56 O14 U2 139.1(4) . . ?
C6 C1 C2 121.0(8) . . ?
C6 C1 H1 119.5 . . ?
C2 C1 H1 119.5 . . ?
C3 C2 C1 120.2(8) . . ?
C3 C2 H2 119.9 . . ?
C1 C2 H2 119.9 . . ?
C4 C3 C2 119.8(7) . . ?
C4 C3 H3 120.1 . . ?
C2 C3 H3 120.1 . . ?
C3 C4 C5 119.7(7) . . ?
C3 C4 H4 120.1 . . ?
C5 C4 H4 120.1 . . ?
C6 C5 C4 121.4(7) . . ?
C6 C5 H5 119.3 . . ?
C4 C5 H5 119.3 . . ?
C1 C6 C5 117.9(7) . . ?
C1 C6 C7 117.9(7) . . ?
C5 C6 C7 124.2(7) . . ?
O4 C7 C8 122.5(7) . . ?
O4 C7 C6 116.3(6) . . ?
C8 C7 C6 121.0(6) . . ?
C9 C8 C7 122.6(7) . . ?
C9 C8 H8 118.7 . . ?
C7 C8 H8 118.7 . . ?
O5 C9 C8 124.0(6) . . ?
O5 C9 C10 116.2(6) . . ?
C8 C9 C10 119.7(6) . . ?
```

```
C11 C10 C15 120.2(7) . . ?
C11 C10 C9 122.1(6) . . ?
C15 C10 C9 117.6(6) . . ?
C10 C11 C12 119.6(7) . . ?
C10 C11 H11 120.2 . . ?
C12 C11 H11 120.2 . . ?
C13 C12 C11 120.8(7) . . ?
C13 C12 H12 119.6 . . ?
C11 C12 H12 119.6 . . ?
C12 C13 C14 120.0(7) . . ?
C12 C13 H13 120.0 . . ?
C14 C13 H13 120.0 . . ?
C15 C14 C13 120.1(7) . . ?
C15 C14 H14 120.0 . . ?
C13 C14 H14 120.0 . . ?
C14 C15 C10 119.3(7) . . ?
C14 C15 H15 120.3 . . ?
C10 C15 H15 120.3 . . ?
C17 C16 C21 120.8(7) . . ?
C17 C16 H16 119.6 . . ?
C21 C16 H16 119.6 . . ?
C16 C17 C18 120.2(7) . . ?
C16 C17 H17 119.9 . . ?
C18 C17 H17 119.9 . . ?
C19 C18 C17 119.6(7) . . ?
C19 C18 H18 120.2 . . ?
C17 C18 H18 120.2 . . ?
C20 C19 C18 121.0(7) . . ?
C20 C19 H19 119.5 . . ?
C18 C19 H19 119.5 . . ?
C19 C20 C21 119.8(7) . . ?
C19 C20 H20 120.1 . . ?
C21 C20 H20 120.1 . . ?
C16 C21 C20 118.5(6) . . ?
C16 C21 C22 118.8(6) . . ?
C20 C21 C22 122.7(6) . . ?
O6 C22 C23 122.9(6) . . ?
O6 C22 C21 116.5(6) . . ?
C23 C22 C21 120.5(6) . . ?
C24 C23 C22 123.5(7) . . ?
C24 C23 H23 118.3 . . ?
C22 C23 H23 118.3 . . ?
O7 C24 C23 123.6(6) . . ?
O7 C24 C25 116.4(6) . . ?
C23 C24 C25 120.0(6) . . ?
C30 C25 C26 118.7(7) . . ?
C30 C25 C24 118.7(6) . . ?
C26 C25 C24 122.6(6) . . ?
C27 C26 C25 120.2(7) . . ?
C27 C26 H26 119.9 . . ?
C25 C26 H26 119.9 . . ?
C28 C27 C26 120.6(7) . . ?
C28 C27 H27 119.7 . . ?
C26 C27 H27 119.7 . . ?
C27 C28 C29 120.1(7) . . ?
C27 C28 H28 120.0 . . ?
C29 C28 H28 120.0 . . ?
C28 C29 C30 120.4(7) . . ?
C28 C29 H29 119.8 . . ?
C30 C29 H29 119.8 . . ?
C29 C30 C25 120.0(7) . . ?
```

```
C29 C30 H30 120.0 . . ?
C25 C30 H30 120.0 . . ?
S1 C31 H31A 109.5 . . ?
S1 C31 H31B 109.5 . . ?
H31A C31 H31B 109.5 . . ?
S1 C31 H31C 109.5 . . ?
H31A C31 H31C 109.5 . . ?
H31B C31 H31C 109.5 . . ?
S1 C32 H32A 109.5 . . ?
S1 C32 H32B 109.5 . . ?
H32A C32 H32B 109.5 . . ?
S1 C32 H32C 109.5 . . ?
H32A C32 H32C 109.5 . . ?
H32B C32 H32C 109.5 . . ?
C38 C33 C34 121.3(7) . . ?
C38 C33 H33 119.4 . . ?
C34 C33 H33 119.4 . . ?
C35 C34 C33 119.6(7) . . ?
C35 C34 H34 120.2 . . ?
C33 C34 H34 120.2 . . ?
C36 C35 C34 120.5(7) . . ?
C36 C35 H35 119.8 . . ?
C34 C35 H35 119.8 . . ?
C35 C36 C37 120.4(8) . . ?
C35 C36 H36 119.8 . . ?
C37 C36 H36 119.8 . . ?
C36 C37 C38 119.5(7) . . ?
C36 C37 H37 120.3 . . ?
C38 C37 H37 120.3 . . ?
C33 C38 C37 118.7(7) . . ?
C33 C38 C39 118.3(7) . . ?
C37 C38 C39 123.0(7) . . ?
O11 C39 C40 122.5(6) . . ?
O11 C39 C38 114.7(6) . . ?
C40 C39 C38 122.8(6) . . ?
C41 C40 C39 123.5(6) . . ?
C41 C40 H40 118.3 . . ?
C39 C40 H40 118.3 . . ?
O12 C41 C40 123.4(6) . . ?
O12 C41 C42 116.2(6) . . ?
C40 C41 C42 120.1(6) . . ?
C47 C42 C43 118.2(7) . . ?
C47 C42 C41 120.2(7) . . ?
C43 C42 C41 121.6(7) . . ?
C44 C43 C42 120.2(7) . . ?
C44 C43 H43 119.9 . . ?
C42 C43 H43 119.9 . . ?
C45 C44 C43 120.1(7) . . ?
C45 C44 H44 120.0 . . ?
C43 C44 H44 120.0 . . ?
C44 C45 C46 120.1(7) . . ?
C44 C45 H45 120.0 . . ?
C46 C45 H45 120.0 . . ?
C47 C46 C45 119.9(7) . . ?
C47 C46 H46 120.1 . . ?
C45 C46 H46 120.1 . . ?
C42 C47 C46 121.6(7) . . ?
C42 C47 H47 119.2 . . ?
C46 C47 H47 119.2 . . ?
C49 C48 C53 119.9(7) . . ?
C49 C48 H48 120.0 . . ?
```

```
C53 C48 H48 120.0 . . ?
C50 C49 C48 121.2(7) . . ?
C50 C49 H49 119.4 . . ?
C48 C49 H49 119.4 . . ?
C49 C50 C51 119.6(7) . . ?
C49 C50 H50 120.2 . . ?
C51 C50 H50 120.2 . . ?
C50 C51 C52 119.8(7) . . ?
C50 C51 H51 120.1 . . ?
C52 C51 H51 120.1 . . ?
C53 C52 C51 120.6(7) . . ?
C53 C52 H52 119.7 . . ?
C51 C52 H52 119.7 . . ?
C52 C53 C48 118.9(6) . . ?
C52 C53 C54 122.9(6) . . ?
C48 C53 C54 118.3(6) . . ?
O13 C54 C55 123.4(7) . . ?
O13 C54 C53 116.1(6) . . ?
C55 C54 C53 120.5(7) . . ?
C56 C55 C54 123.7(7) . . ?
C56 C55 H55 118.2 . . ?
C54 C55 H55 118.2 . . ?
O14 C56 C55 123.8(6) . . ?
O14 C56 C57 115.3(6) . . ?
C55 C56 C57 121.0(6) . . ?
C62 C57 C58 118.9(6) . . ?
C62 C57 C56 118.8(6) . . ?
C58 C57 C56 122.3(6) . . ?
C59 C58 C57 120.7(7) . . ?
C59 C58 H58 119.6 . . ?
C57 C58 H58 119.6 . . ?
C58 C59 C60 120.1(7) . . ?
C58 C59 H59 120.0 . . ?
C60 C59 H59 120.0 . . ?
C61 C60 C59 119.7(7) . . ?
C61 C60 H60 120.1 . . ?
C59 C60 H60 120.1 . . ?
C60 C61 C62 120.2(7) . . ?
C60 C61 H61 119.9 . . ?
C62 C61 H61 119.9 . . ?
C57 C62 C61 120.3(7) . . ?
C57 C62 H62 119.8 . . ?
C61 C62 H62 119.8 . . ?
S2 C63 H63A 109.5 . . ?
S2 C63 H63B 109.5 . . ?
H63A C63 H63B 109.5 . . ?
S2 C63 H63C 109.5 . . ?
H63A C63 H63C 109.5 . . ?
H63B C63 H63C 109.5 . . ?
S2 C64 H64A 109.5 . . ?
S2 C64 H64B 109.5 . . ?
H64A C64 H64B 109.5 . . ?
S2 C64 H64C 109.5 . . ?
H64A C64 H64C 109.5 . . ?
H64B C64 H64C 109.5 . . ?

loop_
 _geom_torsion_atom_site_label_1
 _geom_torsion_atom_site_label_2
 _geom_torsion_atom_site_label_3
 _geom_torsion_atom_site_label_4
```

```
 _geom_torsion
 _geom_torsion_site_symmetry_1
 _geom_torsion_site_symmetry_2
 _geom_torsion_site_symmetry_3
 _geom_torsion_site_symmetry_4
 _geom_torsion_publ_flag
C32 S1 O3 U1 -155.3(6) . . . . ?
C31 S1 O3 U1 97.9(6) . . . . ?
O1 U1 O3 S1 -25.6(4) . . . . ?
O2 U1 O3 S1 154.8(4) . . . . ?
O5 U1 O3 S1 -118.2(4) . . . . ?
O7 U1 O3 S1 63.1(5) . . . . ?
O6 U1 O3 S1 64.4(3) . . . . ?
O4 U1 O3 S1 -113.2(4) . . . . ?
O1 U1 O4 C7 45.9(7) . . . . ?
O2 U1 O4 C7 -135.1(7) . . . . ?
O5 U1 O4 C7 -46.8(6) . . . . ?
O7 U1 O4 C7 -39.9(8) . . . . ?
O6 U1 O4 C7 132.3(6) . . . . ?
O3 U1 O4 C7 136.5(7) . . . . ?
O1 U1 O5 C9 -42.6(6) . . . . ?
O2 U1 O5 C9 136.5(6) . . . . ?
O7 U1 O5 C9 -131.4(6) . . . . ?
O6 U1 O5 C9 -134.8(5) . . . . ?
O4 U1 O5 C9 44.3(6) . . . . ?
O3 U1 O5 C9 49.5(7) . . . . ?
O1 U1 O6 C22 -95.8(7) . . . . ?
O2 U1 O6 C22 85.3(7) . . . . ?
O5 U1 O6 C22 -3.0(8) . . . . ?
O7 U1 O6 C22 -6.5(7) . . . . ?
O4 U1 O6 C22 178.4(6) . . . . ?
O3 U1 O6 C22 174.3(7) . . . . ?
O1 U1 O7 C24 91.1(7) . . . . ?
O2 U1 O7 C24 -88.5(7) . . . . ?
O5 U1 O7 C24 -176.9(7) . . . . ?
O6 U1 O7 C24 0.9(6) . . . . ?
O4 U1 O7 C24 176.4(6) . . . . ?
O3 U1 O7 C24 2.2(8) . . . . ?
C64 S2 O10 U2 -113.9(6) . . . . ?
C63 S2 O10 U2 146.3(5) . . . . ?
O8 U2 O10 S2 10.8(5) . . . . ?
O9 U2 O10 S2 -168.4(4) . . . . ?
O11 U2 O10 S2 -79.4(4) . . . . ?
O14 U2 O10 S2 99.0(5) . . . . ?
O13 U2 O10 S2 101.3(4) . . . . ?
O12 U2 O10 S2 -76.6(6) . . . . ?
O8 U2 O11 C39 48.2(7) . . . . ?
O9 U2 O11 C39 -132.8(7) . . . . ?
O14 U2 O11 C39 -41.3(8) . . . . ?
O13 U2 O11 C39 138.4(6) . . . . ?
O12 U2 O11 C39 -41.0(6) . . . . ?
O10 U2 O11 C39 137.2(7) . . . . ?
O8 U2 O12 C41 -52.4(6) . . . . ?
O9 U2 O12 C41 126.1(6) . . . . ?
O11 U2 O12 C41 37.7(6) . . . . ?
O14 U2 O12 C41 -142.5(7) . . . . ?
O13 U2 O12 C41 -141.7(6) . . . . ?
O10 U2 O12 C41 34.9(8) . . . . ?
O8 U2 O13 C54 -93.2(7) . . . . ?
O9 U2 O13 C54 88.3(7) . . . . ?
O11 U2 O13 C54 176.7(6) . . . . ?
```

```
O14 U2 O13 C54 -3.4(6) . . . . ?
O12 U2 O13 C54 -4.2(8) . . . . ?
O10 U2 O13 C54 177.9(7) . . . . ?
O8 U2 O14 C56 89.0(7) . . . . ?
O9 U2 O14 C56 -91.0(7) . . . . ?
O11 U2 O14 C56 178.5(6) . . . . ?
O13 U2 O14 C56 -1.4(7) . . . . ?
O12 U2 O14 C56 178.1(7) . . . . ?
O10 U2 O14 C56 1.0(9) . . . . ?
C6 C1 C2 C3 -3.4(15) . . . . ?
C1 C2 C3 C4 2.3(14) . . . . ?
C2 C3 C4 C5 -0.9(12) . . . . ?
C3 C4 C5 C6 0.5(11) . . . . ?
C2 C1 C6 C5 2.9(13) . . . . ?
C2 C1 C6 C7 -178.9(8) . . . . ?
C4 C5 C6 C1 -1.5(12) . . . . ?
C4 C5 C6 C7 -179.5(7) . . . . ?
U1 O4 C7 C8 34.3(10) . . . . ?
U1 O4 C7 C6 -150.4(5) . . . . ?
C1 C6 C7 O4 6.6(11) . . . . ?
C5 C6 C7 O4 -175.3(7) . . . . ?
C1 C6 C7 C8 -178.0(7) . . . . ?
C5 C6 C7 C8 0.0(11) . . . . ?
O4 C7 C8 C9 6.8(11) . . . . ?
C6 C7 C8 C9 -168.3(7) . . . . ?
U1 O5 C9 C8 -30.3(10) . . . . ?
U1 O5 C9 C10 152.3(4) . . . . ?
C7 C8 C9 O5 -8.9(11) . . . . ?
C7 C8 C9 C10 168.5(6) . . . . ?
O5 C9 C10 C11 -157.5(7) . . . . ?
C8 C9 C10 C11 24.9(10) . . . . ?
O5 C9 C10 C15 24.5(9) . . . . ?
C8 C9 C10 C15 -153.1(6) . . . . ?
C15 C10 C11 C12 1.2(10) . . . . ?
C9 C10 C11 C12 -176.8(6) . . . . ?
C10 C11 C12 C13 0.9(11) . . . . ?
C11 C12 C13 C14 -1.7(11) . . . . ?
C12 C13 C14 C15 0.3(10) . . . . ?
C13 C14 C15 C10 1.7(10) . . . . ?
C11 C10 C15 C14 -2.5(10) . . . . ?
C9 C10 C15 C14 175.6(6) . . . . ?
C21 C16 C17 C18 0.3(11) . . . . ?
C16 C17 C18 C19 -2.5(12) . . . . ?
C17 C18 C19 C20 1.7(12) . . . . ?
C18 C19 C20 C21 1.4(12) . . . . ?
C17 C16 C21 C20 2.7(10) . . . . ?
C17 C16 C21 C22 -176.4(7) . . . . ?
C19 C20 C21 C16 -3.6(11) . . . . ?
C19 C20 C21 C22 175.5(7) . . . . ?
U1 O6 C22 C23 5.4(11) . . . . ?
U1 O6 C22 C21 -176.4(4) . . . . ?
C16 C21 C22 O6 -12.1(9) . . . . ?
C20 C21 C22 O6 168.9(6) . . . . ?
C16 C21 C22 C23 166.2(7) . . . . ?
C20 C21 C22 C23 -12.9(10) . . . . ?
O6 C22 C23 C24 3.8(12) . . . . ?
C21 C22 C23 C24 -174.3(7) . . . . ?
U1 O7 C24 C23 5.2(11) . . . . ?
U1 O7 C24 C25 -175.1(5) . . . . ?
C22 C23 C24 O7 -8.5(11) . . . . ?
C22 C23 C24 C25 171.8(7) . . . . ?
```

```
O7 C24 C25 C30 -16.7(9) . . . . ?
C23 C24 C25 C30 163.0(7) . . . . ?
O7 C24 C25 C26 162.8(6) . . . . ?
C23 C24 C25 C26 -17.6(10) . . . . ?
C30 C25 C26 C27 -2.3(11) . . . . ?
C24 C25 C26 C27 178.3(6) . . . . ?
C25 C26 C27 C28 1.0(11) . . . . ?
C26 C27 C28 C29 0.3(12) . . . . ?
C27 C28 C29 C30 -0.3(11) . . . . ?
C28 C29 C30 C25 -1.0(11) . . . . ?
C26 C25 C30 C29 2.3(11) . . . . ?
C24 C25 C30 C29 -178.3(6) . . . . ?
C38 C33 C34 C35 -1.3(12) . . . . ?
C33 C34 C35 C36 1.7(13) . . . . ?
C34 C35 C36 C37 -0.2(12) . . . . ?
C35 C36 C37 C38 -1.7(11) . . . . ?
C34 C33 C38 C37 -0.7(11) . . . . ?
C34 C33 C38 C39 -179.9(7) . . . . ?
C36 C37 C38 C33 2.1(11) . . . . ?
C36 C37 C38 C39 -178.7(6) . . . . ?
U2 O11 C39 C40 30.6(10) . . . . ?
U2 O11 C39 C38 -152.7(5) . . . . ?
C33 C38 C39 O11 -3.0(10) . . . . ?
C37 C38 C39 O11 177.9(7) . . . . ?
C33 C38 C39 C40 173.7(7) . . . . ?
C37 C38 C39 C40 -5.5(11) . . . . ?
O11 C39 C40 C41 7.2(11) . . . . ?
C38 C39 C40 C41 -169.2(7) . . . . ?
U2 O12 C41 C40 -23.8(10) . . . . ?
U2 O12 C41 C42 162.3(5) . . . . ?
C39 C40 C41 O12 -10.5(11) . . . . ?
C39 C40 C41 C42 163.1(6) . . . . ?
O12 C41 C42 C47 24.4(10) . . . . ?
C40 C41 C42 C47 -149.6(7) . . . . ?
O12 C41 C42 C43 -157.1(7) . . . . ?
C40 C41 C42 C43 28.9(10) . . . . ?
C47 C42 C43 C44 0.8(11) . . . . ?
C41 C42 C43 C44 -177.7(7) . . . . ?
C42 C43 C44 C45 0.5(11) . . . . ?
C43 C44 C45 C46 -1.1(11) . . . . ?
C44 C45 C46 C47 0.3(11) . . . . ?
C43 C42 C47 C46 -1.6(11) . . . . ?
C41 C42 C47 C46 176.9(7) . . . . ?
C45 C46 C47 C42 1.1(11) . . . . ?
C53 C48 C49 C50 -2.2(12) . . . . ?
C48 C49 C50 C51 -0.1(12) . . . . ?
C49 C50 C51 C52 1.4(12) . . . . ?
C50 C51 C52 C53 -0.4(12) . . . . ?
C51 C52 C53 C48 -1.8(11) . . . . ?
C51 C52 C53 C54 177.9(7) . . . . ?
C49 C48 C53 C52 3.1(11) . . . . ?
C49 C48 C53 C54 -176.6(7) . . . . ?
U2 O13 C54 C55 3.0(11) . . . . ?
U2 O13 C54 C53 -177.7(4) . . . . ?
C52 C53 C54 O13 170.4(6) . . . . ?
C48 C53 C54 O13 -9.9(9) . . . . ?
C52 C53 C54 C55 -10.2(10) . . . . ?
C48 C53 C54 C55 169.4(7) . . . . ?
O13 C54 C55 C56 3.0(11) . . . . ?
C53 C54 C55 C56 -176.2(6) . . . . ?
U2 O14 C56 C55 6.2(11) . . . . ?
```

```
U2 O14 C56 C57 -173.5(5) . . . . ?
C54 C55 C56 O14 -7.2(11) . . . . ?
C54 C55 C56 C57 172.4(6) . . . . ?
O14 C56 C57 C62 -16.1(9) . . . . ?
C55 C56 C57 C62 164.2(7) . . . . ?
O14 C56 C57 C58 163.7(6) . . . . ?
C55 C56 C57 C58 -16.0(10) . . . . ?
C62 C57 C58 C59 -0.8(10) . . . . ?
C56 C57 C58 C59 179.4(6) . . . . ?
C57 C58 C59 C60 -1.1(11) . . . . ?
C58 C59 C60 C61 2.4(11) . . . . ?
C59 C60 C61 C62 -1.9(11) . . . . ?
C58 C57 C62 C61 1.4(11) . . . . ?
C56 C57 C62 C61 -178.9(6) . . . . ?
C60 C61 C62 C57 0.0(11) . . . . ?

_diffrn_measured_fraction_theta_max    0.998
_diffrn_reflns_theta_full              27.49
_diffrn_measured_fraction_theta_full   0.998
_refine_diff_density_max    1.481
_refine_diff_density_min   -1.404
_refine_diff_density_rms    0.108
```

Appendix F

NMR Relaxation Times in Paramagnetic Solutions[65, 182, 183)]

Chemical exchange reactions which occur in a system at equilibrium may be conveniently characterized by the mean lifetime (τ) of the exchanging species in each of the chemical sites between which it exchanges. Thus, for a site A the mean lifetime of the exchanging species in that site (τ_A) is related to the observed and actual chemical exchange rate constants k_A and k, respectively, by Eq. F.1.

$$\tau_A^{-1}[A] = k_A[A] = k[A]^a[B]^b \cdots \tag{F.1}$$

where a, b, ... are the orders of the reaction for the concentrations of the reactants. The order of the reaction may be established by determining the variation of τ_A as the concentrations of each of the reactants are varied, and the activation parameters may be determined from the temperature variation of τ_A using Eq. F.2

$$\tau_A^{-1} = k_A = \frac{k_B T}{h} \exp\left[-\frac{\Delta H^{\ddagger}}{R} \cdot \frac{1}{T} + \frac{\Delta S^{\ddagger}}{R}\right] \tag{F.2}$$

where k_B, T, h, R, $\Delta H^{\ddagger}$, and $\Delta S^{\ddagger}$ are the Boltzmann constant, the absolute temperature, the Planck constant, the gas constant, the activation enthalpy, and the activation entropy, respectively. In the chemical exchange between sites i and j, the mean lifetimes (τ_i, τ_j) and rate constants (k_i, k_j) are related by Eqs. F.3 and F.4, respectively.

$$\tau_i P_j = \tau_j P_i \tag{F.3}$$

$$k_i P_i = k_j P_j \tag{F.4}$$

where the populations (molar fractions) of the nuclei in the sites i and j are denoted by P_i and P_j, respectively.

If one considers both the effects of a relaxation time and a chemical shift in the NMR spectrum of the solution containing paramagnetic species, it is necessary to carry out a rigorous solution of the Bloch equations for the system. For a solution containing a paramagnetic metal ion, the relaxation time is given by,

$$(T_{2\text{obs}}^{-1} - T_{2n}^{-1})\frac{P_L}{P_M} = \tau_M^{-1}\left[\frac{T_{2M}^{-2} + T_{2M}^{-1}\tau_M^{-1} + \Delta\omega_M^2}{(T_{2M}^{-1} + \tau_M^{-1})^2 + \Delta\omega_M^2}\right] \tag{F.5}$$

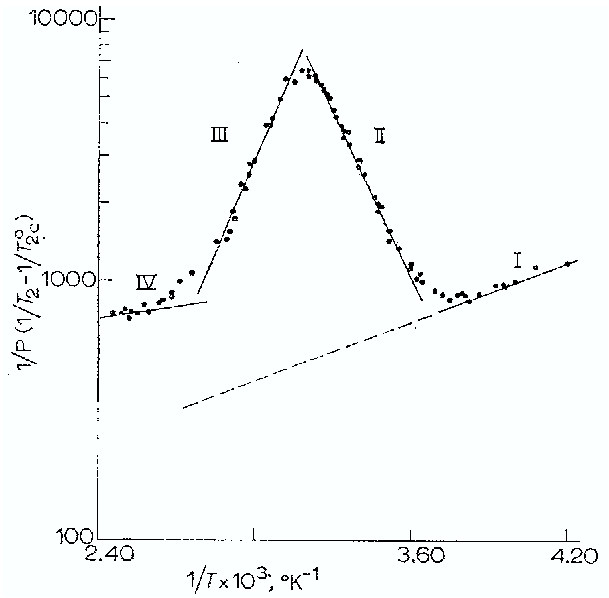

Figure F.1. Temperature dependence of $P_M^{-1}(T_2^{-1} - T_{2A}^{0\,-1})$ for the protons in CH_3CN solutions of $Ni(CH_3CN)_6^{2+}$ at 56.4 MHz quoted from a review by Stengle and Langford,[183] where $T_2 = T_{2osb}$ and $T_{2A}^0 = T_{2n}$ in Eq. F.5. P_L can be neglected because of the dilute solution.

where T_{2obs} and T_{2n} are the transverse relaxation times of a free ligand in the presence and absence of the paramagnetic species, respectively, and T_{2M} is that of the coordinated ligand. P_L and P_M are the molar fractions of the free and coordinated ligand, respectively. Further, τ_M is the mean lifetime of the coordinate ligand, and $\Delta\omega_M$ is the difference between the chemical shifts of the free and coordinated ligand.

At low temperatures, where the exchange is negligible, the line-width of the free ligand show a very slight temperature dependence. This is illustrated in Region I of Figure F.1 which shows the bulk solvent proton resonance of the acetonitrile-Ni^{2+} system over a wide temperature range.

It is convenient to consider the implications of Eq. F.5 for two limiting cases depending on the magnitude of τ_M. If the chemical shift is large, and τ_M not too small ($\Delta\omega_M^2 \gg T_{2M}^{-2}$, τ_M^{-2}), Eq. F.5 leads to,

$$(T_{2obs}^{-1} - T_{2n}^{-1})\frac{P_L}{P_M} = \tau_M^{-1} \tag{F.6}$$

The same result for the line-width is also obtained when the factors other than the chemical shift dominate the relaxation process, *i.e.*, $T_{2M}^{-2} \gg \Delta\omega_M^2$, τ_M^{-2}. Hence, in such a temperature region (Region II in Figure F.1), the exchange rate can be determined regardless of the relaxation mechanism. This is a fortunate result, because the details of the relaxation process are often unclear. The τ_M is related with the first-order rate constant (k_{ex}) of the exchange reaction of L in its metal complex by replacing τ_A and k_A in Eq. F.2 with τ_M and k_{ex}, respectively. Therefore, it is a simple matter to calculate the activation parameters for the first-order exchange reaction from this equation. Many ligand–metal systems have been analyzed using this expression.

If the exchange rate is rapid compared with the conditions for which Eq. F.6 are appropriate, the line-width, $(T_{2obs}^{-1} - T_{2n}^{-1})P_L/P_M$, changes with temperature as shown in Regions III and IV of Figure F.1. Here, the lifetime in the coordination sphere is too short for relaxation

to occur each time the ligand binds to the metal ion. Since several encounters between the ligand and metal ion are required for relaxation, the line-width is no longer directly proportional to the exchange rate. As before, there are two possibilities; effects due to chemical shift may predominate, or, if $\Delta\omega_M$ is small, terms depending on T_{2M} will be important. In the former situation ($\tau_M^{-2} \gg \Delta\omega_M \gg T_{2M}^{-1}\tau_M^{-1}$, Region Ⅲ), we have,

$$(T_{2\text{obs}}^{-1} - T_{2n}^{-1})\frac{P_L}{P_M} = \tau_M^{-1}\Delta\omega_M^2 \tag{F.7}$$

Since the line-width depends upon τ_M, it will change rapidly with temperature but in a direction opposite to Region Ⅱ. If the chemical shift is independently known, τ_M values and hence the exchange rate can be determined.

Finally, when the exchange rate is extremely fast, or the chemical shift is small ($T_{2M}^{-1}\tau_M^{-1} \gg T_{2M}^{-2}$, $\Delta\omega_M^2$, Region Ⅳ), we have,

$$(T_{2\text{obs}}^{-1} - T_{2n}^{-1})\frac{P_L}{P_M} = T_{2M}^{-1} \tag{F.8}$$

Here, the line-width no longer depends on the exchange rate, and it varies but slightly with temperature. This is the limiting high temperature region found in most systems; it is generally called the “fast exchange region”.